Long Wire Notes

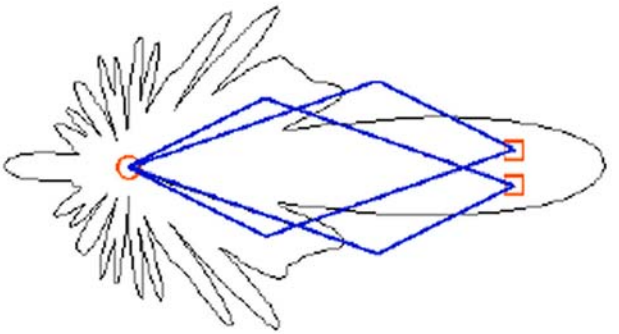

L. B. Cebik, W4RNL

Long-Wire Notes

L. B. Cebik, W4RNL

Published by
antenneX Online Magazine
http://www.antennex.com/
POB 72022
Corpus Christi, Texas 78472 USA

ISBN: 1-877992-77-1

Table of Contents

Dedication

This volume of studies of long-wire antennas is dedicated to the memory of Jean, who was my wife, my friend, my supporter, and my colleague. Her patience, understanding, and assistance gave me the confidence to retire early from academic life to undertake full-time the continuing development of my personal web site (http://www.cebik.com). The site is devoted to providing, as best I can, information of use to radio amateurs and others–both beginning and experienced–on various antenna and related topics. This volume grew out of that work–and hence, shows Jean's help at every step.

Introduction to Long-Wire Technology

> Long wire antennas are very simple, economical, and effective directional antennas with many uses for transmitting and receiving waves in the MF (300 kHz-3 MHz) and HF (3-30 MHz) ranges. Their properties can be enhanced when used in arrays.
>
> Constantine Balanis, *Antenna Theory: Analysis and Design*, 2nd Ed., p.498

Virtually all of the antennas within the amateur arsenal have their origins in the pioneering work done in the 1920s and 1930s. Any true antenna enthusiast has a collection of old books, articles, and manuals from which to read about the old times, the first days of some basic antenna designs. The ubiquitous parasitic beam owes its origins to the early work of Yagi and Uda more than 70 years ago. Even optically based arrays–which include planar, corner, and parabolic reflectors–go back into those early decades of radio communication.

The intervening years have introduced mostly refinements of the early ideas, materials, and design methods. We have developed more complex arrangements of the basic antenna types, accompanied by new and better materials to implement them in superior ways for each new frequency band. Perhaps the most significant development–itself nearly 40 years old–is the growing refinement of computer antenna analysis software that makes daunting and nearly impossible calculations of antenna performance a matter of routine work taking no more than a short time. About mid-way in the life of many antenna types, engineers resorted to a wide array of nomographic design and analysis aids as a means to shortening calculation time for installations. Modern software, such as NEC for round-wire antennas, allows a return to full calculations, where the graphic outputs return to the status of visual aids. As well, contemporary software allows a full accounting of ground conditions, height considerations, and material losses as a matter of course in calculating the likely performance of a given antenna design. Before the 1970s, few design teams could afford the engineering hours required to hand-calculate these factors. Field-testing and adjustment–the engineer's expression for trial and error–ruled

design development.

The effectiveness of computer design and analysis techniques has perhaps proved itself most vividly in the present generation of Yagi antennas. Designs go from software to prototyping and, with little change, into production. We cannot make similar claims for some classes of antennas. Among them is the group of antennas called long-wire arrays and beams. This group includes single end-fed long-wires, V antennas, and rhombics. As bi-directional arrays, they are standing-wave antennas, and when terminated with a proper impedance to form a beam, they are traveling-wave antennas. **Fig. 0-1** shows the general outline of the 3 types of antennas in terminated form. The 3 antenna outlines are not to scale with each other. Nor are the patterns to scale with each other.

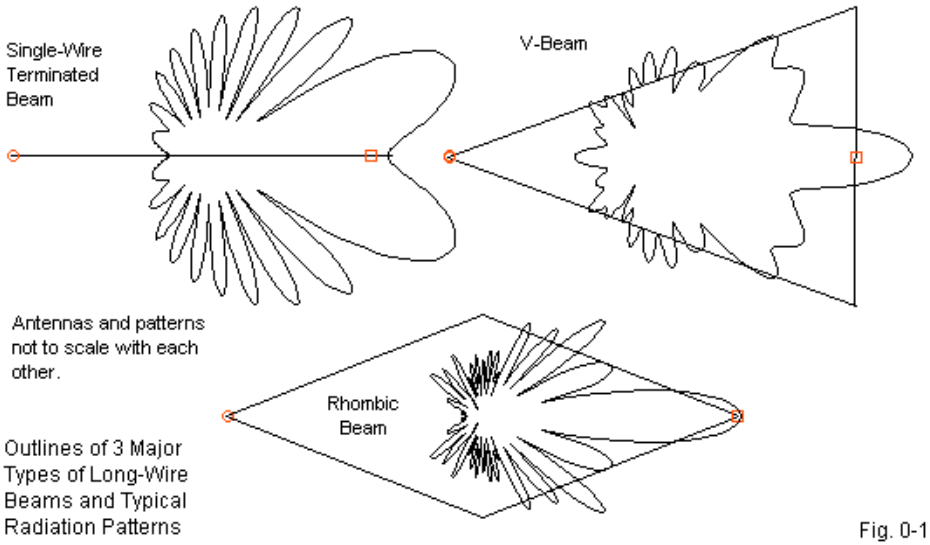

Fig. 0-1

Except for a few remnant installations and the amateur service, these antennas have largely fallen into disuse. Some government services have rediscovered the simpler forms, but few V-beams and rhombics remain in use

outside of amateurs with more acreage than budget. Indeed, the last major volume on traveling-wave antennas appeared in the mid-1960s–before the advent of computer modeling software.

If long-wire antennas have such limited service, then one may fairly ask why we should devote a small volume to their analysis. The answer involves a collection of situations and circumstances that forms the springboard for these notes. First, I regularly receive questions about long-wire antennas from amateurs contemplating installing and using them. Answering the questions has required more information than we tend to find in general antenna handbooks and basic college texts. Second, the antennas are intrinsically interesting, both historically and electrically. They arose in the early days of efforts and analyses aimed at finding ways to enhance antenna performance for more reliable radio communications. Despite being restricted to hand-calculations, antenna engineers developed reasonably reliable equations for designing long-wire antennas. Equally interesting are the practical aspects of antenna installation, testing, and adjustment when wooden supports built like ship masts outnumbered steel masts and towers. Ingenuity, painstaking care, and high levels of craftsmanship accomplished feats that we take for granted with our present-day stock of precision components and digitalized instruments.

Finally, long-wire arrays and beams have not received their just due in terms of analysis via full calculation, otherwise known as computerized analysis. This void has left would-be rhombic designers with no better information than we had in the 1940s. The potential long-wire antenna builder is left with some fundamental equations–mostly dating to the 1930s–and has no guidance as to whether we should assign some limits to them. In general, we treat long-wire equations like simple cutting formulas, assuming their precision without question. The entire class of antennas deserves at least a partial systematic treatment. I have seen entire rhombics designed solely by reference to the initial set of Bruce, Beck, and Lowry equations with little understanding of why those equations have the form that they do and what communications issues were at stake in their formulation. Without that understanding, we can hardly use them intelligently within the amateur antenna situation.

For the radio amateur, long-wire technology proved fascinating since its inception in the early 1930s. The Graham article cited in the short list of sources at the end of this introduction surveys–with mathematical details–the available long-wire designs through 1937. In the same period, the American Radio Relay League erected its own rhombic beam in Connecticut for reliably communicating with the West Coast of the U.S. The antenna remained in service for 4 decades. The League's rhombic inspired many copies and variants by members, as well as continued study by headquarters staff members. Only with the advent of high-performance rotatable Yagis did the rhombic succumb to modernity. Since I am directing these notes principally to the amateur radio community, I also hope to capture with current modeling software something of the history of amateur radio antennas without having to cite any particular examples.

For individuals with acreage and wire, long-wire technology dominated amateur radio antenna thinking. So one way to view these notes might be as a 21st-century homage to those eminently successful communications techniques.

Some Background Ideas

Long-wire antennas and arrays ultimately rest on the basic performance properties of a single end-fed long wire. Different sources use different expressions for the threshold of when an antenna becomes a long-wire antenna. Some treat all wires at least 1 λ long as long wires. Other sources leave the boundary vaguer by using terms like "a few" or "several" wavelengths. In most cases throughout this volume, I shall look at a range of antennas from 1 λ to 11 λ long. Some of the more complex forms of long-wire arrays have poor performance below 2 λ and sometimes below 3 λ. So my rule of thumb is subject to variation.

Long-wire antennas and arrays come in two types: standing-wave and traveling-wave versions. Long-wire antennas do not exhaust these categories, but only represent a small subset of the members of each category. Walter's now-classic volume on *Traveling Wave Antennas* devotes only a few pages specifically to long-wire technology, although the fundamental ideas and equations that he presents throughout the volume are relevant to them.

Again, depending on the source, you may find that accounts of standing waves precede accounts of traveling waves, and vice versa. Since the center-fed dipole–or, in extended frequency use, the center-fed doublet–is perhaps the most familiar antenna, we shall begin with it. The center-fed doublet is a standing-wave antenna. **Fig. 0-2** shows the standing waves of relative current magnitude distribution along the length of the antenna. Note that neither the current peaks nor the current nulls are uniform along the antenna length. (The small peak at the very center or feedpoint region owes to the fact that the model uses a physical length of 5 λ, which makes the antenna very slightly long electrically.)

The diagram emerges from NEC software. Even though the model uses lossless wire and is in free space, the model accounts for two important facts. First, the outgoing energy is not completely reflected back toward the source at the wire ends. As well, the source supplies energy to account for losses from radiation and other factors. Hence, the actual antenna in the figure consists of a standing wave antenna with a small traveling-wave component.

Fig. 0-2

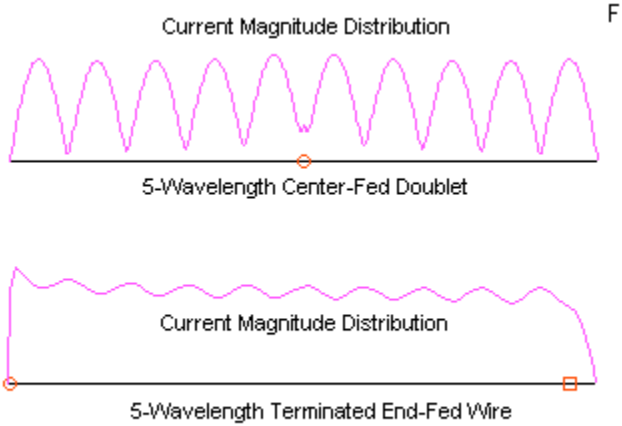

Standing-Wave and Traveling-Wave Current Distribution

Classical calculations related to standing-wave antennas, rest on two

simplifying assumptions. First, the current distribution is sinusoidal. (The diagram shows to what degree the distribution is not sinusoidal.) Second, the system is lossless. In other words, all energy propagating along the wire returns to the source, resulting in perfect standing waves. (Even with lossless wire in free space, the system has losses.) Actual antennas only approximate these conditions, and we shall see some instances in which imperfection can make a difference to antenna operation.

The lower sketch shows an end-fed terminated long-wire antenna, also 5 λ long. It represents a traveling-wave antenna. In a perfect traveling wave antenna, energy propagates along the wire in a single direction, without reflection back toward the source. Real terminated long wire antennas only approximate this condition. Ideally, if we install the proper terminating impedance at the far end of lossless antenna (a subject for extended discussion later), several conditions would exist. The terminating impedance and the source impedance would be identical. The current magnitude would be invariable along the antenna length. The radiation pattern, as suggested in **Fig. 0-1** would be highly directional.

Unfortunately, practical traveling-wave long-wire antennas do not achieve perfection. The most evident cause of imperfection is the use of pure terminating resistances. The actual required impedance is complex. As a result, most long-wire terminated arrays turn out to be traveling-wave antennas with greater or lesser standing-wave components. The lower sketch in **Fig. 0-2** shows the imperfect current distribution. The existence of some rearward radiation in the sample patterns in **Fig. 0-1** is further evidence of imperfection.

Classical calculations used to represent terminated long-wire antennas and arrays tend to ignore the imperfections. As we shall discover, the emergent equations, based on ideal traveling-wave antenna concepts, remain quite serviceable if used within certain limits. They are most accurate in free space. Most early theorists restricted themselves to perfect ground as a reflecting medium, although Harper does introduce some rudimentary accounting for ground losses in his book on rhombic design. At best, then, the classical equations are useful only as starting points in the presence of external influences

on the road to a finished design or analysis.

We shall not examine the derivation of the basic equations most commonly found in handbooks and used in long-wire array design. That material appears in college texts and other extensive literature. (A brief list of useful resources appears at the end of these introductory notes.) Rather, we shall examine some of the common equations–and a few less common ones–in relationship to NEC models of the long-wire arrays. NEC provides for thin, long round-wire antennas a relatively complete and adequate set of calculations that encompass both the internal and external influences on long-wire arrays. The basic calculations account for the source of energy and for wire end effects. For practical antennas, the calculations adjust for material losses associated with the conductivity (and permeability in NEC-4) of the wire itself. The Sommerfeld-Norton ground calculation system is fully adequate to account for influences on long-wire antennas from differences in soil quality and antenna height above ground. In short, the availability of NEC provides a short path to the complete calculations that practical antenna engineers once despaired of making in the design of long-wire arrays. (In fact, rhombic antenna engineers gradually adopted graphic methods of design. Laport of RCA preferred stereographic design aids first introduced by Foster in 1937, while Harper of Bell Labs inclined toward nomographs that captured previous calculations and measurements.)

Before we close these preliminary notes on the relationship of long-wire antennas to standing and traveling waves, we should note a further way in which some authors classify antennas. Standing-wave antennas sometimes receive the label *resonant*. At one or more frequencies, the antennas will show either no or very low reactance at the feedpoint. Without some form of external impedance matching between the feedpoint and the transmission line (or between the transmission line and the transmitting/receiving equipment), the antenna would operate effectively only over a narrow bandwidth.

Traveling-wave antennas sometimes bear the label *non-resonant*. This term sometimes arouses a quizzical expression. For example, one can operate an extended double Zepp antenna (1.25 λ long) in a non-resonant mode, that is, without concern that the feedpoint shows considerable reactance. Hence, we do

not prune the antenna for lowest SWR or purest resistive impedance. Instead, we add the required matching system to convert the impedance to the characteristic impedance of a selected feedline. In the context of long-wire and traveling-wave antennas, the term non-resonant has a different meaning. It suggests that the antenna shows a relatively constant feedpoint impedance over a wide frequency range. The fact that the traveling-wave antenna source impedance is close to resonance in terms of having a low to negligible reactance is accidental to the label. The label indicates that the antenna has a very broad operating bandwidth with little change in feedpoint impedance.

We shall find other distinctions used in classical long-wire technology literature. For example, some authors refer to standing-wave antennas as periodic, indicating that impedance curves repeat themselves as we increase the antenna length. In contrast, traveling-wave antennas are aperiodic, since–in ideal form–they always have virtually the same feedpoint impedance. However, as we shall discover along the way, we shall find neither a perfect standing-wave antenna nor a perfect traveling-wave antenna among the long-wire candidates.

The Goals and Progression of This Volume

NEC makes an excellent vehicle to achieve the goal of this set of notes. The following chapters attempt to make the contemporary early 21st-century radio amateur familiar with the properties of long-wire antennas and arrays. The chief methods, besides a little text, will be data sets and graphical representations of antennas, radiation patterns, and other phenomena connected with the operation long-wires. The data will derive from an internally consistent set of NEC (-4) models that use a common test frequency, a constant wire size, and identical sets of environmental conditions. For each type of antenna that we work with, we shall look at its properties and characteristics from the ideal free-space environment down to several heights above various types of ground. Along the way, we shall explore the relationship of NEC's calculations to classical calculating aids that derive from idealized theory.

The examination of design equations is secondary to the primary goal. I am less interested in performing a critique of these equations than in seeing their

reliability and limitations in relationship to NEC results. The comparisons will permit the prospective long-wire builder to design his or her antenna with some understanding of how traditional methods apply to current computer modeling techniques.

The main course of our work will be to grow familiar with long-wire antennas and arrays by examining progressions of models that are able to display their characteristics–including strengths and weaknesses. To that end, we shall start with a pair of unterminated or standing wave antennas in the first full chapter. Since the center-fed doublet is most likely to be familiar to most readers, we shall begin with its basic properties and compare them to the properties of end-fed long-wires of equal length. We shall be interested in such matters as the angle of the main or strongest radiation lobe to the wire axis and to the elevation angle of the main lobe at various heights above ground. As well, we shall examine the development of lobes in each type of antenna as we increase its length. These factors will prove critical to understanding how more complex long-wire arrays achieve their gain and pattern shapes.

The second chapter will convert the end-fed unterminated long wire antenna into a terminated long-wire, the first of our traveling-wave antennas. The task sounds simple: we need only add a terminating resistor to the far end of the antenna. Actually, the maneuver will present challenges both for modeling the antenna and for practical installations. Most terminated long-wire antennas use vertical lengths of wire at each end in order to allow a common ground termination of both the source and the terminating load–normally a non-inductive resistor. An alternative arrangement places the terminating resistor ¼ λ from the open end of the wire to control both the pattern and the source impedance. We shall explore both forms of installation in order compare their potential performance. We shall also briefly examine two methods of improving performance by aligning the lobes of 2 long-wire antennas. The "bent" long-wire beam and the staggered or echelon long-wire have some very interesting radiation properties, relative to the straight terminated long-wire.

Chapter 3 will examine the first widely used improvement on the simple long-wire antenna. The V array sets up 2 long-wire antennas and feeds them in series

at the source end. The wires diverge from a virtual centerline at an angle related to the angle between the wire axis and the main lobe of a simple long-wire antenna. If the wires are unterminated, the V array yields a bi-directional pattern with a relatively narrow beamwidth for the main lobes. Terminated versions of the antenna require special treatment in practical installations, since the terminating impedance (again, usually a non-inductive resistor) must also connect the wire ends in series. There are several ways to achieve the connection, but not all of them are equally useful when it comes to modeling the antenna. The V beam and its unterminated cousin will reveal some weaknesses, especially with respect to sidelobe suppression. **Fig. 0-3** provides a sample of the pattern differences between terminated and unterminated versions of a V array, and also shows why V antenna sidelobes present a major concern to antenna designers. Although useful, the V array and the V beam do not represent the pinnacle of long-wire array development.

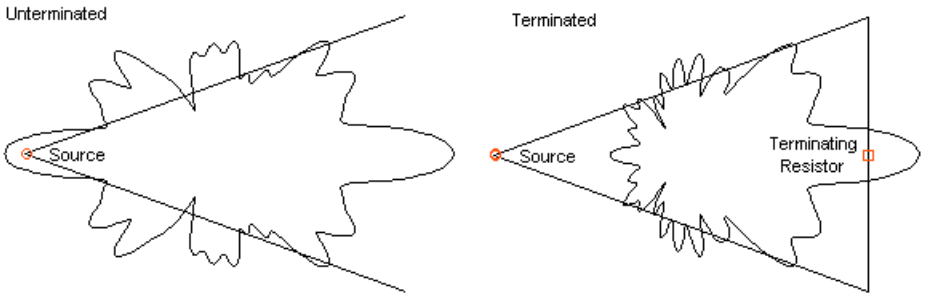

Fig. 0-3 A Sample of Pattern Differences Between Unterminated and Terminated Arrays Using V Antennas with 5-Wavelength Legs.

The fundamentals of rhombic arrays and beams occupy Chapter 4. In one sense, as suggested in **Fig. 0-1**, the rhombic is simply 2 V arrays in mirror formation. We shall explore both open-end and closed-end forms of unterminated rhombic arrays, although unterminated rhombics have seen only rare use. As with all long-wire arrays, unterminated versions give us some standards of design angles and gain measure against which to measure similar parameters in terminated rhombic beams. Because the rhombic far ends join, many of the installation, performance, and modeling limitations that inform

terminated long-wires and V beams do not exist for rhombics. On the other hand, some of the most familiar design equations for long-wire arrays guide common efforts by radio amateurs to design rhombic beams. We shall be very interested in comparing these equations with the results of NEC modeling both in free space and over grounds of various qualities. We shall also want to evaluate the improvements effected by the rhombic over the V beam with respect to sidelobe generation and suppression.

As the highest form of long-wire array and beam development, the basic rhombic has undergone the most study and modification. We shall need a further chapter to survey some of the most important and applicable of them. For example, we shall want to explore the potential for using the rhombic as an effective design for extended frequency coverage. As a case in point, we shall look at the rhombic design that has been a feature in *The ARRL Antenna Book* since the 1970s, when it appeared as a means of covering 20 through 10 meters. A common commercial and amateur modification to the single-wire rhombic is the use of 3 wires to achieve certain aims. It is not clear that all of the claims made about the use of multiple wires have a solid foundation. As well, we shall have to find a viable modeling technique for handling multi-wire rhombics, since there are a number of pitfalls along the way. Completing the list of rhombic "multiples" is the multi-element rhombic, said to increase gain and to improve sidelobe suppression. Even though rhombics have largely fallen into disuse in the HF region, the dual-element rhombic has in recent years been successfully used in the amateur UHF region.

Regardless of whether long-wire antennas and arrays have future uses, they deserve attention and a familiarity that allows you to have reasonable expectations from them. That is the chief goal of these notes. After acquiring the requisite familiarity, you can move in at least two different directions. One path leads back to the underlying theory and mathematics from which we derive basic design equations. The other path leads to a study of the physical requirements for implementing the designs and using them as operating antennas. I hope that the information in these pages is sufficient to allow you to decide in an informed manner whether either path is worth your efforts.

One humorist long ago wished for his ideal antenna, and it was a very long rhombic installed on a rotatable island. Our task will be to see if there is any good sense hiding behind the humor.

A Few Basic References

Many works exist on the subject of terminated directional long-wire antennas, with special attention to the V-beam and the rhombic. However, for a basic introduction to the subject, the following college texts, handbooks, and seminal articles might be useful. There are numerous other articles and texts relevant to a more detailed study of long-wire technology. Some early works are useful in understanding the history of long-wire antennas as part of the growing mastery of the upper MF and the HF ranges. Others provide insight into the variety of design aids developed to ease the problem of calculating the more complex forms of long-wire arrays. The list does not pretend to be complete. Numerous important contributions to long-wire technology appear in other articles. In most cases, the footnotes and references attached to the items in this starting list will provide guidance to further reading.

Balanis, C. A., *Antenna Theory: Design and Analysis*, 2nd Ed., pp. 488-505: a college text.

Boswell, A. G. P., "Wideband Rhombic Antennas for HF," *Proceedings of the 5th International Conference on Antennas and Propagation (ICAP87),* April, 1987: a source of wide-band rhombic design information.

Bruce E., "Developments in Short-Wave Directive Antennas," *Proceedings of the IRE*, August, 1931, Volume 19, Number 8: the introduction of the terminated inverted V and diamond (rhombic) antennas.

Bruce E., Beck A.C., & Lowry L.R., "Horizontal Rhombic Antennas," *Proceedings of the IRE*, January, 1935, Volume 23, Number 1: the classic treatment of rhombic design, repeated in many text books.

Carter P. S., Hansell C. W., and Lindenblad N. E., "Development of Directive

Transmitting Antennas by R.C.A Communications, Inc.," *Proceedings of the IRE*, October, 1931, Volume 19, Number 10: a fundamental treatment of long-wire V antennas, along with the next entry.

Carter P. S., "Circuit Relations in Radiating Systems and Applications to Antenna Problems," *Proceedings of the IRE*, June, 1932, Volume 20, Number 6: the second of the fundamental analyses behind long-wire V antennas.

Foster, Donald, "Radiation from Rhombic Antennas," *Proceedings of the IRE*, October, 1937, Volume 25, Number 10: a more general treatment of rhombic design, with the introduction of stereographic design aids.

Graham, R. C, "Long-Wire Directive Antennas," *QST*, May, 1937: an excellent summary of long-wire technology to the date of publication.

Harper, A. E., *Rhombic Antenna Design* (1941): a fundamental text on rhombics, based on engineering experience, with tables and nomographs as design aids.

Johnson, R. C. (Ed.), *Antenna Engineering Handbook*, 3rd. Ed., Chapter 11, "Long-Wire Antennas" by Laport: similar but not identical material to the relevant pages of Laport's own volume.

Kraus, J. D., *Antennas*, 2nd Ed., pp. 228-234; 502-509: a college text.

Laport, E. A., *Radio Antenna Engineering*, pp. 55-58, 301-339: a summary of long-wire technology up to the date of publication (1950).

Laport, E. A., "Design Data for Horizontal Rhombic Antennas," *RCA Review*, March, 1952, Volume XIII, Number 1: rhombic design data based on the use of stereographic aids developed by Foster.

Laport E. A., & Veldhuis, A. C., "Improved Antennas of the Rhombic Class," *RCA Review*, March, 1960, Volume XXI, Number 1: the introduction of the off-set dual rhombic.

Straw, D. (Ed.), *The ARRL Antenna Book*, 20th Ed., Chapter 13, "Long-Wire and Traveling-Wave Antennas." See also older versions of the volume, for example, Chapter 5 of the 1949 edition, which gives long-wire technology a more thorough treatment on its own ground, rather than in comparison to modern Yagi technology.

Stutzman, W. L., and Thiele, G. A., *Antenna Theory and Design*, 2nd Ed., pp. 225-231: a college text.

Walter, C. H., *Traveling Wave Antennas* (1965): a classic and very thorough text on traveling-wave fundamentals for all relevant types of antennas.

In the course of your reading of materials from the 1930s and 1940s, you may be struck by the use of only selected references in any article. If you then associate both authors and referenced materials to employers–most notably Bell Labs and R.C.A.–you may discover a pattern that we may speculatively suggest is more than accidental. The competition among corporations for ownership or control of patented radio communications technology during the 2 decades preceding World War II had many subtle effects that accompanied its more evident phenomena.

1.

Center-Fed and End-Fed Unterminated Long-Wire Antennas

> The power gain and directive characteristics of electrically long wires (that is, wires that are long in terms of wavelength). . .make them useful for long-distance transmission and reception on the higher frequencies.
>
> *The ARRL Antenna Book*, 20th Ed., p. 13-1

Before we can fully appreciate the early work that developed the V-beam and the rhombic, we must begin our trek in more familiar territory. Since these notes take direct aim at the average amateur radio operator with a yen to understand long-wire technology, we shall largely by-pass mathematical derivations and employ demonstrations via NEC-4 as our vehicle for the journey through long wires. The center-fed doublet is perhaps the most familiar of all wire antennas. If we install a 135' doublet and operate 80 through 10 meters, then by 40 meters, we have a long-wire doublet, that is, a doublet that is 1 λ or longer. Because everything begins with the doublet, that shall be the first leg of our safari.

Some Basic Characteristics of the Center-Fed Long-Wire Doublet

We shall want to examine what happens to a center-fed wire doublet as we change its length in 1-λ increments from 1 to 11 wavelengths. We might extend the exercise further, but the rate of change decreases as the antenna becomes longer, and the limit set here is long enough for us to get hold of all of the fundamental ideas. One key to understanding long-wire antennas is to shift our thinking about antenna size. Instead of thinking in physical lengths, such as X meters or Y feet, we shall think wholly in terms of wavelengths. Hence, as we increase the frequency, the physical length of a wave becomes shorter. So a 10-wavelength antenna at 80 meters is physically 8 times longer than a 10-wavelength antenna at 10 meters.

Fig. 1-1 provides the general layout of a center-fed doublet (using a 3-λ example). It also let's us comment on a common textual convention. The outline of the radiation pattern is a far-field equal-strength diagram. The field limits are

so large that, by comparison, the antenna itself is infinitesimal, no matter how many wavelengths long that we make it. In order to see the antenna orientation to the pattern, we must enlarge the antenna to visible size. In addition, by convention, we center the pattern at the center of the antenna diagram. Shrinking the antenna to its actual size in relationship to the pattern would create a dot at the pattern center.

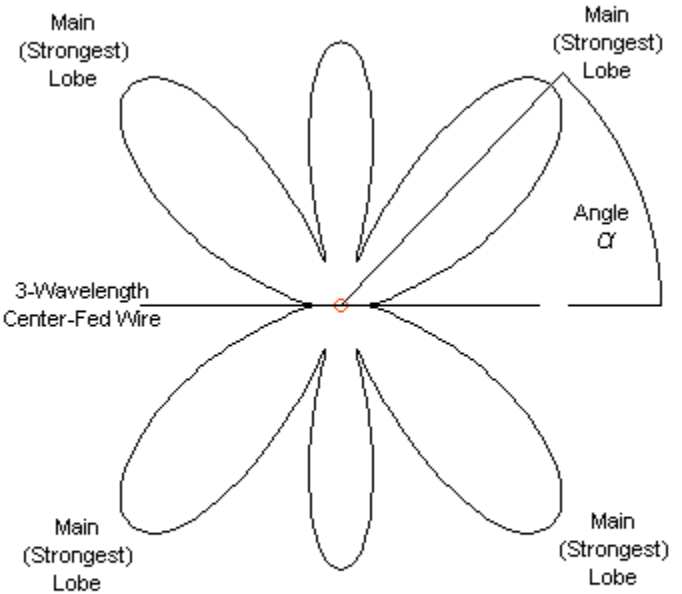

Basic Relationships Between a Center-Fed Doublet and Its Radiation Pattern

Fig. 1-1

The 2-dimensional pattern identifies 4 main lobes. In free-space, these lobes would form rings or tunnels around the virtual wire. We may select any one of the main or strongest lobes and measure the angle between its peak and the axis of the wire. The value of this angle will acquire great importance as we move along

the long-wire trail. By convention, we name this angle α (alpha).

Classical long-wire theory begins in free space, and so we shall begin there also. **Table 1-1** presents the modeled data for a collection of center-fed doublets ranging from 1 to 11 λ. We might well have extended the table, but as the wire grows longer, changes in gain and angle α become much smaller. As well, the increments used for length (1 λ) and for angle α (1°) would not give us the resolution to make good sense of the progression of values that we would encounter.

Center-Fed Doublet in Free-Space				Table 1-1
Lossless Wire				
Len WL	Gn dBi	alpha	BW deg	alpha Calc
1	3.88	90	47.0	85.0
2	4.03	58	26.4	57.0
3	4.74	46	20.6	45.9
4	5.38	40	17.4	39.5
5	5.93	35	15.5	35.2
6	6.41	32	14.0	32.0
7	6.82	29	12.9	29.6
8	7.20	28	12.0	27.6
9	7.55	26	11.3	26.0
10	7.85	25	10.7	24.7
11	8.13	23	10.2	23.5
Len-WL = total wire length in wavelengths				
Gn dBi = maximum gain in dBi				
alpha = angle in degrees between wire axis				
	and main lobe			
BW deg = main lobe beamwidth in degrees				
aphla Calc = calculated value of angle alpha from				
	alpha = arccos[1-(0.912/L)] where			
	L = total wire length in wavelengths			

At a length of 1 λ, we obtain a pattern with 2 lobes, each broadside to the wire and hence 90° relative to the axis of the wire. As we increase the antenna length,

the gain of the strongest lobes increases, and the main lobes tilt toward the wire axis. In principle, no matter how long we make the wire, the main lobes will never quite be in line with the wire.

Every horizontal wire shows some alteration of its free space characteristics as we bring the antenna closer to the ground. **Table 1-2** provides the relevant data for the same wire when it is 1 λ above average ground (conductivity 0.005 S/m, relative permittivity 13). Throughout these tables, we are omitting the feedpoint impedance information provided by the models. In all cases, it will be high. More importantly, we are primarily interested in the relationship between antenna length and the radiation pattern, since this factor ultimately informs the development of long-wire concepts.

Center-Fed Doublet in Free-Space: Lossless Wire

Height: 1 Wavelength above Average Ground

Len WL	Gn dBi	El ang	alpha	HBW deg	VBW deg
1	9.83	14	90	48.4	14.6
2	9.36	14	57	27.6	14.4
3	10.16	14	45	21.7	14.3
4	10.93	14	38	18.7	14.1
5	11.48	13	33	16.5	13.8
6	11.87	13	30	15.2	13.4
7	12.18	13	27	14.3	13.1
8	12.43	13	25	13.5	12.6
9	12.65	13	23	12.8	12.4
10	12.82	13	21	12.5	12.1
11	13.01	13	20	12.0	11.7

Len-WL = total wire length in wavelengths

Gn dBi = maximum gain in dBi

El ang = elevation angle in degrees

alpha = angle in degrees between wire axis and main lobe

HBW deg = horizontal beamwidth in degrees

VBW deg = vertical beamwidth in degrees

Table 1-2

The new table adds 2 columns to the data. One column records the elevation angle of the strongest lobe in the pattern. In theory, the main elevation lobe of a horizontal antenna is tightly connected to the height of the antenna above ground. Texts on long-wire antennas usually give an equation for selecting the height of a proposed antenna in terms of the desired elevation angle required for a communications link.

$H_\lambda = 1 / (4 \sin \alpha)$

H_λ is the height in wavelengths and α is the elevation angle. Since a good bit of science now prefers to count angles from the zenith (overhead) downward as a Θ (theta) angle, α is simply 90 - Θ, and vise versa. Note that the elevation angle has the same label as the angle between the wire and a main lobe. The convention is not accidental. We shall gradually grow clearer on why the 2 angles received the same name, and the background will eventually prove very significant when we approach classical ways of designing rhombic beams. We shall distinguish the two by calling the elevation angle an elevation angle and reserving (for now) the letter α for the azimuth angle between the wire axis and the main lobe.

We may estimate the elevation angle of our antennas if we know its height simply by reversing the equation:

$\alpha = \sin^{-1} [1 / (4 H_\lambda)]$

"Sin^{-1}" is an alternative way to indicate the arcsine or degree-value of a number. Theoretically, our 1-wavelength height should produce elevation angles that are consistently 14.48 degrees. We shall set the software to increment patterns in 1-degree intervals. Since the calculated angle is almost directly between increments, we shall be satisfied if the angles appear as either 14 or 15 degrees. However, as **Table 1-2** shows, as the long-wire antenna grows longer, the elevation angle of maximum radiation–also called the take-off or TO angle–decreases.

The second new column of data involves dividing the beamwidth data into horizontal and vertical components. Once we finish our work with doublets, we shall omit the vertical beamwidth, because the value is very closely related to the value of

the elevation angle. We can more clearly see this fact by surveying the elevation patterns for selected doublet lengths in **Fig. 1-2**. Despite the increasing complexity of the azimuth patterns for these samples that are 1 λ above average ground, the lowest elevation lobe remains almost constant except for variations in gain.

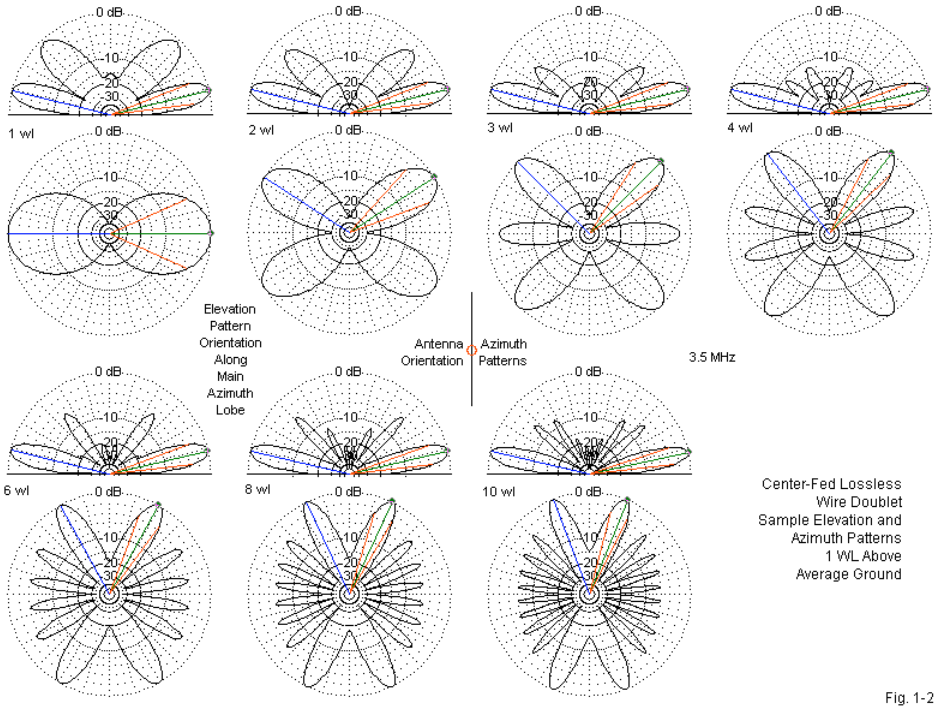

Fig. 1-2

Note that the antenna axis is vertical to the page for the azimuth patterns. Hence, angle α is the angle between an upward line on each pattern toward the lobe containing the beamwidth lines. As shown in the table, as the value of α grows smaller, the horizontal beamwidth also decreases. In addition, as the antenna grows longer, the depth of the null between adjacent main lobes becomes shallower.

Now compare **Table 1-1** and **Table 1-2** with respect to the value of angle α. As the wire length increases, the value of α for an antenna 1 λ over ground becomes smaller than the free-space value. The effect is gradual, but by an 11-λ doublet, the difference is a full 3° or about 13% of the free-space value.

If we raise the antenna to 2 λ above average ground, we obtain somewhat different results, as shown in **Table 1-3**.

Center-Fed Doublet in Free-Space: Lossless Wire					
Height: 2 Wavelengths above Average Ground					
Len WL	Gn dBi	El ang	alpha	HBW deg	VBW deg
1	9.83	7	90	47.4	7.0
2	9.77	7	57	26.6	7.0
3	10.65	7	46	20.8	7.1
4	11.11	7	39	17.8	7.1
5	11.58	7	35	15.7	7.0
6	12.13	7	31	14.4	7.0
7	12.62	7	29	13.2	7.0
8	12.95	7	27	12.3	6.9
9	13.19	7	25	11.7	6.9
10	13.40	7	24	11.1	7.0
11	13.59	7	23	10.6	6.9
Len-WL = total wire length in wavelengths					
Gn dBi = maximum gain in dBi					
El ang = elevation angle in degrees					
alpha = angle in degrees between wire axis					
	and main lobe				
HBW deg = horizontal beamwidth in degrees					
VBW deg = vertical beamwidth in degrees					Table 1-3

With additional height, we expect slightly more gain, and we get it. As well, we expect a lower elevation angle. Using the standard equation, the angle should be 7.18°. The table, which uses 1° elevation-angle increments, shows a constant 7°, roughly confirming the equation. Like the elevation angle for the 1-λ-high doublet, the angle actually decreases slightly. However, the amount of decrease is too little

to show with an integer measure. As well, as we increase the antenna's height above ground, the ground influence on the angle grows smaller, and so even proportionately, the rate of decrease is smaller than for the lower antenna.

The smaller influence of ground shows up in another column of **Table 1-3**. Note that the values for angle α are much closer to those recorded for the free-space model than are the values in **Table 1-2**. In fact, from a height of about 2 λ upward, we may reliably use any computation aids that we may have for free-space models. For example, to independently calculate the value of angle α for free-space models and for models with heights equal to or greater than 2 λ and lengths from 2 to 11 λ, we may use the following equation.

$$\alpha = \cos^{-1} [1 - (0.912/L_\lambda)]$$

In this equation, α is the angle between the wire axis and the main lobe, while L_λ is the total doublet length. The calculated value is close enough to modeled values to provide a preliminary guide for more precise modeling. (See **Table 1-1** to compare modeled vs. calculated values of α for free-space antennas.)

Lobe Development: There is no need to present a set of patterns for the 2-λ-high doublets. The elevation patterns will mostly show a lower main lobe with about twice as many higher lobes, but none stronger than the higher elevation lobes in the 1-λ-high antenna patterns. Except for the small differences in α (1° to 3°), the azimuth patterns would appear virtually identical for antennas at the two heights.

The increment of length change is 1 λ, so that each sampled antenna is at or very close to an integral number of wavelengths long. When we have these conditions, we can calculate the number of lobes in the azimuth pattern very easily:

$$N_{dblt} = 2 L_\lambda$$

N_{dblt} is the number of identifiable lobes and L_λ is the doublet length in wavelengths. Lobes do not suddenly appear, but rather emerge, grow, peak, diminish, and finally disappear. The cycle occurs for every progression from one integral wavelength to the next. For example, **Fig. 1-3** shows the azimuth patterns

for 1-λ-high doublets that are 3 λ, 3.5 λ, and 4 λ long.

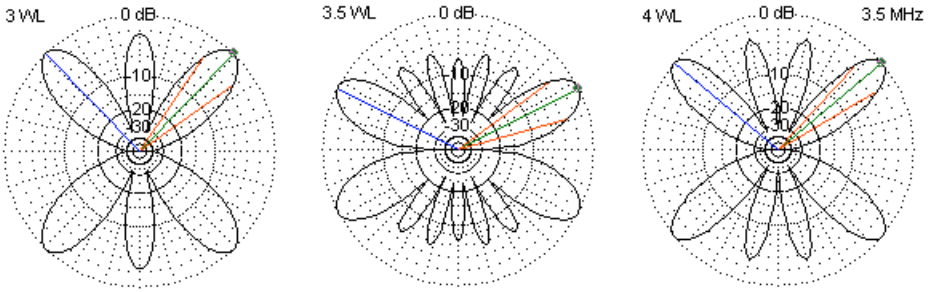

Evolution of Lobe Structure in a Center-Fed Doublet

Fig. 1-3

From the basic equation, we expect 6 lobes from the 3-λ doublet and 8 lobes from the 4-λ doublet. However, as we extend the antenna length beyond 3 λ, the lobes begin to diminish in strength, while the 4-λ lobes set begins to appear. At the 3.5-λ mark, we have a combination of both lobe sets. In other words, for doublet lengths that are close to n.5 λ, where n is an integral number of wavelengths, the total number of lobes will answer to a different equation:

$$N_{dblt} = 2 (L_\lambda + L^{+1}_\lambda)$$

N_{dblt} is the number of lobes. L_λ is the preceding integral wavelength value and L^{+1}_λ is the next integral wavelength value. The sum of the relevant integral doublet lengths in **Fig. 1-3** is 7, giving a total lobe count of 14. In other terms, the 3-λ doublet yields 6 lobes, while the 4-λ doublet has 8. The 3.5-λ doublet has both sets of lobes, that is, 14 lobes.

Fig. 1-3 presents the long doublets oriented horizontally to the pattern diagrams. You may derive the values of angle α of the 3-λ and 4-λ free-space models from **Table 1-1**. However, the presence of many more lobes in the 3.5-λ doublet forces the main lobes to angles that are closer to the wire axis. In fact, for the 3.5-λ doublet, α is 27° (and about 2° less for models that are 1 λ above average ground). Furthermore, the maximum gain (at 5.88 dBi) in the main lobes is higher than the

gain of either the 3-λ or the 4-λ doublets. The narrowing of angle α and the increase in gain above adjacent integral-wavelength doublet sizes will hold true for every doublet that is n.5 λ long.

Environmental and Modeling Considerations: All of the doublet models have adhered to certain constants in order to yield self-consistent results. Each model uses 20 segments per wavelength, plus 1 segment to provide a total number of segments that is an odd number. Thus, the NEC model has an exactly centered feedpoint or source. 20 segments per wavelength is above the NEC minimum, but low enough to allow for systematic modeling of more complex arrays that may use several wires of the longest sampled length. We shall address modeling issues that may arise with more complex long-wire array geometries as they occur in later chapters.

The test models use lossless wire, although the effects of moving from perfect wire to the more common copper or copper-clad wire are minuscule. The test frequency is a uniform 3.5 MHz, with a wire diameter of 0.16" (about AWG #6). If we scale the antennas to other frequencies so that they are the same length in wavelengths and proportionately different in wire diameter, free-space models will show the same results. However, the effects of ground are not constant for all frequencies. Even for a horizontal wire 1-λ above ground, the ground losses change, increasing as we raise the frequency. If we perfectly scale our antenna for other frequencies, then the wire size changes as well. At 7 MHz, it is 0.08" (AWG #12). At 14 MHz, it is 0.04" (AWG #18). At 28 MHz, the size drops to 0.02" (AWG #24). Let's use a 1-wavelength wire at 1 wavelength height and scale it over the set of frequencies to sample the maximum gain values. The results appear in **Table 1-4**. The gain differential between 3.5 MHz and 28 MHz is small: only 0.36 dBi. However, it is a real difference and may vary with the exact height of the antenna over ground. We would expect greater differentials for relatively low antennas and lesser differentials for very high ones. Hence, we should conduct all modeling tests using as consistent a set of values for all possible aspects of the antenna and modeling environment. For any models of actual antennas–existing or proposed–we should set all model parameters as close to reality as a situation permits. As well, we should explore a relevant range of alternatives, whether they involve different materials, different wire diameters, or different heights above ground.

Maximum Gain Values			Table 1-4
1 Wavelength Center-Fed Wire			
1 Wavelength above Average Ground			
Fq MHz	Wire Dia	Gain dBi	
3.5	0.16	9.83	
7.0	0.08	9.67	
14.0	0.04	9.54	
28.0	0.02	9.47	
Fq MHz = Frequency in MHz			
Wire Dia = Wire diameter in inches			
Gain dBi = maximum gain in dBi			

As well, the differential will change with the quality of ground. Our choice of the ground quality also has an effect upon gain values. Indeed, the effect of changing the ground quality is more pronounced than the effect of changing the test frequency. Let's take our 1-λ antenna at its 1-λ height and check it using 3 different levels of soil quality. See **Table 1-5**.

Maximum Gain Values				Table 1-5
1 Wavelength Center-Fed Wire				
1 Wavelength above Various Ground Qualities				
Label	Cond S/m	Permit	Gn 3.5	Gn 28.0
Very Poor	0.001	5	9.41	9.01
Average	0.005	13	9.83	9.47
Very Good	0.0303	20	10.02	9.75
Gain differential: VP to VG Gnd			0.61	0.74
Cond S/m = conductivity in S/m				
Permit = Relative permittivity (vacuum = 1)				
Gn 3.5 = Maximum gain at 3.5 MHz in dBi				
Gn 28.0 = Maximum gain at 28.0 MHz in dBi				

Although the frequency-based differentials between very good (VG) soil and very poor (VP) soil are similar, it is clear that ground effects on antenna losses are not completely linear. Nevertheless, the effects do not change enough to invalidate the general trends in center-fed doublet patterns.

The center-fed doublet often serves as almost a paradigm of standing-wave antennas. Classical antenna accounts make two important assumptions about standing-wave antennas. First, the current distribution along the antenna is sinusoidal. This assumption makes it possible to hand-calculate the principle properties of the antenna, including the field intensity and angle for each lobe produced by the antenna. Second, the unterminated ends of the antenna wire act like a perfect open-ended transmission line and reflect back toward the centered source or feedpoint all current. The result is a series of standing waves that generally show themselves in the relative current magnitude along the length of the wire. Theoretically, each current peak and null should be identical for lossless wire in free space. However, examine **Fig. 1-4**.

Sample Antenna: 241 Segments Fig. 1-4

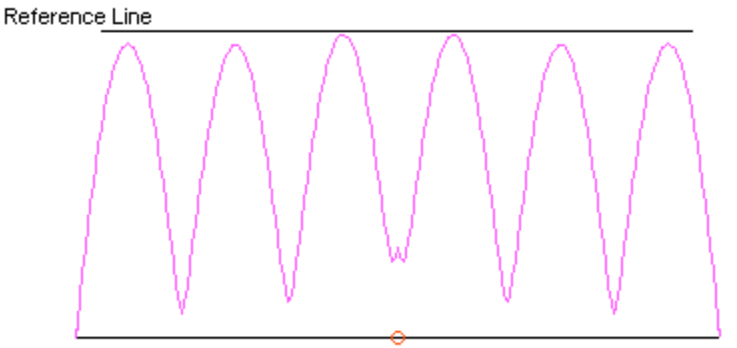

Current Magnitude Distribution: 3-Wavelength Center-Fed Wire

The arbitrary reference line shows not only that the inner current peaks are larger than the outer pair on each side of center, but as well that the outmost peaks are a bit stronger than the middle ones on each side of center. The NEC calculations show small but significant departures from the classical ideal antenna, and the model uses enough segments to show peaks and nulls within very tight error limits. The one deviation from being a perfect model involves the wire length. The model is physically 3 λ long, which makes it very slightly longer than 3 λ electrically. Hence, with enough segments, the source-segment current low shows

up as a very small rise. This rise gradually disappears as the doublet length becomes very large, since the end-effect source of the differential becomes a smaller part of the electrical length of the wires. Nevertheless, the presence of a source to supply energy for losses due to radiation does set a minimum value to the current nulls.

The differences between NEC and classical text calculations for center-fed doublets are not only small, but they are also obscured by the symmetry of the physical layout. Hence, one must look very closely to find deviations between the two calculation methods. However, the effects become very much pronounced if we move the feedpoint from the center to one end of the antenna. Modeled end-fed wires over the same range of lengths will show much more pronounced standing-wave antenna departures. In fact, end-fed wires will show a host of characteristics that differ markedly from those we associated with center-fed long wires. For example, compare the 3-dimensional patterns for 2 4-λ long-wire antennas, one center-fed, the other end-fed. **Fig. 1-5** tells the tale.

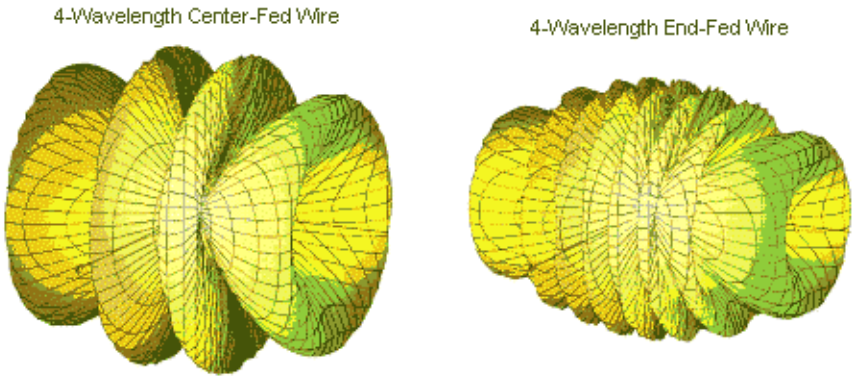

Fig. 1-5 3-Dimensional Free-Space Radiation Patterns
Center-Fed and End-Fed Wire Antennas of Equal Length

The end-fed wire shows twice as many "tunnels" of free-space lobe structures as the center-fed antenna. End-fed wire properties are sufficiently different to

warrant a whole new beginning to our work.

Some Basic Characteristics of the End-Fed Long-Wire

We have a second good reason to investigate with some thoroughness the properties of end-fed long-wire antennas. These antennas form the basis for all of the more complex arrays, whether used as standing-wave antennas or as traveling-wave antennas. **Fig. 1-6** shows the basic outline of the end-fed wire and a representative free-space radiation pattern. (Compare this sketch to **Fig. 1-1**.) Angle α remains the angle between the wire axis and the main lobe. However, for reasons that will become clear, we shall occasionally call the indicated lobe the main forward lobe. If you examine the sketch closely, you will discover that the main lobes toward the feedpoint are slightly weaker than the ones that point away from the feedpoint. Nevertheless, the alignment is correct relative to terminated long-wires in directional arrays.

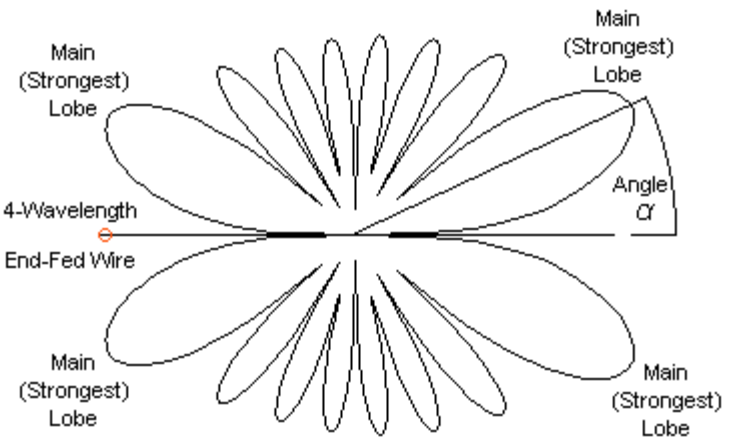

Basic Relationships Between an End-Fed Wire and Its Radiation Pattern

Fig. 1-6

Free-Space Lossless End-Fed Long-Wires: 1-11 WL					Table 1-6
Len WL	Gain dBi	FB dB	alpha	alpha Calc	BW deg
1.0	2.99	0.89	52.8	51.0	41.9
1.5	3.99	1.23	41.5	41.2	32.7
2.0	4.81	1.43	35.7	35.5	27.8
2.5	5.48	1.59	31.4	31.6	24.7
3.0	6.05	1.70	28.5	28.8	22.4
3.5	6.55	1.79	26.6	26.6	20.7
4.0	6.98	1.70	24.5	24.9	19.2
4.5	7.37	1.93	23.1	23.4	18.1
5.0	7.72	1.99	21.8	22.2	17.1
5.5	8.05	2.04	21.1	21.2	16.3
6.0	8.34	2.09	19.9	20.3	15.5
6.5	8.62	2.12	19.4	19.5	14.9
7.0	8.87	2.16	18.5	18.7	14.4
7.5	9.11	2.19	17.9	18.1	13.9
8.0	9.33	2.23	17.2	17.5	13.4
8.5	9.54	2.26	16.6	17.0	13.0
9.0	9.74	2.28	16.2	16.5	12.7
9.5	9.93	2.31	15.7	16.1	12.2
10.0	10.11	2.34	15.3	15.7	12.0
10.5	10.29	2.35	15.2	15.3	11.7
11.0	10.45	2.38	14.8	14.9	11.4
Notes	Len wl = Length in wavelengths				
	Gain dBi = Maximum gain in dBi				
	FB dB = 180-degree front-to-back ratio in dB				
	alpha = Main lobe angle in degrees				
	alpha Calc = Calculated angle in degrees				
	alpha = arccos [1-(0.371/L)], L = wire length in WL				
	BW deg = main lobe beamwidth in degrees				

The first task is to retrace the steps we took in developing the basic properties of center-fed doublets. **Table 1-6** provides data for free-space models that are identical to the center-fed doublets, except that I have moved the feedpoint from the center to one end of the array. In a NEC model, the source placement is not at

the precise wire end, but within the last segment at the antenna end. The source point moves closer to the wire end as we add more segments to the wire without changing its length. However, adding segments does not change the antenna performance significantly in terms of reported values. For example, the 5-λ end-fed wire with 100 total segments returns a free-space gain of 7.72 dBi, a front-to-back ratio of 1.98 dB, an α-angle of 21.8° and a beamwidth of 17.1°. If we increase the number of segments to 800, the gain report increases by 0.02 dB, the front-to-back report by 0.02 dB, and the α-angle by 0.2°

As we might expect, the maximum gain of the forward main lobes increases as we increase the length of the end-fed unterminated wire. The rate of increase, of course, decreases as we extend the wire in linear increments. To the gain specification, we added the word "forward," since the gain away from the feedpoint is slightly higher than the gain toward the feedpoint. The column labeled "FB dB" gives the front-to-back ratio as measured from a forward peak lobe backward to a rearward peak lobe. The gain differential is small, ranging from 0.9 dB for a 1-λ wire to 2.4 dB for an 11-λ wire. Nevertheless, the differential is real and will call for further comments later.

The α-angle values are noticeably smaller than the angles reported for the center-fed doublet series. The end-fed beamwidth values are also lower than for corresponding center-fed doublets. Roughly speaking, the value of α is about 1.28 the beamwidth value, although the multiplier varies from 1.26 for short end-fed wires to about 1.3 for very long wires.

Both the value of α and the beamwidth are directly related to the number of lobes that emerge for any given end-fed wire length. **Fig. 1-5** suggested that for any given length, an end-fed wire that is an integral multiple of a wavelength has twice as many lobes as a center-fed doublet having the same total length. Compare **Fig. 1-7**, a gallery of sample patterns for the end-fed wire, with **Fig. 1-2**, the doublet gallery. Although the patterns are for end-fed wires at a height of 1 λ over average ground, the plots do not change their lobe structure relative to free-space patterns. The elevation patterns do show small but distinct signs of the existence of a front-to-back ratio that is greater than 1:1 for all antenna lengths.

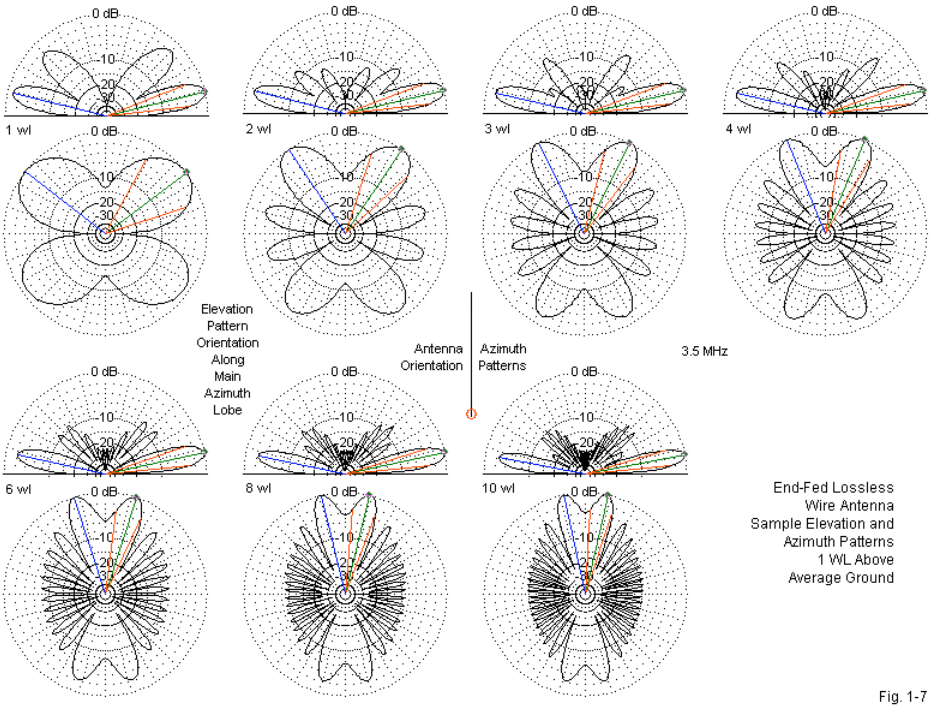

Fig. 1-7

As **Table 1-6** suggests, we may independently calculate the value of the α-angle from the antenna length (L_λ). The required equation appears in many texts, such as Stutzman and Theile (p. 227):

$$\alpha = \cos^{-1} [1 - (0.371/L_\lambda)]$$

The table lists both the values reported by the NEC models and the calculated values. **Fig. 1-8** graphs the two curves to illustrate how closely the classical calculations for free-space values correlate with the reports from NEC models. Like the doublets, the end-fed wires use increments of physical length for convenience, while the independent calculations use electrical lengths.

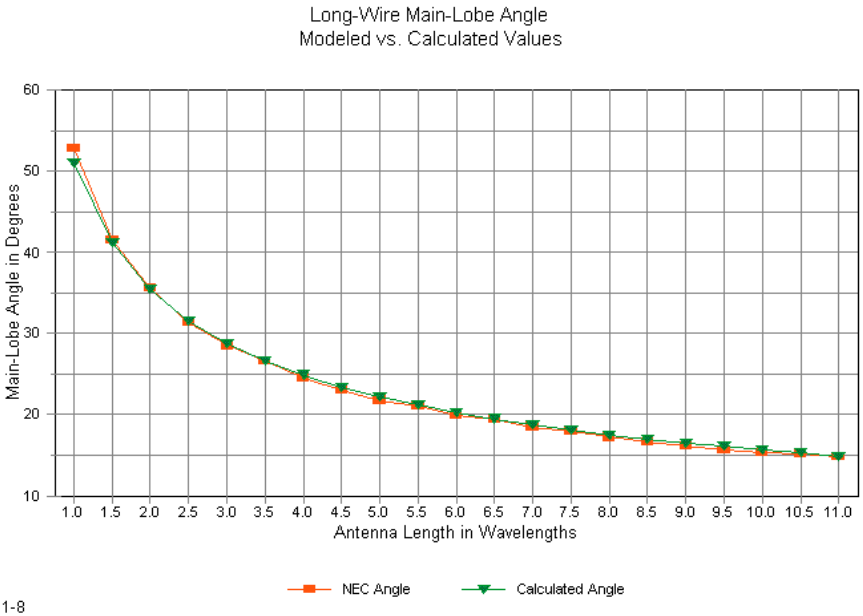

Fig. 1-8

Because the unterminated end-fed wire undergirds all long-wire arrays, whether or not terminated, we should pay close attention to their behavior over ground. One step in this direction is apparent from **Table 1-6**, which used length increments of 0.5 λ. We shall use similar increments of lengths when we examine some essential long-wire characteristics at heights of 0.5 λ, 1 λ, and 2 λ. We shall also show the modeled results for very good, average, and very poor ground. To this span of ground qualities, I have added perfect ground, since that concept plays a role in classic long-wire calculations. Indeed, the calculation of the elevation angle from the antenna height presumes a perfect ground.

If we place the long-wire only 0.5 λ above various grounds, we obtain the interesting results shown in **Table 1-7**. See **Table 1-8** for the same antennas at 1 λ above the same grounds. **Table 1-9** provides equivalent data for a height of 2λ. While the free-space patterns used 0.1° increments, these tables use 1.0°.

End-Fed Unterminated Long-Wires, 1 to 11 Wavelengths, 0.5 Wavelength above Various Grounds								
Ground	Perfect				Very Good (0.0303; 20)			
Len wl	Gain dBi	FB dB	El Ang	alpha	Gain dBi	FB dB	El Ang	alpha
1	8.61	1.00	30	46	8.36	0.97	28	47
1.5	9.48	1.43	30	30	9.08	1.38	28	33
2	10.29	1.64	30	19	9.72	1.60	28	24
2.5	11.01	1.76	30	10	10.26	1.74	27	19
3	11.61	1.82	29	0	10.70	1.84	27	13
3.5	12.07	1.87	27	0	11.07	1.93	27	6
4	12.44	1.89	26	0	11.40	1.99	26	0
4.5	12.73	1.92	25	0	11.66	2.06	24	0
5	12.96	1.94	24	0	11.89	2.11	23	0
5.5	13.16	1.96	23	0	12.07	2.16	22	0
6	13.34	1.99	22	0	12.23	2.19	22	0
6.5	13.48	2.00	21	0	12.37	2.23	21	0
7	13.60	2.02	20	0	12.49	2.28	20	0
7.5	13.72	2.02	20	0	12.58	2.33	19	0
8	13.82	2.04	19	0	12.69	2.36	19	0
8.5	13.90	2.04	19	0	12.77	2.41	18	0
9	13.98	2.05	18	0	12.85	2.43	18	0
9.5	14.05	2.05	18	0	12.91	2.48	17	0
10	14.11	2.07	17	0	12.99	2.51	17	0
10.5	14.19	2.07	17	0	13.02	2.55	16	0
11	14.22	2.07	17	0	13.11	2.58	16	0
Ground	Average (0.005; 13)				Very Poor (0.001; 5)			
Len wl	Gain dBi	FB dB	El Ang	alpha	Gain dBi	FB dB	El Ang	alpha
1	7.99	0.93	27	48	7.38	0.97	25	50
1.5	8.60	1.30	26	36	7.97	1.22	24	38
2	9.11	1.54	25	28	8.45	1.45	23	31
2.5	9.52	1.69	25	23	8.81	1.60	22	26
3	9.85	1.81	24	20	9.11	1.73	21	23
3.5	10.11	1.91	23	17	9.37	1.84	20	21
4	10.33	2.00	22	15	9.59	1.94	19	19
4.5	10.51	2.09	22	12	9.78	2.04	18	17
5	10.68	2.17	21	11	9.96	2.12	17	16
5.5	10.81	2.24	21	9	10.14	2.19	17	15
6	10.90	2.30	21	6	10.30	2.27	16	14
6.5	11.05	2.37	20	6	10.46	2.33	16	13
7	11.19	2.44	19	7	10.61	2.40	15	13
7.5	11.31	2.50	18	7	10.76	2.46	15	12
8	11.40	2.56	18	6	10.90	2.54	14	11
8.5	11.47	2.62	18	2	11.05	2.59	14	11
9	11.60	2.68	17	5	11.20	2.65	14	10
9.5	11.67	2.74	17	0	11.32	2.70	14	9
10	11.79	2.80	16	0	11.48	2.78	13	9
10.5	11.87	2.86	16	0	11.61	2.83	13	8
11	11.97	2.91	15	0	11.75	2.88	13	8
Notes	Len wl = Length in wavelengths							
	Gain dBi = Maximum gain in dBi							
	FB dB = 180-degree front-to-back ratio in dB							
	El Ang = Elevation angle in degrees							
	alpha = Main lobe angle in degrees							Table 1-7

End-Fed Unterminated Long-Wires, 1 to 11 Wavelengths, 1 Wavelength above Various Grounds								
Ground	Perfect				Very Good (0.0303; 20)			
Len wl	Gain dBi	FB dB	El Ang	alpha	Gain dBi	FB dB	El Ang	alpha
1	8.76	0.95	14.2	51	8.63	0.94	14	51
1.5	9.99	1.20	14	40	9.75	1.21	14	40
2	10.95	1.36	14	33	10.64	1.35	14	34
2.5	11.61	1.51	14	29	11.26	1.51	14	29
3	12.12	1.69	14	25	11.73	1.64	14	26
3.5	12.55	1.82	14	23	12.11	1.77	14	24
4	12.92	1.95	14	21	12.43	1.89	13	22
4.5	13.25	2.06	14	19	12.72	1.99	13	20
5	13.55	2.16	14	17	12.98	2.07	13	19
5.5	13.84	2.23	14	16	13.22	2.14	13	18
6	14.11	2.29	14	15	13.43	2.20	13	17
6.5	14.35	2.34	14	13	13.62	2.26	13	15
7	14.59	2.38	14	12	13.80	2.29	13	15
7.5	14.82	2.40	14	12	13.97	2.34	13	14
8	15.03	2.43	14	10	14.12	2.37	13	13
8.5	15.24	2.44	14	10	14.26	2.40	13	12
9	15.44	2.46	14	9	14.38	2.43	13	11
9.5	15.63	2.48	14	8	14.52	2.45	12	11
10	15.81	2.49	14	7	14.65	2.48	12	11
10.5	15.98	2.50	14	6	14.76	2.50	12	11
11	16.15	2.52	14	5	14.87	2.52	12	10
Ground	Average (0.005; 13)				Very Poor (0.001; 5)			
Len wl	Gain dBi	FB dB	El Ang	alpha	Gain dBi	FB dB	El Ang	alpha
1	8.44	0.91	14	52	8.10	0.88	13	53
1.5	9.46	1.21	14	40	9.05	1.20	13	41
2	10.27	1.37	13	34	9.80	1.39	13	34
2.5	10.86	1.50	13	30	10.36	1.52	13	30
3	11.32	1.63	13	27	10.80	1.64	13	27
3.5	11.68	1.75	13	24	11.17	1.73	12	25
4	11.99	1.85	13	22	11.50	1.82	12	23
4.5	12.26	1.92	13	21	11.77	1.88	12	22
5	12.48	2.00	13	19	12.01	1.94	12	20
5.5	12.71	2.06	12	19	12.22	2.00	11	19
6	12.90	2.10	12	18	12.42	2.04	11	18
6.5	13.08	2.15	12	17	12.61	2.08	11	17
7	13.24	2.20	12	16	12.77	2.11	11	17
7.5	13.38	2.24	12	15	12.93	2.14	11	16
8	13.50	2.27	12	14	13.06	2.17	11	15
8.5	13.64	2.31	11	14	13.19	2.20	10	15
9	13.75	2.33	11	14	13.32	2.24	10	14
9.5	13.87	2.36	11	13	13.44	2.25	10	14
10	13.96	2.40	11	12	13.55	2.28	10	13
10.5	14.07	2.41	11	12	13.66	2.30	10	13
11	14.15	2.44	11	12	13.74	2.33	10	12
Notes	Len wl = Length in wavelengths							
	Gain dBi = Maximum gain in dBi							
	FB dB = 180-degree front-to-back ratio in dB							
	El Ang = Elevation angle in degrees							
	alpha = Main lobe angle in degrees							Table 1-8

End-Fed Unterminated Long-Wires, 1 to 11 Wavelengths, 2 Wavelengths above Various Grounds								
Ground	Perfect				Very Good (0.0303; 20)			
Len wl	Gain dBi	FB dB	El Ang	alpha	Gain dBi	FB dB	El Ang	alpha
1	8.92	0.89	7	53	8.85	0.89	7	53
1.5	10.07	1.20	7	41	9.96	1.20	7	41
2	10.78	1.45	7	35	10.66	1.44	7	35
2.5	11.42	1.62	7	31	11.27	1.61	7	31
3	12.07	1.69	7	28	11.88	1.69	7	28
3.5	12.61	1.74	7	26	12.40	1.74	7	26
4	13.03	1.83	7	24	12.80	1.82	7	24
4.5	13.36	1.94	7	22	13.13	1.92	7	23
5	13.68	2.04	7	21	13.41	2.02	7	21
5.5	13.98	2.10	7	20	13.69	2.09	7	20
6	14.28	2.14	7	19	13.95	2.13	7	19
6.5	14.57	2.16	7	18	14.21	2.16	7	18
7	14.85	2.17	7	17	14.46	2.16	7	18
7.5	15.12	2.17	7	17	14.70	2.18	7	17
8	15.37	2.18	7	16	14.90	2.19	7	16
8.5	15.59	2.19	7	15	15.12	2.21	7	16
9	15.82	2.20	7	15	15.30	2.23	7	15
9.5	16.01	2.23	7	14	15.48	2.24	7	15
10	16.21	2.25	7	14	15.63	2.26	7	14
10.5	16.37	2.27	7	14	15.79	2.27	7	14
11	16.54	2.30	7	13	15.92	2.29	7	14
Ground	Average (0.005; 13)				Very Poor (0.001; 5)			
Len wl	Gain dBi	FB dB	El Ang	alpha	Gain dBi	FB dB	El Ang	alpha
1	8.75	0.88	7	53	8.57	0.88	7	53
1.5	9.83	1.20	7	41	9.61	1.21	7	41
2	10.55	1.44	7	35	10.35	1.43	7	35
2.5	11.14	1.60	7	31	10.95	1.59	7	31
3	11.72	1.69	7	28	11.50	1.69	7	28
3.5	12.23	1.75	7	26	11.99	1.76	7	26
4	12.62	1.83	7	24	12.38	1.83	7	24
4.5	12.95	1.91	7	23	12.72	1.90	7	23
5	13.23	1.98	7	22	13.01	1.97	7	22
5.5	13.49	2.06	7	20	13.28	2.03	7	21
6	13.75	2.10	7	20	13.53	2.08	7	20
6.5	13.99	2.13	7	19	13.76	2.12	7	19
7	14.22	2.16	7	18	13.98	2.16	7	18
7.5	14.43	2.19	7	17	14.17	2.19	7	17
8	14.62	2.19	7	17	14.26	2.21	6	17
8.5	14.82	2.23	7	16	14.54	2.24	6	16
9	14.97	2.23	7	16	14.72	2.26	6	16
9.5	15.14	2.26	6	15	14.87	2.29	6	15
10	15.28	2.28	6	15	15.03	2.30	6	15
10.5	15.42	2.31	6	14	15.16	2.32	6	15
11	15.57	2.32	6	14	15.31	2.35	6	14
Notes	Len wl = Length in wavelengths							
	Gain dBi = Maximum gain in dBi							
	FB dB = 180-degree front-to-back ratio in dB							
	El Ang = Elevation angle in degrees							
	alpha = Main lobe angle in degrees							Table 1-9

At relatively how antenna heights, such as 0.5 λ, the standard height vs. elevation-angle equation gradually goes astray as the antenna length increases over any lossy ground. **Fig. 1-9** graphs the elevation angle for each ground quality. Since the models on which this graph rests use 1° increments in the elevation patterns, the tabular data in **Table 1-7** show the reason why the curves for each soil quality have a jagged appearance. Later in these notes, we shall explore the azimuth or angle α column information. However, our present interest lies in the elevation angle information.

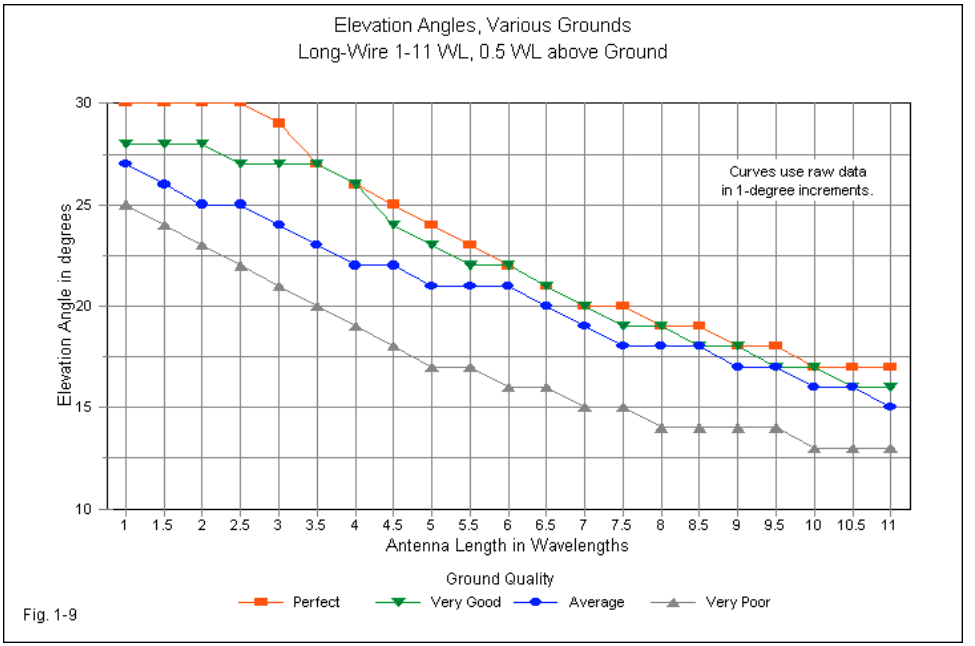

Fig. 1-9

At very low heights the elevation angle quickly drops from its ideal value. The worse the soil quality, the faster the elevation decreases with increasing antenna length. Note that even perfect ground cannot sustain the ideal or calculated elevation angle, since ground quality is not the sole determinant of that angle. Rather, the antenna gain plays a significant role in the final value for the elevation

angle. For any long-wire array design, one must account for the joint effects of the gain that results from wire length and the ground quality in determining the actual elevation angle of maximum radiation.

Doubling the height to 1 λ above ground results in a very large decrease in the affects of ground on elevation angle. **Fig. 1-10** has so few values in the stair-step 1-degrees progression that I linearized the curves in order to separate the lines.

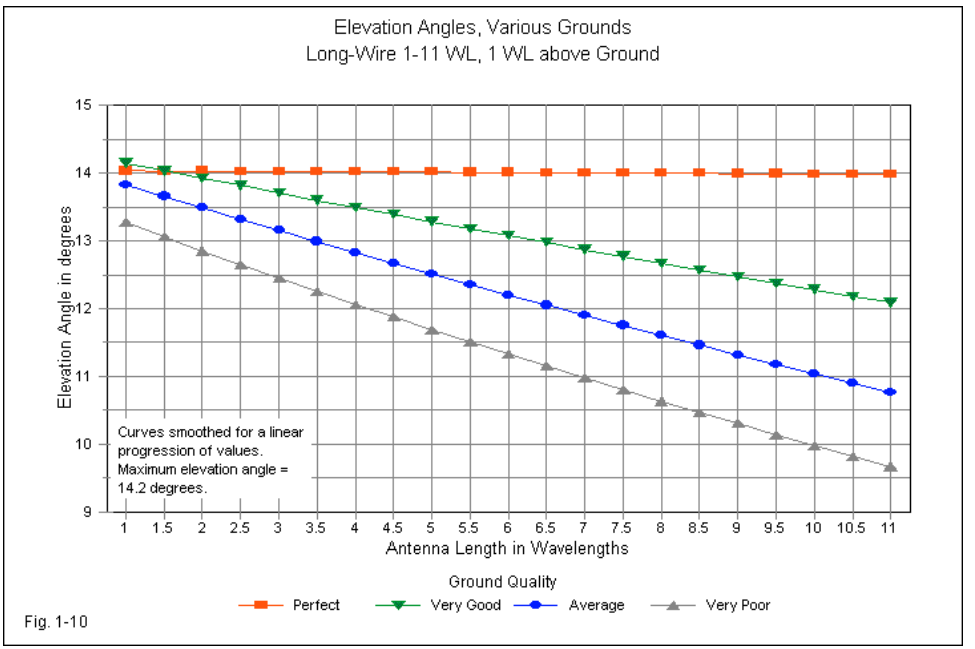

Fig. 1-10

Over perfect ground, the models showed a uniform elevation angle of 14°. However, spot checks at a radiation pattern increment of 0.1° showed the range to be from 14.2° down to 14.0°. The amount is very small, but the decrease with increasing wire length is real. Remember that the calculated value for the angle is closer to 14.5°. **Table 1-8** shows the accumulated data for all soil qualities, but records elevation angles in 1° increments. Both the graph and the table reveal that

the new height results in a much smaller range (3°) for the elevation angle as we move from 1-λ wires to 11-λ antennas. As well, the effects of soil quality are far lower, with a maximum variation of 2°-3° as we move from very good to very poor soil. For most amateur installations of long-wire arrays and beams, 1 λ is a good minimum height at the lowest operating frequency.

There is no need to graph the elevation angles when we again double the height and place the unterminated long-wire at 2 λ above ground. When we gather data using a 1° increment in the radiation pattern reports, the angle is a nearly constant 7°. As shown in Table 1-9, the angle drops to 6° only over average soil (at 10 λ) and over very poor soil (at 8 λ). Although it hardly matters at a height of 2 λ, the rule of thumb is that the worse the ground quality, the lower the elevation angle for wires that are the same length and height above ground.

The result of our survey is a restriction on the use of the standard equation by which we calculate the elevation angle of the main lobe over ground by using the height of the antenna. For long-wire antennas, the equation grows less reliable as we increase the antenna length. As well, the lower the antenna, the less reliable the equation becomes with wires that exceed 1 λ.

As we increase long-wire height, the equation becomes more reliable. At 2 λ and higher, the equation becomes a good guide for all practical long-wire lengths. Equally, the effects of ground quality on the elevation angle also decrease with antenna height. By a height of 2 λ, wide differences in soil quality also create almost no effect on the elevation angle. You may also wish to examine the gain columns in each table to confirm that as we raise the antenna, soil quality has smaller effects on the maximum gain.

Although not a perfectly magical threshold, a 2-λ long-wire height has another benefit. It also represents a height at which the azimuth-angle between the wire and the main radiation lobe (α) stabilizes with very little difference for any soil quality. Indeed, as shown in **Fig. 1-11**, lossy ground has little affect on the angle relative to either perfect-ground or free-space values. The "alpha" angle columns of **Table 1-6** and **Table 1-9** will confirm the absence of a significant difference in the values of α for perfect through very poor ground at a height of 2 λ.

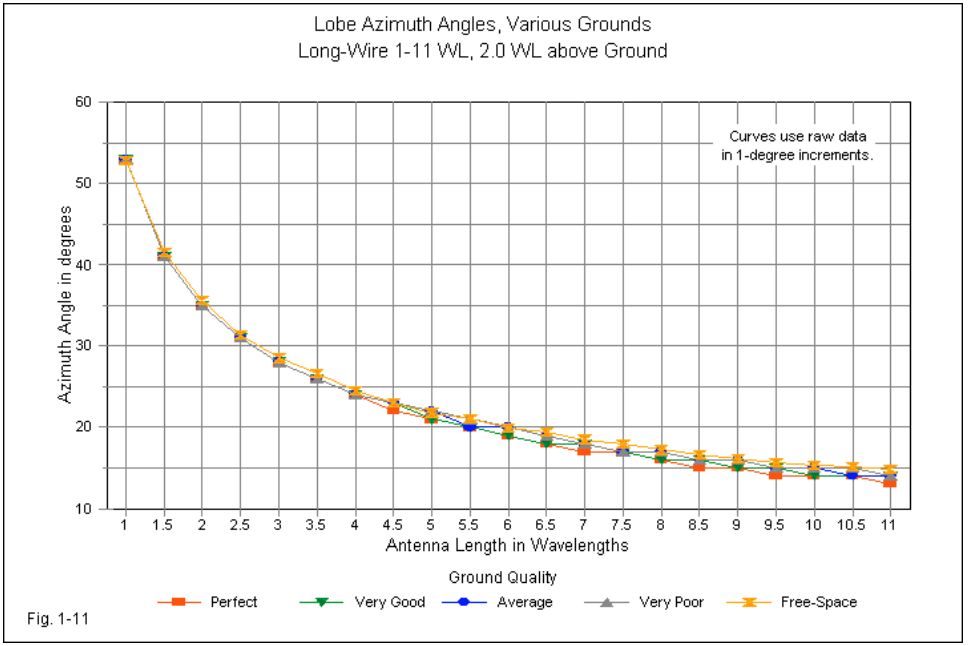

Fig. 1-11

As we reduce the height to 1 λ, we begin to see more significant differences in α over the range of soil qualities from perfect to very poor. (See **Fig. 1-12** and **Table 1-8**.) Possibly contrary to our intuitive expectations, perfect ground shows the widest departure from free-space values for α. Very poor soil shows the closest coincidence with those values.

However, our expectations for the effects of ground on the value of α should not rest on the labels that we associate with ground qualities. Instead, they should rest on the conductivity and relative permittivity values of each ground type. The conductivity of free-space (or a vacuum) is zero S/m, and by definition, the relative permittivity is 1. Very poor soil (0.001 S/m, 5) shows values much closer to a vacuum than does very good soil (0.0303 S/m, 20).

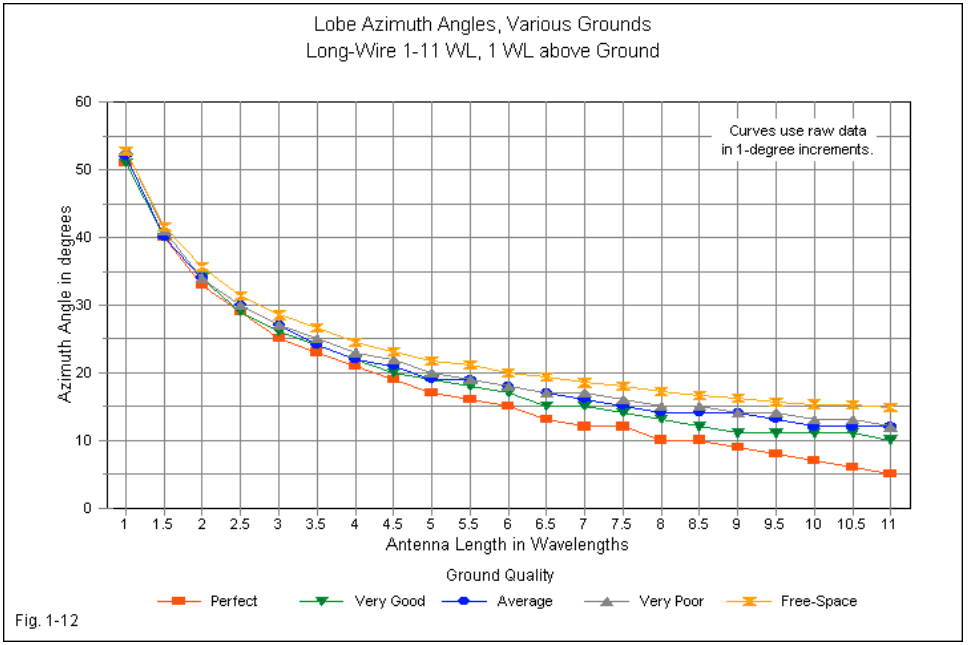

Fig. 1-12

If we further reduce the long-wire height to 0.5 λ, the differences among modeled values of α continue to increase. **Fig. 1-13** collects the azimuth-angle information from **Table 1-7** and graphs it. We find the same divergence among values as in **Fig. 1-12**, but magnified greatly. In fact, all ground types except very poor soil (and free-space, of course) show the azimuth angle reaching and maintaining 0° at certain lengths that increase with decreasing soil quality. A zero-value indicates that the long-wire antenna has a single main forward lobe (and a single main rearward lobe, as well).

Our exploration into the effects of height on the elevation and azimuth angles associated with single unterminated long-wire antennas yields several significant results. First, soil quality has smaller effects on both values than the height of the antenna. However, those effects become increasingly pronounced as we reduce the height of the antenna. At a height of 2 λ, we can scarcely distinguish among the

effects of soil quality, but at 0.5 λ, the differences can be profound–especially with values of α.

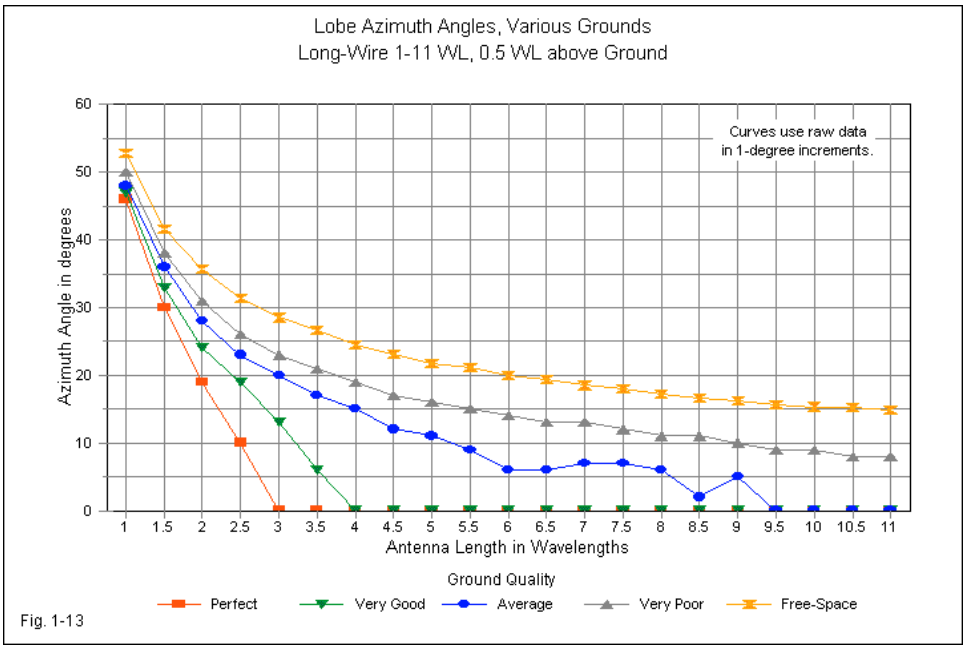

Fig. 1-13

Lobe Development: we have noted that for an integral multiple of a wavelength, an end-fed wire will produce twice as many lobes as a center-fed doublet of the same length. More generally, the proper counting increment for an end-fed wire is the half-wavelength. For any integral multiple of a half-wavelength, an end-fed wire will yield twice as many lobes as it has half wavelengths, or

$$N_{ef} = 4\ L_{\lambda}$$

N_{ef} is the number of lobes, and L_{λ} is the antenna length in wavelengths. So a 10-wavelength end-fed wire has a total of 40 lobes. To squeeze that many lobes into the same 360-degree pattern requires that each lobe have a smaller beamwidth

(that is, be narrower). As well, the main lobes have an angle farther from broadside and closer to the wire end than for a doublet of the same length. In fact, the two main lobes at each end of the antenna wire begin to fuse into a single large lobe with a deep inset. Compare the 10-λ end-fed lobes in **Fig. 1-7** lobes with the very separate lobes of the 10-λ doublet in **Fig. 1-2**.

If the proper increment for full lobe development is 0.5 λ in the end-fed wire and 1.0 λ in the doublet, the two types of antenna must have very different lobe formation characteristics. **Fig. 1-14** shows the difference by tracking both antenna types from 2 to 3 λ in 0.25-λ increments.

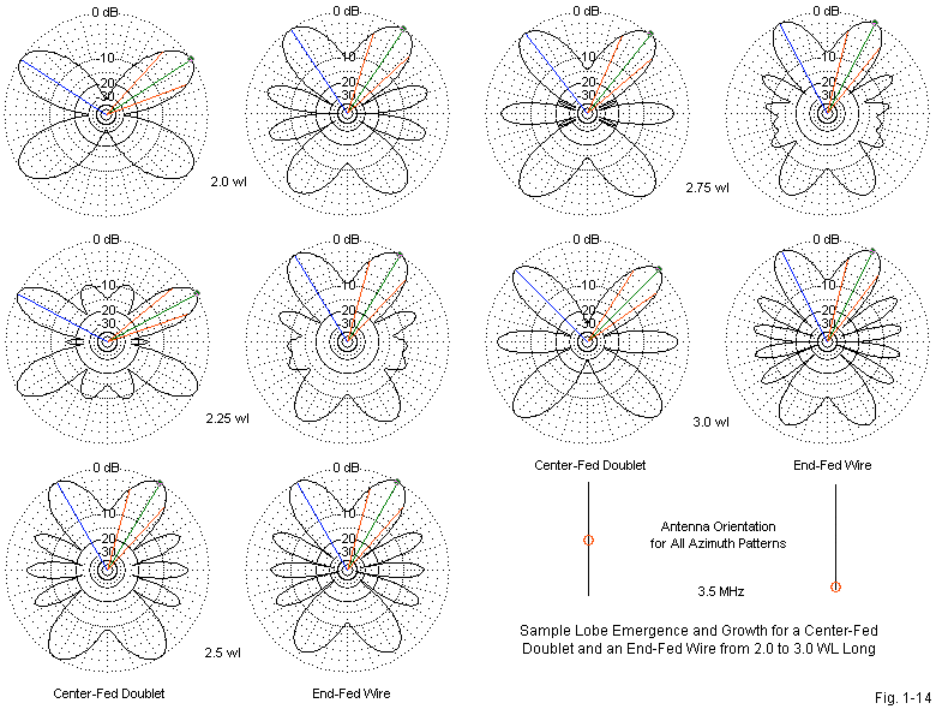

Sample Lobe Emergence and Growth for a Center-Fed Doublet and an End-Fed Wire from 2.0 to 3.0 WL Long

Fig. 1-14

The doublet moves from 4 to 6 total lobes in the 1-λ span. At 2.5 λ, we find the

expected 10 lobes, as the emergent and declining lobes have roughly equal strength. At 2.25 λ, we can see the new lobes suited to the next full wavelength beginning to emerge, and at 2.75 λ, the old lobes have almost completely disappeared. In contrast, the end-fed antenna has complete lobe sets at 2, 2.5, and 3 λ. New lobes appear at both 2.25 λ and 2.75 λ. In each case, the new lobe on each side of the wire forms at an angle that is just over 90° relative to the wire axis as measured from the forward end, that is, the end away from the feedpoint.

The difference in lobe formation between a doublet and an end-fed wire is not a function of current magnitude along the wire. For any given length, the current magnitudes are quite comparable for the two types of antennas. The only other significant variable is the phase of the currents in each excursion. **Fig. 1-15** shows us the difference in this parameter.

Fig. 1-15

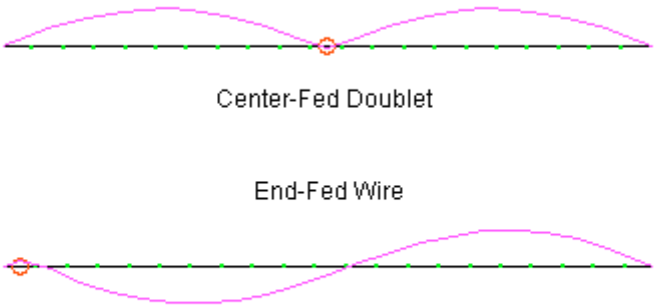

Relative Current Magnitude and Phase on 1-WL Wire Antennas
Center-Fed-Doublet and End-Fed Wire at 1 WL above Ground

The 1-λ center-fed doublet graphic shows that the currents have the same phase in each half of the overall antenna length. Hence, the radiation pattern has only two lobes with contributions from each half of the total wire length. Not until the antenna reaches a significantly greater length (2 λ is the next step in our pattern development sequence) will each half of the doublet show a current phase reversal.

Therefore, we do not find 4 lobes until we reach the 2-λ mark. (Of course, a 1.5-λ antenna will show 6 lobes as the initial 2 diminish and the next 4 emerge and grow.) With the end-fed wire, the currents in each half of the initial 1-λ wire are 180° out of phase relative to each other. Hence, we see 4 lobes at this shorter length.

Certain end-fed antenna properties reported via NEC software do not coincide exactly with classical accounts of these antennas. The off-center emergence of new lobes is one such feature, and the small front-to-back ratio of the antenna is another. There are others.

As we noted for the center-fed doublet, most classical treatments of standing-wave antennas have presumed a sinusoidal current distribution along the wire. Moreover, they also assume a perfect reflection of energy from the lossless open end of the antenna back toward the source, on analogy with standard open-end transmission line conceptualizations. As a result, the calculated lobe structures are symmetrical with respect to the antenna midline, that is, each lobe has a corresponding lobe of equal strength away from and toward the feedpoint. The calculated lobes also have other interesting properties, as shown in **Fig. 1-16**. The graphic is taken from p. 304 of Laport's *Radio Antenna Engineering* but also appear in Chapter 11 of Johnson *Antenna Engineering Handbook*. On the side representing a wire that is 7.75-λ, note the emergence of the new lobe at a heading that is 90° away from the axis of the wire. NEC's calculations of the transition from one length to another, where the lengths are 1/2-wavelength apart, show quite different characteristics.

Note also that the 8-λ end-fed long-wire has main lobes that are stronger than the main lobes of the 7.75-λ antenna. The exact amount is not critical here, only that the addition of 0.25 λ to the wire length increases gain. As well, note the symmetry of the two patterns: both have equal field strength toward and away from the feedpoint. All of these properties are functions of the basic premises of the calculations: a sinusoidal current distribution and perfect energy reflection from the far end of the wire back toward the feedpoint. These premises are fundamental to classical treatments of standing-wave antennas. Theoretically, the end-fed unterminated wire should be a close to a paradigm standing-wave antenna as was the nearly perfect center-fed doublet.

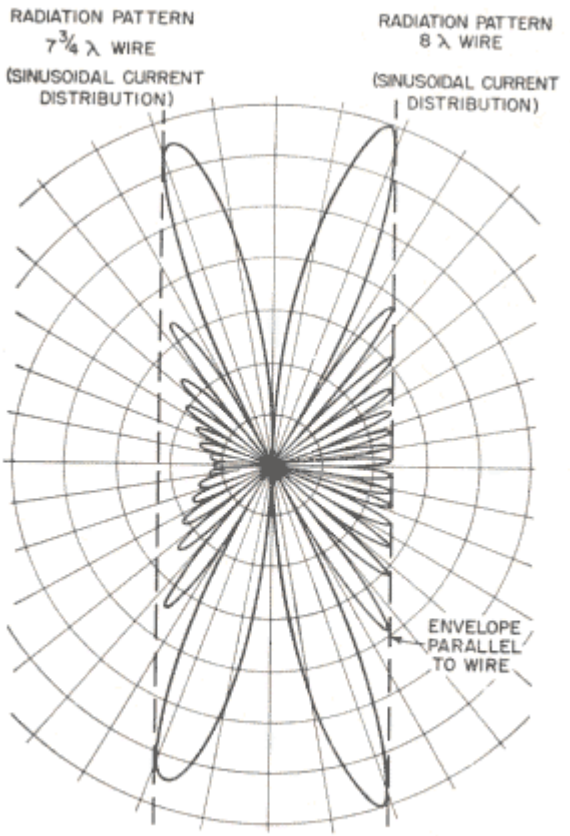

Lobe Structure of 2 Unterminated Long-Wires

Fig. 1-16 Adapted from Lapart, p.304

Unfortunately, an end-fed wire does not achieve full standing-wave status, even when constructed from lossless wire and placed in free space. The current distribution of NEC models is not fully sinusoidal, and reflections are not perfect. **Fig. 1-17** shows the current distribution of a 3-λ wire. Like the comparable current distribution sketch for a doublet in **Fig. 1-4**, the model uses 241 segments in order

to capture accurately current peaks and nulls. The diagram also uses a reference line at the highest current peak to allow easier reading of the relative peak heights.

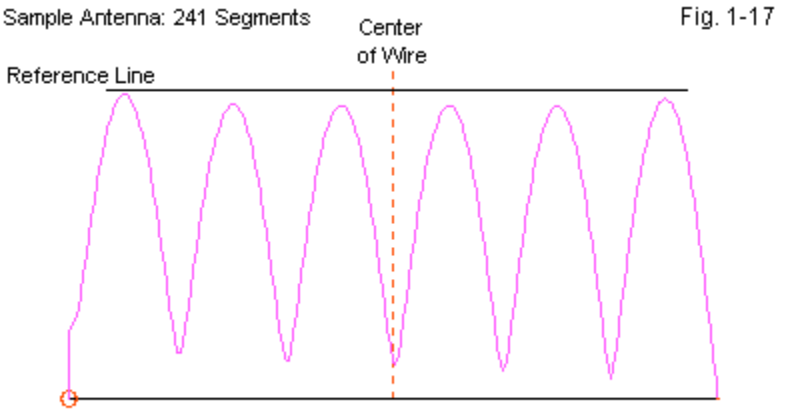

The current magnitude shows its highest peak closest to the feedpoint. The second highest peak occurs closest to the open end of the wire. Intermediate peaks are lower and show a very slightly decreasing peak value as we move away from the feedpoint. Current nulls also show a closer approach to zero as we move away from the feedpoint. These same characteristics appeared on each side of the feedpoint in the center-fed doublet diagram, but were almost too small to detect visually. (Tracking the NEC current tables is a good way to overcome visual obscurity.) In the end-fed wire, the phenomena are quite distinct.

The imperfection of the current distribution on an end-fed long-wire suggests (without proving) that, within the context of NEC models, there is no such thing as a pure standing-wave antenna. Center-fed doublets come close, and their symmetry masks most consequences of any remnant imperfections. End-fed wires, however, reveal the degree to which they fall short of being pure standing-wave antennas when calculated within NEC. **Fig. 1-18** forms a good summary of the consequences of not achieving perfect standing-wave status.

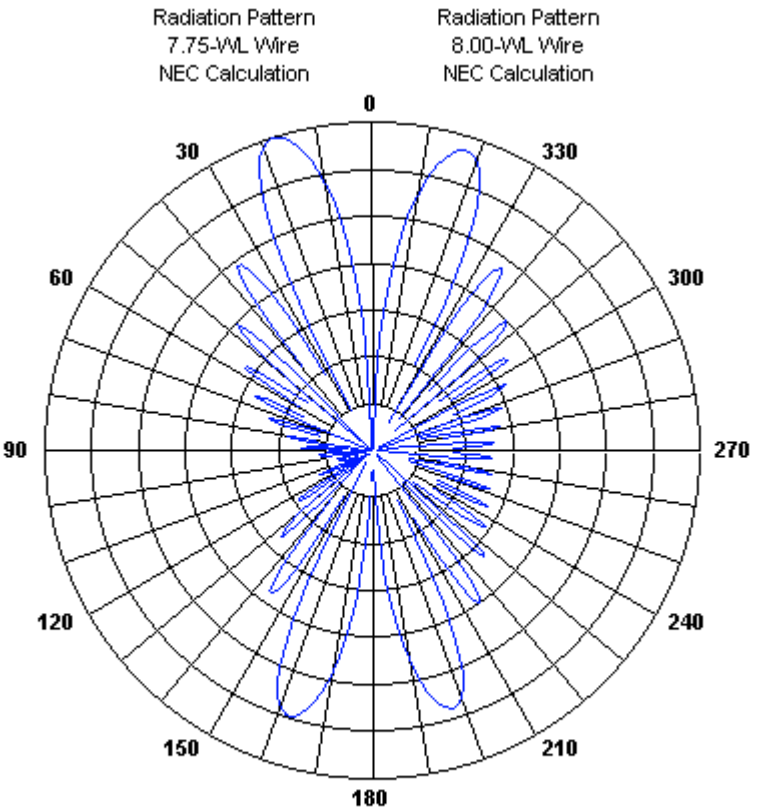

Lobe Structure of 2 Unterminated Long-Wires: NEC Calculation

Fig. 1-18

The new diagram replicates as closely as feasible (without definitive information about the original dual pattern) the characteristics of **Fig. 1-16**. It uses a linear scale for lobe strength with 2.5-dB increments. It places side-by-side NEC modeling results for 7.75- and 8-wavelength long-wire antennas. The outer ring uses the maximum gain of the antenna with the higher gain as the reference. (The graphic

required a change of software to GNEC to access additional facilities for customizing the plot area. Other plots use EZNEC Pro/4 facilities.)

The plots show the higher maximum gain of the 7.75-λ long-wire. Equally evident is the offset of the "new" lobe relative to a line run between 90° and 270°. Furthermore, the forward sidelobes are stronger relative to the main forward lobe than are the rearward sidelobes relative to the rearward main lobe. In contrast, the sidelobes of the 8-λ long-wire show a better balance between forward and rearward directions when we compare them to the forward and rearward main lobes, respectively. However, we do not achieve the straight-line phenomenon–even allowing for the line tilt occasioned by the front-to-rear gain differential–unless we omit both the main lobes and the first sidelobes both fore and aft. A comparison of **Fig. 1-16** and **Fig. 1-18** provides perhaps the most vivid contrast between traditional ideal calculations and method-of-moments calculations applied to seemingly identical free-space lossless unterminated end-fed long-wires.

One more facet of **Fig. 1-16** presents us with a bit of difficulty. Note that the maximum pattern strength for the 7.75-λ wire is lower than for the 8-λ wire. NEC calculations for antennas of the same length appear to contradict the idealized results. Let's determine what the relative gains might be, but use a wider sweep of antenna lengths to make certain the any trends that appear are real and not simple aberrations. I developed a sequence of lossless free-space long-wire models from 8 through 11 λ in 0.25-λ increments. The results appear in **Table 1-10**. The data set reports the maximum gain of the strongest lobe, the front-to-back ratio, the value of angle-α, and the amount of change in α from one step to the next.

The gain for odd multiples of a quarter-wavelength is always greater than the gain of adjacent even multiples of a quarter-wavelength. Indeed, the gain for a length of 9.75 λ is higher than the gain for 11 λ. Equally evident is the fact that the front-to-back ratio is higher at odd multiples of a quarter-wavelength compared to adjacent even multiple of a quarter-wavelength. Finally, the value of α shows a relatively standard downward trend until we examine the increment of change between steps. The amount of change when moving from an even multiple of a quarter-wavelength to an odd multiple of a quarter-wavelength is generally less than when moving from an odd multiple to the next even multiple.

Free-Space Lossless End-Fed Long-Wires: 8-11 WL				
Len wl	Gain dBi	FB dB	alpha	Ang Chng
8.00	9.33	2.23	17.2	
8.25	10.26	2.45	17.0	0.2
8.50	9.54	2.26	16.6	0.4
8.75	10.46	2.46	16.5	0.1
9.00	9.74	2.28	16.2	0.3
9.25	10.65	2.48	16.0	0.2
9.50	9.93	2.31	15.7	0.3
9.75	10.83	2.50	15.5	0.2
10.00	10.11	2.34	15.3	0.2
10.25	11.00	2.51	15.2	0.1
10.50	10.29	2.35	15.2	0.0
10.75	11.17	2.53	15.0	0.2
11.00	10.45	2.38	14.8	0.2
Notes	Len wl = Length in wavelengths			
	Gain dBi = Maximum gain in dBi			
	FB dB = 180-degree front-to-back ratio in dB			
	alpha = Main lobe angle in degrees			
	Ang Chng = Angle change from next			
Table 1-10	shorter length in degrees			

The differences become striking in terms of pattern shape with very long end-fed wires. **Fig. 1-14** showed the transition of patterns between 3.0 λ and 3.5 λ, with the pattern for 3.25 wavelength simply being odd due to the manner in which the new lobe emerges at an angle other than at the midline of wire. (The midline is the line that is 90° to the axis of the wire.) The pattern does not call attention to the differences in the depth of nulls in the forward and rearward directions. However, that difference appears more vividly if we compare plots for 10.75 λ and 11.0 λ wires, as in **fig. 1-19**.

The plot for the 11-λ wire shows deep nulls that accompany all lobes in the pattern, allowing for some slight irregularity that is inevitable when using a finite sampling increment. However, the plot for the 10.75-λ wire shows deep nulls only in directions away from the feedpoint. Toward the feedpoint, the nulls become

considerably more shallow–indeed shallower than the lobe gain differential might otherwise suggest. The difference between the two patterns is partly a function of the fact that at an odd multiple of a quarter-wavelength, the new lobe has already emerged. Moreover, it interacts with the other rearward lobes due to its entrance at an angle greater than 90° relative to the heading away from the feedpoint along the wire. Even at lengths that are so long that end-effect is negligible, with wires as thin as 1E-10-λ in diameter, the shallowness of the side and rearward nulls remains.

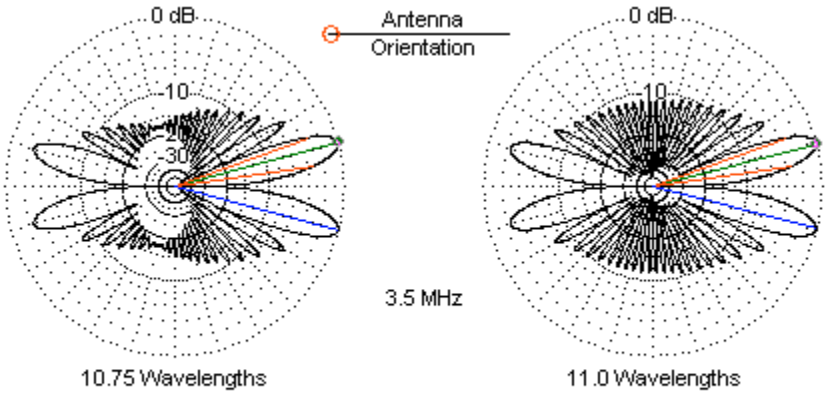

Free-Space E-Plane Patterns: End-Fed Wires
10.75 and 11 Wavelengths

Fig. 1-19

Our exercises have not aimed at challenging classical equations for calculating the properties of long-wire antennas. Instead, they only show that the calculation methods used in NEC differ somewhat from the classical methods and result in different reported data. In some cases, the data is virtually identical in both cases. One primary example is the calculation of angle-α from the wire length in end-fed unterminated long-wire antennas.

In other cases, the data outputs differ between the 2 methods. NEC shows the end-fed long-wire that is an odd multiple of a quarter-wavelength to have a noticeably higher gain than one that is an even multiple of a quarter-wavelength. All NEC-calculated end-fed long-wire antennas have a small but noticeable front-to-

back ratio. As well, new lobes in the radiation patterns for end-fed long-wires emerge with a slight rearward offset at odd multiples of a quarter-wavelength. These small but distinct differences between calculation methods require attention from anyone planning to design or analyze a long-wire antenna via NEC software.

Conclusion

We have sought to familiarize radio amateurs with the basic properties of unterminated center-fed and end-fed long-wire antennas. The center-fed doublet is perhaps the most familiar antenna and so became a comparator to help us better understand the ways in which the end-fed long-wire antenna is both similar and different. Both antennas are examples of standing-wave antennas, but do not exhaust that category by any means.

Because we shall later focus on certain important properties of unterminated long-wire antennas as they apply to long-wire arrays, we emphasized two angles. One was the elevation angle maximum radiation, while the other was α, the azimuth angle between the wire axis and the strongest lobe. In free space, of course, these angles are the same, since the lobe structure does not undergo any modification due to reflection from the ground. However, over ground, we noticed significant changes in the values of these angles.

As we increase the length of a long-wire antenna, the elevation or take-off angle decreases as a function of increasing gain. In addition, as we decrease the height of an antenna, the elevation decreases faster. Poorer soils produced more rapid decreases in elevation angle than better soils. Nevertheless, at antenna heights of 2 λ or more, the elevation angles tended to stabilize, with minimal ground and ground-quality effects on the take-off angle.

Angle-α also shows similar properties. At antenna heights of 2 λ or more, ground effects were minimized and the values reported for α were nearly identical to free-space values. As we brought the antenna closer to ground, ground effects increased, generally decreasing the value of α. Above certain lengths and over certain ground qualities at 0.5 λ, the value of α may reach 0°, indicating a single main lobe in line with the wire. However, values of α were generally closer to free-

space values as the soil quality decreased. In contrast, perfect ground yielded at any antenna height the widest divergence of α from free-space values.

Within the context of NEC calculations, both the center-fed doublet and the end-fed long-wire proved to be imperfect standing-wave antennas. The doublet is only marginally shy of achieving perfect standing-wave status, and its symmetry obscures the tiny departures from being a pure standing-wave antenna. The end-fed long-wire, however, reveals its departures from standing-wave perfection in more obvious ways. These ways include differences in radiation patterns between wires that are an odd multiple of a quarter-wavelength and those that are an even multiple of a quarter-wavelength. As well, the unterminated long-wire antenna has in all NEC models an uneliminable small front-to-back ratio. The ratio is not so great as to disable the antenna as a bi-directional antenna, but one can always find the favored end away from the feedpoint.

The characteristics that we have explored in NEC models of long-wire antennas will carry over into every form of array to come. The next step on our foray into the long-wire jungle is to create a long-wire beam by placing a simple resistor at the end of the end-fed long wire antenna. Although the task sounds simple, it will present some challenges both to practical long-wire applications and to the models we construct to capture the basic properties of terminated long wire antennas.

2.

Terminated End-Fed Long-Wire Directional Antennas

> It is one of the paradoxes of engineering in this field that the simplest antennas are the most difficult to analyze. Long-wire antennas, which permit the simplest structures for a given performance, involve an enormous amount of computation to determine their performance. Furthermore, an accurate analysis is virtually impossible because of the several empirical factors present.
>
> Edmund Laport, *Radio Antenna Engineering*, p. 302

Long-wire antennas and arrays might be very uninteresting is we could not use the length to obtain more than just a bi-directional standing wave antenna. However, if we add an impedance at or near the end of the wire opposite the feedpoint, we can obtain a traveling-wave antenna. C. H. Walter (*Traveling Wave Antennas*, p. 13) broadly defines a traveling wave antenna as one for which the fields and current that produce the antenna pattern may be represented by traveling waves, usually in one direction. With respect to antennas, a traveling wave is an electromagnetic disturbance that propagates with a definite phase velocity. The reason that Walter adds the "one direction" qualifier to his definition of a traveling wave antenna is that some writers treat a standing wave antenna as one along which we have two traveling waves, one in each direction.

The impedance that we add at the correct place at or near the far end of the long-wire dissipates the energy that would form the return traveling wave if we left the wire unterminated. Hence, ideally, we obtain a single traveling wave outward, relative to the feedpoint. The result is a directional antenna pattern roughly pointed away from the source. If we could achieve a pure traveling-wave antenna, there would be virtually no energy radiated to the rear quadrants of the antenna pattern. We have already seen that we cannot achieve a pure standing-wave antenna. The current waveforms are not perfectly sinusoidal; the peaks vary in strength, and the current null values are limited by the presence of a source to supply radiation (and other) losses from the antenna. Likewise, as suggested by **Fig. 2-1**, we shall be unable to achieve a pure traveling-wave antenna. Nevertheless, even impure traveling-wave antennas can serve well for

many communications purposes.

Fig. 2-1

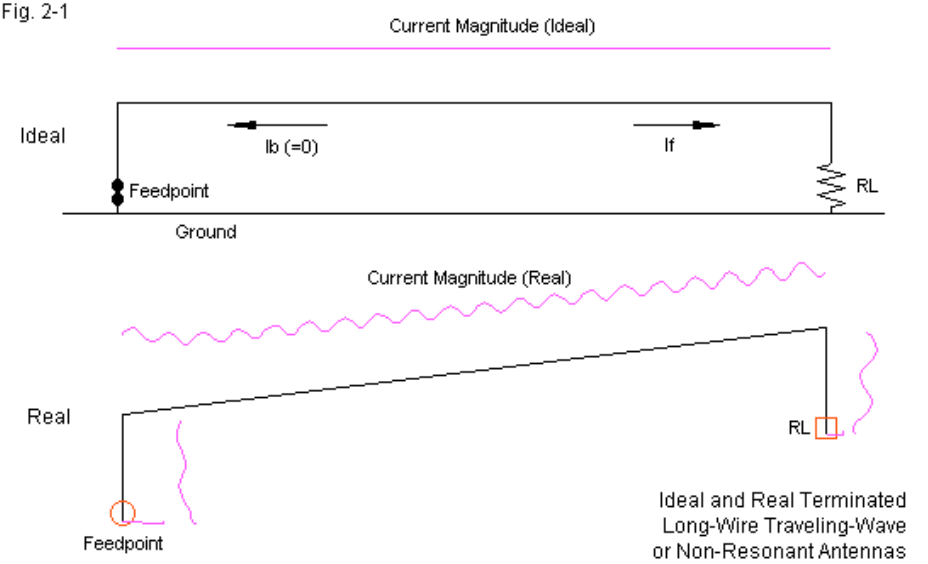

With no return current waveform in a pure traveling-wave antenna, the current magnitude would have the same value everywhere along a terminated long-wire antenna. That unreachable goal appears as an ideal in the upper portion of **Fig. 2-1**. The lower current form, taken from a NEC model, portrays a more real situation. The current does not show the severe peaks and nulls of a standing wave. Instead, it gives the appearance of a standing wave superimposed on a traveling wave current form. Just as there is no pure standing-wave antenna, in long-wire technology, there is no pure traveling-wave antenna.

Among the reasons for the impurity of long-wire traveling-wave antennas is the fact that the most convenient form of termination is not fully adequate to the task. The most common terminating impedance is a non-inductive resistor. With a resistive termination, the antenna achieves the broadest possible operating

bandwidth. For simple terminated long-wires, the bandwidth covers a frequency range of 4:1 or more. The impedance bandwidth may be even greater. We shall discover reasons later on for using the 4:1 frequency ratio as a limiting rule of thumb.

The actual impedance necessary to produce an ideal traveling-wave antenna is complex. However, introducing a reactive component into the termination would severely reduce the operating bandwidth of the antenna, since the lumped component would change reactance with frequency. Moreover, as Kraus notes (*Antennas*, p. 229), we cannot achieve a non-reflecting termination with a lumped impedance, but only greatly reduce the reflections at the termination. Given the other benefits of a resistive termination, most antenna designers and users opt to live with the remaining standing-wave component.

As we shall see along the wave, simple terminated long-wire antennas do create beaming effects, with significant front-to-back ratios to quiet the rearward quadrants of the antenna radiation pattern. However, they also have some significant limitations. Some of those limits are a function of using a resistive termination to produce the forward pattern. For example, the maximum gain of a terminated long-wire is always significantly less than the maximum gain of an unterminated long-wire, without losing the split-forward-lobe structure. Other limits are inherent to end-fed long-wire design, for example, the large number of relatively high-strength side lobes. Despite these limitations, terminated long-wires remain in use, mostly as a function of their simplicity, easy maintenance, and low cost.

Analyzing Terminated Long-Wires: the Laport Configuration

Simple unterminated center-fed and end-fed long-wires lend themselves to analysis via NEC models in both free-space and over a wide variety of ground qualities. The top sketch in **Fig. 2-2** shows the simplicity of the structure that presented no particular modeling difficulties. The middle sketch shows the most common implementation of a terminated long-wire antenna. Both the source and the resistive termination return to ground. A free-floating resistor at the end of a long-wire structured as in the top sketch would not show the desired energy

dissipation that is central to a traveling-wave antenna.

Fig. 2-2

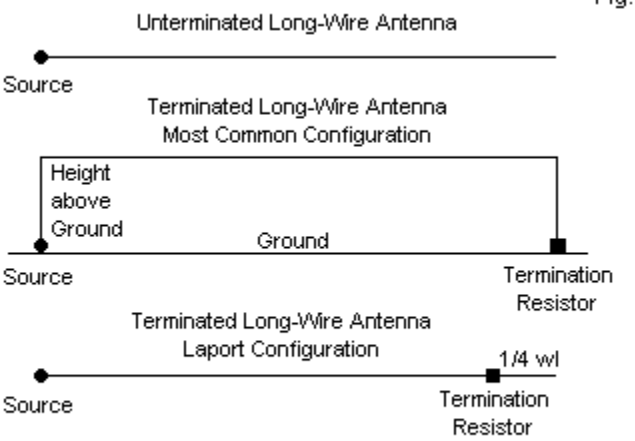

Data Acquisition Options for Terminated Long-Wire Antennas

Although we shall return to the "common-configuration" terminated long-wire antenna, we should first try to find a version of the antenna that does not require the vertical legs. Laport (*Radio Antenna Engineering*, pp. 309 ff) provides us with an alternative configuration, sketched in the lowest part of **Fig. 2-2**. By placing a terminating resistance about ¼ λ from the open end of the antenna, we can obtain a close approximation of pure traveling-wave operation. The required impedance is complex, and in practice, the outer section is extended beyond ¼ λ to supply the required reactive component. The resulting design has significant frequency restrictions, since the electrical length of the outer section changes with changes in frequency. To distinguish this design from the common configuration, I shall arbitrarily call it the Laport configuration.

The Laport configuration finds little practical use today, since most terminated long-wire antennas aim for very broadband service. Nevertheless, the model will serve our initial needs quite well, since we simply need a model that

demonstrates the full capability of a terminated long-wire at the test frequency in both a free-space and a lossy-ground environment. As in the previous chapter, all models will use 3.5 MHz as the test frequency, with 0.16" lossless wire at 20 segments per wavelength.

The first step in our process involves modeling the terminated long-wire in free space to let us compare the results with the free-space unterminated long-wires in Chapter 1. **Table 2-1** provides the results of modeling that antenna in half-wavelength increments between 1 and 11 λ. For all models, the terminating resistor is 690 Ω, and the placement is on the 5th segment from the "far end" of the antenna model. Because the source has no ground return, it always shows a high capacitive reactance. (The Laport text shows a tilted long-wire designed to replicate the elevation angle of maximum radiation; the NEC-4 models are level.)

The data are in many ways completely unexceptional. Gain increases with antenna length in a normal curve. The gain increment per length increment decreases, since the length increments are linear. The front-to-back figures are for 180° relative to the azimuth heading of the main lobe, which the α angle indicates. As a result, we cannot determine the gain to the rear along the array wire axis or centerline. Still the values give a rough idea of the relative suppression of QRM from the rear quadrants.

One aspect of the data cannot escape attention. At 1 λ, the gain is -1.47 dBi maximum. The appearance of being quite low becomes reality when we compare that value to the maximum gain of a 1-λ unterminated long-wire antenna. The relevant comparisons appear in **Table 2-2**, which pulls together data from the previous chapter and our first terminated long-wire models. The gain difference is almost 4.5 dB. As we increase the length of both the terminated and unterminated long-wires, the differential decreases. However, it averages over 2 dB in favor of the unterminated antennas for the 1-11-λ range of free-space models. **Fig. 2-3** graphs the maximum gain difference between unterminated and terminated Laport long-wires. Despite the gain differences, the terminated Laport-configuration terminated long-wire antennas show α angles that are very close to calculated values, where the value of α is

$\alpha = \cos^{-1} [1 - (0.371/L_\lambda)]$

Laport-Terminated Long-Wire Beams					Table 2-1
Free-Space Lossless End-Fed Long-Wires: 1-11 WL					
690-Ohm Terminating Resistor 1/4-Wavelength from Far End					
Len WL	Gain dBi	FB dB	alpha	alpha Calc	BW deg
1.0	-1.47	15.25	52.6	51.0	45.8
1.5	0.58	26.68	42.4	41.2	34.8
2.0	1.89	32.60	36.2	35.5	29.1
2.5	2.86	26.50	31.9	31.6	25.6
3.0	3.63	23.76	28.8	28.8	23.0
3.5	4.28	22.26	26.7	26.6	21.1
4.0	4.83	21.30	24.8	24.9	19.7
4.5	5.31	20.64	23.2	23.4	18.4
5.0	5.75	20.16	22.4	22.2	17.4
5.5	6.13	19.79	21.0	21.2	16.5
6.0	6.49	19.51	20.4	20.3	15.8
6.5	6.81	19.28	19.4	19.5	15.1
7.0	7.11	19.09	18.7	18.7	14.6
7.5	7.39	18.93	18.2	18.1	14.0
8.0	7.64	18.80	17.2	17.5	13.6
8.5	7.89	18.69	16.9	17.0	13.2
9.0	8.12	18.59	16.4	16.5	12.8
9.5	8.33	18.50	15.8	16.1	12.4
10.0	8.54	18.43	15.5	15.7	12.1
10.5	8.73	18.37	15.0	15.3	11.8
11.0	8.92	18.30	14.8	14.9	11.6
Notes	Len WL = Length in wavelengths				
	Gain dBi = Maximum gain in dBi				
	FB dB = 180-degree front-to-back ratio in dB				
	alpha = Main lobe angle in degrees				
	alpha Calc = Calculated angle in degrees				
	alpha = arccos [1-(0.371/L)], L = wire length in WL				
	BW deg = main lobe beamwidth in degrees				

Comparison: Unterminated Long-Wires vs. Laport-Terminated Long-Wires									Table 2-2
Free-Space Lossless End-Fed Long-Wires: 1-11 WL									
690-Ohm Terminating Resistor 1/4-Wavelength from Far End on Laport Long-Wires									
Len WL	Unt Gn	Ter Gn	Gn Diff	Unt alpha	Ter alpha	alpha Diff	Unt BW	Ter BW	BW Diff
1.0	2.99	-1.47	4.46	52.8	52.6	0.2	41.9	45.8	3.9
1.5	3.99	0.58	3.41	41.5	42.4	-0.9	32.7	34.8	2.1
2.0	4.81	1.89	2.92	35.7	36.2	-0.5	27.8	29.1	1.3
2.5	5.48	2.86	2.62	31.4	31.9	-0.5	24.7	25.6	0.9
3.0	6.05	3.63	2.42	28.5	28.8	-0.3	22.4	23.0	0.6
3.5	6.55	4.28	2.27	26.6	26.7	-0.1	20.7	21.1	0.4
4.0	6.98	4.83	2.15	24.5	24.8	-0.3	19.2	19.7	0.5
4.5	7.37	5.31	2.06	23.1	23.2	-0.1	18.1	18.4	0.3
5.0	7.72	5.75	1.97	21.8	22.4	-0.6	17.1	17.4	0.3
5.5	8.05	6.13	1.92	21.1	21.0	0.1	16.3	16.5	0.2
6.0	8.34	6.49	1.85	19.9	20.4	-0.5	15.5	15.8	0.3
6.5	8.62	6.81	1.81	19.4	19.4	0.0	14.9	15.1	0.2
7.0	8.87	7.11	1.76	18.5	18.7	-0.2	14.4	14.6	0.2
7.5	9.11	7.39	1.72	17.9	18.2	-0.3	13.9	14.0	0.1
8.0	9.33	7.64	1.69	17.2	17.2	0.0	13.4	13.6	0.2
8.5	9.54	7.89	1.65	16.6	16.9	-0.3	13.0	13.2	0.2
9.0	9.74	8.12	1.62	16.2	16.4	-0.2	12.7	12.8	0.1
9.5	9.93	8.33	1.60	15.7	15.8	-0.1	12.2	12.4	0.2
10.0	10.11	8.54	1.57	15.3	15.5	-0.2	12.0	12.1	0.1
10.5	10.29	8.73	1.56	15.2	15.0	0.2	11.7	11.8	0.1
11.0	10.45	8.92	1.53	14.8	14.8	0.0	11.4	11.6	0.2
Average Differential		Gain	2.12		alpha	-0.2		BW	0.6
Notes	Len WL = Length in wavelengths								
	Unt Gn = Gain of unterminated long wire in dBi								
	Ter Gn = Gain of terminated long wire in dBi								
	Unt alpha = alpha angle of unterminated long-wire in degrees								
	Ter alpha = alpha angle of terminated long-wire in degrees								
	Unt BW = Beamwidth of unterminated long-wire in degrees								
	Ter BW = Beamwidth of terminated long-wire in degrees								

Table 2-1 shows the correspondence between modeled and calculated values of α. In fact, the comparison of α angles in **Table 2-2** shows an insignificant level of difference between terminated and unterminated antennas. The average difference is a mere 0.2°.

Almost equally small is the difference in overall beamwidth between unterminated and terminated antennas. In all cases, the terminated Laport antennas show a slightly wider beamwidth. Like the maximum gain values, the differences become greater as the antenna length grows shorter.

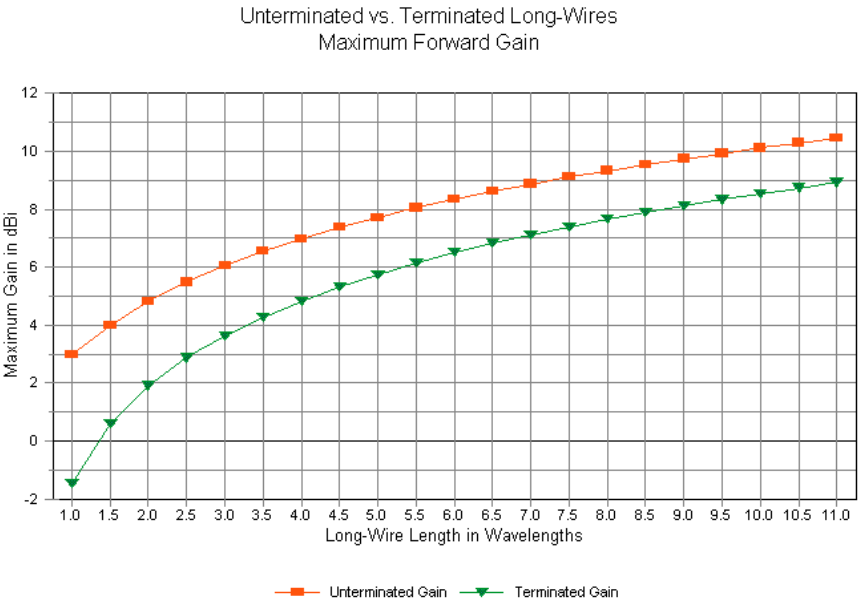

Fig. 2-3

As interesting as the data are the radiation patterns, when we compare unterminated and terminated Laport long-wires. **Fig. 2-4** provides sample free-space patterns for the two antenna types for lengths of 2, 5, and 10 λ. With respect to pattern structure, the Laport configuration of terminated long-wire antennas comes about as close to idealized patterns as one might expect from an actual implementation of the traveling-wave antenna.

Sharp eyes may well note that the terminated 5-λ pattern appears to lose 1 lobe on each side of the wire axis (9 lobes per side vs. the expected 10 in the pattern for the unterminated long-wire). As the lobes of the terminated antenna compress in the rearward quadrant, the rearmost lobes on each side of the wire axis tend to combine into single lobes. We shall see more vivid evidence of this development in a later figure.

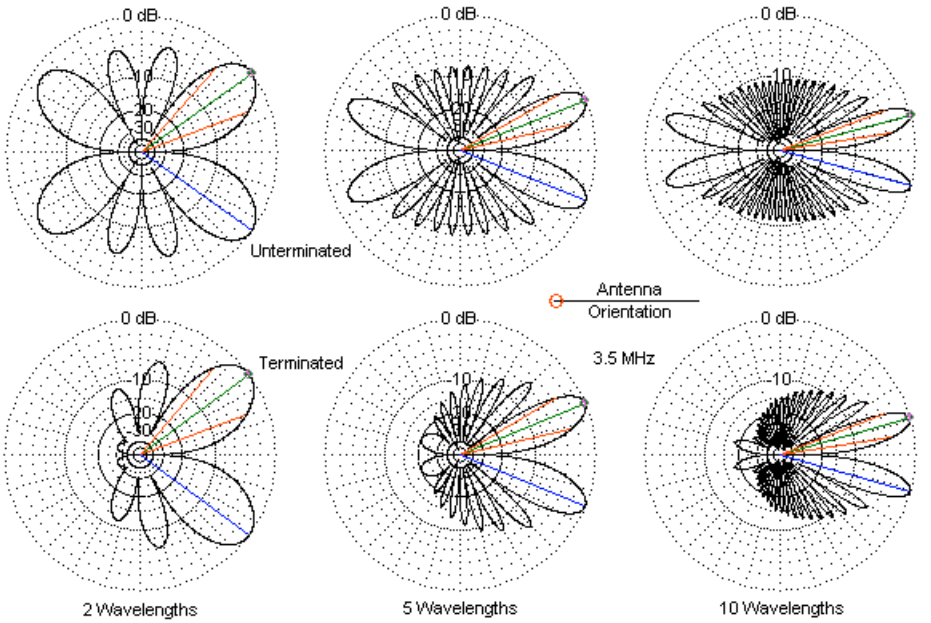

Sample Comparisons of Free-Space Radiation Patterns
Unterminated and Terminated Long-Wire Antennas

Fig. 2-4

Since the Laport configuration is not widely used nowadays, we do not need a complete compendium of its performance over various ground qualities at different heights above ground. Still, we should perform a sample survey over ground to provide for some later comparisons with the common configuration that we can model only over ground. Therefore, I modeled the Laport terminated long-wire at a height of 1 λ above average ground (conductivity 0.005 S/m, relative permittivity 13). The results appear in **Table 2-3**.

The data are once more unexceptional. The gain at 1 λ above average ground shows the expected increase relative to free-space values owing to the ground reflections. The actual increase ranges from about 5.6 dB for a 1-λ antenna down to 3.8 dB for an 11-λ long-wire.

Laport-Terminated Long-Wire Beams: 1-11 WL					Table 2-3
1-WL Above Average Ground					
690-Ohm Terminating Resistor; Lossless Wire					
Len WL	Gain dBi	FB dB	El Ang	alpha	BW deg
1.0	4.16	15.40	14	53	47.1
1.5	6.07	27.18	14	42	36.0
2.0	7.25	33.01	13	35	30.2
2.5	8.14	26.40	13	31	26.8
3.0	8.83	23.57	13	27	24.4
3.5	9.40	22.04	13	25	22.6
4.0	9.86	21.09	13	23	21.3
4.5	10.24	20.46	13	21	20.2
5.0	10.57	20.01	12	20	19.0
5.5	10.87	19.66	12	19	18.3
6.0	11.13	19.38	12	18	17.6
6.5	11.36	19.16	12	17	17.2
7.0	11.57	18.99	12	16	16.8
7.5	11.74	18.84	12	15	16.5
8.0	11.90	18.73	12	14	16.3
8.5	12.06	18.62	11	14	15.5
9.0	12.22	18.51	11	14	15.3
9.5	12.36	18.45	11	13	15.1
10.0	12.48	18.35	11	13	15.1
10.5	12.61	18.32	11	12	15.0
11.0	12.71	18.24	11	12	15.1
Notes	Len WL = Length in wavelengths				
	Gain dBi = Maximum gain in dBi				
	FB dB = 180-degree front-to-back ratio in dB				
	El Ang = Elevation angle of maximum radiation in degrees				
	alpha = Main lobe angle in degrees				
	BW deg = main lobe beamwidth in degrees				

For the various antenna lengths, the elevation angle progression almost perfectly tracks the corresponding progression for unterminated long-wires of the

same length and under the same conditions. **Fig. 2-5** presents a gallery of elevation and azimuth patterns for the Laport terminated long-wire at various lengths, all 1 λ above average ground. See **Fig. 1-7** for comparable unterminated long-wire plots.

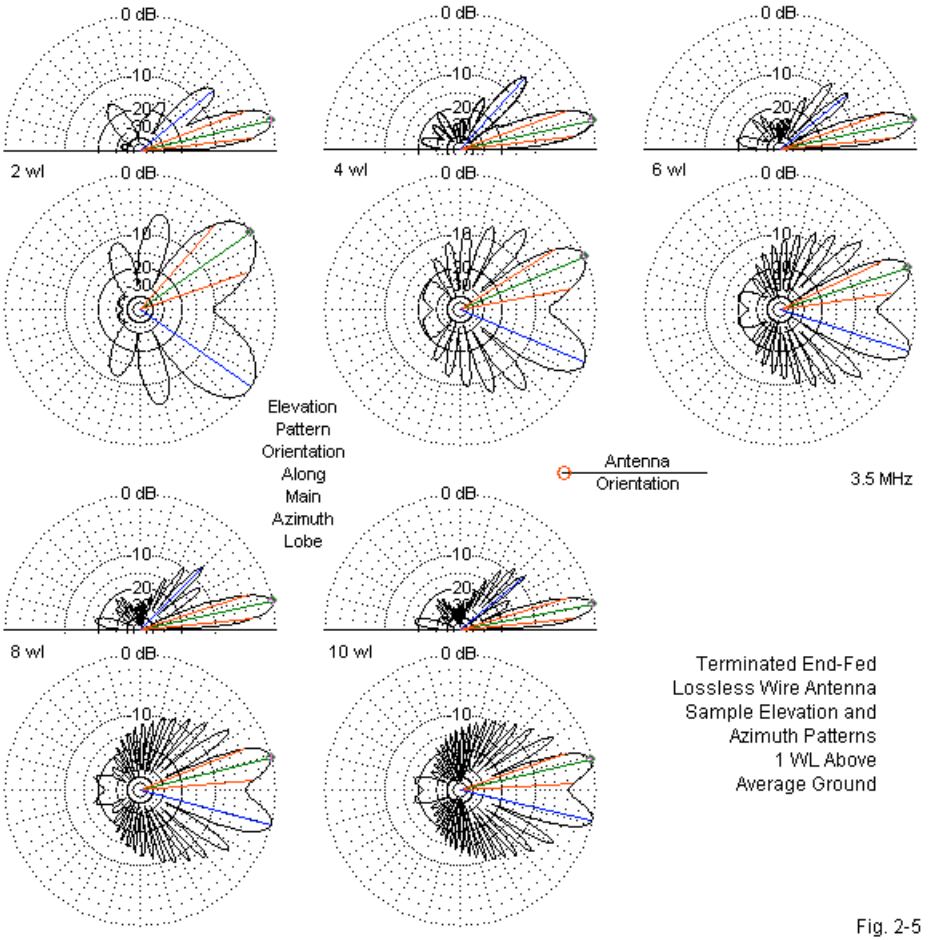

Fig. 2-5

The 4-λ azimuth pattern is perhaps the most interesting. The rear quadrants show the combining of the strongest rearward lobes in the evolution toward a single lobe on each side of the wire axis. By 5 λ, as we saw in **Fig. 2-4**, the process is complete.

A second notable feature of the azimuth patterns is the reduction in the null between the forward-most lobes of the plots over ground compared to the deep null in the free-space patterns in **Fig. 2-4**. Without the decrease in the depth of this null, the terminated long-wire might be relatively useless as a directional antenna.

Laport-Terminated Long-Wire Beams: 1-11 WL									Table 2-4
Some Key Comparisons: 1. Gain of Unterminated and Terminated Long-Wires 1 WL Above Average Ground									
2. Beamwidth and alpha Angle of Free-Space and 1-WL High Terminated Long-Wires									
Len WL	Unt Gn	Ter Gn	Gn Diff	FS alpha	1wl alpha	alpha Diff	FS BW	1wl BW	BW Diff
1.0	8.44	4.16	4.28	53	53	0.4	45.8	47.1	1.3
1.5	9.46	6.07	3.39	42	42	-0.4	34.8	36.0	1.2
2.0	10.27	7.25	3.02	36	35	-1.2	29.1	30.2	1.1
2.5	10.86	8.14	2.72	32	31	-0.9	25.6	26.8	1.2
3.0	11.32	8.83	2.49	29	27	-1.8	23.0	24.4	1.4
3.5	11.68	9.40	2.28	27	25	-1.7	21.1	22.6	1.5
4.0	11.99	9.86	2.13	25	23	-1.8	19.7	21.3	1.6
4.5	12.26	10.24	2.02	23	21	-2.2	18.4	20.2	1.8
5.0	12.48	10.57	1.91	22	20	-2.4	17.4	19.0	1.6
5.5	12.71	10.87	1.84	21	19	-2	16.5	18.3	1.8
6.0	12.90	11.13	1.77	20	18	-2.4	15.8	17.6	1.8
6.5	13.08	11.36	1.72	19	17	-2.4	15.1	17.2	2.1
7.0	13.24	11.57	1.67	19	16	-2.7	14.6	16.8	2.2
7.5	13.38	11.74	1.64	18	15	-3.2	14.0	16.5	2.5
8.0	13.50	11.90	1.60	17	14	-3.2	13.6	16.3	2.7
8.5	13.64	12.06	1.58	17	14	-2.9	13.2	15.5	2.3
9.0	13.75	12.22	1.53	16	14	-2.4	12.8	15.3	2.5
9.5	13.87	12.36	1.51	16	13	-2.8	12.4	15.1	2.7
10.0	13.96	12.48	1.48	16	13	-2.5	12.1	15.1	3
10.5	14.07	12.61	1.46	15	12	-3	11.8	15.0	3.2
11.0	14.15	12.71	1.44	15	12	-2.8	11.6	15.1	3.5
Notes	Len WL = Length in wavelengths								
	Unt Gn = Gain of unterminated long wire in dBi								
	Ter Gn = Gain of terminated long wire in dBi								
	FS alpha = alpha angle of free-space terminated long-wire in degrees								
	1wl alpha = alpha angle of terminated long-wire 1 WL above average ground in degrees								
	FS BW = Beamwidth of free-space terminated long-wire in degrees								
	1wl BW = Beamwidth of terminated long-wire1 WL above average ground in degrees								

There are numerous significant points of comparison between the terminated long-wires over ground and both the unterminated long-wire antennas and the free-space versions of the terminated antennas. **Table 2-4** collects some of the most important comparisons.

First, the gain loss of the terminated antennas relative to unterminated antennas repeats the pattern found for the free-space models. The deficit ranges from 4.3 dB at 1 λ down to 1.4 dB at 11 λ. (The range of deficit ran from 4.5 dB down to 1.5 dB for the free-space models of long-wire antennas.) This pattern has implications for actual practice. If the suppression of rearward radiation and receiving sensitivity is not essential to a communications operation, then the use of a terminated antenna–relative to its unterminated counterpart–may not be justified. Not only does the operator lose detectable gain, but as well, he or she must find the extra component (the non-inductive resistor capable of dissipating the otherwise reflected energy). Whether directivity justifies the loss of gain and the added complexity and expense of the terminated version of the antenna we cannot judge in the abstract, but only with respect to a set of specifications for communications standards applicable to the antenna.

The remaining columns in **Table 2-4** reflect differences between the free-space and over-ground models of the terminated long-wire. The values for angle α and for beamwidth are interrelated. Except for the shortest and least useful antenna lengths, the α angle over ground grows increasingly narrower–relative to free space–as the antenna grows longer. At the same time, the beamwidth grows increasingly larger. The models all have split lobes so that the beamwidth values are for one main lobe on one side of the wire axis. An effect of ground (at least for a height of 1 λ) is to broaden the beam of each main lobe. **Fig. 2-6** graphs the 2 values to show the inverse relationship between the α angle and the beamwidth. The fact that the values do not form smooth curves is a function of the radiation pattern increment used in the models. The patterns sample at 1° increments, resulting in a potential error of +/-0.5° for any entry in the categories of elevation angle, α angle, and beamwidth. These errors can be additive in some cases. A margin of a half-degree in the elevation angle may reflect back upon both the α angle and the beamwidth value, which may also have their margins. Still, the general trends are more than sufficiently accurate for general

guidance. For any practical installation under analysis, one may well wish to construct models that are precise to the situation and that use properly small increments of pattern development.

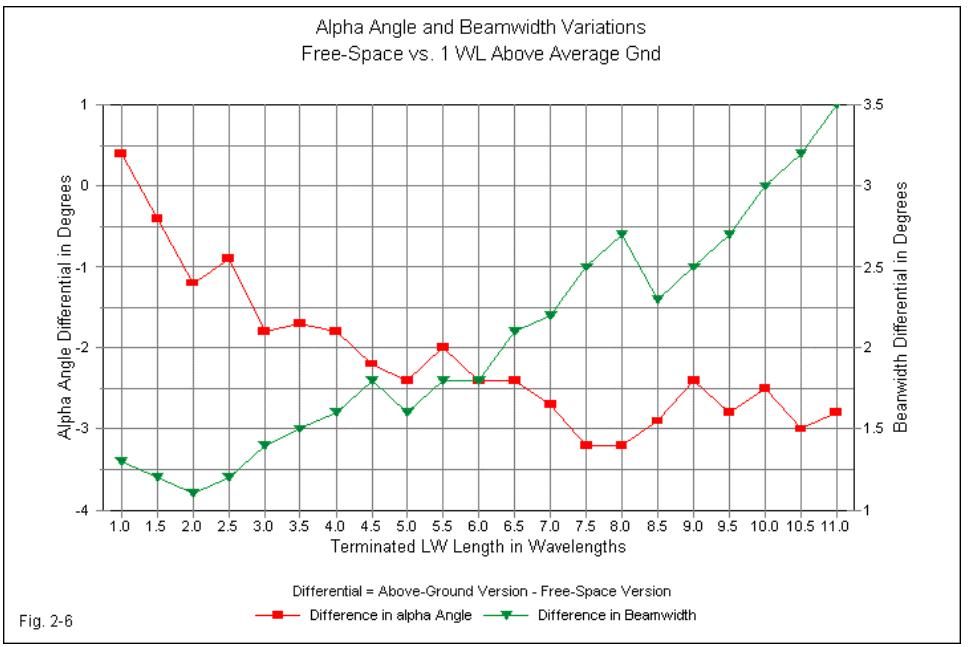

Fig. 2-6

In connection with **Fig. 2-4** and **Fig. 2-5**, we noted the decrease in the depth of the null between forward lobes as we moved the antenna from free-space to a height of 1 λ above ground. At a length of 2 λ, the null is about 10 dB, while at 10 λ, the null shrinks to about 4 dB. The null depth for any antenna length increases with increasing height above ground (as measured in wavelengths). Conversely, the null decreases as we bring the antenna closer to the ground. Under certain conditions, the two forward lobes may join into a single forward lobe.

Even with a sizable null between lobes the terminated long wire does not lose all utility in the direct forward direction along the wire axis. As we showed in the

preceding chapter, the lobe formation takes the form of tunnels. Hence, the distinct azimuth pattern lobes that appear in 2-dimensional plots are part of a "lobe arc." At some higher elevation angle, the lobes reach a junction along the wire axis. **Fig. 2-7** overlays elevation patterns for an 11-λ Laport long-wire at the take-off angle and along the wire axis. In line with the antenna, the peak elevation gain occurs at a slightly higher angle and with about a 2-dB deficit relative to the maximum gain plot. For many communications applications in which a terminated long-wire may be useful, the gain level may be sufficient and the elevation angle may fall within the useful propagation-angle range for the frequency used. Although these notes will normally focus upon the pattern at the take-off angle, a full analysis should always include a detailed scan of all azimuth angles between the α angles on each side of the wire axis.

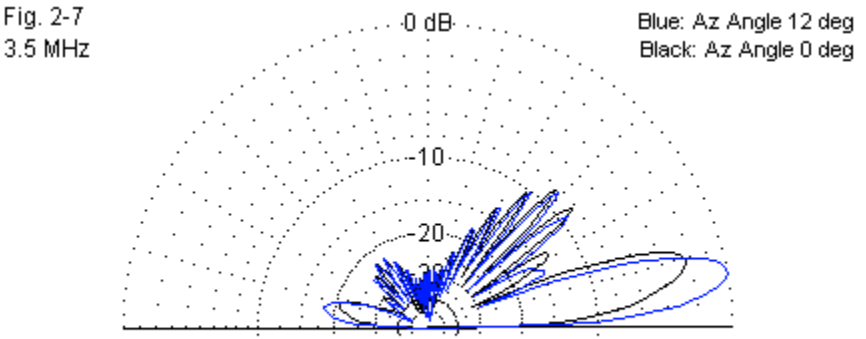

11-Wavelength Terminated End Fed Antenna
Elevation Patterns on Centerline and at Azimuth Angle of Maximum Radiation

The Common-Installation Configuration of the Terminated Long-Wire

The Laport configuration has been useful to our explorations by providing us with free-space and over-ground models that show their clear connection to the unterminated long-wires from which they derive. As well, they show within modeling limits the full potential of a terminated long-wire antenna with respect to gain, pattern shape, and other key properties. What the Laport configuration

lacks is widespread use, since it does not permit broadband use.

The common configuration simplifies construction and maintenance of the terminated long-wire antenna by bringing both the source and the terminating resistor close to ground level. The resistor has a return path that is common to one side of the feedpoint. Hence, we may locate the resistor at the very end of the antenna.

Fig. 2-8

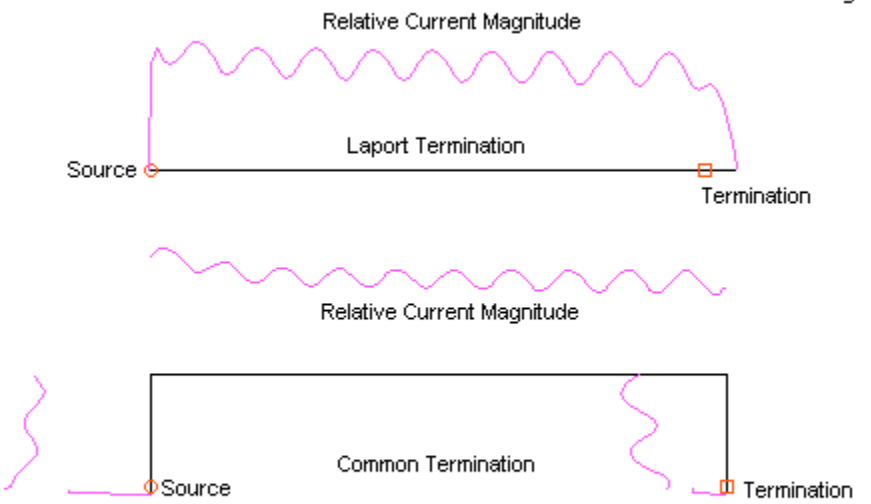

Comparison of Relative Current Magnitude on Long-Wire Beams
Using Inset Termination and Common Near-Ground Termination

Fig. 2-8 shows one immediate consequence of the redesign. Both antennas in the sketch use 5-λ horizontal wires. However, the common configuration also includes two vertical wires (each 1 λ long in this instance). Both vertical wires carry considerable current. As a consequence of the extra wires and their orientation, we can expect that the relatively ideal performance characteristics of

the Laport model will undergo some modification.

Ideally, we can find a load impedance that will provide the proper conditions for achieving full traveling-wave status. The calculation is based once more on treating the wire as a transmission line, and the load impedance must equal the characteristic impedance of the line. Balanis (*Antenna Theory: Analysis and Design*, p. 495) provides the following equation to approximate the proper value of the termination.

$$R_L = 138 \log_{10} (4h/d)$$

R_L is the value of the impedance load in Ohms, h is the height of the wire, and d is the wire diameter, when both are in the same units. Note that the impedance of the line and hence the approximate load value is independent of frequency and dependent only upon a set of physical measurements that use the same units of measurement. For many installations, terminating resistors tend to range between 600 and 800 Ω. We shall use test heights of 0.5 λ, 1.0 λ, and 2.0 λ. The wire diameter is 4.745e-6 λ (for 0.16" wire at 3.5 MHz). Despite the 4:1 ratio of antenna heights, the approximate recommended values of R_L are 776, 818, and 859 Ω, a spread of about 10% of the center value of the three. For a round number, we shall use 800 Ω for all cases, although in the process of developing a usable model, we shall explore some other terminating resistor values.

Modeling Issues: Before we can venture what performance modifications the common configuration might impose, we need to develop a reasonably satisfactory model of the common configuration terminated long-wire beam. Because the ground plays an essential role in the operation of the antenna, we cannot employ free-space models as a starting point. Therefore, all models will be over grounds ranging from very good (conductivity 0.0303 S/m, relative permittivity 20) to very poor (conductivity 0.001 S/m, relative permittivity 5).

Equally important to the model is the configuration that we employ for simulating the termination of the antenna ends at the ground. Essentially, we have 4 options (A though D) as sketched in **Fig. 2-9**.

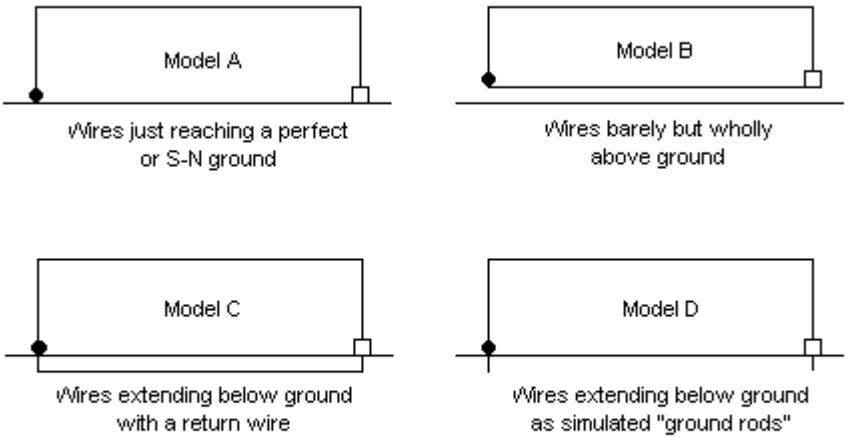

Various Ways of Simulating a Terminated Long-Wire Antenna in NEC Models

Fig. 2-9

Option A brings the vertical elements of the antenna down to ground. The source or feedpoint is the first segment above ground of the left wire, while the terminating load appears on the last segment above ground at the far end of the antenna. In the EZNEC Pro/4 implementation of NEC, we have at least 4 ways to model the structure: over perfect ground, with a Sommerfeld-Norton (SN) average ground using NEC-4, with an SN average ground using NEC-2, and with a MININEC ground. Use of a perfect ground provides a reference baseline for checking the sensibleness of other models. However, neither NEC-2 nor NEC-4 recommends bringing a source wire to ground, since at a minimum, the source impedance is likely to be off the mark. The MININEC ground does not provide accurate impedance reports for the ground quality selected, since it is restricted to using the impedance report for perfect ground.

Despite the limitations, we can tabulate the results. As a test case, I shall use a 10-λ terminated antenna alternately using termination resistors of 600, 800,

and 1000 Ω. For each option, **Table 2-5** lists the maximum gain, the reported 180-degree front-to-back ratio, the elevation angle of maximum radiation, the beamwidth, the source impedance, and the 600-Ω SWR at the test frequency.

Test Performance Values for Modeling Option A					10-WL Horizontal		
Load R	Gn dBi	FB dB	BW deg	El Ang	Feed R	Feed X	SWR 600
Perfect Ground							
600	13.98	29.04	26.4	15	439	24	1.37
800	13.91	26.38	26.2	15	476	43	1.28
1000	13.87	19.57	26.2	15	504	59	1.23
Average S-N Ground, NEC-4							
600	11.54	11.57	35.2	11	460	593	3.01
800	11.49	12.63	35.2	11	495	588	2.85
1000	11.45	12.87	35.2	11	524	587	2.75
Average S-N Ground, NEC-2							
600	10.79	24.23	35.6	11	479	14	1.26
800	10.74	21.78	35.6	11	509	35	1.19
1000	10.72	18.11	35.6	11	532	52	1.16
Average MININEC Ground, NEC-4							
600	11.09	23.58	35.4	11	439	24	1.37
800	11.01	22.71	35.4	11	476	43	1.28
1000	10.98	18.55	35.4	11	504	59	1.23
Load R = Terminating resistance value in Ohms							
Gn dBi = Maximum gain in dBi							
FB dB = 180-degree frnt-to-back ratio in dB							
BW deg = Half-power beamwidth in degrees							
El Ang = Elevation angle in degrees							
Feed R = Feepoint resistance in Ohms							
Feed X = Feedpoint reactance in Ohms							
SWR 600 = 600-Ohm SWR							Table 2-5

Using the sequence over perfect ground as a background reference, the NEC-2 results for the SN average ground and the MININEC average ground data appear to coincide fairly well. However, the NEC-4 runs for the SN average ground appear to yield somewhat high gain values with more than anticipated inductive reactance in the source impedance.

Option B represents an adaptation of a NEC-2 technique for modeling vertical antennas with ground-plane radials. The return line between the load resistor and the source is 0.0001-λ above ground, about 3 times the diameter of the wire. Hence, the model violates no constraints, but as **Table 2-6** for both NEC-2 and NEC-4 shows, it yields a poor model of the terminated long-wire antenna.

Test Performance Values for Modeling Option B					10-WL Horizontal		
Load R	Gn dBi	FB dB	BW deg	El Ang	Feed R	Feed X	SWR 600
Average S-N Ground, NEC-4							
600	7.68	16.93	35.4	11	1170	-97	1.97
800	7.73	14.44	35.4	11	1182	-80	1.98
1000	7.77	13.36	35.4	11	1192	-67	2.00
Average S-N Ground, NEC-2							
600	7.68	16.10	35.4	11	1167	-99	1.96
800	7.72	14.59	35.4	11	1179	-82	1.98
1000	7.76	13.50	35.4	11	1188	-69	1.99
Load R = Terminating resistance value in Ohms							
Gn dBi = Maximum gain in dBi							
FB dB = 180-degree frnt-to-back ratio in dB							
BW deg = Half-power beamwidth in degrees							
El Ang = Elevation angle in degrees							
Feed R = Feepoint resistance in Ohms							
Feed X = Feedpoint reactance in Ohms							
SWR 600 = 600-Ohm SWR							Table 2-6

Although NEC-2 and NEC-4 show a very close coincidence of data, the low gain, low front-to-back ratio, and high feedpoint impedance reports combine to suggest that this model is highly inadequate. However, the beamwidth and elevation-angle reports are consistent with the other models.

NEC-4 does allow the use of a subterranean return wire, shown in *option C* in **Fig. 2-9**. To test this option, I placed a return wire 0.01-λ below ground level, connecting it to the above ground vertical wires with short segments. Both the source and the load for the antenna remain above ground. Since this option is available only in NEC-4, the test-results in **Table 2-7** are quite brief.

Test Performance Values for Modeling Option C					10-WL Horizontal		
Load R	Gn dBi	FB dB	BW deg	El Ang	Feed R	Feed X	SWR 600
Average S-N Ground, NEC-4							
600	10.38	22.53	35.6	11	526	87	1.23
800	10.37	19.94	35.6	11	556	104	1.22
1000	10.36	17.10	35.6	11	579	118	1.23
Load R = Terminating resistance value in Ohms							
Gn dBi = Maximum gain in dBi							
FB dB = 180-degree frnt-to-back ratio in dB							
BW deg = Half-power beamwidth in degrees							
El Ang = Elevation angle in degrees							
Feed R = Feepoint resistance in Ohms							
Feed X = Feedpoint reactance in Ohms							
SWR 600 = 600-Ohm SWR							Table 2-7

The results are modest, but coincide roughly with the NEC-2 results in Option A. The front-to-back reports are consistent with those for perfect ground. The difficulties with the model include the model size, since the return wire requires as many segments as its above-ground counterpart, and the return wire may actually yield slightly low gain reports by carrying more current than the ground itself. A real installation would not likely use a buried ground wire.

Therefore, I tried *option D*, which replaces the below ground structure of option C with 2 simple ground rods. Each rod is a 1-segment wire about 0.05 λ, which is the length of the segments in the vertical wires above ground. Therefore, the source has equal length segments on each side of the feedpoint segment. 0.05-λ is about 4.3 meters or 14'. This length may be longer than the average ground rod, but substituting shorter segments did not change the reports by any significant amount. The results of the test appear in **Table 2-8**.

Except for the predicted very slight increase in maximum gain, all of the values correspond very well with those of the buried-return-wire model (C), but with a 45% reduction in model size. For users of NEC-4, it is likely that this style of model is about as adequate as we may get for a terminated long-wire directional antenna. In fact, for users of NEC-2, the basic model (option A) coincides well enough for general guidance. In physical reality, there will be

structural variables that will inevitably limit the precision attainable by any model. For example, the models presume a flat wire horizontal to the ground, which is not likely to appear with copper wire and real supports. Even if all supports provide the same height, catenary effects will vary the actual wire height above ground along the antenna pathway.

Test Performance Values for Modeling Option D					10-WL Horizontal		
Load R	Gn dBi	FB dB	BW deg	El Ang	Feed R	Feed X	SWR 600
Average S-N Ground, NEC-4							
600	10.49	22.94	35.6	11	513	69	1.22
800	10.47	20.30	35.6	11	544	87	1.20
1000	10.46	17.29	35.6	11	567	102	1.20
Load R = Terminating resistance value in Ohms							
Gn dBi = Maximum gain in dBi							
FB dB = 180-degree frnt-to-back ratio in dB							
BW deg = Half-power beamwidth in degrees							
El Ang = Elevation angle in degrees							
Feed R = Feepoint resistance in Ohms							
Feed X = Feedpoint reactance in Ohms							
SWR 600 = 600-Ohm SWR							Table 2-8

In the process of developing a model configuration for more extensive exploration of the performance of common-configuration terminated long-wires, I briefly examined the effects of using copper wire instead of lossless wire. The 10-λ antenna will maximize copper losses and tell us quickly enough whether such losses are significant in terminated long-wire antennas. **Table 2-9** provides the results of the quick check, with the data for lossless wire at hand for comparison. Both models use option D. Despite the very long length of the wire, copper losses at the test frequency only lower the gain by about 0.2 dB. All other performance values remain quite constant.

The net result of these preliminary tests suggest that option D is a very usable model capable of giving good guidance on the performance of the common-configuration single terminated long-wire antenna. We may without reservation continue to use lossless wire, and a termination of 800 Ω is quite adequate. Note that throughout the exercises, the SWR values are based on a

reference impedance of 600 Ω, a common commercial feedline impedance. In some other long-wire arrays, the terminating impedance and the feedpoint impedance will move in opposite directions, allowing one to center the terminating resistor value very close to the source impedance. However, due to the additional vertical segments of wire, the common-configuration load and source impedance values rise and fall together, forcing us to use other criteria for the selection of both the terminating resistor and the feedline.

Test Performance Values for Modeling Option D with Lossless and Copper Wire							
Load R	Gn dBi	FB dB	BW deg	El Ang	Feed R	Feed X	SWR 600
Average S-N Ground, NEC-4, Lossless Wire							
600	10.49	22.94	35.6	11	513	69	1.22
800	10.47	20.30	35.6	11	544	87	1.20
1000	10.46	17.29	35.6	11	567	102	1.20
Average S-N Ground, NEC-4, Copper Wire							
600	10.28	23.06	35.5	11	518	70	1.21
800	10.27	19.70	35.5	11	548	85	1.19
1000	10.26	17.37	35.5	11	571	97	1.19
Horizontal Section = 10 wavelengths							
Load R = Terminating resistance value in Ohms							
Gn dBi = Maximum gain in dBi							
FB dB = 180-degree frnt-to-back ratio in dB							
BW deg = Half-power beamwidth in degrees							
El Ang = Elevation angle in degrees							
Feed R = Feepoint resistance in Ohms							
Feed X = Feedpoint reactance in Ohms							
SWR 600 = 600-Ohm SWR							Table 2-9

Pattern Evolution: The tables of data will use common-configuration terminated long-wire antennas that range from 3 to 11 λ in 1-λ increments. As we shall see, the gain of a single terminated long wire at 3 λ is below the gain of a simple dipole at the same height. Therefore, using a very short terminated long-wire makes little sense. By increasing the increments between steps, we can more easily survey a larger span of heights and ground qualities. Because model option D includes wires below ground, we shall exclude perfect ground from the survey.

The resulting data progressions will prove very smooth with very consistent feedpoint impedance values from one length to the next. However, we noted in connection with unterminated long-wires that the patterns and performance at odd multiples of a quarter wavelength were not fully consistent with the reports at even multiples of a quarter wavelength. The source of the differences proved to be the emergence on the "new" lobe, with a consequential shift in pattern shape. To see if we encounter a similar phenomenon with common-configuration terminated long-wires, I examined a series of models from 5 to 6 λ in 0.25-λ increments. The results appear in **Table 2-10**.

Terminated Long-Wire Pattern Evolution from 5.0 to 6.0 WL in 0.25-WL Increments
Common Installation; 800-Ohm Termination; Height 1 WL Above Average Ground

Len WL	Gn dBi	FB dB	BW deg	El Ang	Feed R	Feed X	SWR 600
5	8.65	17.35	s53	13	541	89	1.21
5.25	8.94	12.02	s51	13	550	-15	1.01
5.5	8.92	17.87	50.0	13	542	89	1.21
5.75	9.19	12.12	48.6	13	549	-15	1.01
6	9.15	18.30	s48	12	542	89	1.20

Len WL = Length in wavelengths
Load R = Terminating resistance value in Ohms
Gn dBi = Maximum gain in dBi
FB dB = 180-degree frnt-to-back ratio in dB
BW deg = Half-power beamwidth in degrees
El Ang = Elevation angle in degrees
Feed R = Feepoint resistance in Ohms
Feed X = Feedpoint reactance in Ohms
SWR 600 = 600-Ohm SWR

Table 2-10

Just as we found for unterminated long-wires, terminated long-wires show a higher gain at odd multiples of a quarter wavelength than at even multiples. As well, the 180° front-to-back ratio is lower. We also find differences in the values of feedpoint resistance and reactance.

As a side note that is relevant of data tables to come, the beamwidth column shows 2 types of entries. Some entries are simply numerical, while others have a preceding "s." The "s" indicates that the forward structure of the radiation pattern

has split lobes with a null greater than 3 dB between them. Hence, the beamwidth value is an estimate that ignores the null. Purely numerical values indicate a null less than 3 dB so that the program reports the beamwidth directly. **Fig. 2-10** shows the evolution of the patterns from 5.5 to 6.0 MHz.

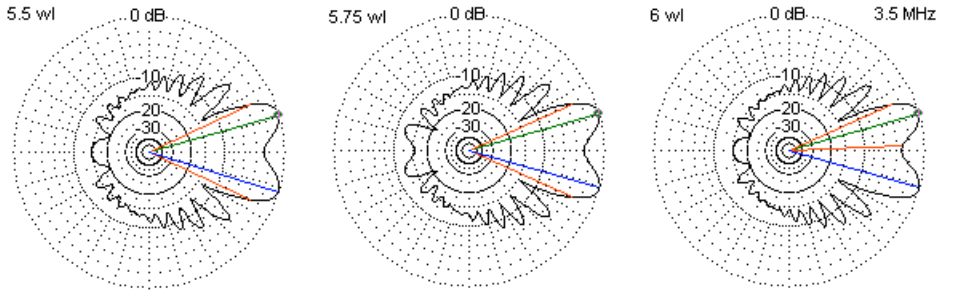

Common-Installation Terminated Long-Wire Beam Azimuth Patterns
5.5 MHz to 6.0 MHz 1 Wavelength Above Average Ground

Fig. 2-10

Corresponding patterns for unterminated long-wires showed patterns at odd multiples of a quarter wavelength to have reduced sidelobe strength in the region 90° to each side of the wire axis. We do not find a similar reduction in side lobes in the sequence of patterns in **Fig. 2-10**. The vertical radiation component from the end wires fills in the sidelobe region to approximately equal strength levels for all patterns, regardless of antenna length. Hence, the radiation pattern shows the antenna length as an odd or even multiple of a quarter wavelength chiefly in the shape of the rearmost lobes.

Using 1-λ increments between sampled antenna lengths can also leave the misimpression that the feedpoint impedance is completely stable from the shortest to the longest antenna length. As **Table 2-10** showed, the actual impedance values vary with finer increments of modeling. To capture something of the actual impedance swings, I ran a 600-Ω SWR sweep of a common-configuration terminated long-wire that is 5 λ at 3.5 MHz 1 λ above average ground. However, the sweep covers a 4:1 frequency range between 1.75 MHz and 7.0 MHz. At the lowest frequency, the antenna is only 2.5 λ long and 0.5 λ

above ground. At the high end of the sweep, the antenna is 10 λ long and 2 λ above ground. **Fig. 2-11** presents the 600-Ω for increments of 0.125 MHz.

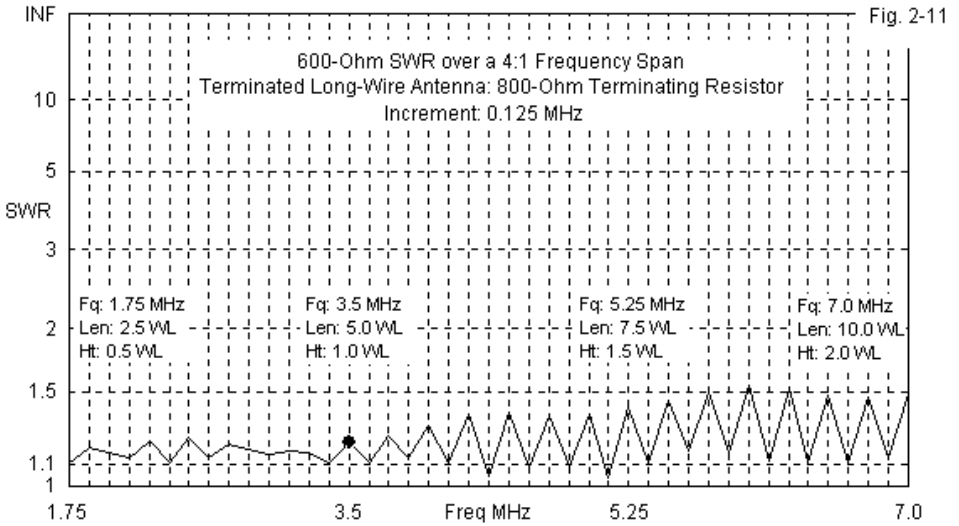

Since the sweep increment is linear while the antenna length increments of interest are multiplicative, the sweep does not catch each peak value. However, it does indicate the ups and down of the impedance relative to the 600-Ω standard. The key variable is reactance, which ranged from -j92 Ω to j248 Ω. Nevertheless, the test antenna would likely prove to have a usable SWR below 2:1 and be amenable to conversion to a 50-Ω coaxial cable via a broadband impedance transformer.

Common-Configuration Modeling Data: To provide some guidance on rational expectations of performance from the common-configuration terminated long-wire, I explored model D at 3 heights: 0.5 λ, 1.0 λ, and 2.0 λ. At each height, I looked at the performance with very good, average, and very poor ground in order to see the effects of ground quality on antenna performance. We can begin with the data for the 1-λ, which appear in **Table 2-11**.

Common-Installation Terminated Long-Wire Beams: 3-11 WL						Table 2-11
Modeling Option D 1-WL Above Average Ground						
800-Ohm Terminating Resistor; Lossless Wire						
Ground	Len WL	Gain dBi	FB dB	El Ang	alpha	BW deg
Very	3	8.33	15.73	16	20	66.6
Good	4	9.25	17.89	15	17	57.0
C: 0.0303	5	9.94	19.09	15	14	49.4
P: 20	6	10.48	20.50	15	12	43.4
	7	10.93	21.28	14	11	40.2
	8	11.30	21.80	14	9	36.4
	9	11.61	23.06	14	8	33.0
	10	11.87	23.44	14	6	30.2
	11	12.09	24.04	14	4	27.4
Ground	Len WL	Gain dBi	FB dB	El Ang	alpha	BW deg
Average	3	7.11	15.32	14	24	s70
C: 0.005	4	7.99	16.48	13	20	s60
P: 13	5	8.65	17.37	13	17	s52
	6	9.15	18.30	12	16	s48
	7	9.57	18.73	12	14	43.8
	8	9.92	19.51	12	13	40.2
	9	10.20	20.12	12	12	37.0
	10	10.47	20.30	11	12	35.6
	11	10.70	20.58	11	11	33.4
Ground	Len WL	Gain dBi	FB dB	El Ang	alpha	BW deg
Very	3	5.78	13.24	13	25	s72
Poor	4	6.66	14.16	12	21	s62
C: 0.001	5	7.32	15.34	12	19	s54
P: 5	6	7.84	15.75	11	17	s49
	7	8.27	16.05	11	15	s45
	8	8.62	16.66	11	14	s42
	9	8.95	16.65	10	13	s39
	10	9.23	16.91	10	12	s37
	11	9.48	17.23	9	12	s35
Notes	Ground = Ground quality (conductivity and relative permittivity					
	Len WL = Length in wavelengths					
	Gain dBi = Maximum gain in dBi					
	FB dB = 180-degree front-to-back ratio in dB					
	El Ang = Elevation angle of maximum radiation					
	in degrees					
	alpha = Main lobe angle in degrees					
	BW deg = main lobe beamwidth in degrees					

Even 1 λ above ground, the quality of ground has a very significant effect on the performance of the antenna. The differential in maximum gain is consistently about 2.5 dB between very poor and very good soil, with comparable differences in the front-to-back ratio. It is very likely that the vertical legs of the common-configuration antenna have a significant role in the size of the differentials based on ground quality.

The elevation data is consistent with comparable data for unterminated long-wire antennas. The better the quality of the ground, the higher that the elevation angle is for any given antenna length. However, the relationship between the value of α and the beamwidth shows an opposite trend relative to the Laport data. The Laport configuration showed an inverse relationship between α and the beamwidth when we compared free-space and average-ground values. (See **Fig. 2-6**.) The common-configuration version of the terminated long-wire antenna shows decreasing values of both α and the beamwidth as we improve the quality of the ground for antennas of equal horizontal length.

Tables do not reveal all the significant differences between terminated long-wire configurations. **Fig. 2-12** presents a gallery of sample elevation and azimuth patterns for common-configuration long-wires 1 λ above average ground. Although the elevation patterns seem smaller, they are in this instance the more important ones for each antenna length. Of special note are the forward and rearward lobes above the lowest level. All of the elevation patterns contain strong upper level lobes at high angles.

For comparison, examine the patterns for the Laport configuration in **Fig. 2-5**. Except for the 2-λ antenna, all of the Laport patterns show very low levels of radiation to the rear of the main lobe at virtually any angle. Equally significant are the upper-angle forward lobes. The Laport radiation patterns show 1 to 2 lobes that are less than -10 dB relative to the main lobe. In contrast, the common-configuration patterns typically show a large front of lobes, some only 3 to 4 dB weaker than the main lobe. The differences between the elevation patterns in the two configurations rest on the radiation contributions of the vertical legs in the common-configuration models.

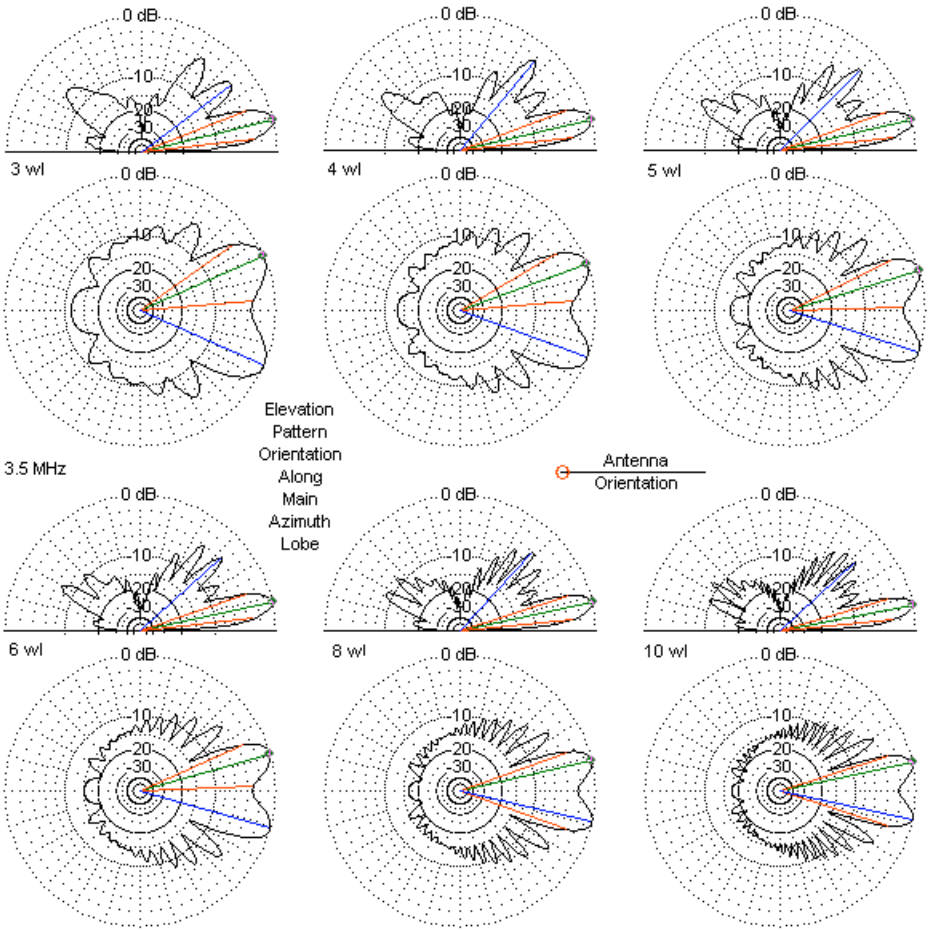

Terminated Long-Wire Antennas with Lossless Wire
Sample Elevation and Azimuth Patterns 1 WL Above Average Ground

Fig. 2-12

The gallery in **Fig. 2-12** clearly shows the weaker null between main lobes for the common-configuration models. The data in **Table 2-11** tells us that as we

improve the ground quality, the null shrinks until it virtually disappears. **Fig. 2-13** compares azimuth patterns for a 10-λ terminated long-wire 1 λ above ground. The models over lossy ground use option D, while the model over perfect ground uses option A. As we improve the ground quality, the split lobe gradually disappears so that with perfect ground, we have only a single lobe with maximum strength in line with the wire axis.

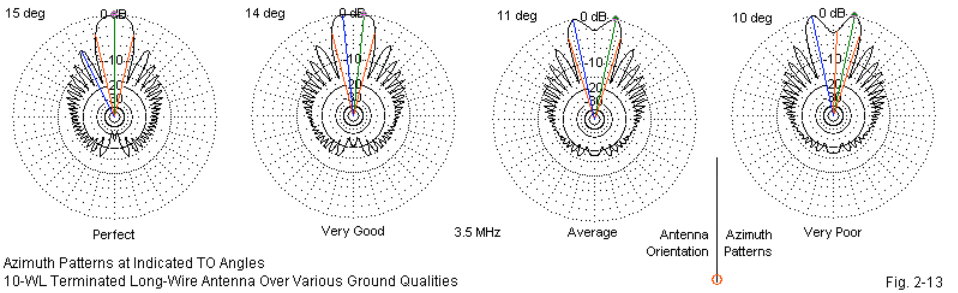

Although we have compared elevation patterns between the Laport and common-configuration terminated long-wires, we bypassed the azimuth pattern. In this case, we cannot easily see the differences between comparable azimuth patterns without close proximity. Therefore, **Fig 2-14** present corresponding Laport and common-configuration azimuth patterns for antennas with 3-λ, 6-λ and 9-λ horizontal wires, each 1 λ above average ground.

If you trace the outer pattern limits, you will find only relatively small differences in pattern shape. Apart from the rearmost lobe structure, the remaining sidelobes have nearly the same strength, relative to the main lobes, in both cases. Of course, the Laport patterns show a deeper null between the two main lobes in all cases. The major distinction in pattern shape occurs with respect to nulls, not only the null between main lobes, but with respect to all nulls. Without vertical legs, the Laport patterns show deep nulls between each lobe. In contrast, most of the sidelobe nulls in the common-configuration models are barely noticeable once we move about 60° away from the wire axis. The vertical components of the radiation pattern, largely a function of the two vertical legs of the antenna, tend to show lobes where the horizontal components show nulls.

The vertical component nulls are not strong enough to remove all signs of a null, but they come very close to that level for sidelobes between about 70° and 120° away from the wire axis. As we shall soon discover, the absence of a null represents a significant amount of energy radiated in directions in which the Laport configuration radiates little or nothing.

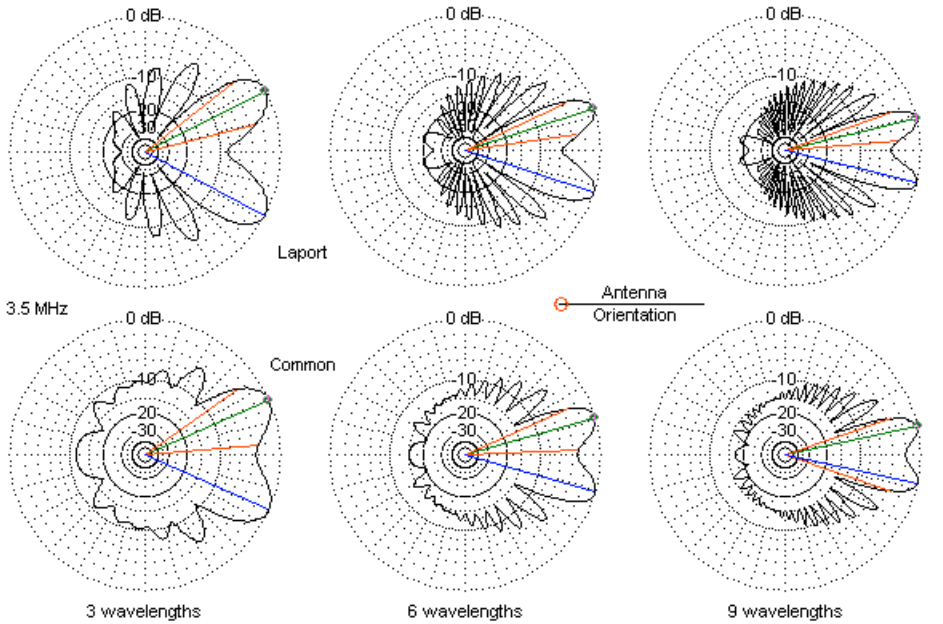

Comparison of Selected Azimuth Patterns of Laport and Common-Installation Long-Wire Beams at 1 Wavelength Above Average Ground

Fig. 2-14

The consequences of having shallow nulls in the common-configuration patterns appear most vividly in a comparison of certain performance data relative to the Laport models. **Table 2-12** provides the data for the maximum forward gain and for the α angle for both types of terminated long-wires. Essentially, the common-configuration loses an average of nearly 2 dB of maximum gain for the convenience of feeding and loading offered by the vertical legs and for the

potential of offering broadband service. The energy that eliminates deep nulls in the sidelobe structure of the common-configuration beam is not available to enhance forward gain.

Laport and Common Long-Wire Installations: Gain and alpha Angle						
1 Wavelength above Average Ground						
	Laport Long-Wire		Common Installation			
Len WL	Gain dBi	alpha	Gain dBi	alpha	Gn Diff	alpha Diff
3	8.83	27	7.11	24	1.72	3
4	9.86	23	7.99	20	1.87	3
5	10.57	20	8.65	17	1.92	3
6	11.13	18	9.15	16	1.98	2
7	11.57	16	9.57	14	2	2
8	11.90	14	9.92	13	1.98	1
9	12.22	14	10.20	12	2.02	2
10	12.48	13	10.47	12	2.01	1
11	12.71	12	10.70	11	2.01	1
Notes	Len WL = Length in wavelengths					
	Gain dBi = Maximum gain in dBi					
	alpha = Main lobe angle in degrees					
	Gn Diff = Laport gain - common gain					
	alpha Diff = Laport alpha - common alpha					Table 2-12

In addition to the comparative loss of gain, the common-configuration long-wire beam also shows a narrowing of the α angle relative to both the Laport configuration and to the unterminated long-wire antennas. Since the reduction in the angle between the wire axis and the main lobe is proportional to the ideal value, the reduction of α in degrees decreases as the antenna grows longer and the ideal value of α becomes smaller. As a result of the variation from the ideal, calculating the headings of the main lobe independently of reasonable models of the antenna becomes less certain. Indeed, for common-configuration terminated long-wires, modeling may become a requisite for obtaining a reasonable prediction of the probable performance of the array. This note applies not only to the long-wire beam itself, but as well to more complex long-wire arrays that use similar feeding or loading schemes. **Fig. 2-15** graphs the gain and α values of

both the Laport and the common-configuration terminated long-wire beams, with the understanding that the particular numbers apply only to beams that are 1 λ above average ground.

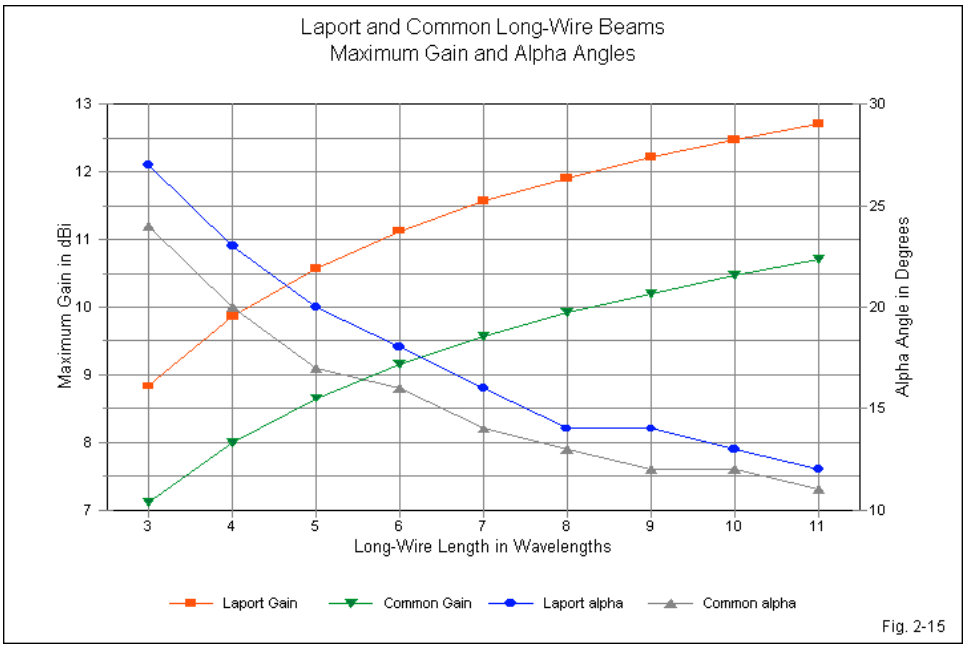

Fig. 2-15

To complete our survey, **Table 2-13** presents data for the common configuration option D models at a height of 0.5 λ. **Table 2-14** presents similar data for the same antennas at 2 λ above ground. In both instances, the models were modified in leg length while retaining a 20-segment/λ density. In both cases, we find lesser variations than at a height of 1 λ. (To make comparisons, consult **Table 1-7** through **Table 1-9** in the preceding chapter.) At a height of 0.5 λ above ground, the vertical legs add only half the extra length relative to the same antenna at a height of 1 λ. When the height reaches 2 λ above ground, the influence of ground on the antenna performance becomes quite variable and intrinsically interesting.

Common-Installation Terminated Long-Wire Beams: 3-11 WL						Table 2-13
Modeling Option D 0.5-WL Above Average Ground						
800-Ohm Terminating Resistor; Lossless Wire						
Ground	Len WL	Gain dBi	FB dB	El Ang	alpha	BW deg
Very	3	7.83	14.04	31	12	59.4
Good	4	8.68	14.06	29	0	45.0
C: 0.0303	5	9.21	13.86	26	0	39.4
P: 20	6	9.59	13.57	24	0	34.8
	7	9.85	13.61	22	0	32.4
	8	10.10	13.23	21	0	29.0
	9	10.28	12.99	20	0	26.6
	10	10.44	12.93	19	0	25.0
	11	10.59	13.03	18	0	24.0
Ground	Len WL	Gain dBi	FB dB	El Ang	alpha	BW deg
Average	3	6.47	12.69	26	21	67.4
C: 0.005	4	7.16	13.06	24	16	55.0
P: 13	5	7.65	13.41	22	13	47.4
	6	8.01	13.56	20	12	42.8
	7	8.34	13.80	19	10	38.4
	8	8.66	14.03	19	6	33.4
	9	8.92	14.29	18	5	31.0
	10	9.16	14.42	17	5	29.2
	11	9.39	14.32	17	0	26.0
Ground	Len WL	Gain dBi	FB dB	El Ang	alpha	BW deg
Very	3	5.08	13.66	21	23	s71
Poor	4	5.82	14.76	19	19	59.0
C: 0.001	5	6.40	15.49	18	16	51.0
P: 5	6	6.90	16.78	16	14	46.2
	7	7.34	17.84	15	12	42.0
	8	7.76	18.42	14	11	38.8
	9	8.14	18.33	14	10	35.4
	10	8.52	19.28	13	9	33.6
	11	8.86	20.39	13	7	31.0
Notes	Ground = Ground quality (conductivity and relative permittivity					
	Len WL = Length in wavelengths					
	Gain dBi = Maximum gain in dBi					
	FB dB = 180-degree front-to-back ratio in dB					
	El Ang = Elevation angle of maximum radiation in degrees					
	alpha = Main lobe angle in degrees					
	BW deg = main lobe beamwidth in degrees					

Common-Installation Terminated Long-Wire Beams: 3-11 WL						Table 2-14
Modeling Option D 2-WL Above Average Ground						
800-Ohm Terminating Resistor; Lossless Wire						
Ground	Len WL	Gain dBi	FB dB	El Ang	alpha	BW deg
Very	3	7.76	15.93	7	26	s74
Good	4	8.94	17.69	7	23	s64
C: 0.0303	5	9.76	18.06	7	20	s57
P: 20	6	10.41	18.47	7	18	s52
	7	10.96	19.33	7	17	s48
	8	11.41	19.93	7	16	s44
	9	11.82	20.34	7	15	s41
	10	12.18	20.61	7	14	s39
	11	12.51	20.78	7	13	s37
Ground	Len WL	Gain dBi	FB dB	El Ang	alpha	BW deg
Average	3	7.09	14.98	7	27	s75
C: 0.005	4	8.24	15.91	7	23	s65
P: 13	5	9.06	16.96	7	21	s58
	6	9.69	17.39	7	19	s52
	7	10.21	17.48	7	17	s48
	8	10.65	17.99	7	16	s45
	9	11.03	18.33	7	15	s42
	10	11.36	18.54	7	14	s39
	11	11.65	18.65	7	13	s37
Ground	Len WL	Gain dBi	FB dB	El Ang	alpha	BW deg
Very	3	6.19	13.46	7	27	s76
Poor	4	7.31	14.42	7	23	s65
C: 0.001	5	8.12	15.49	7	21	s58
P: 5	6	8.75	16.04	7	19	s53
	7	9.25	16.68	6	18	s49
	8	9.71	16.58	6	16	s45
	9	10.10	16.89	6	15	s42
	10	10.44	17.07	6	14	s40
	11	10.77	17.81	6	14	s38
Notes	Ground = Ground quality (conductivity and relative permittivity					
	Len WL = Length in wavelengths					
	Gain dBi = Maximum gain in dBi					
	FB dB = 180-degree front-to-back ratio in dB					
	El Ang = Elevation angle of maximum radiation in degrees					
	alpha = Main lobe angle in degrees					
	BW deg = main lobe beamwidth in degrees					

The vertical legs of the common-configuration long-wire beam raise the elevation or take-off angle of the lowest (0.5-λ) beam by an average of about 2° relative to unterminated long-wires. However, the α angles tends to vary by no more than about 1° from the unterminated values, suggesting that the horizontal portion of the antenna has primary responsibility for the angle at the low height. At the highest sampled height (2 λ), we find a similar 1° change in the α angle and virtually no change in the elevation angle between unterminated long-wires and common-configuration beams.

Within the collection of common-configuration beam samples, we also find some interesting comparisons. **Fig. 2-16** shows the modeled maximum gain values for beams at 1 λ and at 2 λ above ground, for the sampled length range of 3 to 11 λ.

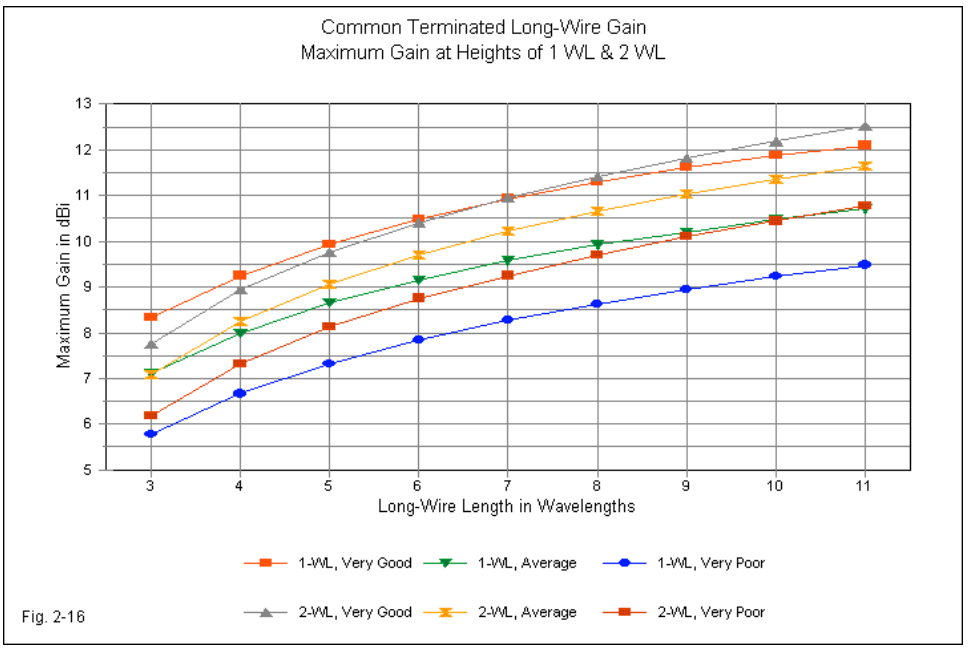

Fig. 2-16

Over very poor ground, the maximum gain of the higher antenna is greater for every antenna length. As we improve the ground to average, the gain difference for the longest antennas is less, and the gain of the 1-λ-high, 3-λ-long beam is actually numerically higher than the same antenna at 2 λ. When we improve the ground to very good. The lower (1-λ-high) model shows a higher gain than the higher (2-λ) model until the antenna length exceeds 7 λ.

We have generally overlooked the variations in feedpoint impedance as we changed the height and the ground quality for the common-configuration long-wire beam. In general, heights of at least 0.5 λ through 2 λ make very little difference in the resistive component of the impedance. However, ground quality does make a difference. Over very good ground, the feedpoint resistance ranged from 490 to 508 Ω over the sampled span of lengths for all antenna heights. Over average ground, the range was 532 to 547 Ω. Above very poor ground, the feedpoint resistance ran from 644 to 667 Ω, again, regardless of height. All models used an 800-Ω termination. We might suggest that a potential long-wire beam builder experiment to arrive at the best value of load resistor. However, the practicalities of obtaining an ideal non-inductive terminating resistor capable of dissipating up to half the applied antenna power suggest that most common-configuration long-wire beams will use the least expensive available resistor (or combination) that permits acceptable SWR performance with the chosen feedline or impedance matching device.

These notes have not exhausted the useful comparisons that we may draw between unterminated long-wires and the two variations on the terminated long-wire beam. Overall, we have seen that adding a terminating resistor–to achieve a directional beam–results in a gain penalty that offsets the reduction in rear quadrant radiation and sensitivity. In addition, using the common-configuration terminated long-wire–to attain feeding and loading convenience as well as very broadband service–results in other penalties that affect the maximum achievable gain and other performance facets. Even in the earliest days of radio communications, engineers and designers considered the terminated long-wire beam to have relatively limited use and numerous drawbacks. Not the least of the limitations were the gain, the split beam, and the large number of strong sidelobes.

Preliminary Ideas for Improving the Long-Wire Beam

One of the earliest ideas to emerge to improve terminated long-wire performance involved combining the split lobes into a single lobe. Before we close the book on single long-wire beams in favor of more complex arrays, let's examine a pair of preliminary ideas on how we might accomplish the feat.

Bending the Terminated Long-Wire Antenna: There is a technique by which we can remove the split radiation lobe of the terminated long-wire antenna, at least when the wire is many wavelengths long. We may bend the antenna horizontally in the middle. In effect, we create a 2-element long-wire antenna, where each element is half the total horizontal wire length. (In this sample, we shall leave the 1-λ vertical wire and the "ground rods" from model option D just as they are.) **Fig. 2-17** shows the general layout.

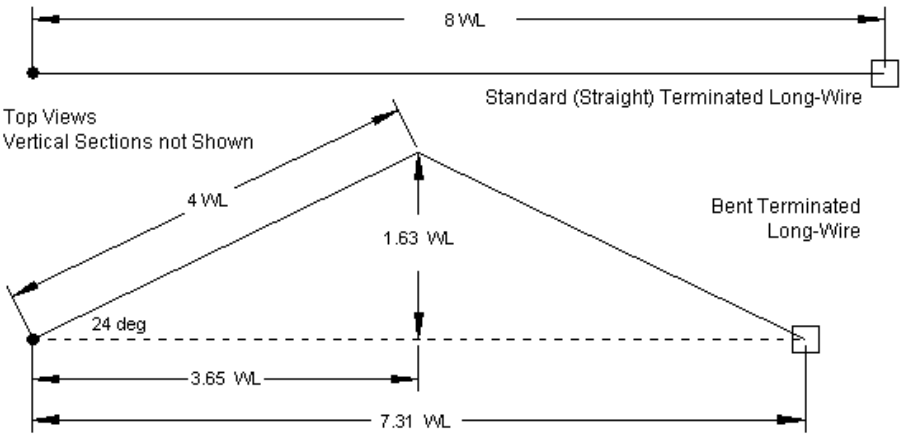

A Sample Straight and Bent Terminated Long-Wire Antenna

Fig. 2-17

One of the forward main lobes from the feedpoint-end section tends to align itself with one of the main forward lobes of the termination-end section, and the two lobes are aligned with the wire termination points. **Fig. 2-17** provides data for

the 8-λ (or dual-4-λ) bent terminated long-wire antenna. The required angle relative to the pattern centerline is 24° for maximum gain. This value is a function of the antenna's 1-wavelength height, the average soil quality, and the wire length. Since the total horizontal wire length is 8 λ, the angle creates a maximum antenna width of 1.63 λ, but shortens the overall length to 7.31 λ.

Comparison: Straight and Bent 8-Wavelength Terminated Long-Wire Antennas							
Both Antennas 1 Wavelength above Average Ground; Model Option D							
Version	Gn dBi	FB dB	BW deg	El Ang	Feed R	Feed X	SWR 600
Straight	9.92	19.51	40.2	12	544	88	1.20
Bent	12.39	15.36	20.3	13	531	71	1.19
Straight = 8-WL straight wire element							
Bent = 8-WL total element length, bent 24 degrees at center (4-WL point)							
Terminating resistor = 800 Ohms							Table 2-15

Table 2-15 compares the performance of the straight and bent 8-λ antennas. Bending the wire adds about 2.5-dB of overall gain, due to the additive affect of aligned lobes. However, the front-to-back ratio suffers by a like amount. The impedance hardly changes between the 2 antennas. The most notable change of all is the reduction in beamwidth from 40° to 20°.

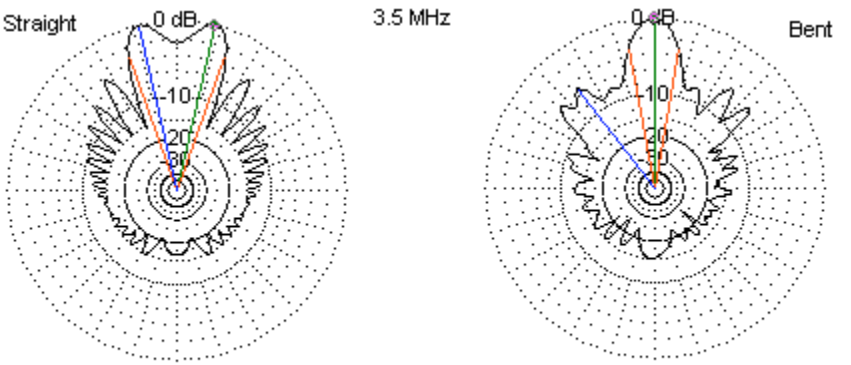

Azimuth Patterns at TO Angles: Straight and Bent
8-Wavelength Terminated Long-Wire Antennas

Fig. 2-18

The difference in beamwidth becomes readily apparent when we examine azimuth patterns for the 2 antennas in the table. **Fig. 2-18** provides the patterns. The bent-beam pattern does not align with either wire, but rather with an angle parallel to the vertical wires at the array ends. The bent version has eliminated the null between peaks by creating a single forward main lobe. As well, the bent antenna's patterns shows irregular sidelobe structures that result from off-axis additions and cancellations, relative to the clean lobe structure of the straight antenna. However, most of the bent antenna sidelobes tend to be weaker than the sidelobes of the straight antenna.

The bent terminated long-wire antenna is rarely used today in its horizontal format. However, a terminated "inverted V" version with the ends terminated at ground is available in commercial packages. Bruce described the terminated inverted V in his classic 1931 article.

The straight terminated long-wire beam has lower gain that the horizontal bent long-wire, but it also enjoys 2 advantages: wider beamwidth and the ability to operate over a very wide frequency range at a constant impedance. The bent antenna might match the straight antenna's SWR curve, but the radiation pattern would become unusable beyond perhaps a 2:1 frequency range. The physical wire angle remains constant, but the electrical length of the wire–measured in wavelengths–changes for every change in operating frequency. The angle simply becomes incorrect to produce maximum gain in a single lobe as the operating frequency goes too high or too low. If we wish to obtain the added gain of the bent antenna's aligned main lobes, there are other designs that achieve the goal with more regular sidelobes and, in some cases, weaker sidelobes.

The Double Laport or Echelon Terminated Long-Wire Beam: An alternative technique uses the same amount of wire as the bent long-wire beam, but requires considerably less real estate. Instead of merely bending an 8-λ wire, we shall cut it in two pieces and offset the pieces. We shall connect the two near ends and feed them at their center. Each far end will use a Laport-type load ¼ λ inward from the tip. **Fig. 2-19** shows the general layout and identifies critical angles and dimensions. Distance *a* represents the amount of offset between the inner and outer tips of the wires, both of which are 4 λ long in this example. Distance *b* is

the side-to-side spacing. Distance *c* is the distance between the tips of each leg at each end of the double long-wire antenna.

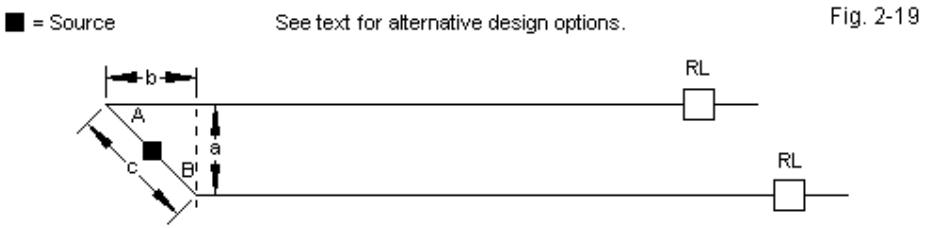

General Outline of a Double Terminated Long-Wire Beam

We know the angle α from either calculation by the equation shown earlier or from models. For the 4-λ single terminated Laport long wire beam, the angle is 22.6°. (Although the angle seems spuriously precise, it will be important to calculations.) From the value of α, we can calculate all necessary values–namely angles A and B and sides *a*, *b*, and *c*.

Type 1 Double Long-Wire Beams: Laport (*Radio Antenna Engineering*, p. 312) provides instructions for calculating the amount of offset and separation for the two wires to arrive at an echelon long-wire beam with only a single forward lobe, although that lobe will not align with the wires. Relative to the sketch in **Fig. 2-19**, it will be offset downward by the value of α. The following equations define the double or type-1 echelon long-wire beam.

$A = 90 - \alpha$ $B = \alpha$

$c = 1/[2 \cos (90 - 2\alpha)]$ $a = c \sin A$ $b = c \sin B$

Angle B = 22.6°, which sets angle A at 67.4°. Distance c = 0.705 λ, with a (the side-to-side separation) becoming 0.651 λ and b (the end offset) 0.271 λ.

Type 2 Double Long-Wire Beams: We may use an alternative set of equations to arrive at dimensions and angles that reverse the direction of the

combined main lobes in the echelon beam. Instead of angling downward relative to the sketch in **Fig. 2-19**, they will angle upward relative to the wires by the amount of α. To arrive at these values, we must alter the equation set.

A = (3 α)/2 B = 90 - A
c = 1/(2 cos B) *a* = *c* sin A *b* = *c* sin B

Angle A becomes 33.9°, while angle B is now 56.1°. Distance *c* is 0.896 λ; *a* (the separation) is 0.5 λ, and *b* (the offset) is 0.744 λ.

Table 2-16 provides a comparison between a single 4-λ Laport long-wire beam and sample models of each type of double or echelon long-wires, where each leg is 4 λ. The models are samples only and would require extreme refinement before becoming useful models to guide the development of a dual long-wire beam using Laport termination methods. The need for a termination reactance is a clear sign that these are preliminary models, but they suffice to illustrate the potential and limits of double long-wire beams.

Single and Double Terminated Long-Wire Beams					Table 2-16
All Antennas 1 Wavelength above Average Ground					
Laport Configuration Models					
Type		Gn dBi	FB dB	BW deg	El Ang
Single		9.86	21.12	s64	13
Double Type 1		12.3	8.3	18.8	13
Double Type 2		12.35	15.83	18.6	13
Single = Laport single-wire terminated long-wire					
Double Type 1 = Standard double long-wire					
Double Type 2 = Alternative double long-wire					
Terminations: Single 690 Ohms; Double 670 - j400 Ohms					

The table shows that we achieve the same general gain level with 2 4-λ wires that we attained with a single bent 8-λ wire. Furthermore, the beamwidth is comparable to the value shown by the bent long-wire model. However, the front-to-back ratio has severely dropped, although further refinement of the model might restore a good bit of its value.

One of the chief limitations of either version of the double long-wire is an inability to control sidelobes. The bent long-wire had very significant forward sidelobes, but their pattern was relatively symmetrical around the main lobe bearing. (Symmetry, of course, is not perfect.) In contrast, the double long-wires show highly irregular patterns once we move away from the main lobe. **Fig. 2-20** provides the patterns, along with antenna sketches to allow orientation between the antenna types and their patterns.

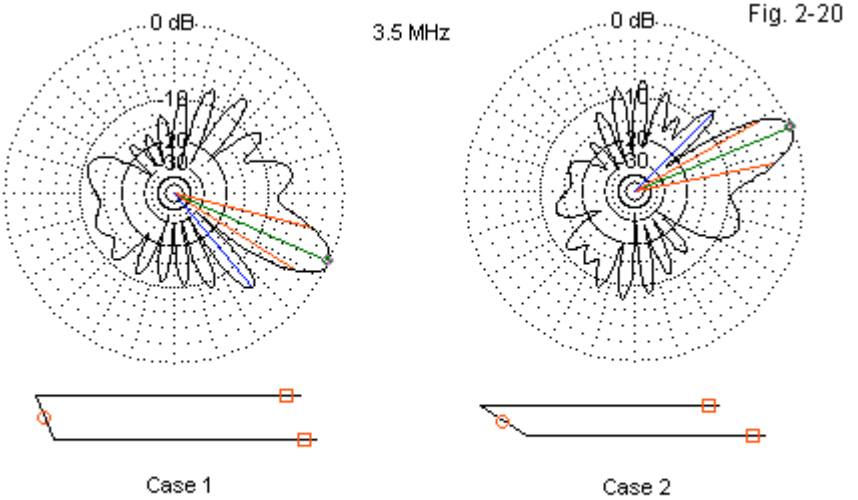

Fig. 2-20

Alternative Designs and Azimuth Patterns for a Double Terminated Long-Wire Beam (1 WL Above Average Ground)

The two general preliminary ideas for improving the performance of long-wire beams share a common core: they both try to align the sidelobes from a long-wire antenna to form a single main lobe that has a controllable direction relative to the antenna's physical layout. The bent long-wire aligns a single main lobe from each straight section of the antenna. The double long-wire uses the phase-shift resulting from the offset and spacing of the two wires to create a single main lobe. Both are less than ideal for general use, but they do provide us with a

fundamental principle of advanced long-wire technology. If we can align main lobes from 2 or more wires, the patterns will add to form a single, stronger main lobe. **Fig. 2-21** shows the basic idea of long-wire lobe addition. Missing from the picture are the sidelobes and what happens when they add to each other.

Fig. 2-21

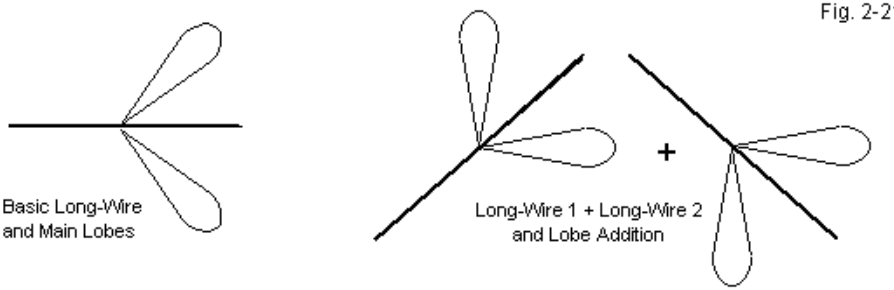

The Basic Idea of Long-Wire Lobe Addition

Our next task will be to explore the first major advance beyond the single long-wire: the V array. If we expect both unterminated and terminated versions of the V, we shall not be disappointed.

Conclusion

When we entered the realm of terminated long-wires, we warned that the path through the topic would not be as simple as it might seem at the portal. Since out goal has been–and continues to be–to naturalize ourselves to the behavior of terminated long-wire beams via extensive NEC modeling of the antenna, we faced both antenna and model design questions. Combined with these questions was the impurity of the resulting traveling-wave antenna, since we would use simple resistive loads rather than complex impedances.

The Laport type of terminated long-wire places the terminating impedance ¼ λ inward from the antenna end opposite the feedpoint. Although restricted in bandwidth, the Laport configuration allowed us to sample models in free-space for direct comparison with free-space data for comparable unterminated antennas

covered in Chapter 1. The Laport models also allowed us to sample the maximum performance of which the terminated long-wire is capable within the range of sampled lengths. Nonetheless, we noted that the terminated long-wires suffered a significant gain deficit relative to unterminated versions. Whether the gain deficit represents a fair trade for the great reduction in rear quadrant radiation and sensitivity is a judgment requiring a set of communication goals and specifications.

We replaced the Laport configuration with the more common configuration of terminated long-wires. These antennas use vertical legs to simplify both feeding and loading, since the source and the terminating resistor appear just above and connected to ground. However, before we could perform an adequate guiding survey of the performance of common-configuration long-wire beams, we had to decide upon an adequate model using NEC-4, the core of choice for this set of exercises. Once we settled on the use of ground rods to provide a model most like those that many amateurs might use, we uncovered the chief reason for employing terminated long-wire beams: their very wide operating bandwidth.

Common-configuration long-wire beams only permit a survey over ground, and we sampled horizontal wire lengths from 3 through 11 λ at heights of 0.5 λ though 2 λ. In the process, we uncovered some lesser-known facts about the antenna. For example, not only does the common-configuration long-wire beam show a gain deficit relative to unterminated long-wires, it also yields lower gain than comparable Laport configuration antennas. The source of the lower gain lies in the vertical legs, which radiate a strong vertically polarized component of the total pattern. The common-configuration azimuth patterns show very shallow to nearly non-existent nulls between sidelobes, reducing the available energy for forward gain. As well, the vertical legs produce numerous relatively strong high-angle lobes in both forward and rearward directions.

Despite the lower gain per unit of horizontal length and the serious elevation and azimuth sidelobes, the common-configuration long-wire beam remains in service. Indeed, new installations have appeared within this century. Modern communications techniques in the HF region call for very high frequency agility, in many instances requiring antennas with exceptionally wide operating bandwidths.

Compared to the log periodic dipole array (LPDA), a terminated long-wire is simple, cheap, and relatively easy to maintain. The cost of installation is acreage and tall supports rather than complex and weather-susceptible electro-mechanical assemblies. A collection of long-wires set radially around a central operating station provides coverage of any desired part of the horizon. As well, such antennas provide excellent back up for more easily injured LPDAs and their rotators.

In the history of long-wire technology, the next developmental step was to discover a way to combine lobes from two wires to form a single main lobe of improved strength. In terms of required acreage for the antenna, a V configuration proved to be the most conservative design. However, as we shall see, terminating a V array will present us with both design and modeling challenges not dissimilar to the ones we faced with simpler single long-wires.

3.

V Arrays and Beams

V antennas have the following characteristics:
1. The structural design is simple and economical.
2. The electrical circuitry is simple, when they are fed from the apex.
3. High gain is secured at relatively low cost.
4. They use low supporting structures but require large areas.
5. The horizontal beam width and the elevation of the point of the main beam are not separately controllable but are mutually dependent on the geometry of the array.

Edmund Laport, *Radio Antenna Engineering*, pp. 311-312

Letters (that is, A through Z) constitute one of the favorite designators for antennas. The two most used English letters for antennas are L and V, both of which come in plain and inverted forms. L will not have a place in these notes to designate a type of long-wire antenna. However, V has become the label of at least 2 long-wire antennas. **Fig. 3-1** shows two shapes, one an inverted or bent V, the other a V array.

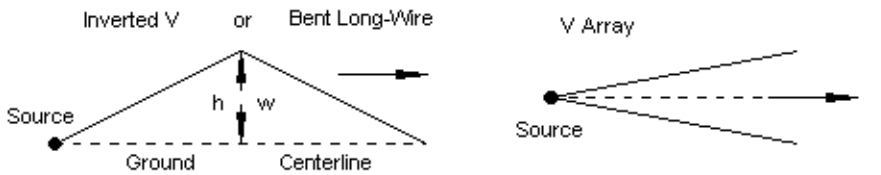

When Is a V "Really" a V?

Fig. 3-1

In Chapter 2, we briefly explored the properties of the bent long-wire, a horizontal V. The dimension at the center (w) marks the widest spread of the antenna. If we rotate the antenna so that the widest point becomes a vertical dimension (h), then we have an inverted V. Adding a terminating resistor at the end of the wire opposite the source gives us a terminated inverted V, an antenna analyzed initially by Bruce in his 1931 article, "Developments in Short-Wave

Directive Antennas." In contrast stand the V arrays and beams, characterized by the quotation that began this chapter. Our chief topic will be the V array and beam, but perhaps we should spend a few moments examining the inverted V.

Long after Bruce analyzed the terminated inverted V, others began to call the antenna a "half rhombic." (The first "half-rhombic" reference to the antenna that I find is Mullaney's January, 1946 *QST* article.) If Bruce's analysis is correct and if we accept his premise for the design, then the "rhombic" label that implies high gain is possibly a misunderstanding of the intended use for the antenna. In fact, the flattop common-configuration terminated long-wire beam finds more favor with those who need a very broadband directional wire antenna. Nevertheless, let's set up a comparison for 8-λ antennas of each type with equal peak heights, as shown in **Fig. 3-2**.

Fig. 3-2

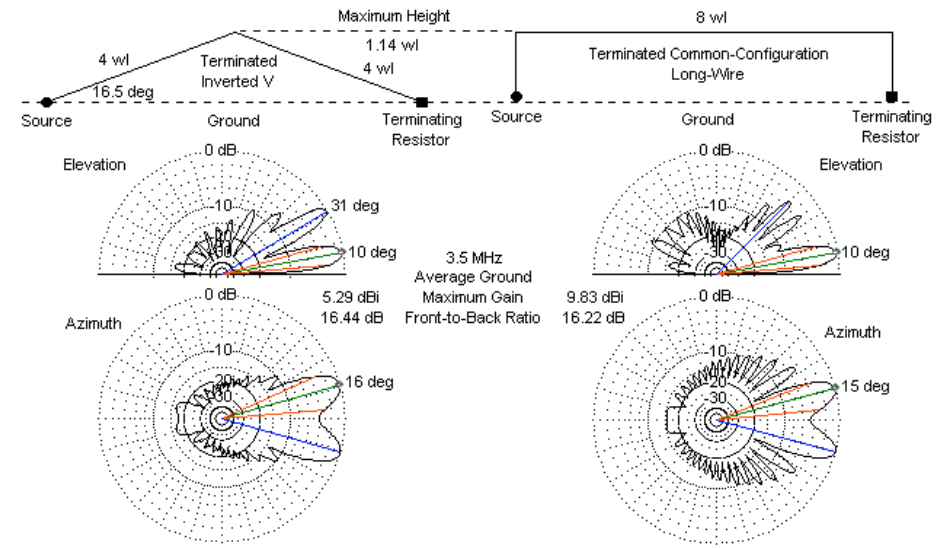

Sample Comparison: Terminated Inverted V and Terminated Common-Configuration Long-Wire

For maximum gain from the lowest inverted V lobe, the required angle between the wires and ground is about 16.5°. One-half the angle between wires at the apex of the V becomes 73.5°. Bruce termed this angle the "tilt" angle. His own chart shows a value of about 70°, but his idealized calculations did not use average ground, the ground quality used for the sample antennas. The total wire length, from ground rod to ground rod, is 8 λ, the same length as the horizontal wire in the common-configuration terminated long-wire. The inverted V uses a 600-Ω terminating resistor in contrast to the 800-Ω resistor used for the level long-wire. As with all models in these notes, the test frequency is 3.5 MHz, while the 0.16" lossless wires use 20 segments per wavelength. The inverted V uses 0.05-λ ground rods similar to those of option D, the model used for all of the common-configuration terminated long-wires.

The patterns in **Fig. 3-2** show one aspect of the inverted V's radiation, especially the elevation pattern. At an angle of 16.5° upward tilt, the lowest lobe is the strongest but just barely so. The second lobe is less than 0.2-dB weaker. If we increase the angle of upward tilt, then the second lobe becomes the stronger of the two. As well, the third lobe begins to grow so that by an angle of 22°, it is less than 1.5 dB weaker than the lower two lobes. Shrinking the upward-tilt angle reduces the forward gain of the array.

Table 3-1 provides comparative data on four 8-λ antennas. The unterminated and Laport antennas from the preceding chapter use data from tables that we have already scanned and appear only for reference. I remodeled the 8-λ common-configuration terminated long-wire at the same peak height as the inverted V, raising an existing 1-λ high model by 0.14 λ. The inverted V falls about 4.5-dB short of the flattop's gain, while the elevation angle, α angle, and front-to-back ratio are all comparable. Remember that the common-configuration long-wire is already 2-dB shy of the Laport version and 3.7-dB weaker than an unterminated 8-λ wire.

In checks from 2 through 5.25 MHz, the inverted V's lowest lobe remained strongest, although forward gain was proportional to frequency. However, with rising frequency, the third lobe grew stronger, and above 5.25 MHz, all three lobes had nearly equal strength. Only the highest of the 3 lobes had an azimuth

pattern resembling those that we shall come to expect from rhombics (in the next chapter).

Comparison of 8-Wavelength Terminated Inverted V and Terminated Common-Configuration Long-Wire over Average Ground						
Antenna	El Tilt deg	Max Ht	Gn dBi	FB dB	El Angle	alpha
Unt LW	na	1	13.50	2.27	12	14
Laport	na	1	11.90	18.73	12	14
CC-LW	na	1.14	9.83	16.22	10	15
Inverted V	16.5	1.14	5.29	16.44	10	16
Notes:	Antenna = unterminated long-wire, Laport terminated long-wire, common-configuration long-wire, and terminated inverted V					
	El Tilt deg = angle of inverted-V wire from ground					
	Max Ht = antenna maximum height in wavelengths; values for Unt LW and Laport antennas shown only for reference					
	Gain dBi = Maximum gain in dBi					
	FB dB = 180-degree front-to-back ratio in dB					
	El Ang = Elevation angle of maximum radiation in degrees					
	alpha = Main lobe angle in degrees					Table 3-1

Given the great gain deficit of the terminated inverted V, we might wonder why one would use such an antenna. The answer lies in the fundamental interests that motivated Bruce to develop and analyze the configuration: reception. One of the principal goals that underlay the 1931 article was obtaining as much freedom from "static" that arose from azimuth headings outside those encompassed by the main split lobes. Comparing the azimuth patterns in **Fig. 3-2** shows us what the inverted V accomplishes by way of contrast to the common-configuration. All side lobes (except perhaps for the rearmost) are much weaker than the corresponding sidelobes for the common-configuration. The elevation patterns also shows a considerable reduction in rearward lobes compared to the flattop antenna. For reception–even in 1931–raw gain was a secondary parameter compared to directivity and sidelobe control. Although the second elevation lobe might invite shorter-range forward "static," the terminated inverted V appeared to offer superior freedom from unwanted natural and man-made signals in all other directions.

The chief advantage of the terminated inverted V beam is the suppression of sidelobes that occur in common-configuration long-wire beams. However, the pattern shown in **Fig. 3-2** only includes the lower lobe. Even at the design frequency (3.5 MHz), the terminated inverted V beam shows considerable disparity in the azimuth patterns of the two main elevation lobes. The lobes occur at 10° and at 30°. **Fig. 3-3** compares the relevant azimuth patterns. The severely reduced sidelobe structure that occurs at the lower angle does not also occur at the high angle. As a consequence, the inverted V beam may show higher than anticipated levels of "static" from shorter-range sources.

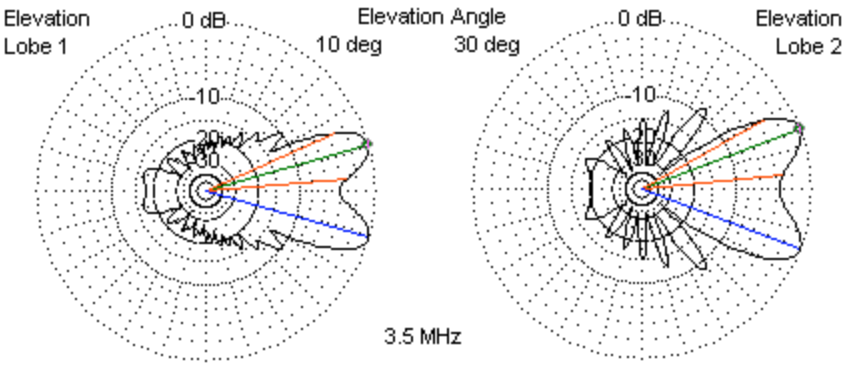

Terminated 8-Wavelength Inverted V
Azimuth Patterns of 2 Main Elevation Lobes

Fig. 3-3

The terminated inverted V beam remains in use today. However, except for its ability to cover a wide range of frequencies, it may not offer all of the advantages attributed to it by authors after Bruce.

Our brief look at the terminated inverted V is preliminary to our main focus in this chapter, the V array and beam. However, we should pause to reconsider the conventions that we shall use, especially to designate angles of interest in these more complex arrays. From earliest times, angle designation has been the seat of some confusion as we move from one text to the next.

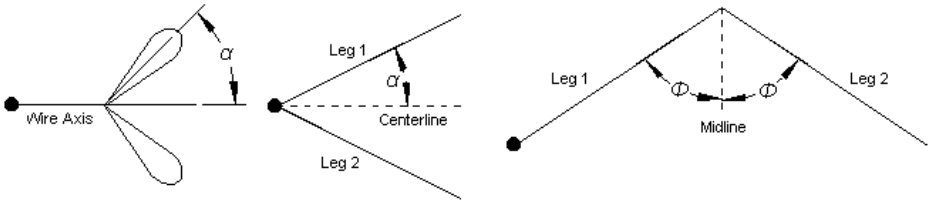

Some Conventional Designations Used in These Notes

Fig. 3-4

We shall eventually explore the calculation of antennas that Bruce called "diamonds" in 1931, but which later become rhombics. Accordingly, we have used the same designation (α) for both the elevation angle and the angle between a long-wire and one of its main lobes, as shown on the left in **Fig. 3-4**. Wherever we need to distinguish a take-off angle from the azimuth angle between a lobe and a wire, we simply refer to the take-off angle as the elevation angle. In free space, of course, we find no difference in lobe angles with respect to a long-wire, since we need not deal with a lossy ground medium. As well, when we arrive at rhombic calculations, using α for both the elevation angle and the wire-to-lobe angle will make eminent sense.

As we examine V arrays and beams, we shall discover that the angle between each V leg and a centerline that splits the wires is intimately related to α. Hence, we shall use α to designate this angle, as shown at the center of the figure. In a V array or beam, the strongest lobe will be along the centerline, so the meaning of α will not have changed. In bent long-wires, inverted Vs, and rhombics, wires will longitudinally join at ends, forming a pair of angles on each side of what we may call the midline. These angles are the tilt angles that bear the designation Φ, as shown on the right in **Fig. 3-4**. Throughout these notes, the angle designations will remain consistent.

Not all early articles and later textbooks use the same conventions. Kraus uses conventions similar to the ones used here. However, for angle α when designating a horizontal angle, Laport uses Φ_m, as do Stutzman and Thiele. Balanis uses Φ_0. Early articles are more highly variable, since rigorous

conventions had yet to develop. Nevertheless, if you look into the history of long-wire technology, you can find your way around with some care.

V Array Basics

V arrays and beams rest on a particular way of combining the main lobes from two long wires. **Fig. 3-5** provides the basic idea behind the use of a V formation to effect the combination. For simplicity, only the main or strongest forward lobes appear in the sketch. However, all lobes participate in the process.

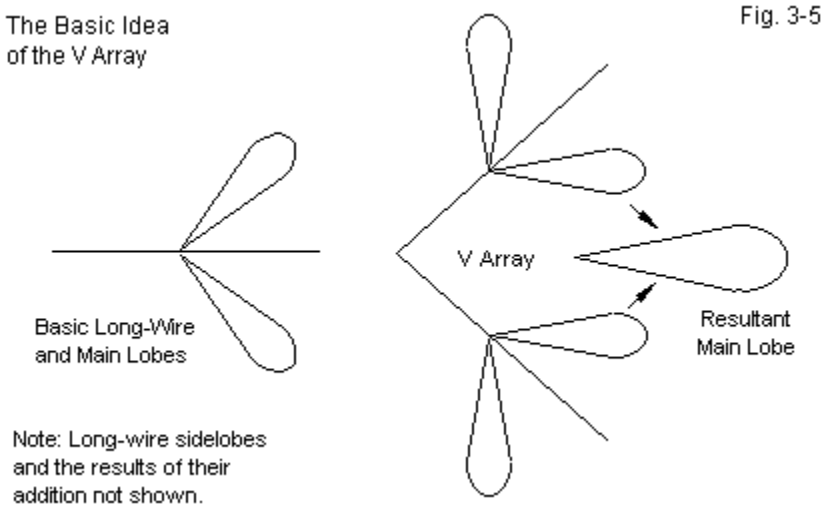

If we select the correct wire angle, two main forward-lobes–one from each wire–combine into a single stronger lobe. Its direction is along the centerline between the two wires. If the array wires are not terminated, then a similar combination forms rearward to the V.

V Arrays in Free Space: The fundamental idea behind the V array is not as simple as it seems. The individual long-wires in free-space produced well-

behaved patterns with lobes that many authors characterize as tunnels. **Fig. 1-5** provided a 3-dimensional outline of such a pattern for a 4-λ long-wire. In contrast, the V array has more than just length: it is a planar array. Consequently, we should not expect to see identical E-plane (in the plane of the structure) and H-plane (at right angles to the structure plane) patterns. The sample patterns in **Fig. 3-6** do not disappoint our expectations.

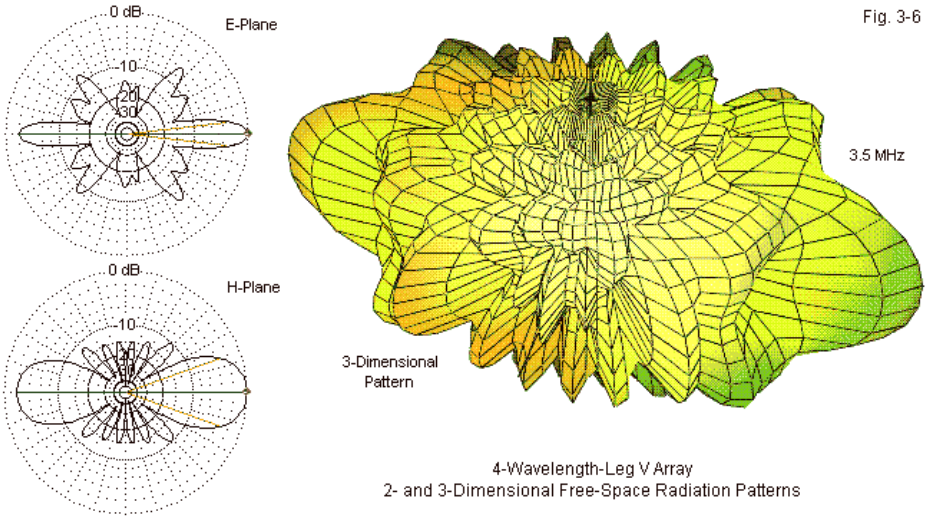

Fig. 3-6

4-Wavelength-Leg V Array
2- and 3-Dimensional Free-Space Radiation Patterns

The H-plane pattern seems well behaved and normal with one exception. It lacks 2 lobes relative to a single long wire. The wide main lobes are actually combinations of 2 lobes. More striking is the E-plane pattern, which would become an azimuth pattern over ground. The same lobes are present, but with revised angles and strengths relative to the H-plane pattern. The combined forward and rear main lobes are both strong and narrow. Since the antenna is optimized for maximum gain from the main lobes, the sidelobes in the E-plane are normally left to become whatever results from the sidelobe angles of each wire in the V. Because the V array is asymmetrical around the centerline, a 3-dimensional representation of the radiation pattern turns out to be almost a confusing bristle of lobes and nulls.

We may model free-space V arrays from 2 through 11 λ using the same standards that we have applied to all models. The 0.16" diameter lossless wire will use 20 segments per wavelength. The length measurement refers to the length of each leg in the V. The total array length will be slightly shorter, the exact amount depending on the angles. In order to create "perfect V shapes, each model uses a split source, with a source segment on each leg in series with each other. **Table 3-2** catalogs the modeling results, along with supplemental information. For the V array, the α angle is the angle between one wire and the array centerline. The total array V-angle is simply 2α.

Free-Space Lossless V Arrays 2 to 11 Wavelengths							Table 3-2
Len WL	Gain dBi	FB dB	alpha	BW deg	alpha Cal	EF Gn	Diff
2	8.26	1.44	33.5	19.4	33.7	4.81	3.45
3	9.66	1.84	28.5	15.4	27.4	6.05	3.61
4	10.83	1.91	24.0	13.6	23.7	6.98	3.85
5	11.61	2.10	21.0	12.2	21.1	7.72	3.89
6	12.33	2.15	20.0	10.8	19.3	8.34	3.99
7	12.95	2.21	18.0	10.2	17.8	8.87	4.08
8	13.42	2.32	16.5	9.6	16.6	9.33	4.09
9	13.88	2.39	16.0	8.8	15.7	9.74	4.14
10	14.31	2.39	15.0	8.4	14.9	10.11	4.20
11	14.67	2.43	14.0	8.2	14.2	10.45	4.22
Notes	Len wl = Leg Length in wavelengths						
	Gain dBi = Maximum gain in dBi						
	FB dB = 180-degree front-to-back ratio in dB						
	alpha = Wire angle to centerline in degrees						
	BW deg = main lobe beamwidth in degrees						
	alpha Cal = Calculated angle in degrees; alpha = 0.95 arccos [1-(0.371/L)]						
	L = wire (leg) length in WL						
	EF Gn = Maximum gain, end-fed wire in free space						
	Diff = Gain difference between V array and end-fed wire						

For single end-fed long-wires, we found an equation to calculate the value of α without modeling. The equation is accurate within about 0.5°. The V array is susceptible to a similar equation.

$$\alpha = 0.95 \cos^{-1} [1 - (0.371/L_{\lambda})]$$

The equation is identical to the one for long-wires in Chapter 1, except that we have added a multiplier (0.95). Essentially, to achieve maximum gain, we must use a slightly narrower angle than the value of α for a single long-wire might suggest. Many authors place the value of the multiplier nearer 0.8, but as the columns for calculated and NEC-derived values for α indicate, 0.95 is far more accurate for free-space models. The NEC values derive from sequences of models that varied the angle in half-degree increments. Hence, there is an inherent ambiguity in the NEC value that may be up to +/-0.5°.

The table also lists the maximum gain values for single end-fed unterminated long-wires, along with the gain advantage of the V array over those wires. Many individuals presume that combining the signal strength or field intensity of two identical lobes would yield a 3-dB power gain advantage. However, if you extract the beamwidth data from **Table 1-6** and compare it with the beamwidth data in **Table 3-2**, you will discover one reason for the additional gain advantage. The V array beamwidths range from 70% to 72% of the single long-wire beamwidths across the 2-λ to 11-λ leg-length span. As the V array grows longer, the gain advantage over a single long-wire increases. As **Table 3-2** shows, the small front-to-back ratio for the unterminated array also remains as an inheritance from the single end-fed long-wire. Like the single long-wire, the unterminated V array is not a pure standing-wave antenna. The front-to-back ratios are almost identical for the two types of unterminated antennas for any given leg length.

With end-fed long-wires, we found that certain performance and pattern-shape characteristics repeat with every half-wavelength increase in leg length. In fact, the pattern shapes and the maximum gain values for odd multiples of a quarter wavelength proved to be significantly different from corresponding properties of even multiples of a quarter wavelength. To see if, and to what degree, the same phenomenon occurs with V arrays, I modeled and optimized for maximum gain a sequence of free-space Vs with legs from 4.0 λ to 5.0 λ using an increment of 0.125 λ. The survey results appear in **Table 3-3**.

Performance Transitions: Free-Space V Arrays				
4 to 5 WL in 0.125-WL Increments				
Len WL	Gain dBi	FB dB	alpha	BW deg
4.000	10.83	1.91	24.0	13.6
4.125	10.87	2.13	23.5	13.2
4.250	11.05	2.19	23.0	13.0
4.375	11.24	2.01	22.5	13.0
4.500	11.26	1.99	22.0	13.0
4.625	11.33	2.26	21.5	12.6
4.750	11.44	2.23	21.0	12.6
4.875	11.60	2.10	21.0	12.6
5.000	11.61	2.10	21.0	12.2
Notes	Len wl = Leg Length in wavelengths			
	Gain dBi = Maximum gain in dBi			
	FB dB = 180-deg. front-to-back ratio in dB			
	alpha = Wire angle to centerline in degrees			
Table 3-3	BW deg = main lobe beamwidth in degrees			

At first sight, the tabulated results appear to be quite orderly. Gain increases steadily from a leg length of 4 λ to a length of 5 λ. Likewise, the values of α and beamwidth show expected declines over the same range. Only the front-to-back ratio–as small as it is–seems to show some possibly random variations.

Even the E-plane patterns seem to vary in only small ways. **Fig. 3-7** shows the pattern sequence from 4.0 λ to 4.5 λ, since the remainder of the total sequence would only replicate the small variations. When the leg length is at a multiple of a half wavelength, the sidelobes nearest 90° from the array centerline are weakest. Between these points, they increase in strength by up to 5 dB relative to the strength of the main forward lobe. Operationally, the difference would be unlikely to be operationally noticeable, since the lobes are inherently the weakest of the entire set of E-plane sidelobes. Nevertheless, the pattern is interesting because it reverses the pattern that we uncovered for single long-wires. The lobes nearest 90° to an end-fed long-wire tended to be weaker when the array was an odd multiple of a quarter wavelength and somewhat stronger when the antenna length approached a multiple of a half wavelength.

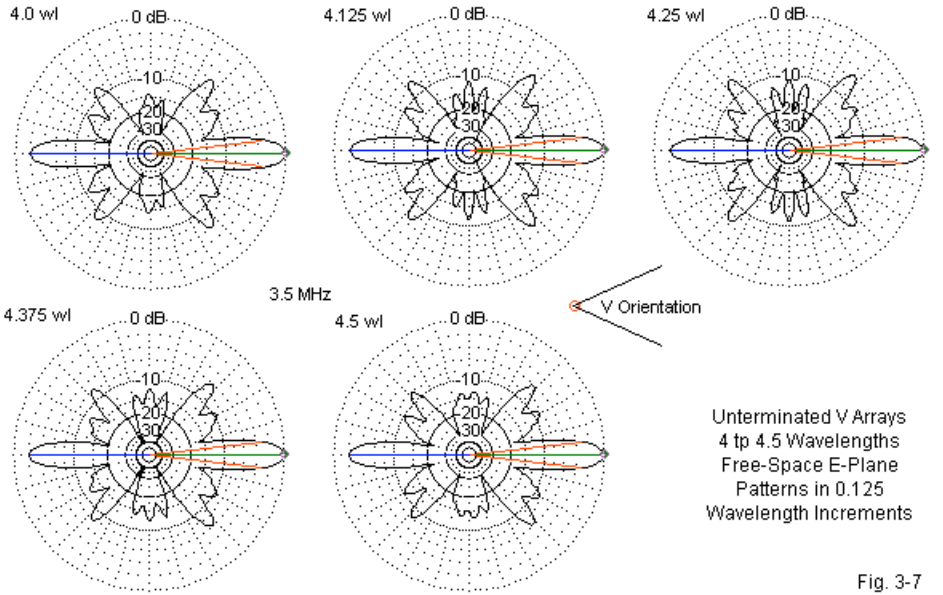

Fig. 3-7

The vestiges of single long-wire behavior show up in more subtle ways if we graph the data. For example, **Fig. 3-8** plots the values of maximum gain and 180° front-to-back ratio for the sequence of V arrays in free space. The presence of 2 cycles with multiples of a half wavelength as end points is an advantage to establishing a pattern rather than simple random variations. The gain values form a virtual plateau for about 1/8 λ on each side of a multiple of a half wavelength. The gain rise between plateaus is relatively steep.

The front-to-back ratio is equally cyclical. Past each multiple of a half-wavelength, the ratio increase is steep and then levels off up to an odd multiple of a quarter wavelength for the leg length. Past that point, the decline is equally steep, followed by another relative leveling of the value as it approaches an even multiple of a quarter wavelength. The curve shapes are not identical due to the small range of values involved and the 0.5° increments of α used in modeling the sequence.

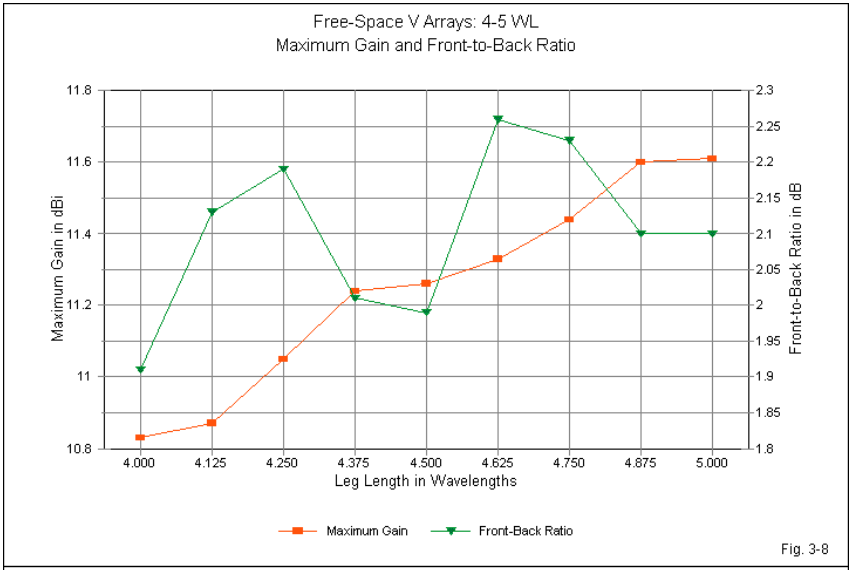
Free-Space V Arrays: 4-5 WL
Maximum Gain and Front-to-Back Ratio
Maximum Gain in dBi
Front-to-Back Ratio in dB
Leg Length in Wavelengths
11.8
11.6
11.4
11.2
11
10.8
2.3
2.25
2.2
2.15
2.1
2.05
2
1.95
1.9
1.85
1.8
4.000
4.125
4.250
4.375
4.500
4.625
4.750
4.875
5.000
Maximum Gain
Front-Back Ratio

Fig. 3-8

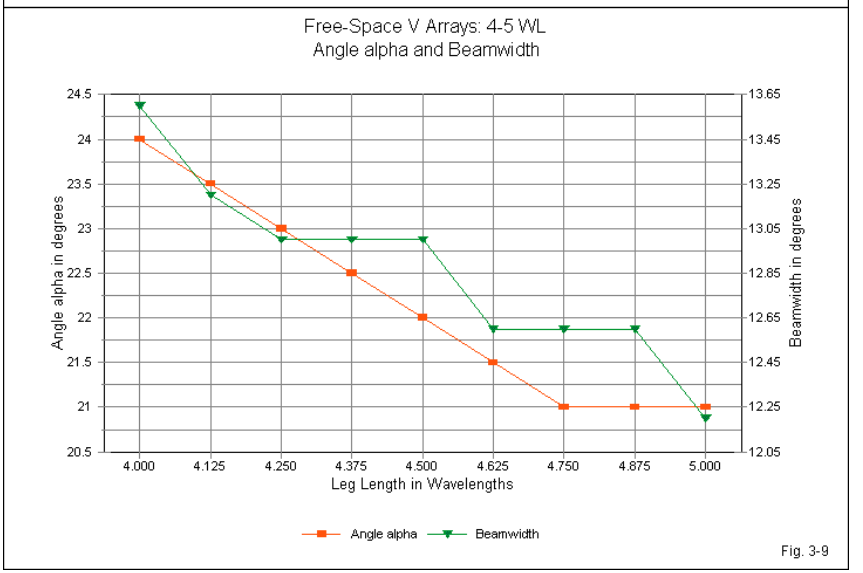
Free-Space V Arrays: 4-5 WL
Angle alpha and Beamwidth
Angle alpha in degrees
Beamwidth in degrees
Leg Length in Wavelengths
24.5
24
23.5
23
22.5
22
21.5
21
20.5
13.65
13.45
13.25
13.05
12.85
12.65
12.45
12.25
12.05
4.000
4.125
4.250
4.375
4.500
4.625
4.750
4.875
5.000
Angle alpha
Beamwidth

Fig. 3-9

As shown in **Fig. 3-9**, value of the α angle is most immune to the cyclical effects of the small transitions in leg length. However, it might have shown some small cycling had I used a smaller angular increment when establishing the value of α for maximum V array gain. Beamwidth values are more susceptible to the effects odd-even multiples of a quarter wavelength. However, the continuous decrease in the beamwidth value with increasing leg length is restricted to a stair-step phenomenon.

In the end, it likely does not matter whether one declares that cyclical long-wire phenomena remain a part of the V array properties or whether one certifies them as too weak to consider. Exploring those characteristics simply reminds us that the V array is electrically an extension of basic long-wire operation.

V arrays over Ground: Terminated V beams have been widely used in HF communications. However, unterminated V arrays have had lesser use, and today, amateurs form the largest group of users. Nonetheless, V arrays have a number of very interesting properties, especially if we compare those properties to comparable ones for single end-fed unterminated wires. For example, a long-wire that is 2 λ or more above ground shows almost no changes in its α angle relative to a free-space or ideal model. At 1 λ above average ground, the α angle narrows significantly below the free-space value for the longest in the sequence of models. Single long-wires also showed considerable differences in α with changes in ground quality. Since the V array is simply two long-wire antennas fed in series at one end and widened to let a main lobe from each wire overlap, we might expect similar results.

For an initial survey, we may move our sequence of models to 2 λ above average ground (conductivity 0.005, relative permittivity 13). At that height, ground influences on the value of α necessary to achieve maximum gain are minimal. **Table 3-4** collects the data for comparison with the free-space data in **Table 3-2**. With respect to the value of α, there is no value that does not fall within the ambiguity of plotting radiation patterns in 1° increments and changing values of α in 0.5° increments. In fact, the elevation angle of maximum radiation is a constant 7° until we reach the longest V array in the sequence. As well, the free-space and the 2-λ front-to-back ratios are virtually identical, as are the

beamwidth values.

Unterminated V Arrays Optimized for Maximum Gain					
2-Wavelengths Above Average Ground					
Len WL	alpha	El Ang	Gn dBi	FB dB	BW deg
2	34.0	7	14.01	1.45	19.8
3	27.5	7	15.33	1.83	16.0
4	23.5	7	16.42	1.91	13.8
5	20.5	7	17.09	2.11	12.6
6	19.5	7	17.69	2.18	11.0
7	17.5	7	18.26	2.20	10.4
8	16.0	7	18.69	2.28	10.0
9	15.0	7	19.02	2.40	9.4
10	14.5	7	19.36	2.42	8.6
11	14.0	6	19.70	2.38	8.2
Len WL = Leg length in WL					
alpha = Wire angle to V centerline					
El Ang = Elevation angle in degrees					
Gn dBi = Maximum gain in dBi					
FB dB = 180-degree front-to-back ratio in dB					
BW deg = Half-power beamwidth in degrees					Table 3-4

As we reduced the antenna height by half to 1 λ above average ground, we anticipate greater shifts in performance between the new environment and free space. The data confirming these expectations appear in **Table 3-5**. 1-λ gain values are lower by an amount that increases as the V arrays grow longer. As well, the front-to-back ratio shows slightly higher values for the longest V arrays at the reduced height.

One factor that affects the smoothness of the data progression is the elevation angle increment of 1°. For the 2-λ data, the front-to-back ratio shows one value that runs against the progression, and it occurs just where the elevation angle changes from 7° to 6° between leg lengths of 10λ and 11 λ. The true elevation angles are close to 6.5°, but the data is for 7.0° and 6.0°

Unterminated V Arrays Optimized for Maximum Gain					
1-Wavelengths Above Average Ground					
Len WL	alpha	El Ang	Gn dBi	FB dB	BW deg
2	33.0	13	13.61	1.41	20.6
3	26.5	13	14.65	1.84	16.8
4	23.5	12	15.48	1.86	14.2
5	19.5	12	16.00	2.03	13.6
6	17.0	12	16.28	2.22	13.0
7	17.0	11	16.62	2.27	11.2
8	15.5	11	16.91	2.29	11.0
9	14.0	11	17.10	2.37	10.2
10	13.0	10	17.24	2.47	10.2
11	12.0	10	17.35	2.56	10.2
Len WL = Leg length in WL					
alpha = Wire angle to V centerline					
El Ang = Elevation angle in degrees					
Gn dBi = Maximum gain in dBi					
FB dB = 180-degree front-to-back ratio in dB					
BW deg = Half-power beamwidth in degrees					Table 3-5

We find some stair stepping in the values for α in the 1-λ data. However, as shown in **Fig. 3-10**, the more significant aspect of the data is the tight fit between values of α for any leg length for any of the tested environments. The maximum differential in α between free-space and 1 λ above average ground is 3°, and that occurs at an elevation angle that is transitioning from 12° to 11°.

Values of α over ground are always less than their free-space counterparts. In contrast, values of beamwidth over ground are always greater than in free space. As we lower the antenna, the beamwidth becomes larger, with long leg lengths showing the highest differential. **Fig. 3-11** graphs the modeled values of beamwidth, subject to the stair-step phenomenon. The free-space and the 2-λ values are almost perfectly coincident, but the values for 1 λ above average ground show an ever-widening divergence. These trends in performance data are consistent with the comparable data in Chapter 1 for unterminated long-wires.

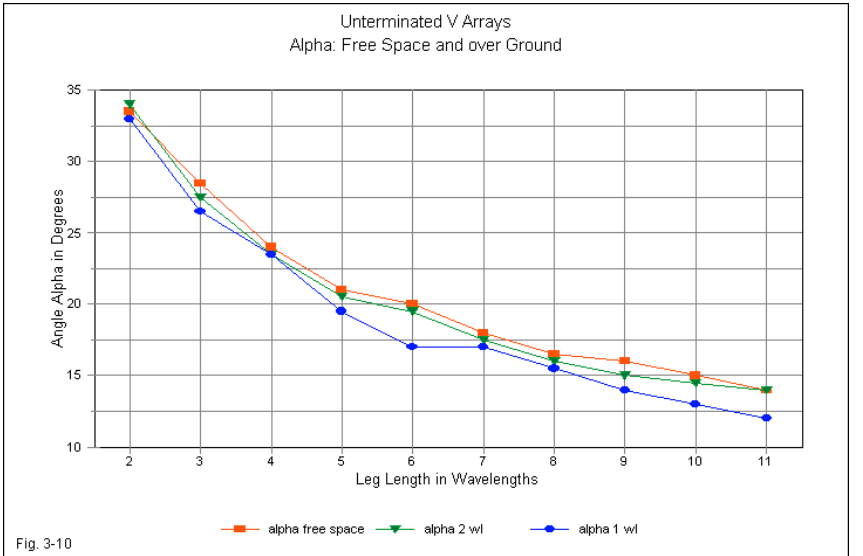

Fig. 3-10

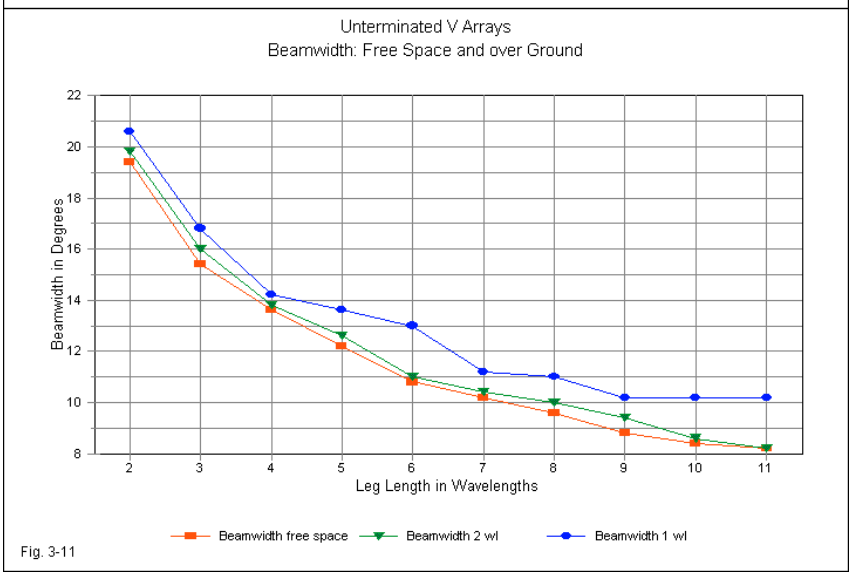

Fig. 3-11

In one respect, we may consider the V array to be better behaved than a single long-wire. The unterminated long-wire showed some significant differences in the value of α as we changed the ground quality over the range from very good (conductivity 0.0303 S/m, relative permittivity 20) down to very poor (conductivity 0.001 S/m, relative permittivity 5). We may sample comparable data for V arrays by using leg lengths of 3, 6, and 9 λ, all at 1 λ above ground. **Table 3-6** supplies the results.

Unterminated V Arrays over Various Ground Qualities: Height = 1 WL above Ground							
Len WL	Ground	alpha	al Range	El Ang	Gn dBi	FB dB	BW deg
3	Very Good	26.5	25.5-27	13	14.82	1.85	17.4
	Average	26.5	25.5-27	13	14.65	1.84	16.8
	Very Poor	26.0	25-26.5	13	14.29	1.84	16.8
6	Very Good	17.0	16.5-17	12	16.32	2.28	13.8
	Average	17.0	16.5-17	12	16.28	2.22	13.0
	Very Poor	17.0	17-17.5	11	16.08	2.16	12.6
9	Very Good	14.0	14	11	17.10	2.46	11.4
	Average	14.0	14	11	17.10	2.37	10.2
	Very Poor	14.0	14	10	17.01	2.28	10.2
Len WL = Leg length in WL							
Ground = Very Good (C 0.0303 S/m, P 20), Average (C 0.005 S/m P 13),							
	Very Poor (C 0.001 S/m, P 5)						
alpha = Wire angle to V centerline							
al Range = Range of alpha values in degrees for maximum gain							
El Ang = Elevation angle in degrees							
Gn dBi = Maximum gain in dBi							
FB dB = 180-degree front-to-back ratio in dB							
BW deg = Half-power beamwidth in degrees							Table 3-6

The value of α for maximum gain is less critical for short V arrays, so I have included the range of values that produced the listed gain. The listed values of α for maximum gain result from averaging the rate of change of other performance parameters on each side of the value. Note that only for the shortest V array is there a difference in the alpha column based on ground quality. As well, note the very small change in maximum gain as the ground quality changes. As a V array grows longer, it appears more immune to performance changes occasioned by ground losses.

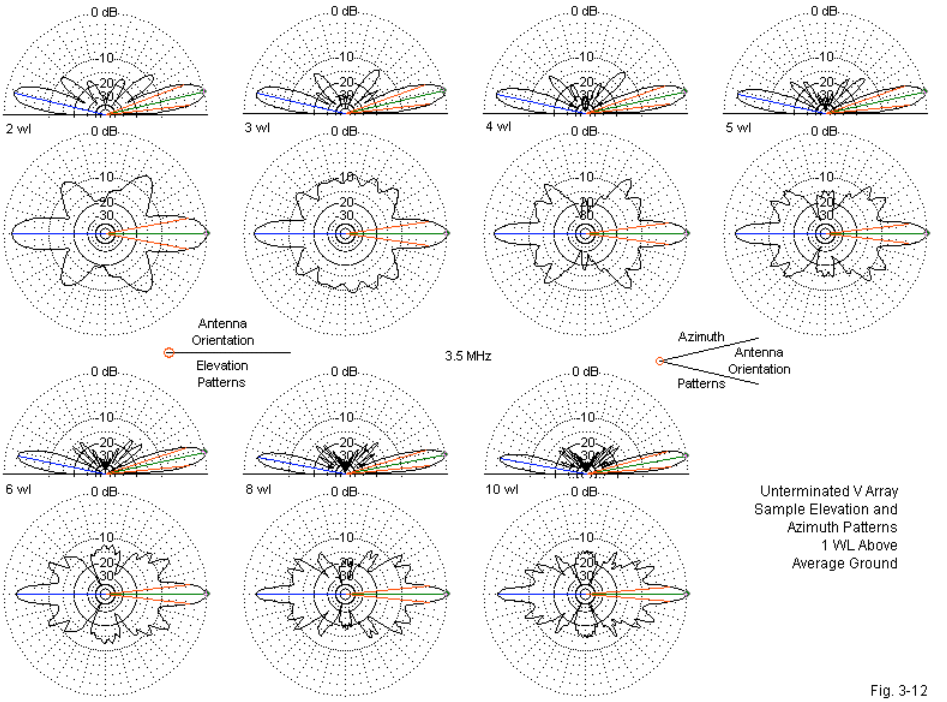

Fig. 3-12

Lest we overstate the advantages of the unterminated V array, we should examine the sample elevation and azimuth patterns in **Fig. 3-12**. The elevation patterns do show very good suppression of higher-angle lobes, and the suppression increases as the V array legs grow longer. However, the chief disadvantage of the V array in the original HF point-to-point context of use is the strength of the azimuth sidelobes. In the forward direction, the V array presents a broad transmitting and receiving front that is only 6-7-dB weaker than the narrow main lobe. Static, man-made interference, and signal security were issues that occasioned developments beyond the V array. Even the terminated V beam could not overcome the azimuth sidelobe issues.

For the amateur user of a V array, perhaps the key issue is the narrow

beamwidth. A long wire V array or beam is economical, but very confining. Even a collection of V arrays would leave much of the radio horizon with weak or negligible coverage.

Before we terminate our work with V arrays and beginning terminating the array to form a directional beam, we should satisfy at least one point of curiosity: What happens to the performance of a V array if we depart in either direction from the optimized value of angle α? We can find part of the answer in **Table 3-7**, which records at 2° α-intervals the free-space performance of a V array with 4-λ legs.

Free-Space Unterminated V Array with 4-WL Legs				
Performance Evolution with Changing Values of alpha				
alpha	Gain dBi	FB dB	BW deg	Notes
14	8.37	2.08	26.8	Max BW
16	9.32	1.97	21.1	
18	9.92	2	18.2	
20	10.33	2.07	16.2	
22	10.67	2	14.6	
24	10.83	1.91	13.6	Max Gain
26	10.68	1.92	12.6	
28	10.27	1.94	12	
30	9.61	1.85	11.6	
32	8.55	1.72	11.8	
34	7.51	1.81	11.4	3 lobes
alpha = Wire angle to V centerline				
Gain dBi = Maximum gain in dBi				
FB dB = 180-degree front-to-back ratio in dB				
BW deg = Half-power beamwidth in degrees				Table 3-7

With each incremental departure from the optimum value of α, the gain decreases, slowly at first, and then more precipitously. If α is 10° off the mark, the gain is down by 2.5-3 dB, depending on the direction of departure. Equally notable is the fact that the beamwidth increases as the angle grows smaller. As the α-angle increases, the main lobe beamwidth decreases. However, the

immediate sidelobes increase in strength. As a result, when the value of α is 10° high, the pattern shows three lobes, and the central lobe that aligns with the V centerline is no longer the strongest. **Fig. 3-13** provides a sample of pattern development across the surveyed range of α values, using 5° intervals. All polar plots use the same power gain value for the outer ring, that is, the gain of the array with an optimal value of α. Therefore, the differences of maximum gain also appear in the pattern sequence. For the 34° pattern, if we ignore the nulls between the three forward lobes, the overall beamwidth is about 37°. If the reduced gain level is acceptable, one might develop a radial array of 4-λ long-wires and feed any single adjacent pair, arriving at full horizon coverage in 34° steps.

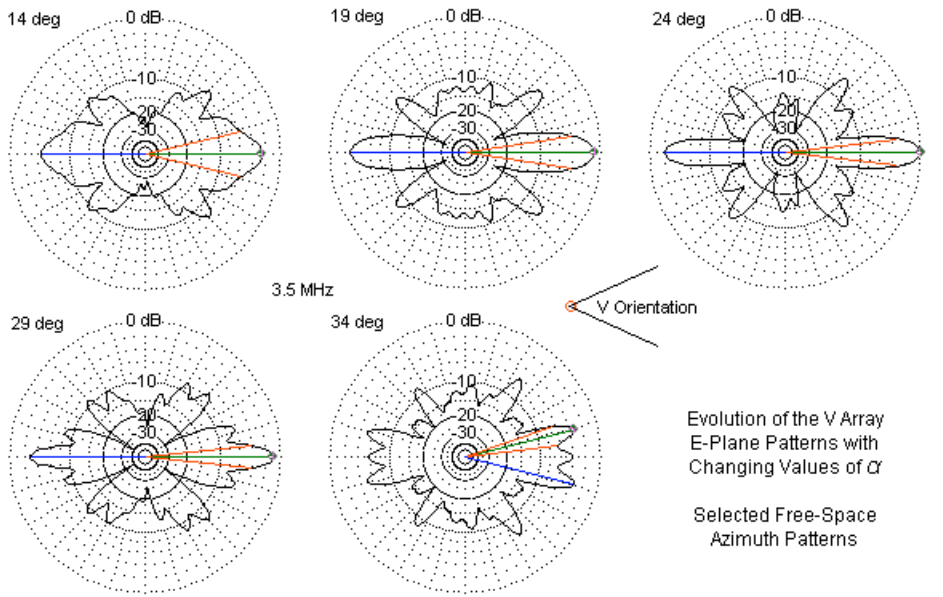

Fig. 3-13

Also apparent from the sample patterns is the changing sidelobe structure as the α-angle changes. As we alter the value of α, secondary lobes for each long-

wire leg add in differing combinations. Whether a given pattern is acceptable for a particular communications need depends upon the detailed objectives and specifications for the project as a whole.

V Beam Basics

Radio amateurs are perhaps the largest group of V antenna users for both unterminated and terminated versions. Terminated V beams come in many forms, but to make our survey relatively comprehensive, we cannot begin with any of the most common implementations. Our initial models should have free-space versions for ready comparison to the free-space models of unterminated V arrays. Virtually all terminated V beams either are wedded intimately to the ground or use construction modes that would make free-space models misleading relative to the unterminated V arrays that we have examined.

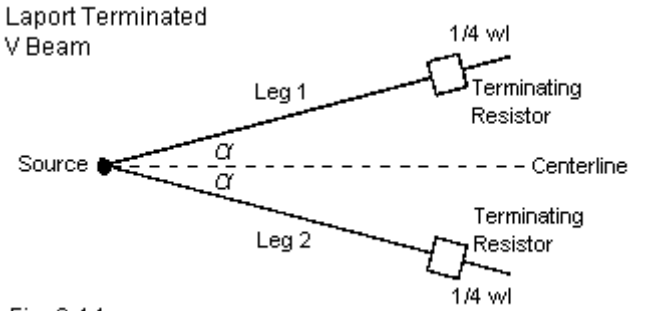

Fig. 3-14

Fortunately, the Laport method of placing terminating resistors on single long-wires also applies to the legs of a V beam. **Fig. 3-14** provides a generalized outline for the antenna. Each load is just about ¼ λ from the far end of the leg, with adjustments in the actual finishing length for reactance compensation. One result will be to make the antenna frequency-specific, since the finishing length will change with the frequency of operation. Our use of the Laport models only include comparing them to free-space unterminated V arrays and providing a frame of reference to determine if common installations penalize the user relative

to more ideal installations. When we examined common-configuration long-wire beams, the vertical legs needed on both the source and termination ends of the wire cost about 2 dB in forward gain compared to what the more ideal but frequency-limited Laport long-wire might produce. As well, the common configuration long-wire beam patterns showed a number of fairly strong high-angle elevation lobes that more ideal installations lack. We shall be interested along the way in seeing if we encounter similar costs associated with the common method of V beam installation that we select for detailed exploration.

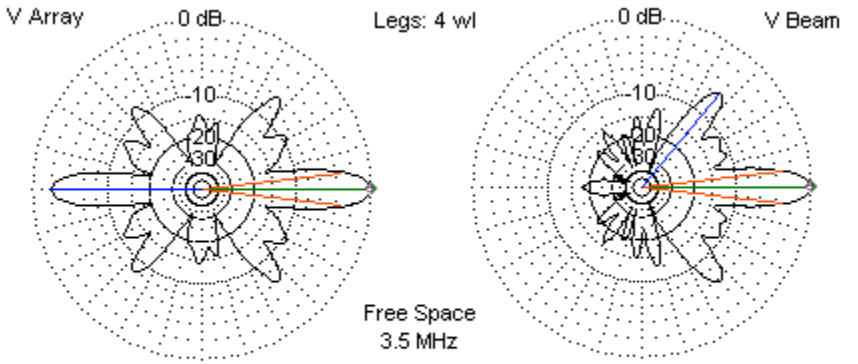

Sample E-Plane Pattern Comparison
4-WL V Array and 4-WL V Beam

Fig. 3-15

Fig. 3-15 gives us a good reason for examining V beams in some detail. Compared to an unterminated V array, the V beam provides a high degree of lobe attenuation in the rear quadrants. Even though all traveling-wave antennas are imperfect–especially those using only resistive terminations–the rear-lobe suppression level of the V beam has provided good reasons historically for antenna builders to obtain the needed non-inductive terminating resistor (or resistors) to develop a directional antenna. However, the termination process does not reduce the forward sidelobe structure significantly, so the forward front-to-sidelobe ratio remains fairly low.

The Laport terminated V beams used in the survey placed twin 800-Ω resistors about ¼ λ inboard from the tips of the V legs. As usual, the antenna model used 0.16" diameter lossless wire at 20 segments per wavelength. The free-space scan sampled models from 2 to 11 λ as the leg-length measure. Besides the data typical of these surveys, **Table 3-8** includes the front-to-sidelobe information, where the ratio is between the main forward-lobe power gain and the strongest sidelobe gain. As suggested by **Fig. 3-15**, the strongest sidelobe is rarely the sidelobe nearest the main lobe. The result is a broad front of forward gain that is down by only a few dB relative to the main lobe.

Free-Space Lossless Laport V Beams 2 to 11 Wavelengths								Table 3-8
Terminating Resistors: 800 Ohms x 2								
Len WL	alpha	Gn dBi	FB dB	BW deg	F/SL dB	alpha Cal	Unter Gn	Diff
2	36.0	4.82	24.47	19.8	7.76	35.5	8.26	3.44
3	29.0	6.64	20.12	15.8	6.13	28.8	9.66	3.02
4	25.0	7.88	18.50	13.2	5.59	24.9	10.83	2.95
5	22.0	8.85	17.69	12.0	5.69	22.2	11.61	2.76
6	20.0	9.63	17.14	10.8	5.71	20.3	12.33	2.70
7	18.5	10.28	16.89	10.0	5.74	18.7	12.95	2.67
8	17.5	10.85	16.66	9.2	5.82	17.5	13.42	2.57
9	16.5	11.35	16.46	8.6	5.86	16.5	13.88	2.53
10	15.5	11.79	16.38	8.4	5.92	15.7	14.31	2.52
11	15.0	12.19	16.31	7.8	5.98	14.9	14.67	2.48
Notes	Len WL = Leg Length in wavelengths							
	alpha = Wire angle to centerline in degrees							
	Gain dBi = Maximum gain in dBi							
	FB dB = 180-degree front-to-back ratio in dB							
	BW deg = main lobe beamwidth in degrees							
	F/SL dB = Front-to-sidelobe ratio in dB							
	alpha Cal = Calculated angle in degrees							
	alpha = arccos [1-(0.371/L)]; L = wire (leg) length in WL							
	Unter Gn = Maximum gain of free-space unterminated V array in dBi							
	Diff = Gain difference between unterminated and terminated V antennas							

The table has a number of interesting data trends. First, the value of angle α for these terminated arrays corresponds more closely to the values modeled and calculated for free-space unterminated long-wires than to the modified calculation used for unterminated V arrays. The difference is about 5%, with the V beam showing the larger value.

Second, the front-to-back ratio and the front-to-side ratio both tend to decrease as the V legs grow longer. The front-to-back ratio decline is continuous, but the front-to-sidelobe ratio tends to be more variable once the legs are longer than about 4 λ. Longer V beams have front-to-sidelobe ratios between about 5.5 and 6.0 dB.

Third, there is a gain penalty to be paid for terminating the V antenna to produce a directional beam. As the legs grow longer, the gain deficit of the V beam relative to its unterminated counterpart decreases by a full dB–falling from nearly 3.5 dB down to just below 2.5 dB. The remaining data tend to show a high degree of correspondence between values of unterminated and terminated V arrays.

Lossless Laport V Beams 2 to 11 WL, 1 WL Above Average Ground								Table 3-9
Terminating Resistors: 800 Ohms x 2								
Len WL	alpha	El Ang	Gn dBi	FB dB	BW deg	F/SL dB	alpha FS	Diff
2	35.5	13	10.02	24.18	20.4	6.73	36.0	0.5
3	28.0	13	11.55	19.90	16.6	7.20	29.0	1
4	23.5	12	12.49	18.22	14.6	6.55	25.0	1.5
5	20.5	12	13.15	17.63	13.2	6.55	22.0	1.5
6	19.0	11	13.62	17.06	11.8	5.92	20.0	1
7	17.0	11	14.01	16.71	11.4	6.29	18.5	1.5
8	16.0	11	14.29	16.62	10.6	6.03	17.5	1.5
9	15.0	10	14.52	16.53	10.0	5.95	16.5	1.5
10	14.0	10	14.74	16.35	9.6	6.08	15.5	1.5
11	13.0	10	14.91	16.22	9.4	5.63	15.0	2
Len WL = Leg length in WL								
alpha = Wire angle to V centerline								
El Ang = Elevation angle in degrees								
Gn dBi = Maximum gain in dBi								
FB dB = 180-degree front-to-back ratio in dB								
BW deg = Half-power beamwidth in degrees								
F/SL dB = Front-to-sidelobe ratio in dB								
alpha FS = Value of alpha angle in free-space models								
Diff = Difference between free-space and 1-wl over ground values of alpha angle								

Although the Laport version of the V beam is an unlikely candidate for installation, **Table 3-9** catalogs the performance data at 1λ above average ground. We shall have occasion to compare this data to a more common way of

installing a V beam later on. For the moment, we may note that the value of α over ground is lower than in the free-space models. The near-constancy of the difference in the value is actually an increase with growing leg length. Every degree of shrinkage in over-ground α, relative to free-space α, is a greater percentage of the actual value of α for the longer legs.

Since the terminating resistor on each leg of a V beam cannot simply float at the end of the wire, broadband implementations of V beams over ground have two basic choices that evolve into several different configurations. One option is to bring the terminated end of the leg wire to ground. Alternatively, we may run a wire between the two terminated wires end and place the non-inductive resistor at the center. **Fig. 3-16** sows general outlines of some (but not all) ways of implementing the options.

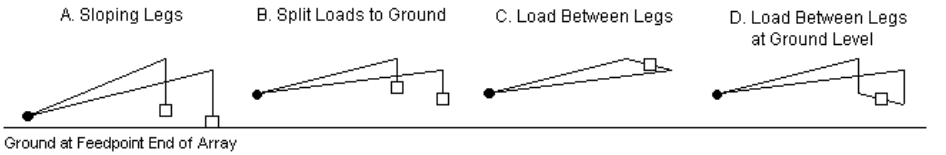

Variations of the Basic Terminated Long-Wire V Beam

Fig. 3-16

Models A and B use the ground as the antenna element and the resistor termination. Both techniques normally involve a vertical wire to ground from each side of the V. (Note that we do not use a vertical wire and a common feedpoint near ground with a V beam. Such a system would feed the legs in parallel, which would yield quite different patterns. The junction of the V legs must use a series feed.) Option A shows that feedpoint near ground, with the far ends of the V legs elevated, in this case to 1 λ above average ground. A reverse arrangement is also possible, raising the feedpoint and lowering the far ends near ground. In both cases, the net result is simply to lower the effective height of the wire to between half and two-thirds the tallest point in the antenna. Option B is similar to either form of option A. The difference lies in placing the antenna at the same height throughout.

Option C is one classical solution to the V beam structure that uses a single resistor for the termination. A wire runs straight across from one leg end to the other, with the terminating resistor at the center. Since it is likely that the cross wire affects performance by being an active part of the radiating structure, option D is an alternative to remove the cross wire from the radiating pattern. Legs run to near the ground, and the cross wire and the centered terminating resistor are very low. In models, this distance is about 0.001 λ.

The fundamental question is not whether these implementations work. They all work. Our evaluation of the options is to find an implementation that fairly represents the operation of the V beam over ground and as a broadband antenna. Selecting the correct values of the terminating resistors is not so simple as it was with the single long-wire beam. The value is not exceptionally critical, although we may have reasons for choosing one value over another. For design purposes, the reasons may involve the best compromise among gain, front-to-back ratio, and impedance. In practical installations, the reasons generally focus on what non-inductive resistors may be available. All models in the trials used V beams with 5-λ legs with a peak height of 1 λ over average ground. The results appear in **Table 3-10**.

The tilted models (A and A1) show that tilting a V beam does virtually nothing to improve its performance. For both models, gain is down by over 4 dB relative to the other options. As well, the take-off angle is higher as a result of the antenna having a lower effective height.

Model B uses the same layout as model A, but raises the feedpoint to the same height as the remainder of the antenna. Like model A, B uses a pair of terminating resistors. The gain and the elevation angle of maximum gain return to normal values, as shown in the test table. The gain level of this model changes very slowly with changes in the values of the terminating resistors. Hence, the table proceeds in 200-Ω increments. Selecting the most optimal combination requires some decision-making based on external criteria, such as a desired feedline characteristic impedance. Note that the feedpoint impedance tends to parallel the value of each terminating resistor, although the feedpoint impedance falls more slowly than the resistance values.

Test Values for Modeling Options: 5 WL legs, 1 WL above Average Ground							
Option A							
Load R	Gn dBi	FB dB	BW deg	El Ang	Feed R	Feed X	SWR 1000
600x2	8.89	23.15	12.2	15	988	184	1.20
700x2	8.91	22.40	12.4	15	1043	145	1.16
800x2	8.93	20.58	12.4	15	1091	109	1.14
Option A1							
Load R	Gn dBi	FB dB	BW deg	El Ang	Feed R	Feed X	SWR 1000
400x2	8.60	18.90	21.0	14	1032	107	1.12
500x2	8.60	18.06	21.2	14	1096	-6	1.10
600x2	8.63	15.99	21.2	14	1141	-109	1.18
Option B							
Load R	Gn dBi	FB dB	BW deg	El Ang	Feed R	Feed X	SWR 800
600x2	13.00	20.62	13.8	12	830	133	1.18
800x2	13.02	18.41	13.8	12	926	190	1.30
1000x2	13.07	16.00	13.8	12	1002	242	1.42
Option C							
Load R	Gn dBi	FB dB	BW deg	El Ang	Feed R	Feed X	SWR 900
800	14.38	12.73	12.6	12	981	192	1.25
900	14.35	13.76	12.6	12	949	147	1.18
1000	14.34	14.73	12.6	12	919	110	1.13
Option D							
Load R	Gn dBi	FB dB	BW deg	El Ang	Feed R	Feed X	SWR 750
600	13.02	21.26	13.4	12	761	-49	1.07
800	13.03	20.64	13.4	12	754	-55	1.08
1000	13.03	20.19	13.4	12	749	-59	1.08
1200	13.03	19.85	13.4	12	744	-63	1.09
Notes	Load R = Terminating resistance value in Ohms						
	Len WL = Total wire length in WL						
	Gn dBi = Maximum gain in dBi						
	FB dB = 180-degree front-to-back ratio in dB						
	BW deg = Half-power beamwidth in degrees						
	El Ang = Elevation angle in degrees						
	Feed R = Feepoint resistance in Ohms						
	Feed X = Feedpoint reactance in Ohms						
	SWR nnn = nnn-Ohm SWR						Table 3-10

The models with resistors that terminate at ground use ground rods similar to

those used in the common-configuration long-wire beams in the preceding chapter. Compare the general values of model B with the 5-λ leg values in **Table 3-9** for the Laport model that is also 1 λ above average ground. The general coincidence suggests that model B is a potential candidate for our extended survey.

Model C uses a single cross wire at the height of the antenna legs, with the terminating resistor at the center of the cross wire. For the 5-λ legs of the test model, the crossing wire is about 3.4 wavelengths. The crossing horizontal wire between the V-leg ends contributes to the array gain in both directions. Hence, the peak forward gain is slightly higher than for model B, but the front-to-back ratio is much lower. Although the model is the structure of a perfectly plausible V beam installation, it would not allow us to make detailed comparisons with the idealistic Laport models.

Model D also uses a crossing wire with a single terminating resistor at its center. However, it brings the crossing wire much closer to ground level. In the model, the wire is 0.001-λ above ground, just enough for the wire to clear the ground by several wire diameters. Each end of the V assembly runs a vertical wire down to the junction with the low crossing wire. As the table shows, this arrangement produces one of the most stable configurations relative to changes of gain with changes of the terminating resistor value. Not only is the gain stable across a 2:1 range of resistor values, but as well, both the front-to-back ratio and the feedpoint impedance are equally stable. Using a very low crossing wire removes it from having a significant affect on the radiation pattern. In fact, the data for models B and D are quite similar, although model D appears to be the more stable. Further tests of the V-beam using various leg lengths will employ model D and a 750-Ω resistor.

The selection of 750 Ω for the terminating resistor is not accidental. Note that for models C and D, as the value of the terminating resistor rises, the feedpoint resistance falls. There is a value of terminating resistor that–at least for the test case–will match the resulting feedpoint resistance. Since the termination does not attempt to compensate for reactance, we shall always find a remnant reactance in the feedpoint impedance. 750 Ω turns out to be a useful value for all

leg lengths using the model D configuration.

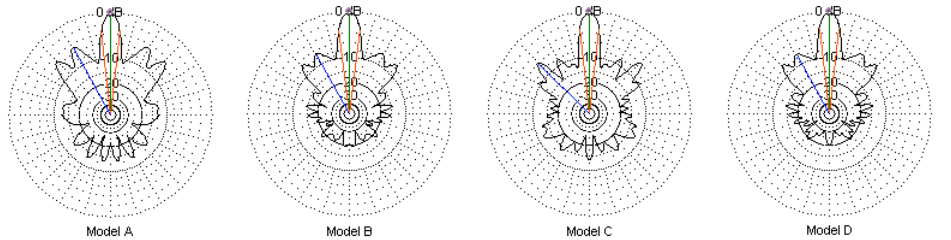

Fig. 3-17 provides azimuth patterns for each of the 5-λ V beam models. They show a family resemblance, especially in the forward structure of the lobes. The sidelobes of model A appear stronger because the forward gain is 4-dB (or more) weaker than for the other models. The data had suggested a close correlation between model B and model D, and the azimuth patterns tend to confirm the suggestion.

Although the 4 models of a V beam use different arrangements and terminating resistor values to arrive at their patterns, all of them have the wide-band characteristic that we saw in the case of single long-wire beams. **Fig. 3-18** provides the SWR curves over a 2:1 frequency range using the optimal feedpoint impedance relative to the indicated values of terminating resistor or resistors. In each case, for the range tested and beyond, a single impedance-transformation device would suffice to match the antenna to most equipment. What all the SWR patterns share in common is the existence of ripples of non-harmful but noticeable proportions. The ripples result in part from the fact that V beams–like the unterminated V arrays that we earlier examined–retain vestiges of the behavior of both terminated and unterminated long-wire antennas. Besides slight gain fluctuations, we also find small variations in the feedpoint resistance and reactance. As a consequence, terminated V beams will almost always show impedance ripples and–as a result–SWR ripples for any selected reference impedance.

Comparative 2:1 Frequency Sweep SWR Curves of 4 Different Implementations of a 5-WL V-Beam 1-WL Above Average Ground

Fig. 3-18

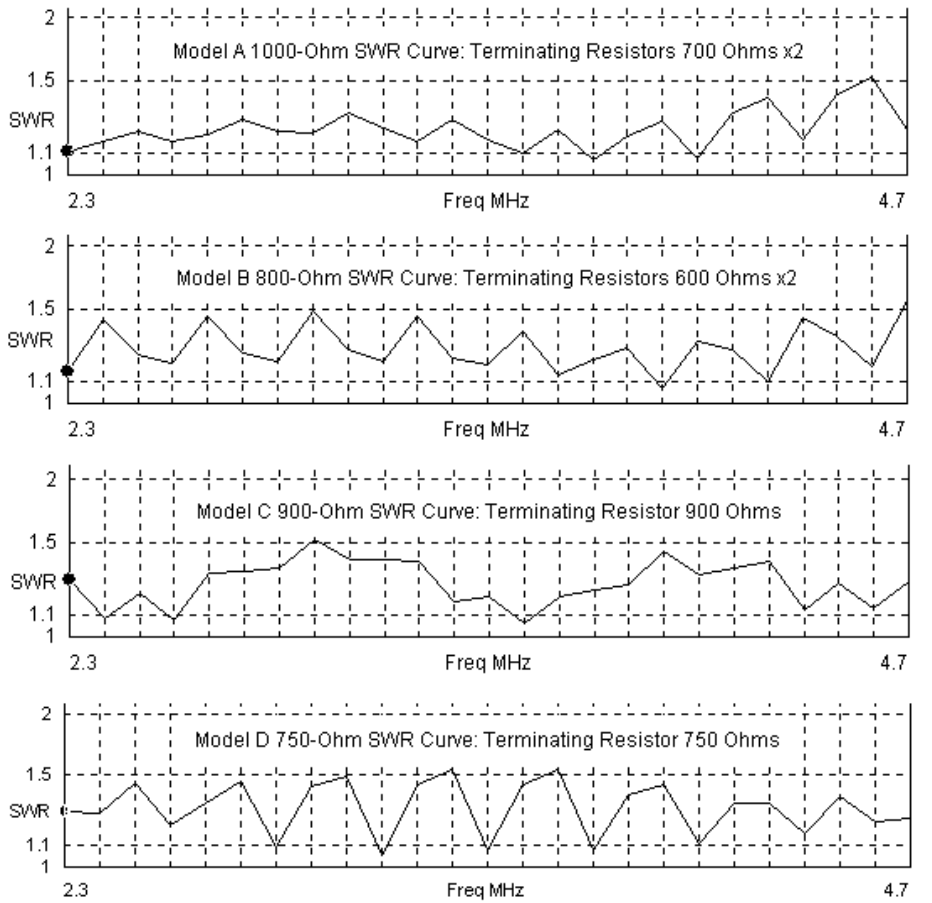

The SWR curves cover only a 2:1 frequency range with the design frequency (3.5 MHz) at the center. Before we close the discussion of the terminated V beam, we shall try to see just how wide the actual operating range might be, at

least for model D.

The test models used 5-λ legs. However, we are interested in the performance of V beams with leg lengths from 2 to 11 λ. At 1 wavelength above average ground, **Table 3-11** gives us a usable data set. For each leg length, I optimized the model for maximum gain by altering the value of angle α in 0.5° increments. Elevation angles change in 1° increments. The terminating resistor is 750 Ω in all models within the set.

Performance of Terminated V Beams Optimized for Maximum Gain (R = 750 Ohms) — Table 3-11

Model D; 1-Wavelength Above Average Ground

Len WL	alpha	El Ang	Gn dBi	FB dB	BW deg	F/SL dB	Feed R	Feed X	SWR 750
2	33.5	13	9.89	31.32	21.2	7.36	754	-5	1.01
3	26.0	13	11.41	23.05	17.4	6.92	761	-54	1.08
4	23.0	12	12.35	21.97	14.8	6.92	760	-37	1.05
5	20.0	12	13.03	20.78	13.4	6.93	755	-53	1.07
6	18.5	11	13.50	20.10	12.2	6.49	746	-42	1.06
7	16.5	11	13.88	20.01	11.6	6.47	743	-43	1.06
8	15.0	11	14.17	19.73	11.2	5.98	736	-47	1.07
9	14.5	10	14.41	19.37	10.4	6.19	730	-45	1.07
10	13.5	10	14.63	19.47	10.0	5.85	726	-44	1.07
11	12.5	10	14.85	20.05	9.8	5.39	716	-35	1.07

Notes:
- Len WL = Leg length in WL
- alpha = Wire angle to V centerline
- El Ang = Elevation angle in degrees
- Gn dBi = Maximum gain in dBi
- FB dB = 180-degree front-to-back ratio in dB
- BW deg = Half-power beamwidth in degrees
- F/SL dB = Front-to-sidelobe ratio in dB
- Feed R = Feepoint resistance in Ohms
- Feed X = Feedpoint reactance in Ohms
- SWR 750 = 750-Ohm SWR

Model D does manage to slightly improve the front-to-back ratio relative to the Laport models. The front-to-sidelobe values are also slightly higher, although the amount would likely not be operationally noticeable. In other comparative terms, use of short V beams seems unwarranted. For example, the version with 2-λ legs has less gain than a simple 2-element Yagi, and a leg-length of 5 λ is necessary before the gain exceeds that of a 3-element monoband Yagi. The V beam is not simply a substitute for parasitic beams that we commonly use today. Rather, long V beams with their very narrow beamwidths are most apt for point-to-point skip communications, a much more common governmental and commercial enterprise in the 1930s and 1940s.

For comparison with the gallery of sample elevation and azimuth patterns for

unterminated V arrays in **Fig. 30-12**, **Fig. 3-19** provides a corresponding gallery for terminated V antennas. The elevation plots show that upper-angle lobes tend to lose strength as the legs of the V grow longer. Except for the strongest secondary elevation lobes, the remainder are about 20 dB or more weaker than the main lobe. The azimuth patterns also show an interesting trend affecting the sidelobes. As the legs become longer, the angle of the strongest sidelobes grows narrower, in step with the narrowing of the main forward lobe.

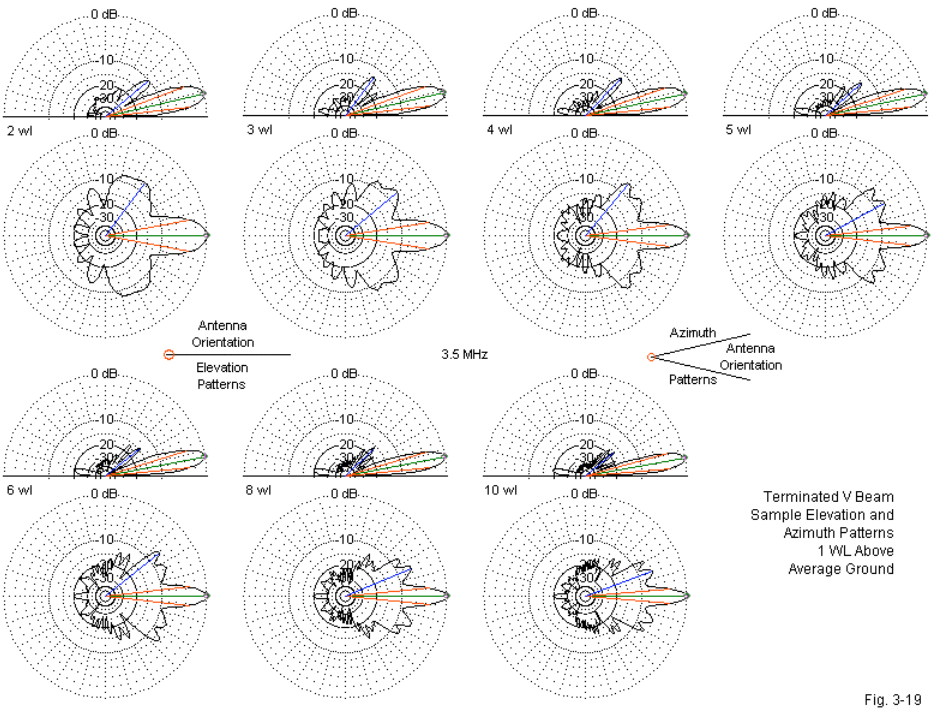

Fig. 3-19

To complete the survey of modeled results, **Table 3-12** provides performance data for the same set of antennas 2 λ above ground. The cross wire and terminating resistor remain 0.001 λ above ground, necessitating a lengthening of the vertical legs. Despite the longer vertical legs, the performance is relatively

smooth across the span of beam sizes and fully consistent with the performance of the model-D antennas at 1 λ above ground. For longer V beams, the additional antenna height results in larger values of α and narrower beamwidths, relative to the same antennas at 1 λ above ground.

Performance of Terminated V Beams Optimized for Maximum Gain (R = 750 Ohms)									Table 3-12
Model D; 2-Wavelengths Above Average Ground									
Len WL	alpha	El Ang	Gn dBi	FB dB	BW deg	F/SL dB	Feed R	Feed X	SWR 750
2	33.5	7	10.47	25.83	20.4	7.93	782	-48	1.08
3	27.5	7	12.18	21.90	16.2	6.81	762	-28	1.04
4	23.5	7	13.16	24.20	13.8	6.51	786	-5	1.05
5	21.0	7	14.24	20.46	12.4	6.32	748	-35	1.05
6	19.0	7	14.93	20.16	11.4	6.28	740	-23	1.03
7	17.5	7	15.48	19.85	10.4	6.23	735	-27	1.04
8	16.5	7	15.95	19.42	9.8	6.18	726	-38	1.05
9	15.5	7	16.36	19.25	9.2	6.18	720	-30	1.06
10	14.5	6	16.72	18.95	8.8	6.15	714	-32	1.06
11	14.0	6	17.06	18.96	8.2	6.06	714	-35	1.07
Notes:	Len WL = Leg length in WL					BW deg = Half-power beamwidth in degrees			
	alpha = Wire angle to V centerline					F/SL dB = Front-to-sidelobe ratio in dB			
	El Ang = Elevation angle in degrees					Feed R = Feepoint resistance in Ohms			
	Gn dBi = Maximum gain in dBi					Feed X = Feedpoint reactance in Ohms			
	FB dB = 180-degree front-to-back ratio in dB					SWR 750 = 750-Ohm SWR			

Terminated V beams have a considerable impedance frequency range. However, many authors limit the effective operating range to a 2:1 frequency ratio. To sample what might happen to a V beam over an extended frequency range, I used the model (version D) of a V beam with 5-λ legs and a 750-Ω terminating resistor in a 4:1 frequency sweep. The sweep ran from half the design frequency (3.6 MHz) to twice the design frequency, that is from 1.75 to 7.0 MHz. The antenna was 1 λ above average ground.

The most immediate consequences involved array gain and take-off angle. **Fig. 3-20** graphs both properties. The sweep increments are linear. The elevation angle of maximum gain shows a steady decline in the elevation angle, since the antenna changes height–when measured as a function of the wavelength of the operating frequency. The graph line would be smoother if the elevation angle increment was smaller than 1°. Although the antenna is optimized for maximum gain at the design frequency, the gain continues to increase until it peaks at 5.75 MHz, 1.6 times the design frequency.

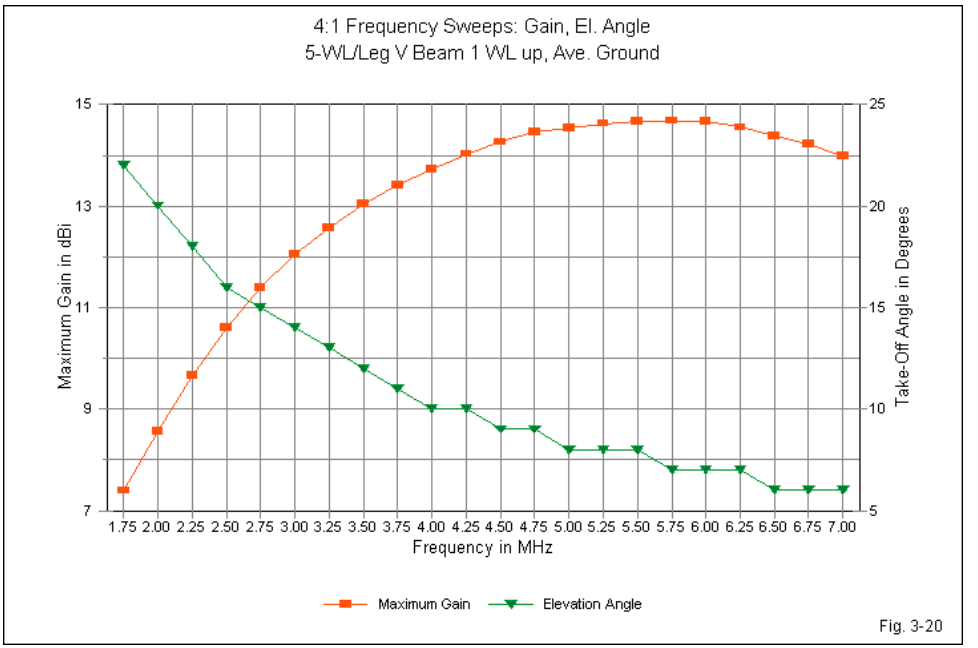

Fig. 3-20

Performance of a 5-Wavelength 3.5-MHz V-beam 1 Wavelength Above Average Ground								Table 3-13
Model D: Terminating Resistor: 750 Ohms								
Fq MHz	Gn dBi	FB dB	BW deg	El Ang	F/SL dB	Feed R	Feed X	SWR750
1.75	7.39	34.85	27.8	22	6.03	854	-51	1.16
2.33	9.98	25.76	21.6	17	4.36	865	-56	1.17
3.5	13.03	20.78	13.4	12	6.93	755	-53	1.07
5.25	14.63	22.13	9.0	8	5.01	756	34	1.05
7	13.99	22.14	24.0	6	0.31	740	97	1.14
Notes:	Fq MHz = Frequency in MHz				F/SL dB = Front-to-sidelobe ratio in dB			
	Gn dBi = Maximum gain in dBi				Feed R = Feepoint resistance in Ohms			
	FB dB = 180-degree front-to-back ratio in dB				Feed X = Feedpoint reactance in Ohms			
	BW deg = Half-power beamwidth in degrees				SWR 750 = 750-Ohm SWR			
	El Ang = Elevation angle in degrees							

The simple graph cannot show all of the relevant sweep properties. **Table 3-13** records values for frequencies that are 0.5, 0.67, 1.0, 1.5, and 2.0 times the

design frequency. Through the entry for 5.25 MHz, the progressions of values are very orderly, as the gain increases and as the beamwidth and elevation angle decrease. The front-to-back and the front-to-sidelobe ratios are both stable within this range. However, the entries for 7.0 MHz have several anomalies, especially in the front-to-sidelobe ratio column. **Fig. 3-21** shows the azimuth patterns for the array at the tabulated frequencies and easily explains the odd reading.

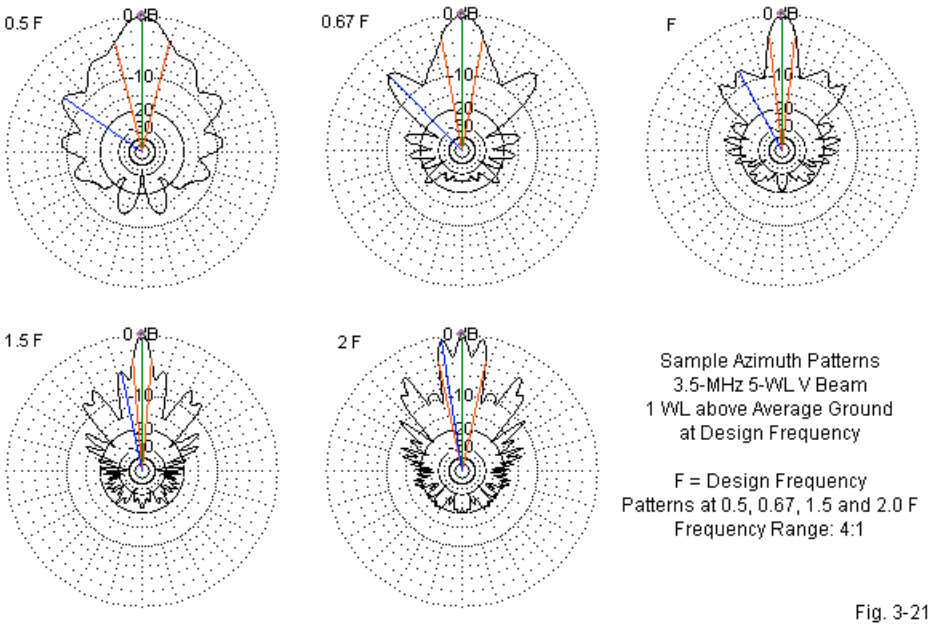

Fig. 3-21

At 1.5F, we see that the first sidelobes begin to become prominent, although at lower frequencies, they are nearly indistinguishable. Note the small bulges at the nulls on either side of the main lobe at F. As the first sidelobes grow, as shown for 1.5 F, they eventually become dominant. At 2F, the sidelobes are stronger than the central lobe, so that the forward radiation takes the form of split lobes. Since the nulls at 2F do not reach a -3dB value, the recorded beamwidth value encompasses all 3 lobes.

Below the design frequency, the chief performance disadvantage of the V beam is forward gain. The forward gain drops to ½-λ dipole level at 0.5F, despite the 5-λ legs. The final evaluation of the V beam's effective operating range thus becomes a composite judgment based upon both gain and azimuth pattern shape factors. However, as shown by **Fig. 3-22**, the 750-Ω SWR curve remains usable throughout the sampled range and beyond.

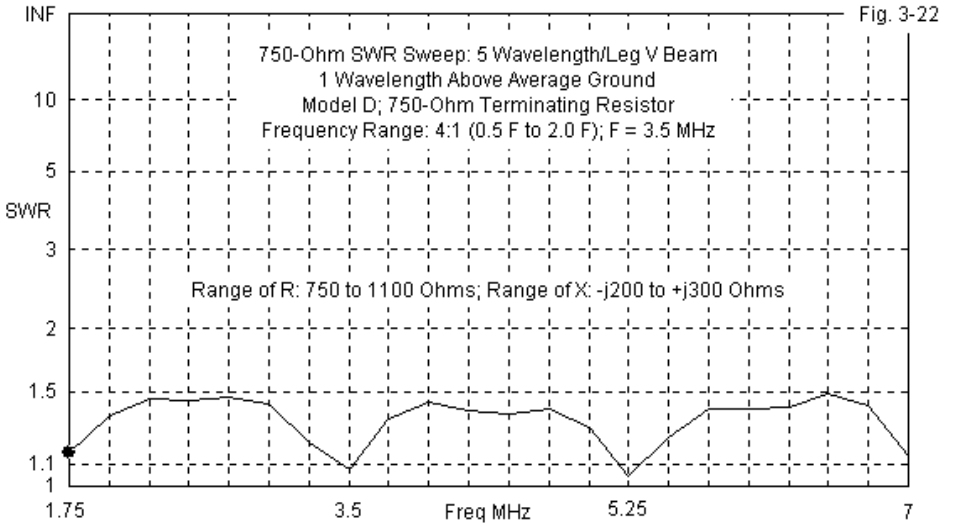

Because the original design used a terminating resistor that provided the lowest SWR value at the design frequency, that value periodically replicates itself. The 0.25-MHz increments in the SWR sweep do not capture all of those points. Hence, some SWR excursions simply do not appear on the sweep. The actual resistance range (750 to 1100 Ω) creates no major matching problems across the swept frequencies, relative to a 750-Ω standard. However, the reactance range is larger, from -j200 Ω to about +j300 Ω. These values only reflect the sampled frequencies, not the absolute limits of variation.

In order to provide space for interesting facets of V beam performance, we

have overlooked the influence of various ground qualities on the antenna. Since these effects diminish at increasing heights above ground, we may sample the effects with a 5-λ V beam at 1 λ above ground. **Table 3-14** shows the results.

5-Wavelength Terminated V Array						
1-Wavelength Above the Indicated Soil Type; Terminating Resistor 750 Ohms						
alpha = 20 degrees; Elevation Angle = 12 degrees						
Gnd Type	Gn dBi	FB dB	BW deg	Feed R	Feed X	SWR 750
Very Good	13.17	19.39	14.4	751	-76	1.11
Average	13.03	20.78	13.4	755	-53	1.07
Very Poor	12.72	24.13	13.0	781	-23	1.05
Gn dBi = Maximum gain in dBi						
FB dB = 180-degree front-to-back ratio in dB						
BW deg = Half-power beamwidth in degrees						
Feed R = Feepoint resistance in Ohms						
Feed X = Feedpoint reactance in Ohms						
SWR 750 = 750-Ohm SWR						Table 3-14

As we saw in the case of the unterminated V array (**Table 3-6**), the effects of ground are somewhat smaller than for the single long-wire beam. The gain decrease from very good to very poor soil is only 0.45 dB, and the front-to-back ratio rises as ground quality becomes worse. The variation in performance properties across the range of sampled ground qualities decreases as the V beam legs grow longer.

A second remnant question concerns how closely the model D implementation of the V beam approaches the more idealized performance of the Laport configuration. **Table 3-9** provides the Laport figures, while **Table 3-11** provides comparable numbers for model D. However, to provide a more ready reference, **Table 3-15** extracts the values of maximum gain and α from those tables for direct comparison. Although the common-configuration long-wire beam showed a significant gain deficit relative to the comparable Laport models, the V beam presents a very different picture. The average gain deficit of model-D beams is only about 0.1 dB compared to Laport models in the same environment. The vertical legs of the D model do result in a small decrease on the value of α to

optimize the array for maximum gain. The comparison does establish that the model used for detailed exploration of the V beam above ground provides a fair sampling of the likely beam performance.

Maximum Gain Comparison: Laport and Model D V Beams						Table 3-15
1 WL above Average Ground						
Len WL	Gain L	Gain D	Gn Diff	alpha L	alpha D	alpha Diff
2	10.02	9.89	0.13	35.5	33.5	2
3	11.55	11.41	0.14	28.0	26.0	2
4	12.49	12.35	0.14	23.5	23.0	0.5
5	13.15	13.03	0.12	20.5	20.0	0.5
6	13.62	13.50	0.12	19.0	18.5	0.5
7	14.01	13.88	0.13	17.0	16.5	0.5
8	14.29	14.17	0.12	16.0	15.0	1
9	14.52	14.41	0.11	15.0	14.5	0.5
10	14.74	14.63	0.11	14.0	13.5	0.5
11	14.91	14.85	0.06	13.0	12.5	0.5
Len WL = Total wire length in WL						
Gain L = Maximum gain of Laport version in dBi						
Gain D = Maximum gain of model D version in dBi						
Gn Diff = Gain difference between Laport and model D versions in dB						
alpha L = alpha angle of Laport version in degrees						
alpha D = alpha angle of model D version in degrees						
alpha Diff = angle difference between Laport and model D versions in degrees						

The V beam's erratic sidelobe structure and its requirement for significantly greater installation area may raise questions about why one would use a V beam in preference to the simpler common-configuration long-wire beam. **Table 3-16** provides one sort of answer by drawing together data for both antennas from 3 through 11 λ. The V beam enjoys a 4-dB forward gain advantage over the long-wire beam. The much narrower beamwidth holds advantages for point-to-point communications. In contrast, the long-wire beam has lower gain. Its much wider beamwidth is accompanied by a significant null between peak lobes, especially at shorter lengths. However, the table does not tell us everything that we need to know before opting for one or the other antenna.

Comparison: Terminated Long-Wire and Terminated V Antennas					
3-11 Wavelengths, 1 Wavelength Above Average Ground					
	Long-Wire			V-Beam	
Len WL	Gn dBi	BW deg		Gn dBi	BW deg
3	7.11	s70		11.41	17.4
4	7.99	s60		12.35	14.8
5	8.65	s52		13.03	13.4
6	9.15	s48		13.50	12.2
7	9.57	43.8		13.88	11.6
8	9.92	40.2		14.17	11.2
9	10.20	37.0		14.41	10.4
10	10.47	35.6		14.63	10.0
11	10.70	33.4		14.85	9.8
Len WL = Total wire length in WL					
Gn dBi = Maximum gain in dBi					
BW deg = Half-power beamwidth in degrees					Table 3-16

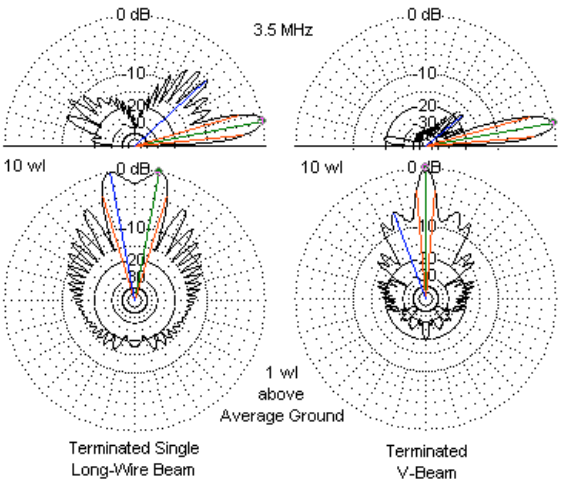

Comparative Elevation and Azimuth Patterns
10-WL Long-Wire and V-Beams

Fig. 3-23

Fig. 3-23 compares the elevation and azimuth patterns of the 2 types of antennas with 10-λ legs. Compared to the long-wire, the V beam has far lower upper-angle radiation, as shown in the elevation patterns. Both antenna models use 1-λ vertical legs. The azimuth patterns provide a reason for us to reconsider a common criticism of the V beam: its fairly small attenuation of forward side lobes. Although the criticism is a motivation to continue to seek designs with higher levels of sidelobe attenuation, longer V beams do improve upon the sidelobe situation of long-wires.

Conclusion

We have not explored the V array and the V beam to reach a final conclusion about which of the numerous long-wire antennas to use. That decision would require a set of communications goals and specifications against which to measure various antenna performance properties. Instead, we have looked at the V antennas to familiarize ourselves with their characteristics.

The unterminated V array combines one main lobe from each leg into a single stronger lobe in each direction. The required angle between each wire and the V centerline is about 95% of the value of α that we might derive from an unterminated long-wire whose length is equal to the leg-length of the V array. The maximum gain that we achieve is greater than the expected 3 dB from lobe addition, since the resulting forward and rearward main lobes have very narrow beamwidths when we optimize the array for maximum gain. Compared to a single unterminated long-wire, the V array also enjoys more immunity to ground effects that tend to change values of α, gain, and beamwidth in long-wires.

However, the V array has limitations built into its design. The azimuth patterns for V arrays of all lengths show a very erratic sidelobe structure when we choose a value of α to achieve maximum gain for a given height. The addition of main lobes of individual long-wires does not achieve a full nulling of other lobes from the wires. Hence, the V array tends to present broad forward and rearward patterns only a few dB down from the main lobes. As well, varying the α angle by more than a few degrees yields rapid gain losses. Increasing the value of α too much results in split main lobes.

Terminating the legs of a V antenna to form a traveling-wave array attenuates rearward radiation to create a directional beam. The gain penalty that we pay for obtaining a directional antenna is less than for long-wires. In longer V beams, the deficit is just over 2.5 dB relative to unterminated V arrays of the same size. Idealized V beams using the Laport configuration require α angles that tend to coincide with the α values calculated for long-wires.

Since the Laport configuration is frequency-specific, broadband implementations of the V beam yield a number of configurations that either bring the terminating resistors to ground or that employ a cross wire with a single terminating resistor at its center. To facilitate a more detailed survey of properties, we selected a model that used a cross wire close to ground level. The model is equally applicable to NEC-2 or NEC-4. Eventually, the model proved to have performance characteristics very close to those of a Laport model at the same leg height.

In the forward direction, the V beam retained all of the properties associated with the V array. Among these properties were the very narrow beamwidth, the broad forward minor-lobe structure, and the relative immunity to ground effects. Despite the erratic sidelobe structure, the V beam tends to have lower sidelobe strength than terminated long-wire beams of the same leg length. However, while the common-configuration terminated long-wire tends to find use over a 4:1 frequency range, pattern degradation tends to limit the usable frequency limits. Although we cannot specify an absolute limit, it is less than the SWR bandwidth of the terminated V beam.

Through our examination of long-wire and V antennas, we have used a convention common to amateur radio installation. We have set an antenna within a given environment–whether in free space or at a height over ground–and then optimized it for maximum gain. The elevation angle of maximum radiation was an emergent value and not a design value. To be true to history, we shall eventually have to change that procedure. The quotation from Laport that began this chapter suggests that we should have done so in our design of V beams. However, we shall save the maneuver for terminated rhombic arrays.

4.

Rhombic Arrays and Beams

> The pattern of a rhombic antenna may be calculated as the sum of the patterns of four tilted wires each with a single outgoing traveling wave. The effect of a perfectly conducting ground may be introduced by the method of images. For a horizontal rhombic of perfectly conducting wire above a perfectly conducting plane ground, Bruce, Beck, and Lowry give the relative field intensity E in the vertical plane coincident with the rhombic axis as a function of α, Φ, L_λ, and H_λ. . .
>
> John D. Kraus, *Antennas*, 2nd Ed., p. 505

For the most part, modern radio amateurs bypass much of the critical information in Kraus' succinct summary of the classic Bruce-Beck-Lowry rhombic equations, and also never examine the context within which these formulations arose. Edmond Bruce was not only instrumental in the development of the standard rhombic (originally called the diamond antenna in his 1931 article), but as well in the development of numerous other large arrays in the early 1930s. All of these antenna designs and the calculations underlying them arose in a period in which we were just coming to grips with the 3-dimensional control of antenna radiation in the MF and HF ranges.

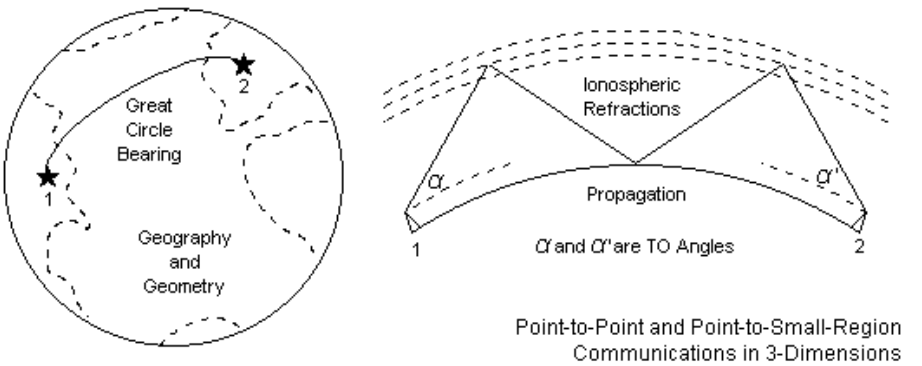

Fig. 4-1 provides a simplified view of the challenge. The aiming of an array relative to the correct azimuth heading for a great circle bearing to a desired communications target is perhaps the simpler project, since it relied upon well-established geographic calculations and very precise surveying techniques. By the 1930s, we were intensively monitoring propagation angles for skip communications in the upper MF and the HF regions. The design of large wire arrays, as one standard technique for effecting reliable point-to-point communications, required attention to both elevation and azimuth headings, especially if the subject antenna produced a radiation pattern with very narrow beamwidths in the favored direction(s).

The era in which the rhombic arose as the so-called king of wire beams differed from the 21st-century use of satellites for intercontinental communications. Goals of the period included establishing the HF region for reliable point-to-point communications over vast distances. 19th-century telegrams expanded into undersea cablegram service and finally into radiograms. The widely used Phillips code initially provided a compact means for news transmission via cable and later via radio. The teletype machine eventually replaced the telegraph key as the chief messaging device for commercial services, although telegraphy remained in wide and important use. Business and governmental transactions also made use of radio services as they became available. Harper reports that by 1941, Bell used rhombic antennas exclusively in its point-to-point communications system. Eventually, some of the antennas developed for point-to-point communications proved effective in targeted short-wave broadcasting.

V-beams, rhombics, and even bi-directional arrays such as the Bruce and the Sterba curtains permitted the generation of main lobes having very narrow beamwidths as measured horizontally. Indeed, all of these antennas obtained their gain by means of narrowing the beamwidth. For operations with fixed termini and fixed frequencies, azimuth control of the beams proved insufficient by the late 1920s. To make use of skip refractions required control of the vertical angle of radiation. Moreover, gain eventually proved to be a secondary consideration as receivers improved. Indeed, Bruce's classic 1931 article (see the reference list in the Introduction) devotes about a third of its pages to discussions of receiver capabilities and "static," that is, interfering man-made and natural signals. Narrow

beamwidth was only part of the solution; sidelobe reduction was the other part.

Out of these concerns the rhombic or diamond antenna emerged. It remained under active study and improvement into the 1960s with Laport's introduction of the multiple rhombic. We shall review that design in the next chapter. However, we must first examine some rhombic basics. The unterminated rhombic has seen virtually no use. However, we must linger over it for two reasons. First, it is the baseline against which we measure terminated rhombic performance. Second, it provides a ready reference for comparisons with the other terminated long-wire antennas in Chapters 2 and 3.

Unterminated Rhombic Basics

The rhombic antenna derives its name from its shape: the rhombus (or diamond). In geometry, a rhombus is an equilateral parallelogram, that is, a closed 4-sided figure with all sides the same length, but with all corner angles normally using other than right angles. **Fig. 4-2**, at the top, shows a basic rhombus, with indications of the key dimensions.

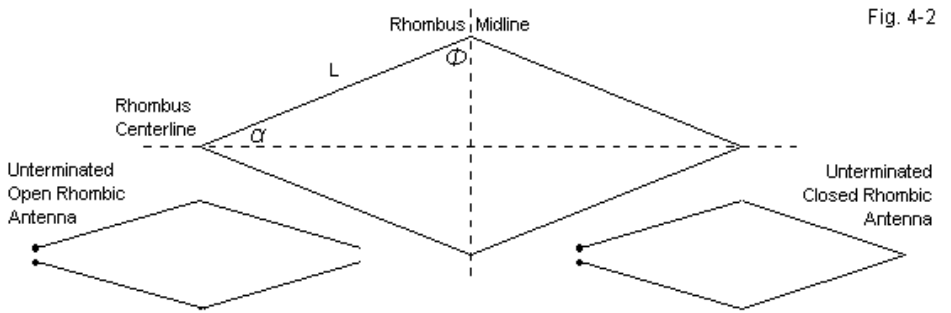

Fig. 4-2

Basic Rhombus Parameters and
Alternative Unterminated Rhombic Antenna Shapes

An alternative way to look at the rhombus is to see it as 2 V antennas end-to-end. This orientation makes clear that the centerline is correctly identified, and it gives the elongated shape some sense, assuming that Chapter 3 has had its

impact. The length L, in wavelengths, defines the length of each leg, suggesting that each rhombic antenna that we examine will likely be twice as long overall as a corresponding V antenna with the same leg length.

Also apparent in the sketch are key angles. When we examined V antennas, we used the angle of the strongest lobe of a single long-wire of length L to determine the value of angle α. We then found that angling each V wire from the centerline by the value of α produced additive lobes along the centerline. Since the far end of any rhombic antenna is a mirror image of the feedpoint end, the lobes for the far-end wires will also be aligned with the centerline. Hence, we can expect more gain from a rhombic antenna than from a corresponding V antenna.

The earliest literature began the practice of referring to angle Φ in **Fig. 4-2** as the tilt angle. Angle Φ is simply 90° minus angle α. Because early literature had no pre-set standard, you will find other designations for the angles. For example, Laport–following Foster– uses the entire acute rhombic angle as his baseline, and he calls it angle A (A = 2α). Nevertheless, we shall follow Kraus in these notes.

The lower portion of **Fig. 4-2** shows two ways of modeling an unterminated rhombic antenna. We may separate the far end point by a small space. This configuration is perhaps the most common understanding of an unterminated (sometimes called a resonant) rhombic. However, we may equally bring the ends together to short-circuit the gap. The options expose something of a misimpression of the rhombic antenna. If we were given to extreme (and unfortunately, contentious) modes of expression, we might suggest that there is no such thing as an unterminated rhombic antenna.

The single long-wire unterminated antenna and the V array both make good sense of the idea of a wire without a resistive termination. Any form of termination requires extra wires and ultimately a ground connection–although we have examined forms that do not use ground at the far end of the array. The rhombic returns the 2 wires of the antenna to close proximity. In the models that we shall explore, the gap will be 0.002-λ. At 3.5 MHz, that distance is 170 mm, while a wavelength is over 85.6 m long. If we leave the gap open, we can treat the terminating resistance as simply indefinitely large. One modeling technique

for rhombics is to use a short wire to bridge the gap. To create a terminated rhombic–as the term is generally used–we place a load resistor of a desired value on the bridge wire. To create an open circuit, we might specify the load resistance as 1e10 Ω or higher. To short out the gap, we can either remove the load resistor or give it a value of 0 Ω. Alternatively, we can remove the bridge wire and simply bring the 2 legs to the same point on the coordinate scheme.

Despite the existence of a reasonably plausible claim that all rhombics are terminated to one or another degree, we shall adhere to the common referential terms. Without a mid-range non-inductive resistor at the far end of the antenna, the rhombic will be unterminated in either the open or closed configuration. The chief difference between the open and closed versions of the unterminated rhombic antennas lies in the sidelobes, not in the small differences in gain and inherent front-to-back ratio that is a part of all end-fed long-wire antennas. **Fig. 4-3** contrasts the structure of the sidelobes for sample open and closed unterminated rhombics. Note that the closed version shows larger sidelobes than the open version, suggesting less complete cancellation of lobes from the parallel legs.

For comparison and contrast, **Fig. 4-3** also presents two azimuth patterns from corresponding unterminated V arrays. The pattern on the lower left uses 3-wavelength legs, the same length as the legs of the rhombic. The pattern on the lower right has 6 λ legs. The longer legs give the V array the same overall length as the rhombic, with a small margin of difference due to the difference in the value of angle α. (Both rhombic are 5.39 λ long, while the long V is 5.71 λ overall.) On the whole, the long V antenna pattern resembles in general sidelobe strength the closed rhombic pattern. However, the V patterns show the combination of many sidelobes that combine to form fewer distinct lobes and nulls. In contrast, the double-V configuration of the rhombic reduces these indefinite lobe formations down to distinct lobes and nulls. In fact, both rhombic azimuth patterns show a total of 20 lobes. The lower strength levels of the lobes at near-right-angles to the 2 main lobes for the open version of the antenna make lobe counting impossible at the scale of **Fig. 4-3**, but expanded renderings of the plot reveal them all. In contrast, even large renderings of the V-antennas do not permit an accurate count of the lobes and the bulges that form incipient lobes.

Even in unterminated form, the rhombic shows its potential for sidelobe reduction.

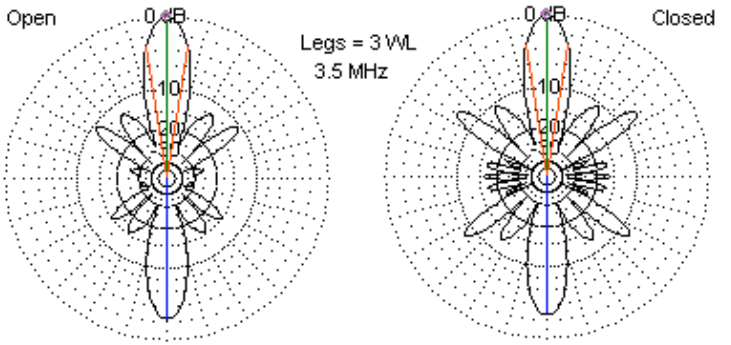

Open and Closed Unterminated Rhombic Antennas
Comparative Azimuth Patterns

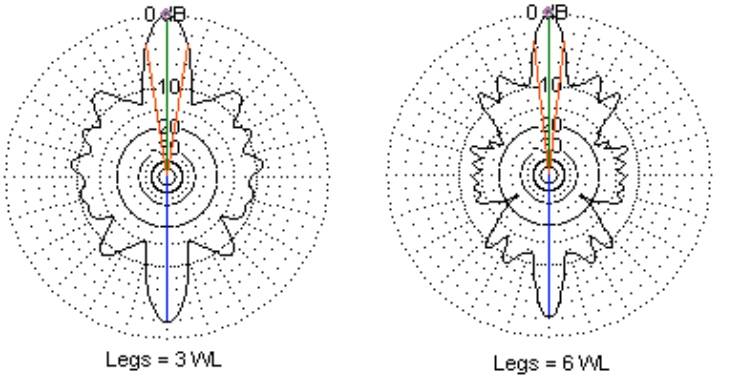

Comparable V-Array Azimuth Patterns

Fig. 4-3

Clear definition and numeric limitation of lobes together comprise one of the advantages of the rhombic over corresponding V antennas. The other major rhombic advantage is gain. **Table 4-1** provides modeled data for both open and closed unterminated rhombics in free space with varying leg lengths from 2 through 11 λ. Compare gain values at 2, 4, and 8 λ: each length doubling

provides about 3 dB more gain (11.1, 14.1, and 17.1 dBi for the open versions). The increase rate diminishes when we place the antenna over ground.

Open and Closed Unterminated Rhombic Arrays: Free-Space									Table 4-1
	Open End Version				Closed End Version				
Len WL	alpha	Gn dBi	FB dB	BW deg	alpha	Gn dBi	FB dB	BW deg	alpha Cal
2	39.0	11.08	2.53	17.8	38.5	10.62	2.97	18.4	39.0
3	31.5	12.88	2.60	14.4	31.0	12.60	2.88	14.9	31.7
4	27.5	14.13	2.65	12.2	27.0	13.96	2.80	12.4	27.4
5	24.5	15.10	2.63	10.8	24.0	14.95	2.79	11.0	24.4
6	22.0	15.89	2.64	10.0	22.0	15.77	2.77	10.0	22.3
7	20.5	16.56	2.63	9.2	20.5	16.56	2.73	9.2	20.6
8	19.0	17.14	2.64	8.6	19.0	17.04	2.73	8.6	19.3
9	18.0	17.65	2.63	8.0	18.0	17.57	2.70	8.0	18.2
10	17.0	18.11	2.63	7.6	17.0	18.04	2.69	7.6	17.2
11	16.5	18.51	2.61	7.0	16.0	18.44	2.67	7.4	16.4
Notes:	Len wl = Leg Length in wavelengths								
	alpha = Wire angle to centerline in degrees								
	Gain dBi = Maximum gain in dBi								
	FB dB = 180-degree front-to-back ratio in dB								
	BW deg = main lobe beamwidth in degrees								
	alpha Cal = Calculated angle in degrees; alpha = 1.1 arccos [1-(0.371/L)]								
	L = wire (leg) length in WL								

The closed versions of the unterminated rhombic show a small gain deficit relative to the open versions. The difference is highest for the smallest rhombics, but is still under 0.5 dB. For the longest rhombics, the difference shrinks to under 0.1 dB. In all cases, α angles for the 2 versions are within a 0.5° of each other. The open version shows the larger angle wherever it occurs. Since the increment of α angle change is 0.5°, resolving the angular difference further is not possible.

Among the most interesting comparative features of the unterminated long-wire arrays that we have surveyed are the independent equations by which we may approximate the value of α. For single end-fed long-wires, we found a reasonably accurate tracking equation:

$$\alpha = \cos^{-1} [1 - (0.371/L_\lambda)] \qquad \text{End-Fed Long-Wires}$$

For the long-wire, α is the angle between the wire axis and the main lobe (in degrees), and L_λ is the wire length in wavelengths. When we moved to V arrays,

we had to adjust the equation by about 5%:

$$\alpha = 0.95 \cos^{-1} [1 - (0.371/L_\lambda)] \qquad \text{Unterminated V Arrays}$$

Angle α is now the angle between the wire for one leg and the V centerline. Angle α has the same meaning with rhombics, but requires a different adjustment factor, this time upward for free-space unterminated rhombics:

$$\alpha = 1.1 \cos^{-1} [1 - (0.371/L_\lambda)] \qquad \text{Unterminated Rhombic Arrays}$$

For each type of unterminated long-wire array, the indicated equation tracks quite well, given the increment between modeled values of α.

Texts on various long-wire arrays provide a number of other α-tracking equations. Some of them are parts of equation systems that analyze the entire geometry and electrical performance of the arrays. However, the equations shown here appear to track best with NEC-4 models of the arrays in free space. For maximum-gain models of the arrays over lossy ground, the values of α diminish, although the effect is most pronounced for antennas well below 2 λ in height. For any given height above ground, the difference of α from its free-space value varies with the quality of the ground. Because the effect of ground is subject to two complex variables (height and ground quality), I have not tried to develop tracking equations for these situations. However, the tabular data provide guidance for initial models that may use specific leg lengths, antenna heights, and ground qualities. In general, wire loss has almost no effect on α.

Since we have compiled data on a considerable number of unterminated long-wire arrays, we might well pause to compare the maximum gain values attained by each of them. **Table 4-2** and **Fig. 4-4** provide the data. The center-fed doublet and the end-fed long-wire values are for angles that diverge from the wire axis, while the V and rhombic array values are in line with the array centerline. The length values are for legs of an array. Hence, the unterminated rhombic antennas are about twice as long as the corresponding V arrays and just short of twice as long as the center- and end-fed wires. The overlapping lines for the two rhombic arrays show the insignificance of their gain differences.

Unterminated Free-Space Long-Wire Arrays					Table 4-2
Comparative Maximum Gain Values					
Len WL	CFD	EF	V	O RH	C RH
2	4.03	4.81	8.26	11.08	10.62
3	4.74	6.05	9.66	12.88	12.60
4	5.38	6.98	10.83	14.13	13.96
5	5.93	7.72	11.61	15.10	14.95
6	6.41	8.34	12.33	15.89	15.77
7	6.82	8.87	12.95	16.56	16.56
8	7.20	9.33	13.42	17.14	17.04
9	7.55	9.74	13.88	17.65	17.57
10	7.85	10.11	14.31	18.11	18.04
11	8.13	10.45	14.67	18.51	18.44
Notes:	Len wl = Leg Length in wavelengths				
	CFD = Center-fed doublet				
	EF = End-fed long-wire				
	V = V array				
	O RH = open-end rhombic array				
	C RH = Closed-end rhombic array				

Fig. 4-4

The unterminated rhombic–for several good reasons–finds little service. However, to complete our data baselines for later comparisons, we may re-model the arrays 1 λ over average ground. **Table 4-3** provides the data for the exercise. Except for small differences of α for short rhombics, the most prominent feature is the similarity of performance values between open and closed versions.

Performance of Unterminated Rhombic Antennas						Table 4-3
1-Wavelength Above Average Ground						
Type	Len WL	alpha	El Ang	Gn dBi	FB dB	BW deg
Open	2	37.0	14	16.55	2.42	18.8
Closed	2	35.5	14	15.91	3.00	19.8
Open	3	28.5	14	18.04	2.50	15.6
Closed	3	28.0	14	17.67	2.81	16.0
Open	4	24.5	13	18.98	2.61	13.4
Closed	4	24.0	13	18.65	2.90	13.6
Open	5	21.0	13	19.63	2.62	12.2
Closed	5	21.0	13	19.41	2.83	12.2
Open	6	18.5	13	20.13	2.58	11.4
Closed	6	18.0	13	19.94	2.71	11.6
Open	7	17.0	12	20.61	2.57	10.4
Closed	7	16.5	12	20.43	2.67	10.8
Open	8	15.5	12	20.96	2.51	10.0
Closed	8	15.0	12	20.79	2.60	10.2
Open	9	14.0	12	21.24	2.42	9.6
Closed	9	14.0	12	21.08	2.55	9.6
Open	10	13.5	11	21.54	2.43	9.0
Closed	10	13.5	11	21.41	2.53	9.0
Open	11	12.5	11	21.76	2.37	8.6
Closed	11	12.5	11	21.63	2.46	8.6
Len WL = Leg length in WL; double for total rhombic length						
alpha = Wire angle to V centerline						
El Ang = Elevation angle in degrees						
Gn dBi = Maximum gain in dBi						
FB dB = 180-degree front-to-back ratio in dB						
BW deg = Half-power beamwidth in degrees						

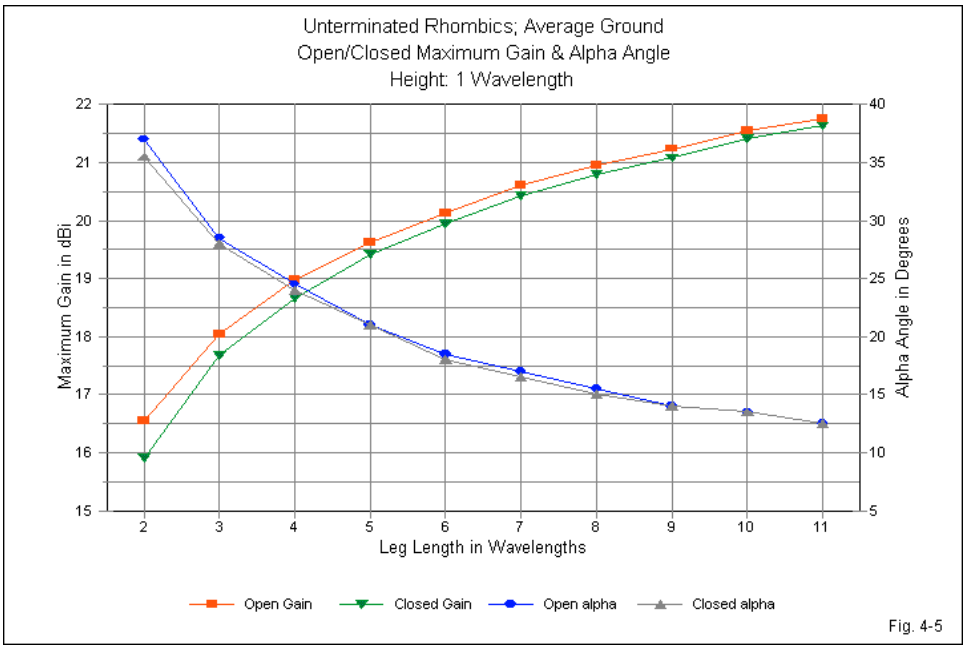

Fig. 4-5 graphs the maximum gain values and the values of α. Over average ground at a height of 1 λ, the gain values for open and closed rhombic versions differ slightly more than in free space. The differential ranges from about 0.6 dB to 0.1 dB across the leg lengths in the survey. Only at the shortest length does the α angle vary by more than 0.5° for the two versions of the unterminated rhombic array.

To show the evolution of the unterminated rhombic array patterns with increasing leg length, **Fig. 4-6** presents a small gallery of sample patterns for the open version of the array at 1 λ above average ground. Rhombics show good attenuation of higher-angle elevation lobes, and the lobes diminish as the legs grow longer. As well, with increasing leg length, the major azimuth sidelobes (the first and second on each side of the main lobe) move inward toward the centerline. In addition, these major sidelobes decrease their beamwidth as the

main lobe also decreases its beamwidth to accommodate new small sidelobes.

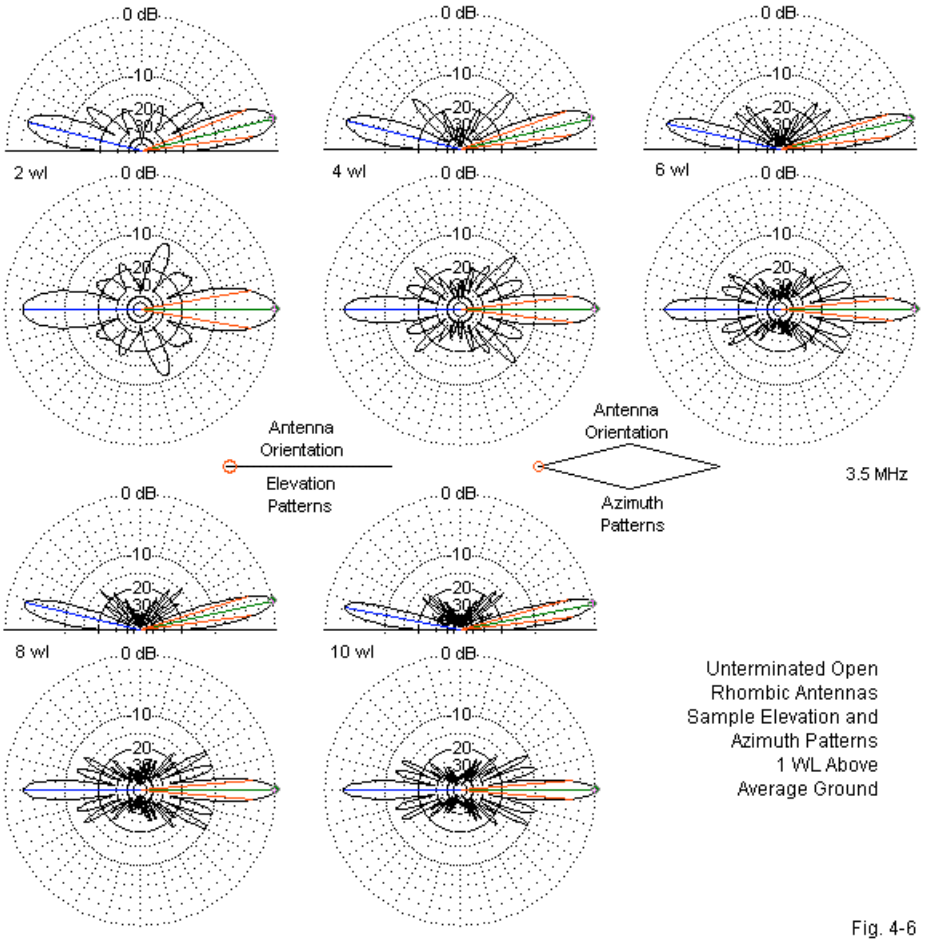

Fig. 4-6

One limitation of the survey that we have also noted for other long-wire arrays is the use of 1-λ increments of leg-length between samples. However, we saw in

connection with the V arrays that the more complex long-wire arrays show only vestiges of the behavior that made end-fed long wires so interesting. Performance and pattern behaviors for rhombics using leg lengths between the sampled values show similar small variations, as recorded in **Table 4-4** for a sample of open rhombic behavior between 3 and 4 λ leg lengths.

Unterminated Open Rhombics				Table 4-4
3-4 Wavelength Legs in Free Space				
Len WL	alpha	Gn dBi	FB dB	BW deg
3.00	31.5	12.88	2.60	14.4
3.25	30.3	13.05	2.85	14.3
3.50	29.0	13.55	2.63	13.2
3.75	28.3	13.73	2.78	13.1
4.00	27.5	14.13	2.62	12.2
Len wl = Leg Length in wavelengths				
alpha = Wire angle to centerline in degrees				
Gain dBi = Maximum gain in dBi				
FB dB = 180-degree front-to-back ratio in dB				
BW deg = main lobe beamwidth in degrees				

As the leg length increases from a multiple of a half-wavelength to an odd multiple of a quarter-wavelength, the front-to-back ratio increases and the beamwidth remains almost constant. The gain rises more slowly in this interval. From the odd multiple of a quarter-wavelength to the next multiple of a half-wavelength, the front-to-back ratio decreases and the beamwidth narrows more rapidly, and the gain also rises more rapidly. However, unlike the gain progression for the single unterminated long-wire, we do not find retrograde movements in the rhombic gain curve.

Terminated Rhombic Basics

As we turn to terminated rhombics, we face two significant questions. How shall we model them? How shall we design them? Both questions have more than 1 answer.

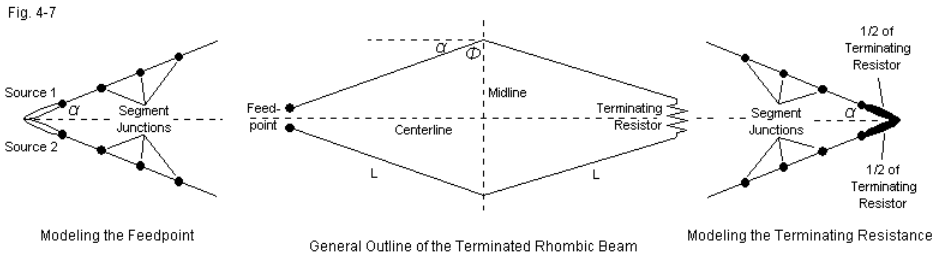

Fig. 4-7 shows, at the center, the general outline of terminated rhombic array with a finite terminating resistor. In fact, we shall select a terminating resistor whose value (in rounded terms) approximately equals the feedpoint impedance. Since the rhombic beam is a closed figure, with no required appendages to provide a return path for the termination, the value of the terminating resistor and the value of the feedpoint resistance change in opposite direction. Where the two values match provides the closest approach to a match between the terminating and feedpoint impedances.

The diagram also indicates the relationship between angles α and Φ. Angle Φ bears the name "tilt angle," and is the angle between a leg (L) wire and the rhombus midline across the narrow peaks of the figure. Angle α is sometimes called the "acute angle." However, in some texts, authors use the term "acute angle" to represent 2α, that is, the total angle between the two wires rather than simply the angle between the wire and the rhombus centerline.

Modeling the terminated rhombic presents some options. We may create a short wire at each end of the rhombus and place the source on one and the load resistor on the other. Effective modeling normally requires that these end wires use 3 segments, especially at the source end of the antenna. This practice ensures that the segments on each side of the center source segment have the same current, a measure that tends to yield the highest accuracy of current calculation by NEC. (In MININEC, we would use a 2-segment wire and place the source at the junction of the segments.) This technique presents 2 relatively undesired alternatives. If we make the end wires short enough to preserve the value of α, then the segments are very short. The legs of the rhombic should

have segment lengths that do not vary much from the length of source and load segments. We would end up with highly segmented legs and very large and slow-running models, or we would need to use some form of length tapering of the segments.

For the V beam, we adopted a simpler procedure. We used a split source. A split source simply places a source on each of the two wires at the feedpoint. The net impedance of the array is the sum of the two source impedances, since they are in series. For the rhombic, we may supplement the feedpoint treatment by a comparable technique for implementing the terminating resistor. We place resistive loads of one-half the total value of the terminating resistance on each of the two wire segments at the far junction. **Fig. 4-7** shows both the feeding and terminating techniques at the left and right ends of the sketch. The technique permits finite-size models and a very good correlation between the unterminated and terminated versions of the rhombic antenna.

Not all rhombic configurations allow the use of the simplified model. Some complex rhombics will require the use of end wires. We shall encounter a specific case in the next chapter. At that time, we can compare and evaluate the modeling techniques more thoroughly.

When we turn to designing the rhombic, we face a number of choices. We may design a rhombic beam using nomographs of the sort presented in the Harper 1941 volume. We may also follow Laport and use the stereographic techniques first introduced by Foster in his 1937 article. A third way to proceed is to use the technique introduced by Bruce, Beck, and Lowry in 1936 as a follow-up to Bruce's introduction of the rhombic "diamond" in 1931. Finally, we may proceed along the lines of design that we have used for all other long-wire arrays, modeling the antennas at each leg length in free space and over lossy ground, altering the model's value of α until we achieve maximum gain.

The last two methods provide perhaps the greatest contrast in design procedures. The Bruce technique begins by selecting an elevation angle, called α (or Δ in some sources). From that angle, we calculated the correct height and leg length, where α is also the angle between the wire and the centerline. The

modeling technique selects a height, and finds the value of α that yields maximum gain. The elevation angle becomes whatever the antenna configuration dictates. If we wish to change the elevation angle, we may change the antenna height and again seek out the required value of α for maximum gain. Since we have presented every other long-wire antenna in these terms, let's start with the modeling procedure and then compare it to the classic design equations.

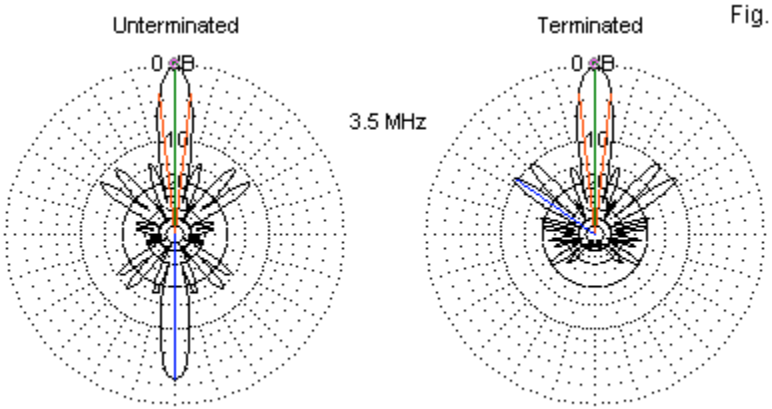

Fig. 4-8

Free-Space E-Plane Patterns: Unterminated and Terminated Rhombic Arrays with 4-WL Legs

Fig. 4-8 provides us with the motivation for terminating the rhombus to create as pure as traveling-wave antenna as a non-inductive terminating resistor will permit. Both rhombics use the same leg lengths and the same values of α. Both have the same overall length, just shy of 8 λ. The terminated beam attenuates rearward lobes to a very high degree, while leaving the forward lobes relatively intact. Since the terminated rhombic used the maximum-gain technique for design, the two strongest secondary lobes on each side of the main lobe are slightly stronger (by about 2 dB) than the ones associated with the unterminated array. Nevertheless, the lobes are about 4-5 dB weaker than for a V beam, and the lobes are narrow compared to the broad front of lobes associated with the V beam.

We shall begin with free-space models, using 1-λ increments of leg length for rhombic beams between 2 and 11 λ (or about 4 to 22 λ overall length). As always, the test frequency is 3.5 MHz, and the 0.16" diameter lossless wires use 20 segments per wavelength. The terminating resistor is 850 Ω, a rounded value that we shall use with all of our initial rhombic models. The tables will present the feedpoint resistances and reactances as a measure of how close the terminating resistor corresponds to the feedpoint resistance. Where the leg length uses a value closer to an odd multiple of a quarter-wavelength, the resistive component of the impedance does not change much, but the reactance may vary somewhat.

Performance of Terminated Rhombic Beams Optimized for Maximum Gain (R = 850 Ohms)

Free Space

Len WL	alpha	Gn dBi	FB dB	BW deg	F/SL dB	Feed R	Feed X	SWR 850
2	38.5	9.43	29.22	18.2	7.52	851	8	1.01
3	31.0	11.30	45.38	14.6	8.94	865	22	1.03
4	27.0	12.59	44.22	12.4	9.32	868	18	1.03
5	24.0	13.57	38.68	11.0	9.10	872	22	1.04
6	22.0	14.36	37.26	10.0	8.94	872	20	1.04
7	20.5	15.03	36.44	9.2	8.86	871	22	1.04
8	19.0	15.60	36.16	8.6	8.87	871	22	1.04
9	18.0	16.11	36.14	8.0	8.96	869	22	1.03
10	17.0	16.56	36.17	7.6	9.00	867	22	1.03
11	16.0	16.96	36.46	7.4	8.95	866	23	1.03

Len WL = Leg length in WL; double for total rhombic length
alpha = Wire angle to V centerline
Gn dBi = Maximum gain in dBi
FB dB = 180-degree front-to-back ratio in dB
BW deg = Half-power beamwidth in degrees
F/SL dB = Front-to-sidelobe ratio in dB
Feed R = Feepoint resistance in Ohms
Feed X = Feedpoint reactance in Ohms
SWR 850 = 850-Ohm SWR

Table 4-5

Table 4-5 provides data for the free-space models. The 850-Ω SWR column provides a measure of the impedance match between the termination and the feedpoint. The values of α are identical to those that produced maximum gain for the closed unterminated rhombic arrays shown in **Table 4-1**. The 180° front-to-back ratios are uniformly high, while the beamwidths are comparable to those for unterminated rhombics. The front-to-sidelobe rejection averages close to 9 dB.

Each long-wire terminated array that we have encountered has suffered a significant reduction of maximum gain relative to unterminated versions of the same array. However, the V beam showed a smaller deficit than did the single terminated long-wire. The terminated rhombic shows an even smaller deficit, as illustrated by the data in **Table 4-6**. In general, the gain loss created by termination is so small that designers have viewed it as insignificant relative to the improvement in the suppression of rear quadrant lobes. Since point-to-point communications rarely requires aiming at 2 points that oppose each other by 180° relative to the antenna, unterminated rhombics have seen virtually no use.

Free-Space Rhombics: Unterminated and Terminated						Table 4-6
Gain Differentials						
Len WL	Unt Open	Unt Close	Ter 850		Diff Open	Diff Close
2	11.08	10.62	9.43		1.65	1.19
3	12.88	12.60	11.30		1.58	1.30
4	14.13	13.96	12.59		1.54	1.37
5	15.10	14.95	13.57		1.53	1.38
6	15.89	15.77	14.36		1.53	1.41
7	16.56	16.56	15.03		1.53	1.53
8	17.14	17.04	15.60		1.54	1.44
9	17.65	17.57	16.11		1.54	1.46
10	18.11	18.04	16.56		1.55	1.48
11	18.51	18.44	16.96		1.55	1.48
Len WL = Leg length in WL; double for total rhombic length						
Unt Open = maximum gain in dBi for unterinated open rhombic						
Unt Close = maximum gain in dBi for unterminated closed rhombic						
Ter 850 = maximum gain in dBi for rhombic terminated 850-Ohms						
Diff Open = Gain difference in dB: unterminated open vs. terminated rhombic						
Diff Close = Gain difference in dB: unterminated closed vs. terminated rhombic						

We are now positioned to compare more directly the gain potential the various terminated long-wire arrays that we have developed. **Table 4-7** supplies data on both the maximum gain and the beamwidth of free-space models of the terminated long-wire, the V beam, and the rhombic. The long-wire and V beam models use the Laport configuration.

Maximum Gain of Various Terminated Long-Wire Antennas						Table 4-7
Free-Space Models			Gain in dBi; Beamwidth in degrees			
	Single Long-Wire		V Beam		Rhombic	
Len WL	Gain	BW	Gain	BW	Gain	BW
2	1.89	29.1	4.82	19.8	9.43	18.2
3	3.63	23.0	6.64	15.8	11.30	14.6
4	4.83	19.7	7.88	13.2	12.59	12.4
5	5.75	17.4	8.85	12.0	13.57	11.0
6	6.49	15.8	9.63	10.8	14.36	10.0
7	7.11	14.6	10.28	10.0	15.03	9.2
8	7.64	13.6	10.85	9.2	15.60	8.6
9	8.12	12.8	11.35	8.6	16.11	8.0
10	8.54	12.1	11.79	8.4	16.56	7.6
11	8.92	11.6	12.19	7.8	16.96	7.4
Notes:	Rhombics are twice as long overall as the other antennas.					
	Single long-wire main lobes not in l;ine with wire axis.					
	Len WL = Leg length in WL					

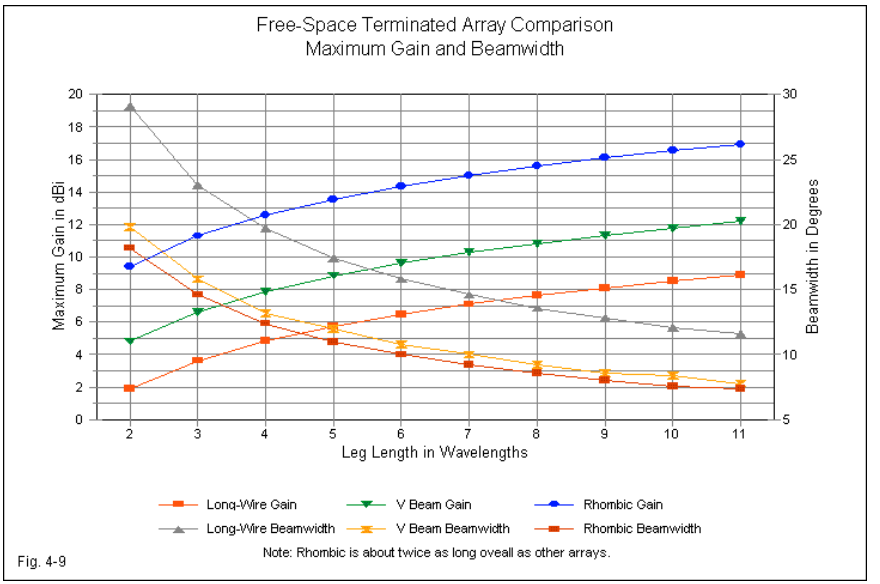

Fig. 4-9

The ascending curves show the maximum potential gain of each array at each length. The wide gain margin for the rhombic is a combined function of its configuration and its doubled overall length. The descending curves represent the beamwidth. The values for the long-wire represent one lobe on one side of the wire axis, since the null between lobes is considerable. The nearly parallel values of beamwidth for the V beam and the rhombic suggest that doubled rhombic length makes only a small difference in this value.

The free-space models of the terminated rhombic required, for maximum gain, the same values of α as the closed unterminated rhombic. However, when we place both antenna types 1 λ over average ground, the terminated rhombic at each leg length requires a value of α that is about 0.5° higher. Values for α decrease relative to free-space models, while beamwidth values increase. As we might expect, the elevation angle decreases as the rhombic grows longer, although these values are comparable to V beam values for antennas having about half the total length of the rhombics. Impedance values vary only slightly between free-space models and those 1 λ over the lossy ground

Performance of Terminated Rhombic Beams Optimized for Maximum Gain (R = 850 Ohms) — Table 4-8

1-Wavelength Above Average Ground

Len WL	alpha	El Ang	Gn dBi	FB dB	BW deg	F/SL dB	Feed R	Feed X	SWR 850
2	36.0	14	14.77	28.23	19.4	7.58	860	17	1.02
3	28.5	13	16.39	38.85	15.8	8.26	863	28	1.04
4	24.5	13	17.39	45.68	13.4	8.75	871	25	1.04
5	22.0	12	18.08	46.84	11.6	8.89	867	25	1.04
6	19.0	12	18.62	43.51	11.2	8.97	865	26	1.04
7	17.5	12	19.01	44.82	10.2	9.05	866	25	1.04
8	15.5	12	19.30	45.11	10.0	9.31	862	24	1.03
9	14.5	11	19.59	44.04	9.4	9.26	859	23	1.03
10	14.0	11	19.83	45.22	8.6	9.13	858	24	1.03
11	13.0	10	20.00	43.98	8.6	9.22	855	24	1.03

Len WL = Leg length in WL; double for total rhombic length
alpha = Wire angle to V centerline
El Ang = Elevation angle in degrees
Gn dBi = Maximum gain in dBi
FB dB = 180-degree front-to-back ratio in dB
BW deg = Half-power beamwidth in degrees
F/SL dB = Front-to-sidelobe ratio in dB
Feed R = Feepoint resistance in Ohms
Feed X = Feedpoint reactance in Ohms
SWR 850 = 850-Ohm SWR

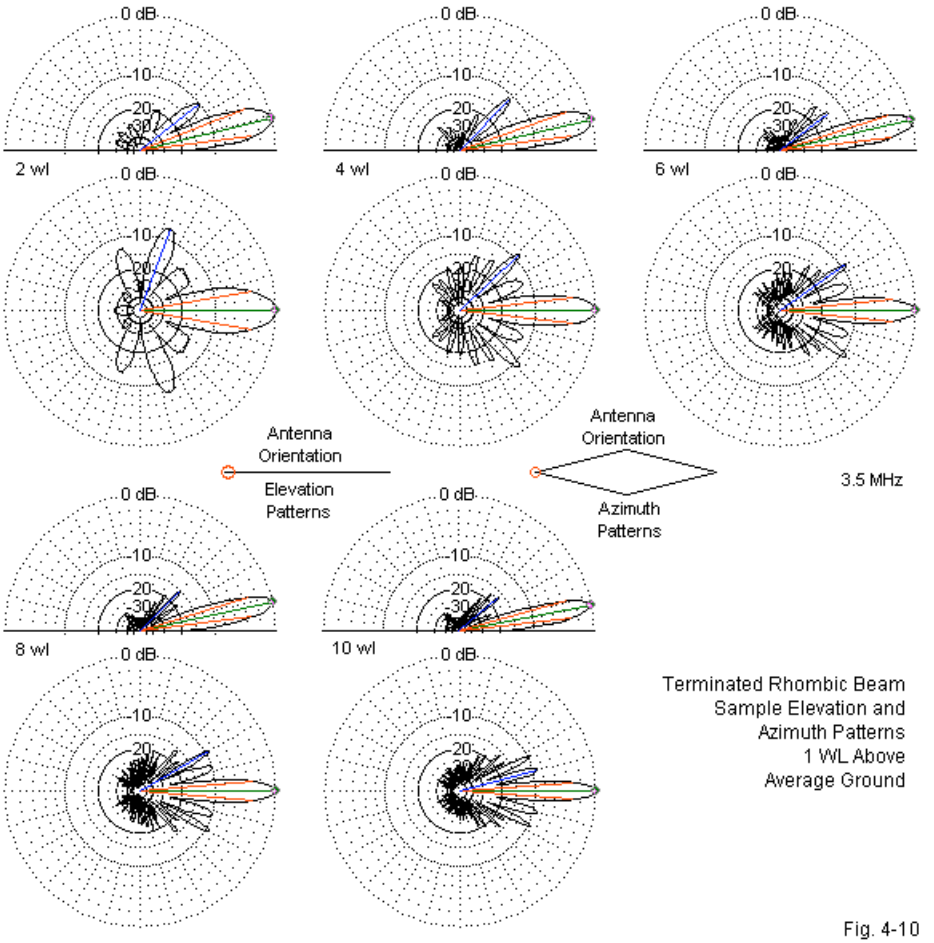

Fig. 4-10

To facilitate comparisons with both unterminated and terminated versions of the entire set of long-wires arrays, **Fig. 4-10** presents a gallery of selected elevation and azimuth patterns for the rhombic beam 1 λ above average ground. As the rhombic grows longer, high-angle elevation lobes grow weaker. As well–

just as we saw in the case of unterminated rhombics–the major sidelobes move inward toward the narrowing main lobe. Also as a function of the growing rhombic length, the rearward lobes become ever weaker.

The values of α for the rhombic at 1 λ above average ground are about 2.5° to 3° smaller than the free-space or ideal values. If we raise the antenna to 2 λ above average ground, the differential in α angles relative to free-space models drops to between 0.5° and 1°. Beamwidth values at 2 λ are only slightly wider than in free space. **Table 4-9** presents the detailed information for models at the 2-λ level.

Performance of Terminated Rhombic Beams Optimized for Maximum Gain (R = 850 Ohms) — Table 4-9

2-Wavelengths Above Average Ground

Len WL	alpha	El Ang	Gn dBi	FB dB	BW deg	F/SL dB	Feed R	Feed X	SWR 850
2	38.0	7	15.19	28.87	18.4	7.53	851	18	1.02
3	30.5	7	17.00	48.31	14.8	8.85	864	21	1.03
4	26.5	7	18.23	50.87	12.6	9.72	871	20	1.04
5	23.5	7	19.14	40.98	11.2	9.87	870	25	1.04
6	21.0	7	19.87	38.93	10.4	10.07	871	22	1.04
7	19.5	7	20.47	38.45	9.4	9.94	869	21	1.03
8	18.0	7	20.98	38.44	8.8	10.25	868	22	1.03
9	17.0	7	21.40	39.02	8.2	10.16	868	22	1.03
10	15.5	7	21.78	39.39	8.2	10.20	865	22	1.03
11	15.0	7	22.12	39.89	7.6	10.66	863	23	1.03

Len WL = Leg length in WL; double for total rhombic length
alpha = Wire angle to V centerline
El Ang = Elevation angle in degrees
Gn dBi = Maximum gain in dBi
FB dB = 180-degree front-to-back ratio in dB
BW deg = Half-power beamwidth in degrees
F/SL dB = Front-to-sidelobe ratio in dB
Feed R = Feepoint resistance in Ohms
Feed X = Feedpoint reactance in Ohms
SWR 850 = 850-Ohm SWR

Despite having overall lengths of up to nearly 22 λ, the rhombic elevation angles remain at 7° above the horizon. The use of 1° elevation-angle increments limits the precision of these numbers. Nonetheless, the rhombic at 2 λ or higher does achieve a high degree of stability in its elevation angle, making it almost purely a function of height above ground. Stronger variations in elevation angle with changes in leg length occur when the antenna is closer to ground.

Increasing the antenna height improves both the front-to-back and the front-to-sidelobe ratios, although the latter improvement is limited to an average of about 1 dB. The feedpoint impedance remains stable for all sampled leg lengths.

Because we shall be considering an alternative design method for rhombic beams, we should summarize at least part of our efforts using NEC models to derive maximum-gain rhombic designs. **Table 4-10** presents the gain and angle-α data for the free-space and the over-ground models.

Terminated Rhombics in Free Space and over Average Ground						Table 4-10
	Maximum Gain in dBi			alpha angle in Degrees		
Len WL	1 WL	2 WL	FS	1 WL	2 WL	FS
2	14.77	15.19	9.43	36.0	38.0	38.5
3	16.39	17.00	11.30	28.5	30.5	31.0
4	17.39	18.23	12.59	24.5	26.5	27.0
5	18.08	19.14	13.57	22.0	23.5	24.0
6	18.62	19.87	14.36	19.0	21.0	22.0
7	19.01	20.47	15.03	17.5	19.5	20.5
8	19.30	20.98	15.60	15.5	18.0	19.0
9	19.59	21.40	16.11	14.5	17.0	18.0
10	19.83	21.78	16.56	14.0	15.5	17.0
11	20.00	22.12	16.96	13.0	15.0	16.0
Len WL = Leg length in WL; double for total rhombic length						
1 WL = rhombic 1 wavelength above average ground						
2 WL = rhombic 2 wavelengths above average ground						
FS = rhombic in a free-space environment						

The tabular data serves as a reference for possibly more revealing graphs of the 2 data sets. For example, the gain data in **Fig. 4-11** show virtual congruence between the free-space and the 2-λ curves. However, the gain data for 1 λ has a different slope. With respect to the value of α, in **Fig. 4-12**, each curve has a slightly different slope within the limits of the 0.5° increments of α used in model construction. However, in this case, the 1-λ and 2-λ curves are more similar to each other than either curve is to the free-space curve.

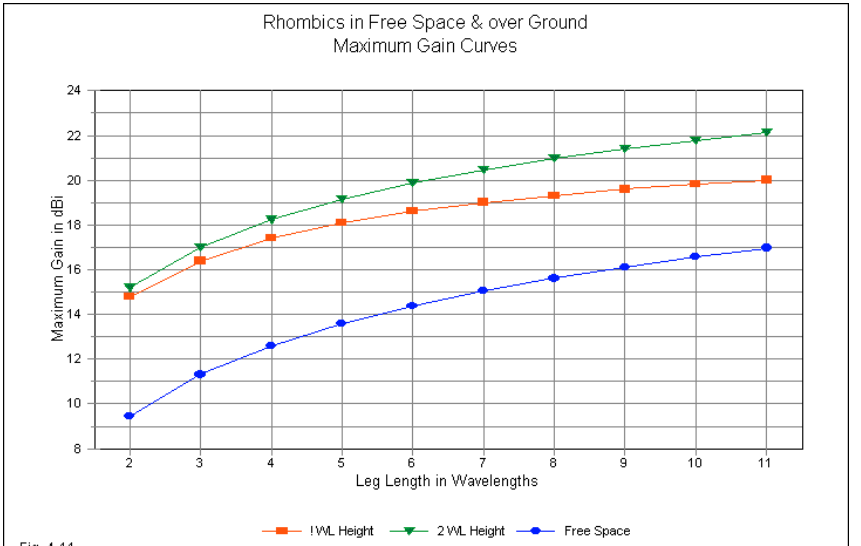

Fig. 4-11

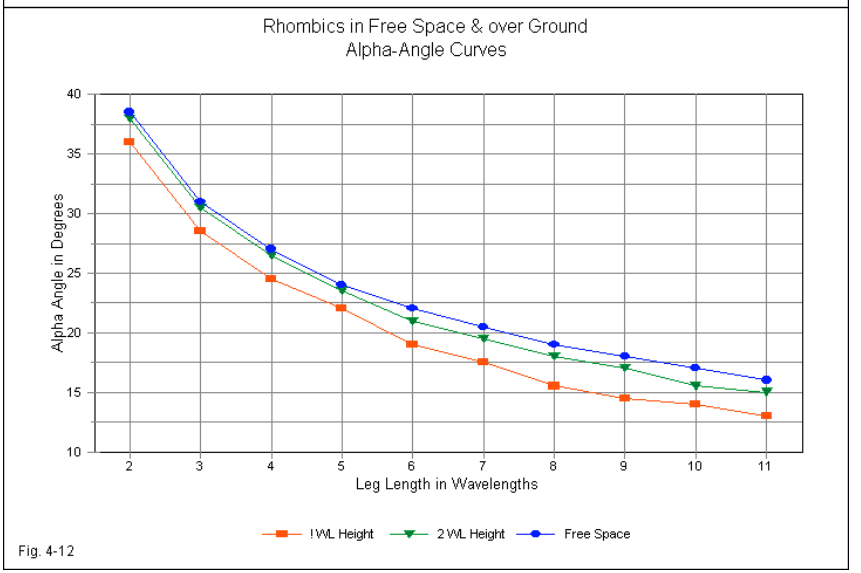

Fig. 4-12

The terminated rhombic beam has a very wide impedance bandwidth. **Fig. 4-13** shows the 850-Ω SWR values for a 4:1 frequency span from half the design frequency to twice the design frequency (1.75 to 7.0 MHz for a 3.5-MHz design frequency). The frequency increment is 0.1 MHz to show a maximum number of high and low values. The resistance for the sample frequencies ran from a low of about 790 Ω to a high of 1165 Ω. The reactance range went from -j155 Ω to +j325 Ω. These ranges coincide very well with those of the V beam with similar leg lengths, covered in the preceding chapter.

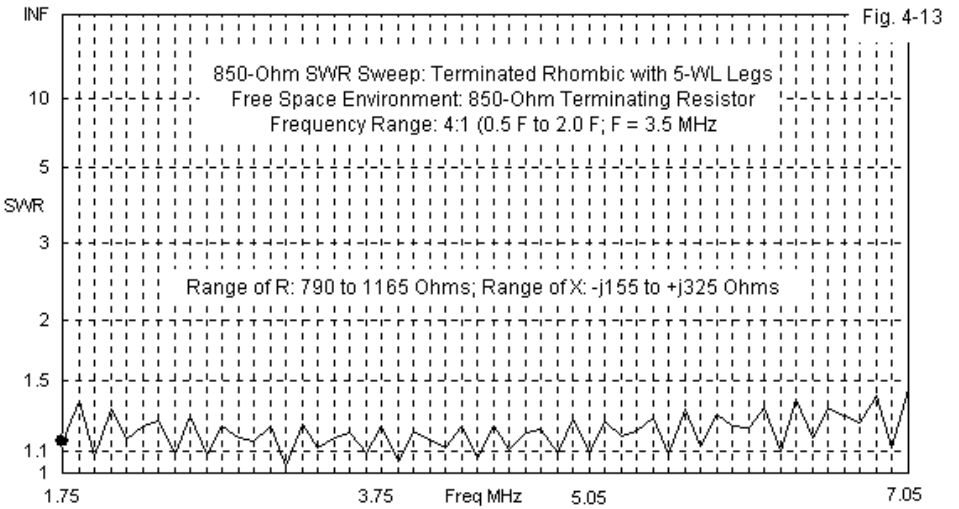

The SWR bandwidth does not necessarily indicate the effective operating range of a terminated rhombic. However, we shall withhold detailed coverage of that topic until the next chapter.

The design method that we have employed rests on achieving maximum gain for a given leg length by adjusting the value of α in a free space model. As well, we redesigned the value of α to obtain maximum gain at antenna heights of 1 λ and 2 λ above average ground (with samples of alternative ground qualities

readily available). As Bruce, Beck and Lowry noted in their 1935 paper, "one might be led to believe that the theoretical effectiveness of a horizontal rhombic receiving antenna would increase without limit, for a stable wave direction, as the properly related dimensions are increased. It will be shown that, for a given incident wave angle above the horizontal, the optimum dimensions have quite definite values." (Page 25; see introduction for the full reference.) Both in the present paper and in Bruce's 1931 article that introduced the diamond or rhombic antenna, the key interest lies in the incident angle of arriving skip radiation. Indeed, Bruce was very much more concerned about reception than about transmission. By 1931, receiver improvements had made the skip or elevation angle more significant to Bruce than the raw or maximum gain of the antenna.

As a consequence of these premises, Bruce noted that we must design the elevation angle of the radiation into the basic antenna calculations. **Fig. 4-14** shows the general principle involved.

Fig. 4-14

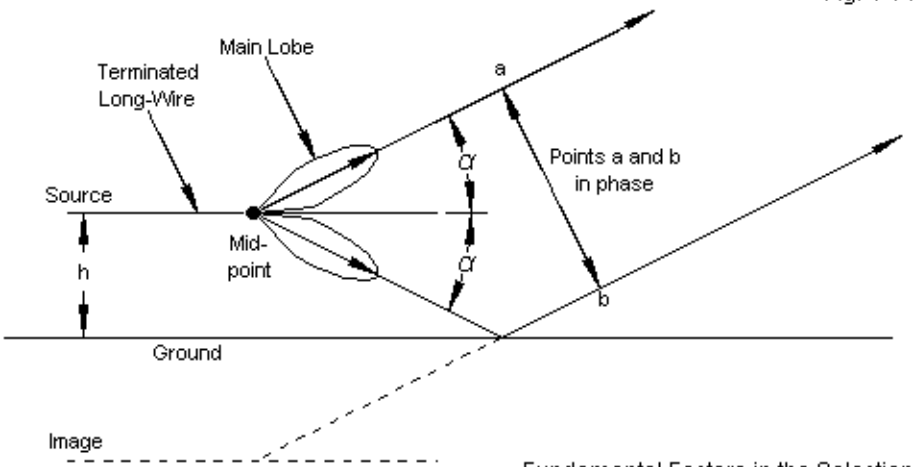

Fundamental Factors in the Selection
of a Height for a Terminated Rhombic

A long-wire antenna of any arrangement ideally projects a "tunnel" of main-lobe radiation surrounding the axis of the wire. For any given height above (perfect) ground, the portion of the tunnel projected upward forms the incident wave at an angle to the wire. By correctly selecting the antenna height, the portion of the tunnel projected downward will intercept the ground and be reflected upward according to calculations based on the theory of images. For maximum radiation at the angle indicated in the sketch, the wave fronts from the incident and reflected components must be in phase. A long-wire tunnel yields main lobes at a fixed angle to the wire, regardless of the plane in which we measure the angles in free space. The angles depend upon the length of the long-wire, whether alone or in an array of wires. As a consequence, the desired elevation angle and the leg lengths are intimately related.

The theory of long-wire antennas and arrays therefore rests on the inter-relationship between frequency, the dominant propagation angle, the antenna main-beam elevation angle, and the leg-length of a long-wire array. Since almost all texts give a prominent place to the Bruce-Beck-Lowry equations for calculating the dimensions of a rhombic beam, we should spend some time with them. Our goal will be first, to understand them, and second, to see if they are consistent with findings developed through NEC modeling, our main approach to long-wire arrays in these notes. The first step, then, is to set aside our common practices and to grow comfortable the new (old) starting point.

For the design of a rhombic, we begin with the elevation angle of the antenna's main lobe. When we match this angle to the dominant propagation angle for the frequency of choice, we best ensure reliable communications between the points for which we calculate the propagation angle. At the same time, due to the long-wire "tunnel," we fold together the elevation angle and the azimuth angle of the main lobe with respect to the array wire into a single angle that we have called angle α. This angle corresponds to textbook use of α as the angle name.

Classically, for lossless very thin wire over a perfect ground, we calculate the required height of a long-wire array from the standard lobe equation for horizontal antennas:

$$H_\lambda = [1 / (4 \sin \alpha)]$$

H_λ is the antenna height above perfect ground in wavelengths and α is the desired elevation angle. Let us suppose that we determined that the optimal elevation angle for our main beam is 14° above the horizon. H_λ is then 1.033 λ above a perfect ground.

Summary treatments of the Bruce-Beck-Lowry calculations then move on to the calculation of L_λ, the length of the each leg of a rhombic that uses a value of 14° for angle α. (14° for angle α gives us a value of 76° for angle Φ, the tilt angle or one-half the total angle between side wires at the midline of the rhombic.) We find two conditions. One of the conditions is obtaining *maximum relative field intensity* (*E*) at the prescribed radiation angle, assuming a uniform antenna current. We have already seen that a practical rhombic using a non-inductive resistive termination does not yield a pure traveling wave antenna with uniform current along even a lossless wire. As well, the peak field intensity of the beam–or the lobe's alignment–does not coincide with the prescribed angle. Nevertheless, for maximum field intensity or gain at the selected elevation angle, the required leg length (L_λ) is as follows:

$$L_\lambda = 0.5/\sin^2\alpha$$

A second condition *aligns the main lobe peak value with the desired elevation angle α*. To obtain this condition, we use a smaller constant for the calculation of L_λ.

$$L_\lambda = 0.371/\sin^2\alpha$$

The overall gain of an alignment design will be lower than the gain of the maximum-E design, since the rhombic legs will be shorter. As we shall later see, neither of these designs carries into a region where the main lobes from the 4 wires fail to coincide. So the main lobe is always aligned with the rhombic centerline.

If we again use a 14° angle for α, then the alignment design yields legs that are 6.339 λ long. The maximum-E design requires 8.543-λ legs. **Fig. 4-15** shows the general outlines of our test-case antennas. The additional dimensions in the sketches guide the setting of coordinates for test NEC-4 models using various ground qualities for each of the two cases. The total rhombic length is twice the

value of the length from the source to the midline (HL), and the total width is twice the value of W. The test models use the 4-wire construction method with a split source and a divided terminating resistor. The shorter rhombic, uses a 920-Ω terminating resistor for the best coincidence of termination and source impedances. The longer version uses a 900-Ω resistor. (These values and the 850-Ω values of terminating resistances used in models with integer leg lengths are consistent with Harper's range of actual installations.) As in past models, the test frequency is 3.5 MHz, and rhombic uses lossless 0.16"-diameter wire. Each model ran over a range of grounds from perfect to very poor, where the labels have the same values of conductivity and permittivity as in preceding chapters. For the initial modeling test of the equation-based rhombics, the aligned version checked the gain at 13° and 15° elevation to determine if maximum gain indeed aligned with the 14°-elevation angle. The maximum-E version checked gain at both the TO angle and at 14°.

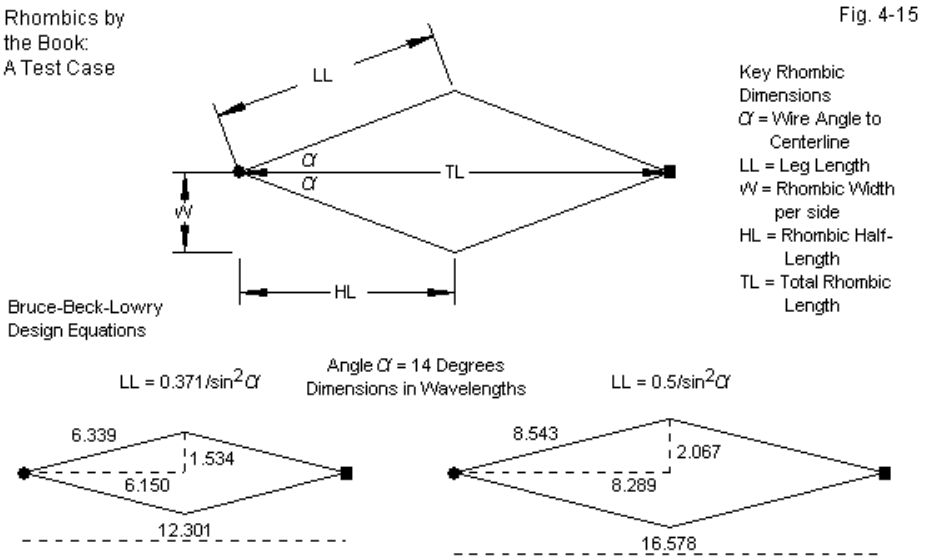

The results appear in **Table 4-11**. Peak gain and hence maximum field

strength intensity indeed occurs at 14° elevation for the aligned version of the rhombic. Ground losses did not change the elevation angle of maximum radiation within the 1° increments used in the survey of patterns. The maximum-E version of the rhombic showed a take-off angle 2° lower than the aligned version. However, for the present test, the "Gn 14" column (gain value at an elevation angle of 14°) is more significant. The equation promises maximum gain at 14° regardless of the actual TO angle. The initial test shows the gain at that angle to average about 1.2 dB higher than the aligned model.

Equation-Based Rhombic Design with Angle alpha Set at 14 Degrees; Constant = 0.371									
Antenna Height 1.033 WL; Leg Length 6.339 WL; Terminating Resistor 920 Ohms									
Gnd Type	El Ang	Gn dBi	Gn 15	Gn 13	FB dB	BW deg	F/SL dB	Feed R	Feed X
Perfect	14	17.78	17.70	17.65	37.17	15.6	5.53	922	8
Very Good	14	17.65	17.56	17.55	37.17	14.4	7.27	922	8
Average	14	17.46	17.34	17.39	37.18	13.6	9.22	923	8
Very Poor	14	17.09	16.92	17.05	37.21	13.0	11.18	922	8
Equation-Based Rhombic Design with Angle alpha Set at 14 Degrees; Constant = 0.5									
Antenna Height 1.033 WL; Leg Length 8.543 WL; Terminating Resistor 900 Ohms									
Gnd Type	El Ang	Gn dBi	Gn 14	FB dB	BW deg	F/SL dB	Feed R	Feed X	
Perfect	12	19.60	19.00	31.98	10.8	6.04	903	47	
Very Good	12	19.51	18.89	31.97	10.4	7.80	902	47	
Average	12	19.38	18.72	31.97	10.2	10.01	902	47	
Very Poor	12	19.10	18.35	31.96	10.0	10.92	902	47	
Gnd Type = Ground quality by standard label					Gn 15 = Gain at 15 degrees elevation in dBi				
El Ang = Elevation angle in degrees					BW deg = Half-power beamwidth in degrees				
Gn dBi = Maximum gain in dBi					F/SL dB = Front-to-sidelobe ratio in dB				
FB dB = 180-degree front-to-back ratio in dB					Feed R = Feepoint resistance in Ohms				
Gn 13 = Gain at 13 degrees elevation in dBi					Feed X = Feedpoint reactance in Ohms				
Gn 14 = Gain at 14 degrees elevation in dBi									Table 4-11

With respect to the aligned version of the array, the test establishes the validity within the context of NEC models for the rhombic design equations. However, it is not clear that the maximum-E version of the antenna achieves the highest gain possible at 14° elevation, but only that the gain is higher at that angle than the gain of the aligned version. To provide at least a preliminary estimate of the NEC-context validity of the maximum-E calculation, we need a second test.. In this case, I used a set of models optimized for maximum gain regardless of the elevation angle. At the test height (1.033 λ), each model uses a value of angle α that yields maximum gain, with the elevation angle being a secondary result. These models

come from the set of maximum-gain models developed earlier in this chapter.

The set of gain-optimized models used a leg-length increment of 1 λ. Therefore, none of the models had legs that are 6.339 λ or 8.543 λ. In the test, I used models that bracketed these leg values. Due to differences in the required value of angle A for maximum gain and the values required by the equation-based models, total rhombic length became an interesting figure. The 6- and 7-λ models are 1 λ shorter and longer than the aligned model, while the 8- and 9-λ models are 1 λ shorter and longer than the maximum–E version. For each model, I recorded the maximum gain at the TO angle and the gain at an elevation angle of 14°, the angle used for the equation-based designs. The results of this small survey appear in **Table 4-12**.

Comparison of Equation-Based Rhombics and Rhombic Optimized for Maximum Gain

Antenna Height: 1.033 WL above Average Ground

Antenna	Tot Len	alpha	El Ang	Gn dBi	FB dB	BW deg	F/SL dB
Eq-Align	12.30	14.0	14	17.46	37.18	13.6	9.22
Gn-6wl	11.35	19.0	12	18.70	44.08	11.2	9.04
			14	18.26	50.28	10.8	9.14
Gn-7wl	13.35	17.5	11	19.10	42.64	10.4	9.03
			14	18.38	51.22	9.6	8.13
Eq-MaxE	16.58	14.0	12	19.38	31.97	10.2	10.01
			14	18.72	30.11	9.6	8.56
Gn-8wl	15.42	15.5	11	19.38	43.06	10.2	9.22
			14	18.58	48.21	9.2	8.09
Gn-9wl	17.42	14.5	11	19.69	44.45	9.4	9.35
			14	18.46	46.55	8.6	7.02

Antenna = Antenna model: Eq = equation-based; Gn = optimized for maximum gain

Tot Len = Total rhombic length in wavelengths

alpha = Wire angle to rhombic centerline

El Ang = Elevation angle in degrees

Gn dBi = Maximum gain in dBi

FB dB = 180-degree front-to-back ratio in dB

BW deg = Half-power beamwidth in degrees

F/SL dB = Front-to-sidelobe ratio in dB

Table 4-12

The shorter maximum-gain models clearly show higher gain than the aligned version of the equation-based design, even at 14° elevation. Note that optimizing

gain requires a much larger value for angle α than the equations permit. However, the most interesting result emerges from the maximum-E rhombic and its surrounding gain-optimized models. The equation based model value for angle α is only slightly narrower than angle α for either of the maximum-gain models. Since the value of angle α is not optimal for maximum gain, the gain-optimized models show equal or higher gain at their respective take-off angles. However, at 14° the equation-based maximum-E model shows the highest gain. Although the test is not completely definitive, it does indicate the general validity of the maximum-E equation within the context of NEC modeling.

We should not overlook secondary trends within the data. For example, the models optimized for maximum gain tend to show much higher 180° front-to-back ratios than the equation-based models. Perhaps more important and more subtle is the overall pattern of sidelobes. The number and strength of sidelobes always concerned rhombic designers, whether as a matter of wasted energy or as an obstruction to secure or interference-free communications. **Fig. 4-16** shows azimuth patterns at take-off angles for the shorter set of test rhombic designs. For both models based on optimizing gain, the sidelobes are stronger, and the strongest sidelobe is the second from the main lobe. The aligned equation-based model shows overall a weaker set of sidelobes. Although the differences might not make much of a difference to amateur installations, the pattern differences might be significant to at least some commercial installations.

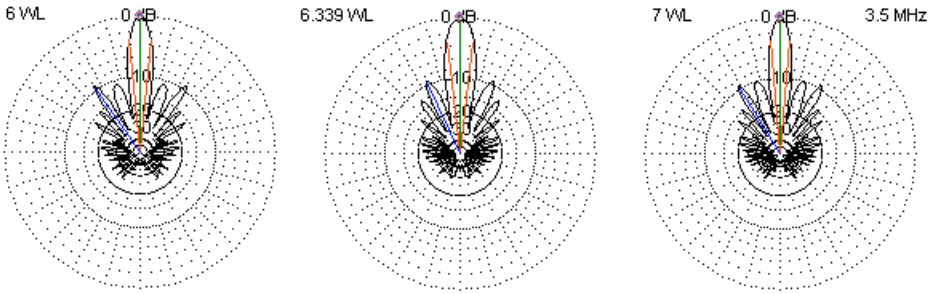

Azimuth Patterns at TO Angles: Smaller Equation-Based Rhombic
Bracketed by Nearest Rhombics Optimized for Maximum Gain

Fig. 4-16

Although the differences are subtler, the larger rhombic designs show similar trends, as revealed by the patterns in **Fig. 4-17**. Despite the similarities in the values of angle A, both gain-optimized designs again show maximum sidelobe strength in the second sidelobe. By contrast, the maximum-E array places maximum sidelobe strength in the first sidelobe. These values apply to the azimuth patterns for the indicated take-off angles. In addition, the rearward sidelobe structure of the maximum-E version of the rhombic is a bit more modest in strength.

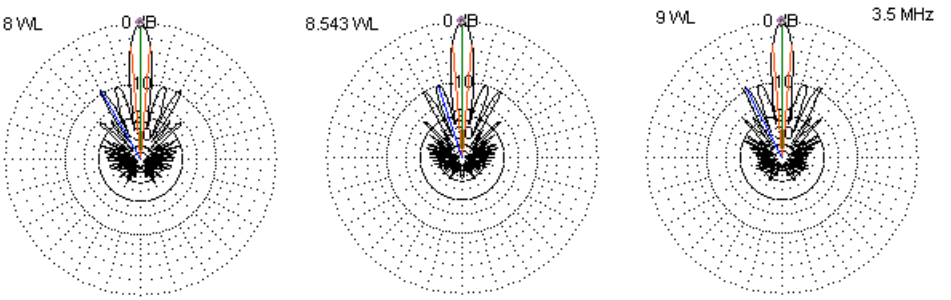

Azimuth Patterns at TO Angles: Larger Equation-Based Rhombic
Bracketed by Nearest Rhombics Optimized for Maximum Gain

Fig. 4-17

In general, then, NEC models are in close agreement with the Bruce-Beck-Lowry calculations for rhombic designs based on the selection of an optimal elevation angle to match the propagation angles for a given frequency. Our exploration has given the classical equations only a spot check, but the test suffices at least partially to validate the approach.

One interesting question raised by the Bruce-Beck-Lowry equations is whether there might be an equation to give us the value of α for the case of designs that aim for maximum gain. If we use existing design equations to solve for α, then for maximum-E and for lobe-alignment, respectively, we obtain the following equations:

$\alpha_{deg} = \sin^{-1} \mathrm{SQRT}(0.5/ L_\lambda)$ and $\alpha_{deg} = \sin^{-1} \mathrm{SQRT}(0.371/ L_\lambda)$

Only in the case of lobe alignment does α correspond to the elevation angle. As we

saw earlier, the maximum-E version of the equation accompanies a rhombic design whose elevation angle is lower than α.

The next step is to determine at what height over ground the tracing equation for α will apply. If the height is too low, then the value of α becomes very much dependent upon both the height above ground and the ground quality. Figure **4-12** showed us that the slopes of the angles for curves that track α for rhombics with leg lengths from 2 to 11 λ have different slopes and therefore answer to different equations. However, at heights of 2 λ and above, the slope of the curve for α stabilizes, as does the elevation or take-off angle. At this height and upward, an effective tracking equations has the following form:

$$\alpha_{deg} = \sin^{-1} \text{SQRT}(0.742/ L_{\lambda})$$

Note that the requisite constant is twice the value of the constant for the aligned-lobe version of the original equations. **Table 4-13** shows both the calculated and the modeled values of angle α for maximum gain. Within reasonable margins, the two columns track each other very well.

The table also shows the value of angle α for a 1-λ height. The differences in the values of angle α tend to be irregular, largely due to the more rapid changes in elevation angle for the lower rhombics. The single table cannot show the further variations in elevation angle created by changing values of ground quality. Hence, the utility of the new equation for optimizing gain is marginal beyond its use as a starting point in finding angle α via models. For that reason, I tend to call it a "tracking equation" rather than a "design equation."

The original Bruce-Beck-Lowry equations included versions for compromise relationships between the desired elevation angle and the desired leg-length of the rhombic. However, for most cases, it is simpler to create a NEC model using the desired antenna height, the desired α angle, and the desired leg-length and to examine the outcome. One may then adjust any of the factors in a systematic manner to explore the design options. As well, NEC calculates the structure and the strength of all sidelobes within the azimuth increment in the radiation pattern.

Angle alpha Estimates for Rhombic Beams					Table 4-13
	2 Wavelengths above Average Ground or Higher				
Leg Len.	alpha Cal	NEC 2WL	NEC-Calc	NEC 1WL	NEC 2-1
WL	degrees	degrees	Difference	degrees	Difference
1	59.5				
1.5	44.7				
2	37.5	37.75	0.2	36.25	1.5
2.5	33.0				
3	29.8	30.25	0.4	28.75	1.5
3.5	27.4				
4	25.5	26.25	0.7	24.50	1.75
4.5	24.0				
5	22.7	23.25	0.6	22.00	1.25
5.5	21.5				
6	20.6	21.00	0.4	18.75	2.25
6.5	19.7				
7	19.0	19.25	0.2	17.25	2
7.5	18.3				
8	17.7	17.75	0.0	15.75	2
8.5	17.2				
9	16.7	16.75	0.1	14.50	2.25
9.5	16.2				
10	15.8	15.75	-0.1	14.00	1.75
10.5	15.4				
11	15.1	15.00	-0.1	13.00	2
Notes:	Leg Len. WL = Leg length in wavelengths				
	alpha Cal degrees = Calculated alpha for 2-wavelength				
	heights and higher from A = arcsin [SQRT (0.742/L)]				
	NEC 2WL degrees = alpha for NEC models 2				
	wavelengths above average ground. NEC entries use				
	n.25 or n.75 whenever 2 adjacent values for angle A				
	show a gain difference of 0.01 dB or less.				
	NEC-Calc Difference = Difference between NEC model				
	and calculated angle in degrees.				
	NEC 1WL degrees = alpha for NEC models 1				
	wavelength above average ground.				
	NEC 2-1 Difference = Difference in alpha for				
	models 2 and 1 wavelength above average ground.				

A second question that arises as a result of the Bruce-Beck-Lowry equations involves an appreciation for what happens as we vary the value of α in a conventionally designed rhombic, that is, one designed for maximum gain at a given height or in free space. To sample this set of conditions, I selected a rhombic with 5-λ legs. The legs are long enough so that changes occur fast enough to include in a finite table, but short enough that the increments of change did not result in wholesale shifts of performance properties. The subject antenna is 1 λ above average ground in order to see if varying the α angle alone is sufficient to produce significant changes in the elevation angle of the main lobe. Perhaps the one performance characteristic that changes least is the feedpoint impedance with the 850-Ω terminating resistor.

Results of Varying Angle alpha in a 5-Wavelength-Leg Rhombic Beam 1 Wavelength above Average Ground

alpha	El Ang	Gn dBi	FB dB	HBW deg	VBW deg	F/SL dB	Feed R	Feed X	SWR 850
12	16	13.91	38.37	18.4	11.2	7.97	846	26	1.03
14	16	15.35	40.93	16.8	11.7	8.34	852	23	1.03
16	15	16.54	43.08	15.4	11.9	8.97	856	23	1.03
18	14	17.43	42.93	14.2	12.0	9.86	863	25	1.03
20	13	17.97	44.71	12.8	11.9	9.02	867	23	1.03
22	12	18.08	46.84	11.6	11.7	8.89	867	25	1.04
24	11	17.64	54.61	10.4	11.2	8.84	870	28	1.04
26	10	16.48	46.21	9.0	10.6	5.90	873	25	1.04
28	10	14.39	38.19	7.6	9.9	1.57	870	23	1.04

alpha = Wire angle to rhombic centerline
El Ang = Elevation angle in degrees
Gn dBi = Maximum gain in dBi
FB dB = 180-degree front-to-back ratio in dB
HBW deg = Horizontal half-power beamwidth in degrees
VBW deg = Vertical half-power beamwidth in degrees
F/SL dB = Front-to-sidelobe ratio in dB
Feed R = Feepoint resistance in Ohms
Feed X = Feedpoint reactance in Ohms
SWR 850 = 850-Ohm SWR

Table 4-14

Table 4-14 tracks the data in α angle increments of 2°. The value of α for maximum gain is 22°, as indicated by the peak gain value at this angle (18.08 dBi). The value is not the center value of the table, nor does the highest value of α (28°) represent a gain level that is equal to or lower than the value for the other table extreme (12°). The asymmetry of the table results from the fact that for α angles of more than 28°, the main forward lobe no longer is in line with the centerline of the array. In fact, the azimuth patterns undergo considerable change as we alter the value of α without changing either the height of the leg-length of the array. (Of course, as we change the value of α, the overall length and peak width of the rhombus will change.) **Fig. 4-18** samples the pattern evolution.

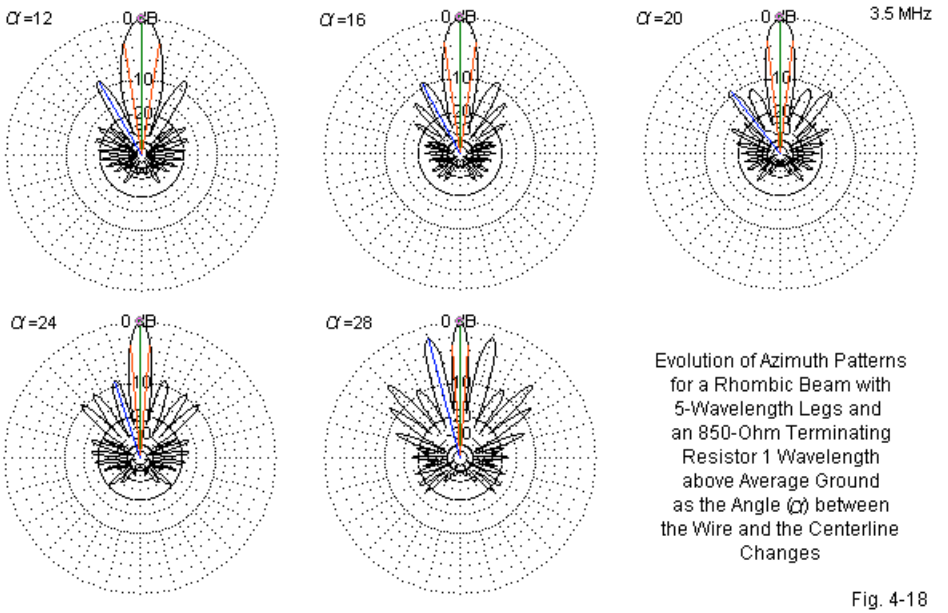

Evolution of Azimuth Patterns for a Rhombic Beam with 5-Wavelength Legs and an 850-Ohm Terminating Resistor 1 Wavelength above Average Ground as the Angle (α) between the Wire and the Centerline Changes

Fig. 4-18

As we increase the value of α–sampled at 4° intervals in the figure–the number of major forward sidelobes increases. At 12°, we find only one major sidelobe on each side of the main lobe, but at 28°, we find five. For values of α below 25°, the strongest sidelobes are at least 9 to 10 dB below the strength of the main lobe. However, as we further increase the value of α, the innermost sidelobes become very strong. Above 28°, the former sidelobes become the twin major lobes, and the center lobe becomes weaker. Hence, an α angle value of 28° is a practical upper limit for the exercise.

As revealed in **Fig. 4-19**, the value of α also has a bearing on the strength of higher-angle elevation lobes. However, the progression is slower, and so 3 patterns will serve to show the phenomenon. The higher-angle lobes are weakest when α is closest to its optimal value for maximum gain. When α departs significantly from the optimal value, the higher-angle lobes become stronger. Elevation sidelobe strength grows considerably at high values of α, as the take-off angle diminishes.

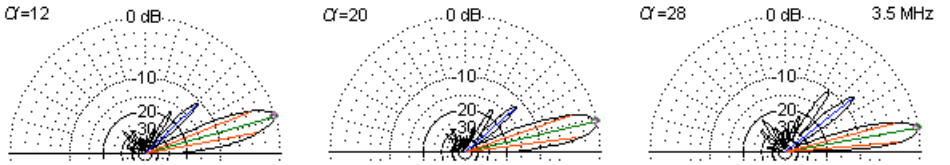

Evolution of Elevation Patterns for a Rhombic Beam with 5-Wavelength Legs and an 850-Ohm Terminating Resistor 1 Wavelength above Average Ground as the Angle (α) between the Wire and the Centerline Changes

Fig. 4-19

Fig. 4-20 graphs the main lobe maximum gain values and elevation angles over the sampled range of α values. The gain curve is unexceptional, although we may note the 4-dB difference between maximum and minimum values.

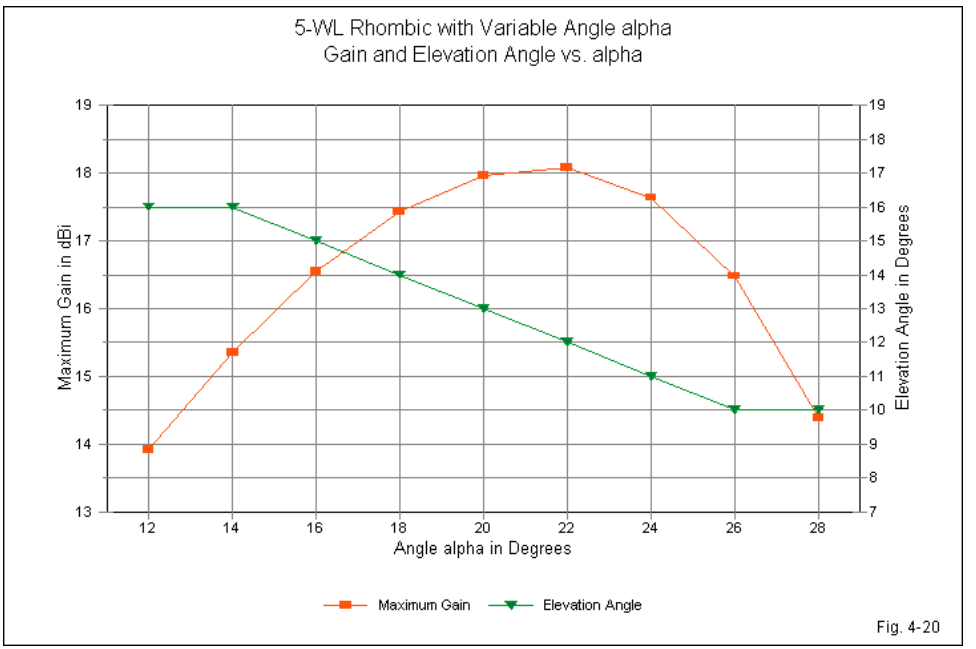

Fig. 4-20

More significant perhaps is the change in the elevation angle of maximum radiation with changes in the value of α. The leg lengths remain constant, so that with an increasing value of α, the overall rhombic length becomes shorter. However, increasing the value of α yields a lower take-off angle. Over the range of sampled values of α, the elevation angle decreases by 6°, a significant amount if a design goal is to place the main elevation lobe within a desired range of angles for either reception or transmission via skip phenomena.

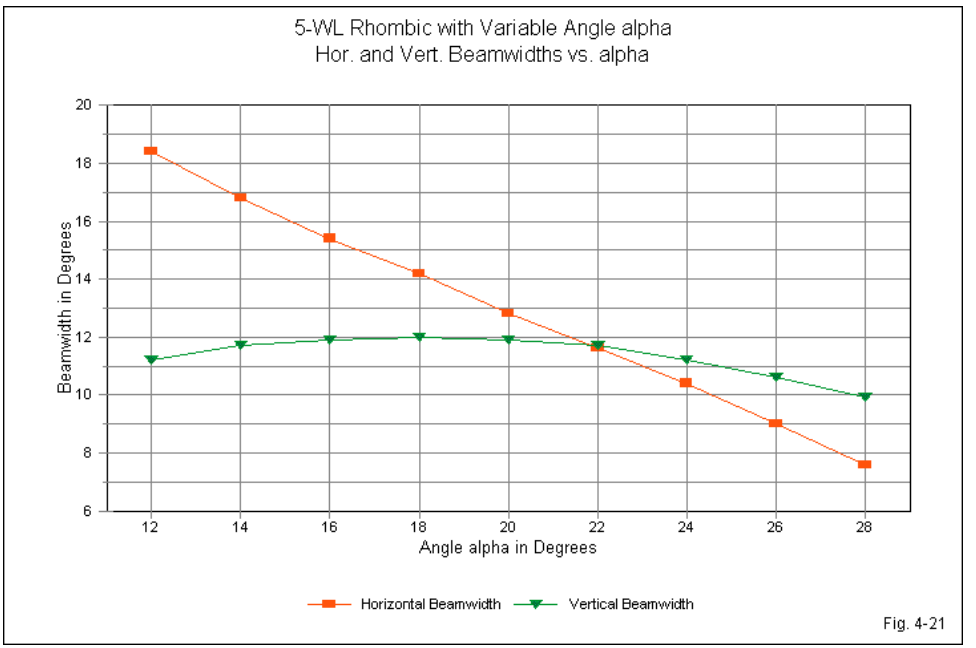

Fig. 4-21 tracks the horizontal and vertical beamwidth data from **Table 4-14**. The horizontal beamwidth shows a linear decline with increasing values of α. The decrease in beamwidth results in large measure from the growth of the major forward sidelobes. As these sidelobes become stronger, they also become wider, shrinking the available beamwidth for the main forward lobe. Although the patterns shown in **Fig. 4-18** may seem initially random in their development, the beamwidth

data strongly suggests otherwise. A random development of forward sidelobes could not yield such a linear curve for the main lobe beamwidth.

The vertical beamwidth curve may seem worth little notice. However, it also contains a surprise for the uninitiated. For most horizontal antenna designs, the vertical beamwidth is a function of the elevation angle of the main lobe, and the two values will usually be nearly equal as measured in degrees. However, we do not reach that equality until we use the widest value of α. Then the elevation angle and the vertical beamwidth are both about 10°. For smaller values of α, the vertical beamwidth value is considerably smaller than the elevation angle.

Although we have explored the effects of varying α while holding other factors constant for only one size of rhombic beam, you may easily replicate the exercise for any of the other rhombics in the collection found in the various tables in this chapter. Design techniques ranging from classical equations to graphical aids may result in the development of a professionally acceptable rhombic beam for almost any situation. However, the facility offered by antenna modeling software for varying individual rhombic parameters allows a more complete analysis and understanding of the antenna's performance characteristics. Even if long-wire technology has passed its prime, even for point-to-point communications in the HF range, understanding the capabilities and limitations of long-wire arrays remains a useful enterprise. These notes are only a small beginning in that direction.

Intermission

We cannot call this summary section of the chapter a conclusion, because we have further paths to explore in the rhombic portion of our safari. The rhombic proved so successful, relative to its era of development and the HF communications needs of the time, that it has experienced the greatest effort at improvement and re-design of any of the long-wire antennas.

We began, almost as a side-note and reference section, with the unterminated rhombic array. Because the rhombus is inherently a closed geometry, we uncovered an equality between open and closed unterminated rhombic arrays, on the one hand, and rhombics terminated by indefinitely large

and infinitesimally small termination impedances, on the other. The open rhombic array managed a slightly higher gain and somewhat smaller sidelobes than the closed version.

Although unterminated rhombic arrays showed gain increases over unterminated V arrays as a function of the additional wire sections that doubled the array length for any given leg length, the beamwidth values for the two array types are very comparable. However, the tracking equations for the two types of arrays differ. The V array requires a 5% reduction relative to the tracking equation for simple long-wires of the same leg length. In contrast, the unterminated rhombic required a 10% increase over the same basic formula.

When we turned to terminated rhombic beams, we found two design roads. One route was simply an extension of the design procedures used throughout these notes: to develop rhombic models for maximum gain at the sampled leg lengths by finding the optimal value of α. This method of design produced high performance beams with a minimal gain deficit relative to unterminated rhombics–a contrast to the other forms of long-wire arrays.

The other pathway returned us to the origins of classical design equations for rhombics, as well as to their motivation. The most basic element in rhombic design was the desired elevation angle for receiving HF skip signals. That angle determined the value of α for use in designing the horizontal arrangement of wires. Sample NEC models established the general validity of the method for designing rhombics with main lobes aligned with the desired elevation angle and rhombics with maximum field strength or gain at the desired elevation angle. The results led us to explore further, first for a tracking equation for maximum gain rhombics at heights that minimized ground influences and second for a further understanding of the effects of varying α for rhombic performance.

Despite our long trek through rhombic pathways, we have a significant amount of unfinished business with the rhombic.

1. *Multiple Rhombic Solutions*: For any installation, we can find multiple rhombic designs to suit the even rigid specifications of wave angles and site

boundaries. The latter condition is exceptionally important to amateur installations.

2. *Multi-Band Rhombics*: In both professional and amateur service, the rhombic has served on multiple frequencies. In fact, *The ARRL Antenna Book* has shown a rhombic design for 20 through 10 meters since the mid-1970s. We need to explore the operating frequency limits for an effective rhombic to see how far short they may fall relative to the SWR operating limits.

3. *Multi-Modeling Potentials*: We have noted that the modeling technique used in this chapter is but one of at least two ways to model a rhombic. Before we reach any final conclusions on the modeling adequacy of these notes, we need to compare techniques and to evaluate the results

4. *Multi-Wire Rhombics*: One common method of trying to improve rhombic beam performance is to use more than 1 wire for each leg. The usual arrangement consists of 3 wires that come together at the rhombic points and spread in the middle by relatively arbitrary distances. The arrangement presents both theoretical and modeling challenges, and careless modeling of a 3-wire rhombic can lead to erroneous results.

5. *Multi-Element Rhombics*: In the late 1950s, Laport developed the multi-element rhombic beam to improve both gain and sidelobe suppression. Since the antenna has seen use on the UHF amateur bands, the design bears at least an initial exploration to look at both design and modeling issues.

Although the subjects in our list of unfinished business are diverse, perhaps multiplicity itself may serve to bind them together into a final chapter of notes.

5.

Rhombic Multiplicities

> Considerable control of the main beam of the rhombic can be obtained by varying the element length and angle between elements and tilting the plane of the rhombic. Arrays of rhombics are also employed to control the radiation pattern. Arrays are principally used to increase gain and decrease sidelobes. A great deal of design data on rhombic antennas is available in the literature.
>
> Carlton H. Walter, *Traveling Wave Antennas*, p. 321

With the exception of the Yagi-Uda parasitic array, perhaps no antenna has undergone so much study and modification as the rhombic beam. For more than 30 years, the rhombic–in one or another guise–served as the principal HF point-to-point communications antenna. We cannot hope to cover all modifications and variations on the rhombic (and other long-wire arrays), but perhaps we can examine some of them. At the close of the preceding chapter, I identified several items that form the theme of this chapter: multiplicity. In brief form, the list includes the following items.

–Multiple rhombic solutions
–Multi-band rhombics
–Multi-modeling potentials
–Multi-wire rhombics
–Multi-element rhombics

We shall look at each item in its turn. However, we might first spend a moment summarizing our approach to long-wire antennas in order to avoid certain misconceptions that might arise. The best place to begin is with the contrast between the modeling approach and traditional design-calculation approaches.

Multiple Rhombic Solutions

Classic long-wire design approaches begin with the geometry formed

between an end-fed long wire antenna and its main lobes. In free space, that geometry involves an angle that we have labeled α. Idealized phase calculations then yield an initial relationship between α and the length of the long-wire antenna:

$L_\lambda = .5 / (1 - \cos \alpha)$ and $\alpha = \cos\text{-}1 [1 - (.5 / L_\lambda)]$

The term L_λ is the wire length in wavelengths, while α is the angle between the wire axis and the peak of the main lobe on either side of the wire. For simple long wire antennas, whether terminated or unterminated, the modeling data tracked better with a modification of the idealized equations, one that has been well published in engineering literature:

$$\alpha = \cos^{-1} [1 - (0.371 / L_\lambda)]$$

Moreover, this tracking equation for the value of α for simple long-wires applied only to free-space models. When we placed the long-wire over ground of any kind, from perfect to very poor, the value of α at the elevation angle of maximum radiation changed. Furthermore, the value of the elevation angle changed with the length of the wire, even for models without vertical connections to ground. The amount by which the elevation angle changed varied with the height of the antenna and with the quality of ground. The lower the antenna and the poorer the ground, the greater that the angle changed with increasing antenna length.

The earliest or most idealized calculations of the proper angle for a V array or for a rhombic assume that the required wire angle to make main lobes from each wire join for maximum gain along the array centerline is the same angle α that we tracked with simple long-wires. However, for free space models, we discovered that if each of these antennas is to arrive at maximum gain, then we need to modify the tracking equation. For V arrays, the required equation is approximately the following one.

$$\alpha = 0.95 \cos^{-1} [1 - (0.371 / L_\lambda)]$$

For terminated V beams, the value of α tracked more closely with the unmodified

equation. Once more, the height of the antenna and the quality of the ground beneath the antenna modified antenna performance in terms of the elevation angle.

Free-space models of the rhombic required a different modification to the long-wire equation for α to achieve maximum gain.

$$\alpha = 1.1 \cos^{-1} [1 - (0.371/L_\lambda)]$$

This tracking equation proved equally applicable to terminated and unterminated rhombics. Nevertheless, introducing ground into the antenna environment again altered the value of α relative to the production of maximum gain from the antenna.

Classical calculations of optimal V and rhombic beams not only assume that the same values of α apply to all long-wire antenna type and that they also apply over ground. As well, the calculations also assume an idealized or perfect ground. The motivation is to apply to the equations image concepts to arrive at a condition for optimizing element lengths. Let's call the elevation angle over perfect ground–also called the wave angle in much early literature–α_E. For contrast, we shall call the azimuth angle α_A. From a purely geometric perspective, we can define an optimizing condition, namely the following one:

$$\alpha_A = \alpha_E$$

Under this condition, we can initially define for an desired wave angle, α_E, an initial pair of optimizing equations for both V and rhombic beams to determine the best antenna height, H_λ, and the best leg length, L_λ.

$$H_\lambda = [1 / (4 \sin \alpha_E)] \quad \text{and} \quad L_\lambda = 0.5 / \sin^2 \alpha_E$$

Optimizing the leg length for a rhombic has more than one meaning. In this case, it is the length of rhombic leg that yields the highest gain at the desired wave or elevation angle. However, the peak gain of the lobe does not align with value of α_E. To achieve alignment between the peak gain and the elevation angles requires that we use a modified calculation for leg length.

$L_\lambda = 0.371 / \sin^2 \alpha_E$

As the modeling exercises showed, neither equation yields a rhombic that achieves maximum gain regardless of the elevation or wave angle. The general purpose of these exercises was to see what a monoband long-wire array might achieve. However, a long-wire array optimized for maximum gain may not be suitable for all proposed installations. The first consideration raised by this fact involves the typical amateur rhombic installation. **Fig. 5-1** shows the general limiting conditions.

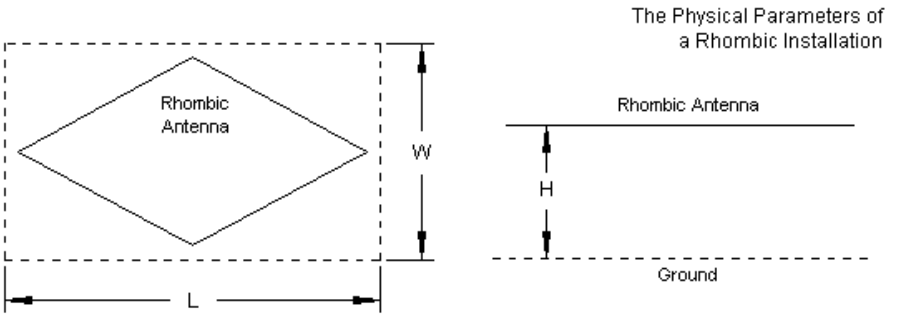

Fig. 5-1

The sketch in all its simplicity carries a relatively profound meaning: amateur installations generally operate within physically defining limitations. The left sketch obviously shows the maximum overall length and width that any rhombic might have. The maximum height generally emerges from a variety of factors, including the availability of supports and any codes or regulations that govern the maximum height of an antenna at the intended location.

The next consideration is the desired wave angle or signal elevation angle at the design frequency. At this point, you must not assume that a certain angle is best. First, signal angles tend to come in groups. Second, there may be more than one group of angles with a statistically high percentage of signal occurrences. Current editions of *The ARRL Antenna Book* carry an accompanying CDROM with

statistical tables summarizing signal angles over a full 11-year sunspot cycle for multiple locations relative to numerous regions of the world. Focusing in on a single elevation angle may prove less productive than examining a span of promising angles.

The merit of modeling is that it allows the long-wire array designer to vary the leg length, the α_A angle, and the antenna height to arrive at the best combination relative to a given site. Of course, siting considerations take into account all of the environmental conditions affecting the antenna. These factors would include both real wire losses from intended materials, the real value of the terminating resistor(s), and the ground quality for the antenna region (including the area of initial ground reflection). Except in highly restricted circumstances, more than one possible combination of long-wire variables will satisfy the modeling limits, and the array builder must then select the best combination. That combination may or may not fit the terms of classical design formulations.

To see how we may customize the highest-performance terminated rhombic for a given space, let's return to **Fig. 5-1** and set some values for L, W, and H. For the design frequency, the maximum length will be 8 λ in the direction of the communications target. The maximum width will be 3.5 λ. The tallest manageable supports will be 1.2 λ. (At 20 meters, the available space would be about 560' by about 245', with 84' supports.) The soil quality is very poor (conductivity 0.005 S/m, relative permittivity 5). The desired elevation angle (α_E) is centered at 12°.

Multiple Solutions												Table 5-1
Maximum Area: 8 WL by 3.5 WL (aligned with target)						Ground Quality: Very Poor (conductivity 0.005 S/m, relative permittivity 5)						
Leg Len	alpha	Ttl Len	Ttl Width	Height	El Ang	Gn dBi	FB dB	BW deg	F/SL dB	Feed R	Feed X	SWR 850
5.0	22.0	9.272	3.746	1.0	12	17.79	46.15	11.6	9.55	866	26	1.04
4.0	24.5	7.280	3.318	1.1	12	17.55	47.51	13.4	8.78	876	22	1.04
4.4	23.0	8.100	3.438	1.1	12	17.87	24.49	12.9	8.93	1025	3	1.21
4.3	22.5	7.945	3.292	1.1	12	17.72	23.08	13.6	8.84	929	108	1.16
4.3	23.0	7.916	3.360	1.1	12	17.78	23.18	13.2	8.90	931	110	1.17
4.3	23.5	7.887	3.430	1.1	12	17.82	23.31	13.0	8.95	934	111	1.17
4.3	24.0	7.856	3.498	1.1	12	17.82	23.46	12.6	9.07	937	113	1.17
4.3	24.5	7.826	3.566	1.0	12	17.59	23.60	12.2	8.97	941	114	1.18
Notes:	Leg Len = Leg length in wavelengths						FB dB = 180-degree front-to-back ratio in dB					
	Ttl Len = Total rhombic length in wavelengths						BW deg = Half-power beamwidth in degrees					
	Ttl Width = Total rhombic width in wavelengths						F/SL dB = Front-to-sidelobe ratio in dB					
	Height = Height above ground in wavelengths						Feed R = Feepoint resistance in Ohms					
	El Ang = Elevation angle of maximum radiation in degrees						Feed X = Feedpoint reactance in Ohms					
	Gn dBi = Maximum gain in dBi						SWR 850 = 850-Ohm SWR					

Table 5-1 summarizes the modeling work required to select an apt rhombic. Note that standard calculations from Chapter 4 will not allow us to arrive at a solution, since even the smaller aligned rhombic requires 8.6-λ legs for an overall length of about 17 λ. We might use one of the compromise calculation vehicles supplied in the Bruce-Beck-Lowry collection, but modeling is faster, especially since we have reference models for 4- and 5-λ legs already available as a guide. See the first two lines of the table. Of course, the model with 5-λ legs is too large for the plot, while the 4-λ-leg model is smaller than it might be and still fit the plot outline.

The next step using 4.4-λ legs was a trial model at an estimated optimized value of α, and it also proved too large, although just barely so. The next series of models used 4.3-λ legs, but used the exercise at the end of Chapter 4 as a guide to finding the best compromise between the correct size and the best performance. The models vary the value of α between 22.5° and 24.5°. As we dropped the leg length below 5 λ, we had to increase the antenna height to 1.1 λ to obtain the desired elevation angle. In the sequence of models with 4.3-λ legs, the largest value of α required a return to 1 λ as the height. As we saw in Chapter 4, varying the value of α adds another variable to the collection that can influence the elevation angle.

The most promising models appear to be the 4.3-λ versions using 23.5° and 24° as the values of α. These models are close enough to an odd multiple of a quarter-wavelength to show vestiges of simple long-wire behavior. For example, the front-to-back ratio is lower than for models that are a multiple of a half-wavelength. The gain level is slightly higher than for a 5-λ model, although certainly not enough for more than numerical notice. As well, the feedpoint impedance is higher than for models that are multiples of a half-wavelength. For this specific installation, you might even wish to change the value of the terminating resistor to reduce the feedpoint reactance. Both models fit the property limits, although the version using 23.5° as the value of α leaves a little room for support posts outside the perimeter of the antenna proper.

The exercise required less than 30 minutes. As well, it made available a complete set of elevation and azimuth patterns, along with additional information on all lobes of the antenna at all angles. The technique offers options, some of which

we can instantly exclude and others that may give us reason to ponder before making a final decision.

These practical notes do not in any way void the classical design formulations. Nor do they suggest that use of the classical equations will produce a poor array. Indeed, striving for maximum gain may in some cases be just the wrong tack to take. At the end of Chapter 4, we saw that we may vary the value of α over a considerable range and still wind up with a working rhombic beam of considerable performance potential. In some cases, we may also select an alternative value of α for reasons that involve neither gain nor siting limitations.

Multi-Band Rhombics

The American Radio Relay League used an unterminated rhombic at its Newington, Connecticut, site from 1937 onward in order to provide coverage to the west coast of the U.S. The antenna came down when the League moved its headquarters to a new building on the site. A 3-element Yagi set up to replace the rhombic did not match the performance of the earlier antenna, So the League re-installed the rhombic in the mid-1960s. New generations of Yagis that were better able to implement the theoretic capabilities of the antenna eventually supplanted the long-wire array. Even western red cedar poles have a finite lifetime as antenna supports.

When ARRL first started publishing its *Antenna Book*, it provided a strong chapter (5) on long-wire antennas. Around 1970 or so, it added to the chapter a multi-band terminated rhombic designed to cover 20 through 10 meters. The antenna design, derived from data taken from Harper's 1941 volume, sought to take advantage of the published ability of rhombics to operate effectively over at least a 2:1 frequency range. **Fig. 5-2** shows the published dimensions of the antenna. I have added the angular data. The antenna uses 3-λ legs at 14 MHz, with an α of 26° (and a Φ or tilt angle of 64°). At the highest frequency, the legs are about 6 λ long. The height of 1 λ is at the lowest operating frequency (14 MHz), or about 70'. The terminating resistor is 600 Ω to coincide with the use of 600-Ω transmission line. We can presume that the antenna consists of AWG #12 copper wire, and that the ground quality is average.

Fig. 5-2

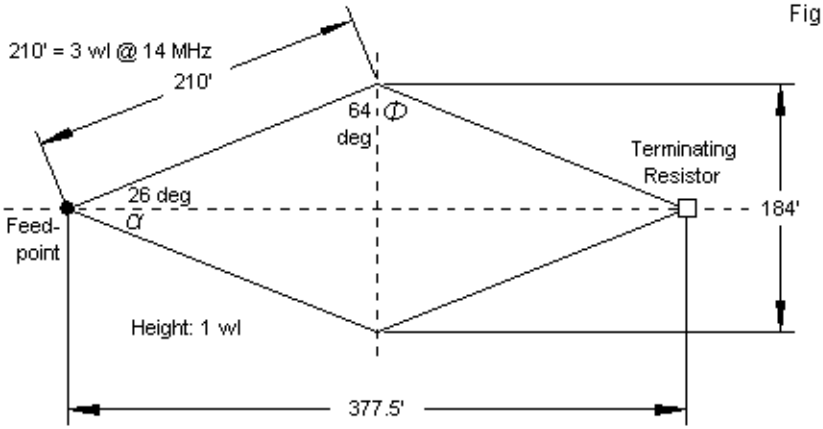

Dimensions of the ARRL Multi-Band Rhombic Beam for 14-28 MHz

The multi-band ARRL rhombic design does not coincide either with the maximum gain designs shown in Chapter 4 or with basic Bruce-Beck-Lowry calculations. The maximum-gain design using 3-λ legs yields a 28.5° value for α. A lobe-aligned basic design for the 14°-elevation angle calls for longer elements. The design is quite evidently a compromise.

We may translate the design to our basic test frequency (3.5 MHz) for some initial comparisons. We shall scale the antenna, use lossless 0.16" diameter wire, and model it using 20 segments per wavelength. (We shall eventually return more directly to the original design.) However, the first test involves seeing how much the design compromise might compromise performance. **Table 5-2** compares the two versions of the antenna at the test frequency. The table examines both antennas with terminating resistors ranging from 600 Ω to 900 Ω. Perhaps the first notable comparison is that there is no significant difference in feedpoint impedance created by the difference in the value of α. More significant to general rhombic design is the fact that we find a value of terminating resistor that most closely coincides with the feedpoint resistance (about 850 Ω).

Selecting the Most Nearly Correct Rhombic Termination						Table 5-2
Terminated Rhombics with 3-Wavelength Legs; 1 WL above Average Ground						
Optimized for Maximum Gain			alpha = 28.5 degrees			
R Load	Gn dBi	FB dB	BW deg	F/SL dB	Feed R	Feed X
900	16.39	29.82	15.8	8.31	887	41
850	16.39	38.85	15.8	8.26	863	28
800	16.39	38.99	15.8	8.20	838	16
750	16.39	29.19	15.8	8.14	812	3
700	16.39	24.46	15.8	8.08	785	-9
650	16.40	21.24	15.8	8.02	758	-22
600	16.41	18.76	15.8	7.94	729	-24
ARRL Rhombic			alpha = 26.0 degrees			
R Load	Gn dBi	FB dB	BW deg	F/SL dB	Feed R	Feed X
900	16.04	30.71	17.2	8.49	887	37
850	16.04	41.16	17.2	8.44	864	23
800	16.04	35.97	17.2	8.38	839	8
750	16.04	28.07	17.2	8.32	813	-7
700	16.04	23.74	17.2	8.25	786	-21
650	16.05	20.71	17.2	8.18	758	-36
600	16.06	18.32	17.2	8.10	729	-50
Notes:	R Load = Terminating resistor in Ohms					
	Gn dBi = Maximum gain in dBi					
	FB dB = 180-degree front-to-back ratio in dB					
	BW deg = Half-power beamwidth in degrees					
	F/SL dB = Front-to-sidelobe ratio in dB					
	Feed R = Feepoint resistance in Ohms					
	Feed X = Feedpoint reactance in Ohms					

Early amateur designs suggested the use of a 600-Ω terminating resistor due to the early difficulty in constructing parallel transmission lines with higher impedance values. However, modern materials make such construction routine, since RF-rated plastics have supplanted the old wood separators boiled in paraffin. Over a 2:1 frequency ratio, The difference in the system's characteristic impedance can make a difference in the measured SWR values. When radio amateurs had only 10, 15, and 20 meters has their upper HF bands, the

differences would not show up. However, the addition of the non-harmonic 17- and 12-meter bands suggests that one may encounter more problematical impedance values for these bands. **Fig. 5-3** plots the 2 SWR curves. The lines are dark because they overlay plotted SWR values for both versions of the antenna, showing that–even with extending frequency coverage–the difference of α values creates no noticeable change in the SWR curves.

Fig. 5-3

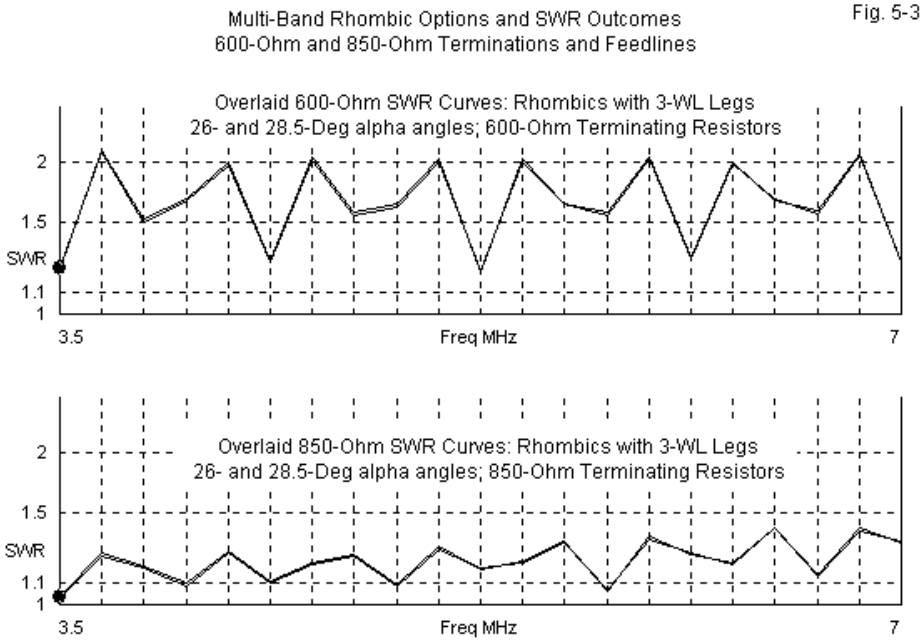

Fig. 5-4 plots the values of resistance and reactance across the same frequency range using the more optimal 850-Ω termination. On the chart, 3.5, 5.25, and 7.0 MHz represent the scaled values of the original beam's coverage of 14, 21, and 28 MHz. We might as easily have used the corresponding plot of resistance and reactance for the maximum-gain model. Notable in the graph is the relative stability of the resistance curve, but the rising character of the

reactance curve. As we increase frequency, the average reactance for any segment of the curve becomes more inductive.

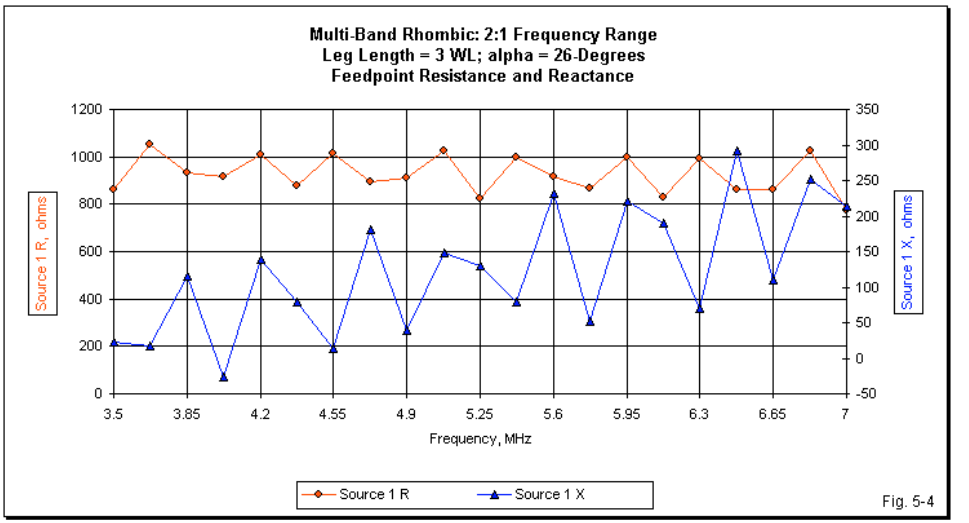

The data for the optimal termination of the antenna suggests that (for the model used) an 850-Ω terminating resistance is significantly better than the possibly more convenient 600-Ω standard amateur value. The next question concerns what the best value might be for the value of α for a tri-band rhombic. **Table 5-3** presents a preliminary comparison between the optimized gain model and the 26° ARRL model. The frequency span is 2:1. The intermediate frequencies corresponding to the lower edges of the amateur 17-and 12-meter bands.

The table shows 2 versions of the ARRL design using 850-Ω and 600-Ω terminating resistors. Between these two models, we find that as we lower the value of the terminating resistor, the front-to-back ratio suffers a significant decay. In addition, we find the anticipated higher values of SWR on the 600-Ω line on 17 and 12 meters. The table highlights those values. The remaining values–including forward gain, beamwidth, and front-to-sidelobe ratio–show no

operationally significant differences across the span of operating frequencies.

Selecting the Correct Value of alpha								Table 5-3
Terminated Rhombics with 3-Wavelength Legs; 1 WL above Average Ground at Lowest Frequency								
Optimized for Maximum Gain				alpha = 28.5 degrees			R load = 850 Ohms	
Fq MHz	El Ang	Gn dBi	FB dB	BW deg	F/SL dB	Feed R	Feed X	SWR 850
3.5	13	16.39	38.85	15.8	8.26	863	28	1.04
4.517	10	**17.28**	22.66	11.6	8.81	1055	72	1.26
5.25	8	16.81	31.34	9.2	5.55	829	129	1.17
6.2225	7	14.86	18.38	7.4	**3 lobes**	1005	258	1.38
7	6	16.68	23.36	6.9	**3 lobes**	775	206	1.31
Optimized for Balanced Gain				alpha = 26.0 degrees			R load = 850 Ohms	
Fq MHz	El ang	Gn dBi	FB dB	BW deg	F/SL dB	Feed R	Feed X	SWR 850
3.5	14	16.04	41.16	17.2	8.44	864	23	1.03
4.517	10	17.76	22.81	13.2	9.16	1040	76	1.24
5.25	9	**18.23**	29.93	10.8	8.98	825	131	1.17
6.2225	7	17.95	21.20	8.6	6.13	998	253	1.37
7	6	16.84	25.30	6.8	2.52	772	214	1.32
Optimized for Balanced Gain				alpha = 26.0 degrees			R load = 600 Ohms	
Fq MHz	El ang	Gn dBi	FB dB	BW deg	F/SL dB	Feed R	Feed X	SWR 600
3.5	14	16.06	18.32	17.2	8.10	729	-50	1.23
4.517	10	17.81	14.16	13.2	9.16	1182	217	**2.06**
5.25	9	**18.25**	18.55	10.8	8.68	714	47	1.21
6.2225	7	17.99	14.86	8.4	6.03	916	400	**1.96**
7	6	16.85	18.03	6.8	2.50	701	109	1.26
Notes:	Fq MHz = Frequency in MHz, see text for selection rationale							
	El Ang = Elevation angle in degrees							
	Gn dBi = Maximum gain in dBi							
	FB dB = 180-degree front-to-back ratio in dB							
	BW deg = Half-power beamwidth in degrees							
	F/SL dB = Front-to-sidelobe ratio in dB							
	Feed R = Feepoint resistance in Ohms							
	Feed X = Feedpoint reactance in Ohms							
	SWR nnn = nnn-Ohm SWR							

When we turn to the maximum gain version of the antenna, we find that it is unsuitable for multi-band operation beyond a 1.5:1 frequency ratio (although operation below the design frequency was not explored in this test). At the two highest test frequencies, the innermost sidelobes became the main lobes, with the gain of the central lobe that is aligned with the array centerline falling to a

lower level. We can see in the ARRL design data that the 26° model is approaching this condition at 7 MHz, as the front-to-sidelobe ratio drops below 3 dB.

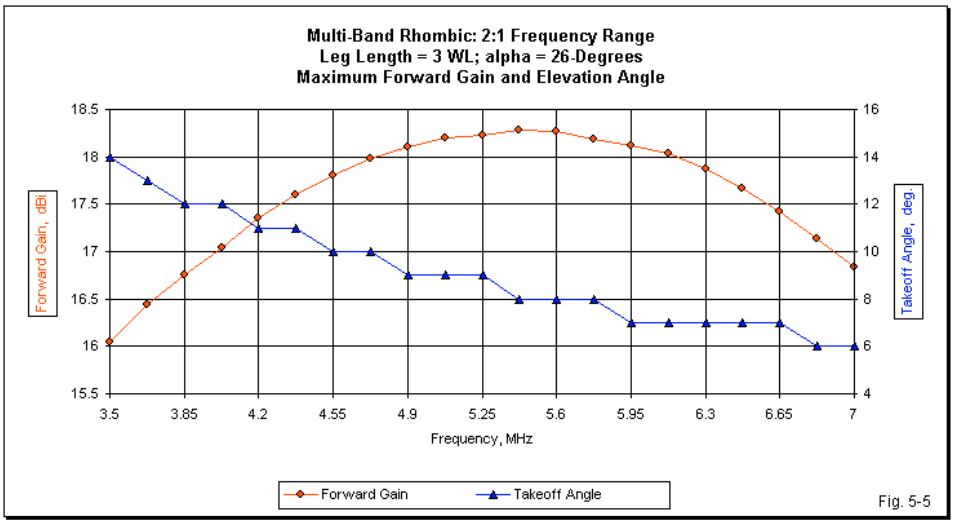

Fig. 5-5

If we assume for the moment that the front-to-sidelobe ratio is not a significant problem for the 26° design, we can explore the gain across the operating span, as shown in **Fig. 5-5**. The gain peaks just above the mid-point of the scanned frequency range. The total gain spread is only about 2.3 dB over the entire operating range. The plot also shows the continuous descent of the elevation or take-off angle across the 2:1 frequency span. The stair-step quality to the curve is an artifact of using 1° increments in elevation plot angles.

The performance differences between the optimum gain model and the 26° model opens the question of whether the 26° value for α is itself optimal for a 2:1 frequency range. We have discovered that 28.5° is too high a value for α, but we have not explored values below 26°. **Table 5-4** corrects this data vacuum by examining the 2:1 frequency range performance of models using α values between 24° and 27°. The table uses the same intermediate frequencies that

correspond to the non-harmonic amateur bands in the upper HF range. The table also highlights certain key entries.

Multi-Band Performance Variations with Variations in alpha								Table 5-4
Terminated Rhombics with 3-Wavelength Legs; 1 WL above Average Ground at Lowest Frequency								
alpha = 24 degrees								
Fq MHz	El Ang	Gn dBi	FB dB	BW deg	F/SL dB	Feed R	Feed X	SWR 850
3.5	15	15.42	41.04	18.4	9.19	866	21	1.03
4.517	11	17.57	23.17	14.2	8.74	1025	75	1.23
5.25	9	18.55	29.04	12.2	9.53	823	128	1.17
6.2225	7	**19.10**	21.32	10.0	8.81	985	247	1.36
7	6	18.97	24.03	8.4	7.68	767	216	1.33
alpha = 25 degrees								
Fq MHz	El Ang	Gn dBi	FB dB	BW deg	F/SL dB	Feed R	Feed X	SWR 850
3.5	14	15.76	41.72	17.8	8.61	865	21	1.03
4.517	11	17.71	23.01	13.6	8.95	1032	76	1.23
5.25	9	18.48	29.46	11.6	10.03	824	129	1.17
6.2225	7	**18.65**	21.22	9.2	8.05	991	251	1.37
7	6	18.09	24.56	7.6	5.13	770	216	1.33
alpha = 26 degrees								
Fq MHz	El Ang	Gn dBi	FB dB	BW deg	F/SL dB	Feed R	Feed X	SWR 850
3.5	14	16.04	41.16	17.2	8.44	864	23	1.03
4.517	10	17.76	22.81	13.2	9.16	1040	76	1.24
5.25	9	**18.23**	29.93	10.8	8.98	825	131	1.17
6.2225	7	17.95	21.20	8.6	6.13	998	253	1.37
7	6	16.84	25.30	6.8	2.52	772	214	1.32
alpha = 27 degrees								
Fq MHz	El Ang	Gn dBi	FB dB	BW deg	F/SL dB	Feed R	Feed X	SWR 850
3.5	14	16.23	39.97	16.6	8.34	863	25	1.03
4.517	10	17.68	22.71	12.6	9.51	1047	75	1.25
5.25	8	**17.81**	30.34	10.2	8.06	827	131	1.17
6.2225	7	16.94	21.27	7.8	3.77	1002	255	1.38
7	6	15.42	22.61	6.9	**3 lobes**	774	210	1.32
Notes:	Fq MHz = Frequency in MHz, see text for selection rationale							
	El Ang = Elevation angle in degrees							
	Gn dBi = Maximum gain in dBi							
	FB dB = 180-degree front-to-back ratio in dB							
	BW deg = Half-power beamwidth in degrees							
	F/SL dB = Front-to-sidelobe ratio in dB							
	Feed R = Feepoint resistance in Ohms							
	Feed X = Feedpoint reactance in Ohms							
	SWR 850 = 850-Ohm SWR							

Obviously, for full coverage, 27° is too high a value for α. At the high end of the frequency range, the sidelobes have become the dominant lobes. However, notice the trend in the highlighted peak gain values for each model. As we increase the value of α, the gain peak rises in frequency, and the gain at the lower end of the frequency range rises. For smaller operating ranges relative to the base design frequency, the wider angle at α might prove useful.

Relative to a full 2:1 frequency range, we shall have to reach a compromise. As we decrease the value of α, the overall gain decreases at the lowest frequency, but the front-to-sidelobe ratio increases at the highest frequency. As well, with lower values of α, the frequency of peak gain decreases toward the mid-point on the operating range. Lower values of α also yield wider beamwidth values. A decision on the best geometry for the array requires the introduction of communications specifications for a specific task.

Having surveyed the properties of rhombics having the same relevant properties as the ARRL antenna, we should not fail to survey that antenna itself. **Table 5-5** presents the data for the antenna using AWG #12 copper wire over the amateur bands from 20 through 10 meters, with an 850-Ω terminating resistor and average ground.

ARRL Rhombic: 14 - 28 MHz			AWG #12 Copper Wire			Terminating Resistor: 850 Ohms		
3-Wavelength Legs			1 WL above Average Ground at Lowest Frequency					
Fq MHz	El Ang	Gn dBi	FB dB	BW deg	F/SL dB	Feed R	Feed X	SWR 850
14	14	15.94	27.54	17.0	8.71	804	-108	1.14
18.068	10	17.73	22.71	13.0	9.40	868	-41	1.10
21	9	18.17	27.07	10.8	9.10	788	-54	1.07
24.89	7	17.89	35.52	8.4	5.96	821	-14	1.03
28	6	16.76	26.16	6.8	2.36	775	3	1.03
Notes:	Fq MHz = Frequency in MHz					Special note: Segmentation		
	El Ang = Elevation angle in degrees					40 segments / wavelength		
	Gn dBi = Maximum gain in dBi							
	FB dB = 180-degree front-to-back ratio in dB							
	BW deg = Half-power beamwidth in degrees							
	F/SL dB = Front-to-sidelobe ratio in dB							
	Feed R = Feepoint resistance in Ohms							
	Feed X = Feedpoint reactance in Ohms							
	SWR 850 = 850-Ohm SWR							Table 5-5

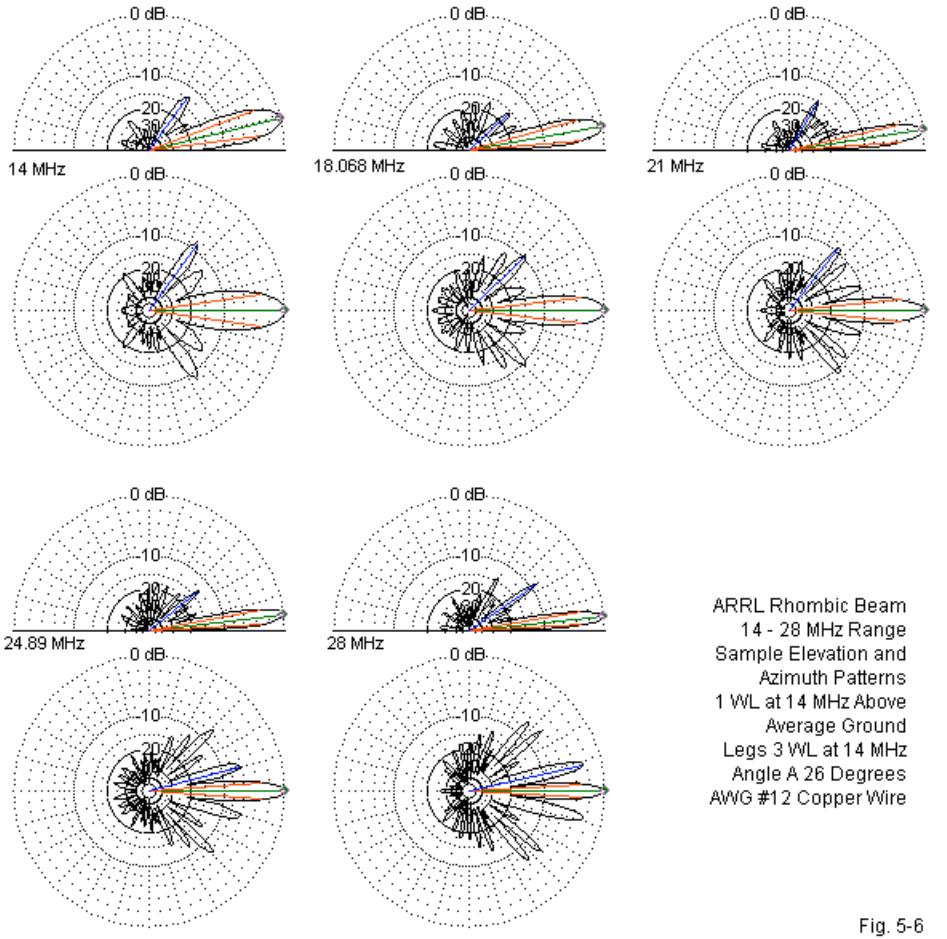

ARRL Rhombic Beam
14 - 28 MHz Range
Sample Elevation and
Azimuth Patterns
1 WL at 14 MHz Above
Average Ground
Legs 3 WL at 14 MHz
Angle A 26 Degrees
AWG #12 Copper Wire

Fig. 5-6

To ensure minimally adequate segmentation at all frequencies, the model uses 40 segments per wavelength at the lowest frequency. We may note the movement in the reactance values in the capacitive direction, a subject that will occupy our next discussion in this collection of multiplicities. However, for the

moment, we may focus on the gallery of elevation and azimuth plots in **Fig. 5-6**. Most notable in the collection are the patterns for 28 MHz. Not only do we see increasing strength in the azimuth sidelobes, reflecting the tabular values, but we also find increasing strength in the secondary elevation lobes at the highest frequency. We cannot say in the abstract whether the 26° value for α falls within or passes over the line of acceptable design values for a wide-band rhombic, but the patterns and the tabular data suggest that it is close to the limit.

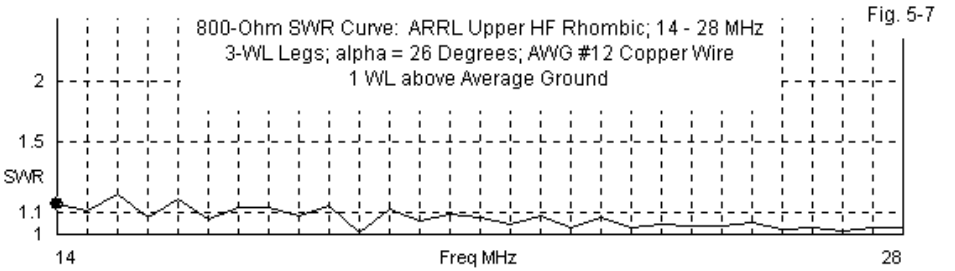

Fig. 5-7 presents the 800-Ω SWR curve for the ARRL rhombic across its operating range, using the 850-Ω terminating resistor in favor of the 600-Ω resistor that has been fairly standard amateur practice. The sampling points use a 0.5-MHz increment, and within this limit, the curve shows no significant aberrations. Even though we might select alternative values of α to match a refined list of operating needs and goals, the ARRL upper HF rhombic remains a strong candidate for use wherever one might need a rhombic antenna.

These notes, of course, rest on the use of a certain type of model for rhombic antennas (and for long-wire antennas in general). Altering the segmentation of the model appeared to have an effect on certain performance values, most significantly, the feedpoint reactance. Although those values are only a small part of the data and do not affect the overall trends that mark the goal of these notes, the shifts in reactance do raise some interesting questions about modeling rhombics. We noted early on in Chapter 4 that we had alternative ways of modeling rhombic antennas. Perhaps a comparison of these techniques might prove useful.

Multi-Modeling Potentials

The models in these notes provide general guidance, but not refined analysis suitable for use as a final pre-building design. Besides lacking the environmental inputs relevant to a prospective building site, there are some fundamental modeling issues that preclude the use of these models as precision replications of some particular rhombic or other long-wire array. First, the models use one of several possible input configurations possible in NEC. Each configuration has its own strengths and weaknesses relative the NEC calculations. Second, the models use a somewhat minimal segmentation density at 20 segments per wavelength. The final model of the ARRL rhombic used a higher segmentation density: 40 segments per wavelength at the lowest frequency. Both segmentation density and modeling configuration can alter some of the output data. The differences are not extreme, but neither are they negligible.

Fig. 5-8

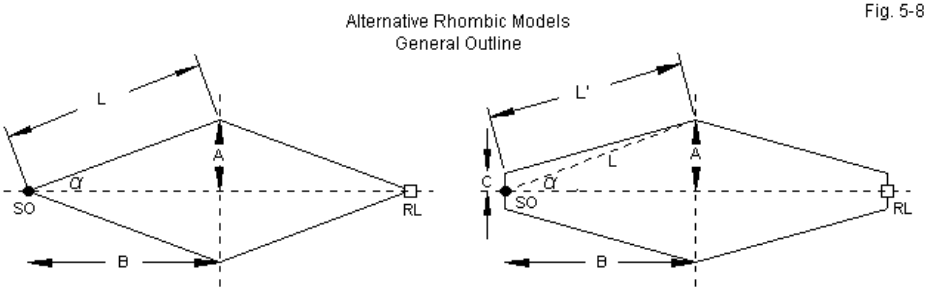

Fig. 5-8 shows the pointed-end configuration used for all rhombic models thus far in these notes. L is the leg length and is the square root of the sum of the squares of dimensions A and B. One advantage of this model is that it replicates angle α accurately. However, it does require the use of split sources and loads. An alternative configuration that we shall have to use shortly is on the right. The model places a single source and a single load on short end wires that create a blunt-end rhombic. The dashed line shows the virtual leg that has length L. However, the actual leg length is L' + C. As well, the wire labeled L' has a shallower angle relative to the junction with C than given by α. If we make

dimensions A and B the same as for the configuration on the left, then we have slightly distorted the rhombic shape. The degree of distortion is a function of 2 factors: the length of C and the leg length L. If C is very short and L is very long, then the distortion will be small relative to the pointed-end model.

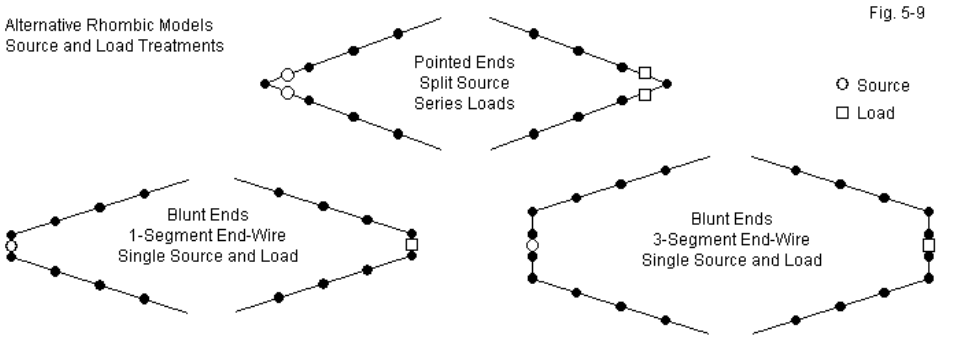

Fig. 5-9 illustrates the source and load treatments that accompany the two general configurations. Assume that all segments or distances between dots on the sketch have the same length. The pointed-end model places source excitation on the left-most segments of each of the two wires forming the feedpoint end of the rhombic. These sources are in series, and the net impedance of the source is the simple sum of the resistive and reactive components of each source. If we increase the segmentation density of the model, then the sources move closer to the actual tip of the rhombic. A similar condition applies to the series loads placed on the right-most segments of each wire approaching the termination end of the rhombic. The net resistive load is the sum of the two resistances, but if we increase segmentation density, the loads move closer to the actual tip of the rhombic.

The lower sections of the sketch show alternative methods of placing sources and loads at the furthest extremes of the rhombic. The method on the left uses a single segment wire for the source and another for the load. If we carefully size the 1-segment wires so that their length just about equals the length of each segment, NEC should yield accurate results, although it is preferable to have

equal-length segments in a line on each side of the source segment. The lower right sketch shows a 3-segment wire at each end of the rhombic that achieves this goal. However, even with careful sizing of the wire length to equalize segment lengths throughout the model, the 3-segment wires increase the distortion of the rhombic shape relative to either the pointed-end or the 1-segment blunt-end versions.

Physical Dimensions of the Test Rhombic with 4-WL Legs						Table 5-6
Pointed End 4-Wire Version: All Segmentation Densities						
	A	B	C	L	L'	L'+C
	1.6588	3.6398	0	4	4	4
Blunt-End 6-Wire Design with Source and Resistor on 1-Segment End Wires						
Seg/WL	A	B	C	L	L'	L'+C
20	1.6588	3.6398	0.025	4	3.9897	4.0147
40	1.6588	3.6398	0.013	4	3.9946	4.0076
80	1.6588	3.6398	0.007	4	3.9971	4.0041
Blunt-End 6-Wire Design with Source and Resistor on 3-Segment End Wires						
Seg/WL	A	B	C	L	L'	L'+C
20	1.6588	3.6398	0.07	4	3.9715	4.0415
40	1.6588	3.6398	0.04	4	3.9836	4.0236
80	1.6588	3.6398	0.02	4	3.9918	4.0118
Notes:	Seg/WL = Models segments per wavelength of wire.					
	See Fig. 5-8 for explanation of dimension designations.					

The amount of distortion in the rhombic shape is not large, even with a 3-segment wire at each end. **Table 5-6** provides information on the dimensions of a test rhombic using 4-λ legs and an α angle of 24.5°, the angle needed to optimize for maximum gain in the original pointed-end model. The tables shows the dimensions for all three versions, including the changing value of C as the segments in the main legs (L') grow shorter with increasing segmentation density. The worst case of distortion occurs with a segmentation density of 20 segments per wavelength while using a pair of 3-segment end wires. For 20 segments per wavelength, the end wires have individual lengths of 0.14 λ (or C = 0.07 λ). The distortion amounts to adding about 4% to each leg wire overall, although the angular portion of the wire is under 4 λ. Nonetheless, the combination of

configuration, source, and load changes can affect the modeling outputs.

Varying Segmentation Density in 4-Wavelength-Leg Rhombic Beams 1 Wavelength above Average Ground									
Pointed-End 4-Wire Design with Split Sources and Series Terminating Resistors at the Sharp Ends									
Seg/WL	Tot Segs	El Ang	Gn dBi	FB dB	HBW deg	F/SL dB	Feed R	Feed X	SWR 850
20	320	13	17.39	45.04	13.3	8.75	871	28	1.04
40	640	13	17.38	29.42	13.4	8.75	871	-104	1.13
80	1280	13	17.37	25.48	13.4	8.75	856	-177	1.23
Blunt-End 6-Wire Design with Single Source and Terminating Resistor on 1-Segment End Wires									
Seg/WL	Tot Segs	El Ang	Gn dBi	FB dB	HBW deg	F/SL dB	Feed R	Feed X	SWR 925
20	322	13	17.38	32.00	13.4	8.78	924	-41	1.05
40	642	13	17.37	26.71	13.4	8.82	900	-124	1.15
80	1282	13	17.35	24.23	13.4	8.82	885	-174	1.22
Blunt-End 6-Wire Design with Single Source and Terminating Resistor on 3-Segment End Wires									
Seg/WL	Tot Segs	El Ang	Gn dBi	FB dB	HBW deg	F/SL dB	Feed R	Feed X	SWR 975
20	326	13	17.42	32.46	13.2	8.46	970	-29	1.03
40	646	13	17.47	28.37	13.4	8.71	934	-92	1.11
80	1286	13	17.48	24.00	13.4	8.83	908	-148	1.19
Notes:	Seg/WL = Segments per wavelength in model								
	Tot Segs = Total number of segments in model								
	El Ang = Elevation angle in degrees								
	Gn dBi = Maximum gain in dBi								
	FB dB = 180-degree front-to-back ratio in dB								
	HBW deg = Horizontal half-power beamwidth in degrees								
	F/SL dB = Front-to-sidelobe ratio in dB								
	Feed R = Feepoint resistance in Ohms								
	Feed X = Feedpoint reactance in Ohms								
	SWR nnn = SWR referenced to value of terminating resistor in Ohms								Table 5-7

Table 5-7 provides the results of running all models under identical environmental conditions by placing each rhombic 1 λ over average ground at the test frequency. We need to scan the table in several different ways. First, if we compare the 3 models regardless of segmentation, we note that the terminating resistor increases value as we add the blunt end wire and increase their length. The terminating resistor was set with a segmentation of 20 segments per wavelength and remains unchanged as we increase the segmentation density for each model. The SWR reference impedance is also the resistance of the termination. For each model, as we increase the segmentation density, the feedpoint reactance grows more capacitive, and the feedpoint resistance decreases. The change in reactance is more radical than the decrease in resistance. However, reducing the terminating resistance in each model for a better match with the feedpoint impedance for a given segmentation density will also reduce the magnitude of the reactance. The higher capacitive reactance

that we saw in the 20-meter feedpoint data for the copper ARRL rhombic is thus a function of having increased the segmentation density by a factor of 2 relative to the model used to detect general trends.

Second, we can scan each model's table for other trends occasioned by increasing the number of segments per wire. The most dramatic case is the 180° front-to-back ratio, which is also a measure of the relative size of the lobe projecting directly rearward along the rhombic centerline. In all cases, it decreases as we increase the segmentation density, leveling off in the 24-25-dB region for all three models with 80 segments per wavelength. The beamwidth is stable for all models. So too is the front-to-sidelobe ratio, although the 3-segment end-wire model shows the greatest internal variation with changes in segmentation density.

With respect to the reported forward gain, the pointed-end and 1-segment blunt-end models show the closest coincidence in two respects. First, the gain levels closely match at all levels of segmentation, as do most of the other data related to radiation patterns. Second, both models show a slowly decreasing gain value as the segmentation density increases. In contrast, the blunt-end model using 3 segments in each cross wire shows an initially higher gain value, and that value continues to increase with the segmentation density.

The relatively close values that we find in **Table 5-7** with respect to the performance of the pointed-end and blunt-end arrays, when each uses an optimized terminating resistor, can hide some differences. To show one of the differences, I varied the value of the terminating resistor across a wide set of values. The data in **Table 5-8** selects 3 values that surround the final value and suffices to reveal the critical differences in model performance.

The data columns related to the radiation patterns reveal a consistent set of curves. The gain shows almost no change, with a slight numerical increase as the value of the terminating resistor increases. The front-to-side ratio also increases with the value of the terminating resistor. The front-to-back ratio peaks at mid-range, a characteristic of rhombics as the terminating resistor approaches its optimal value. In these respects, the two models are fully consistent. Since

the terminating resistor values are not too far apart, even the feedpoint resistance values are not distant from each other.

Single Wire Rhombic Performance Trends					Table 5-8
	with Varying Terminating Resistances				
4-Wavelength Legs; 1 Wavelength above Average Ground					
Pointed-End 4-Wire Model: 20 Segments/WL					
	Optimum R 850 Ohms				
R Load	Gn dBi	FB dB	F/SL dB	Feed R	Feed X
700	17.39	23.57	8.63	795	-9
900	17.39	31.99	8.78	894	41
1100	17.42	20.22	8.91	980	115
Blunt-End 6-Wire Model: 20 Segments/WL, 1-Segment End-Wire					
	Optimum R 925 Ohms				
R Load	Gn dBi	FB dB	F/SL dB	Feed R	Feed X
700	17.38	22.71	8.65	807	-11
900	17.38	36.23	8.77	912	-38
1100	17.40	21.29	8.86	1004	-64
R Load = Terminating resistor value in Ohms					
Gn dBi = Maximum gain in dBi					
FB dB = 180-degree front-to-back ratio in dB					
F/SL dB = Front-to-sidelobe ratio in dB					
Feed R = Feepoint resistance in Ohms					
Feed X = Feedpoint reactance in Ohms					

The key difference between the progression of values lies in the reactance column. The pointed-end model shows a reactance that becomes more inductive as the value of the terminating resistor increases. In contrast, the blunt-end model, even though it uses only 1 segment on the short end wire, shows a reactance that becomes more capacitive as the value of the terminating resistor increases. Older literature from the 1940s suggests that the rhombic builder should use a set of perhaps 3 to 4 resistors in series rather than a single terminating resistor. The goal is to reduce the capacitance across the total termination by creating several capacitors in series. If the models reflect reality (a major presumption in the absence of a physical test rhombic), then the reactance

columns might be natural. The pointed-end model already uses 2 resistors in series, and they extend from a position on one side wire to a position on the other. In contrast, the one-segment blunt-end model uses a single resistive load on a very short wire.

With respect to physical reality, much of the variation among models falls below the level of practical measurement in HF arrays, and almost all lies outside operational concerns. However, internal to a series of interrelated modeling tasks, such as those that we have conducted (and will conduct) in these notes, the data in **Table 5-7** and in **Table 5-8** are important. Some models to appear soon cannot use the pointed-end model and so must use some form of the blunt-end model. The data at hand strongly suggests that if we are eventually to compare the results of the new models with past models in this series, the 1-segment end-wire blunt model yields results that are most consistent with the pointed-end models. Since our goal is to detect and appreciate general trends in rhombic performance, consistency is a virtue, if not an absolute necessity.

Multi-Wire Rhombics

Many references on rhombic design recommend the use of multiple side wires to improve performance. The wires come together at each end of the rhombic to form a single source and a single terminating resistor. However, at the midline from which we measure the tilt angle or Φ, the wires are vertically separated by a space that runs from a few feet at lower frequencies to a few inches in the upper HF range. Some literature warns about ensuring that the center wire of the set–the one that is level with respect to ground–is not shorter than the outer wires. However, the warning is misplaced, since the actual length difference is a small part of 1%. The key caution to use in creating a multi-wire rhombic is to ensure that all wires place equal tension on the connecting points. Although some 5-wire rhombics have existed, the most common configuration uses 3 wires.

The multi-wire rhombic has enjoyed many claims of advantages over the single wire rhombic. Some have reported quieter operation, suggesting that the 3-wire array has weaker sidelobes. As well, the 3-wire array shows more forward

gain than its 1-wire counterpart with the same leg length. In some places, we find claims that the 3-wire array shows a better SWR curve over an extended frequency span due to interaction among the wires that compensates for reactance. It also provides a better match for a 600-Ω terminating resistor and common 600-Ω transmission line. To evaluate the foundation of some of these claims, we must figure out how to model a 3-wire rhombic in a relatively reliable manner.

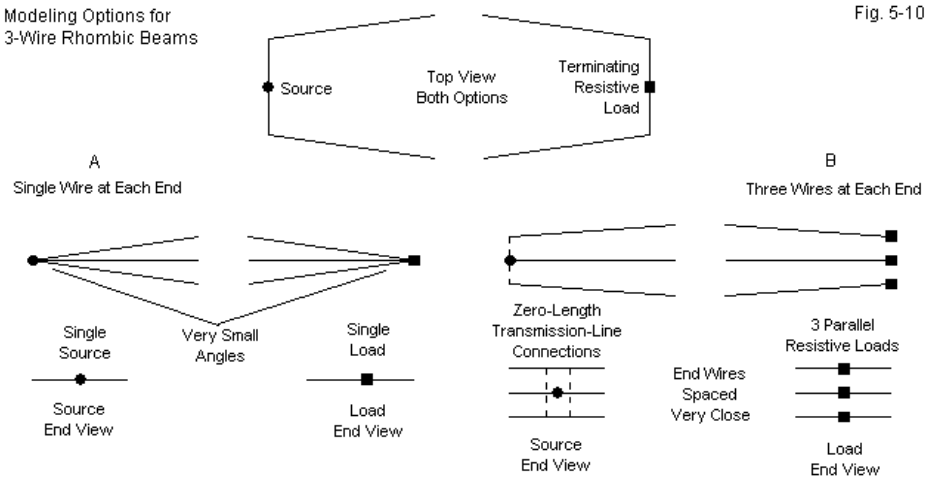

Fig. 5-10 shows two alternative methods of modeling the 3-wire rhombic. The top view would be the same for both models. It only indicates that we must use a blunt-end technique for the model. Given the discussion of blunt-end vs. pointed-end models in the previous section, we shall use a 1-segment end wire to form the blunt ends.

When we turn to end treatments in the lower portion of the figure, we can see more clearly our options. The simplest option (A) uses a single end wire at the source and load ends of the rhombic. The three side wires come together at each end of these wires. The source and the load are effectively centered within

each end wire. The configuration presents two challenges to NEC as a calculating instrument. First, the three side wires approach the junction at very shallow angles, allowing for significant inter-penetration in the segments that form the junction. Second, NEC prefers a single segment on each side of a source segment prior to any division of the current.

The alternative to the single end wire is the use of separate end wires for each side wire (B). We may place these wires very close together so long as we allow spaces that are several times the wire radius. We may model the separate end wires using a spacing of 0.001 λ to achieve a simulation of a single wire. At the load end of the array, we may use separate terminating resistors on each line. The value for a 3-wire rhombic is simply 3 times the desired equivalent single terminating resistor, since the loads are in parallel. Since the loads do not have a physical dimension, they do not affect the wire spacing.

The source wires call for slightly different treatment, although we might use 3 sources and calculate their parallel value. A simpler procedure is to create a transmission line between each outer wire and the center wire. Since lines have no physical dimensions due to the wire geometry, we can assign them any desired length. Because we wish to simulate a parallel connection, we can assign a length of 1e-10 m or similar. The line's characteristic impedance can be virtually any value, since virtually nothing happens over a near-zero line length. However, using an impedance of about 600 Ω will satisfy the situation. Of course, we place a single source on the center end wire, since transmission lines are in parallel with any source on the same segment.

One way to evaluate the alternative modeling techniques is to track what happens if we vary the value of the terminating resistor. As a test case, we can create 3-wire rhombics with 4-λ legs. **Table 5-9** provides the comparison. Since the two types of models call for different optimized terminating resistors, the resistor ranges differ. As well, they differ from the ranges used in **Table 5-8**, which compared pointed-end and blunt-end models of 1-wire rhombics with 4-λ legs. The data in that earlier table will also be important to the evaluation of 3-wire models. The 3-wire models use 1-segment end wires, so the 1-segment blunt-end model of the single wire rhombic is the appropriate comparator. All

models will be 1 λ above average ground and use 0.16" diameter lossless wire.

Three-Wire Rhombic Performance Trends with Varying Terminating Resistances					Table 5-9
4-Wavelength Legs; 1 Wavelength above Average Ground					
Single End Wires: 20 Segments/WL. Optimum R 700 Ohms					
R Load	Gn dBi	FB dB	F/SL dB	Feed R	Feed X
500	19.14	21.57	8.26	627	118
700	19.15	26.27	8.41	702	119
900	19.17	19.51	8.52	763	120
Triple End Wires: 20 Segments/WL; Optimum R 600 Ohms					
R Load	Gn dBi	FB dB	F/SL dB	Feed R	Feed X
400	18.73	20.57	8.30	525	-67
600	18.74	30.17	8.48	599	-79
800	18.77	19.31	8.60	656	-96
R Load = Terminating resistor value in Ohms					
Gn dBi = Maximum gain in dBi					
FB dB = 180-degree front-to-back ratio in dB					
F/SL dB = Front-to-sidelobe ratio in dB					
Feed R = Feepoint resistance in Ohms					
Feed X = Feedpoint reactance in Ohms					

The use of a single end wire with 3 side wires joining at very small angles yields rather optimistic gain estimates compared to the 3-end-wire version of the model. In addition, the reactance undergoes virtually no change as we vary the value of the terminating resistor by 400 Ω. Both of these data columns are at odds with the results for a 1-wire blunt-end rhombic model. In contrast, the 3-wire model that uses 3 end wires shows a more modest gain. As well, the pattern of capacitive reactance parallels the pattern shown in **Table 5-8** for the blunt-end 1-wire rhombic. Finally, the triple end-wire model shows an optimized terminating resistor value of about 600 Ω, a value that corresponds well with actual practice.

A second relevant test of the modeling options is to compare them by varying the spacing between side wires at the midline point. As a sample, I ran the models for both options at 3 spacing increments: 0.0125 λ (narrow), 0.025 λ

(medium), and 0.05 λ (wide). Wide spacing is 4 times narrow spacing. The total distance at the midline between the top and bottom wires is twice the spacing increment. The end-wire spacing for the triple end-wire model does not change. The results of these tests appear in **Table 5-10**.

Three-Wire Performance of Rhombics with 4-WL Legs							Table 5-10
	with Varying Midline Separation Distances						
All Models 1 WL Above Average Ground: 13-Degree Elevation Angle							
1-Segment End Wires 0.04-WL Long							
Single End Wire Models with Single Sources and Loads							
Mid Sp	Gn dBi	FB dB	BW deg	F/SL dB	Feed R	Feed X	SWR 700
0.013	19.15	26.27	13.2	8.41	702	119	1.18
0.025	19.27	24.22	13.2	8.42	672	123	1.20
0.050	19.40	22.36	13.2	8.44	638	127	1.24
Triple End Wire Models with Zero-Length Transmission Lines to Source and							
	Paralleled Terminating Resistors, 1 Resistor Per Line						
Mid Sp	Gn dBi	FB dB	BW deg	F/SL dB	Feed R	Feed X	SWR 600
0.013	18.74	30.17	13.2	8.48	599	-79	1.14
0.025	18.88	30.51	13.2	8.43	600	-52	1.09
0.050	19.01	29.74	13.2	8.40	593	-42	1.07
	Mis Sp = Midline maximum wire spacing in wavelengths						
	Gn dBi = Maximum gain in dBi						
	FB dB = 180-degree front-to-back ratio in dB						
	BW deg = Half-power beamwidth in degrees						
	F/SL dB = Front-to-sidelobe ratio in dB						
	Feed R = Feepoint resistance in Ohms						
	Feed X = Feedpoint reactance in Ohms						
	SWR nnn = nnn-Ohm SWR (= terminating resistance)						

The weakness of the model using single end wires shows up in the table. The key datum is the feedpoint resistance, especially as we compare it with the corresponding datum for the triple end-wire model. As we increasing the wire spacing for the triple end-wire model, the reactance undergoes some change, but the resistance remains essentially constant. In contrast, the single end wire model shows only a small change of reactance, but a large change of resistance. As we increase the angle of the side wires as they approach their junction at the end wires, the resistive component moves closer to the 600-Ω value of the triple

end-wire model. The resistance change suggests that widening the angle at the junction reduces any calculation aberrations produced by wire inter-penetration.

Option B, the triple end-wire model provides results that are thus superior to those of option A in at least 2 ways. First, they are consistent with the results for the blunt-end 1-wire rhombic model. Second, the results are internally consistent relative to widening the midline spacing between wires. Although the reported gain is lower for the triple end-wire model, it nevertheless shows an increase with respect to increasing wire spacing. Moreover, it shows a useful gain over a 1-wire rhombic. For wide 3-wire rhombic midline spacing, the gain improvement can be up to about 1.6 dB, as shown in **Fig. 5-11**. The gain advantage is slightly less for narrower midline wire spacing.

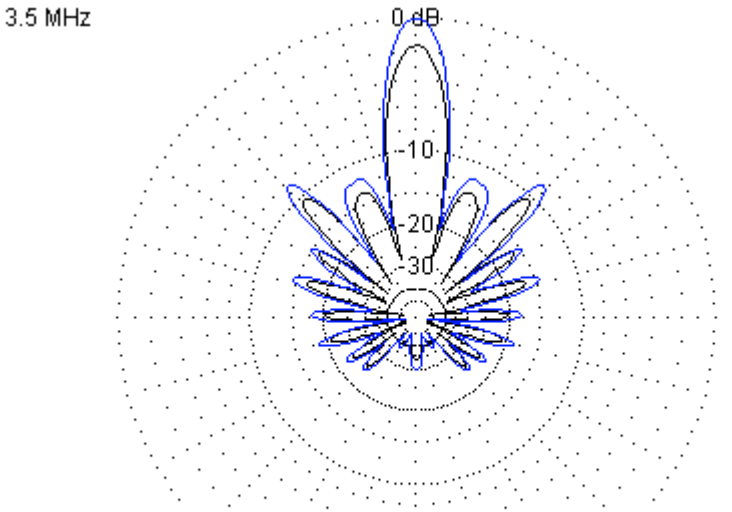

Overlaid Azimuth Patterns: Rhombic Beams with 4-WL Legs
Blue: 3-Wire, Wide-Spaced, with 1-Segment End Wires
Black: 1-Wire with 1-Segment End Wires

Note that the 3-wire rhombic not only magnifies the main forward lobe. As

well, it enlarges virtually every other lobe in the radiation pattern proportionally, and without changing either the angle or the general shape of each lobe. Especially interesting in the pattern are the two innermost forward sidelobes. From the shapes, we can tell that they are in fact pairs of overlapping lobes. Both the 1-wire and the 3-wire models use an α of 24.5° to maximize gain. The lobe structure might change slightly with other values of α. For example, if we widen the angle further, the combined innermost sidelobes on each side of the present main lobe will eventually become stronger than the central lobe, resulting in a 3-lobe forward pattern.

To assure ourselves that we have fairly represented the advantages of the 3-wire rhombic over its 1-wire counterpart, we can perform one further test. We can increase the segmentation density of the triple end wire model and compare the progression with the one that we examined in the case of the blunt-end 1-wire rhombic. The comparison appears in **Table 5-11**. For both antennas, the steps use 20, 40, and 80 segments per wavelength, and the length of the end wire is reduced to maintain length parity with the adjacent segments of the side wires.

Varying Segmentation Density in 4-Wavelength-Leg Rhombic Beams 1 Wavelength above Average Ground									
Blunt-End Single-Wire Design with Single Source and Terminating Resistor on 1-Segment End Wires									
Seg/WL	Tot Segs	El Ang	Gn dBi	FB dB	HBW deg	F/SL dB	Feed R	Feed X	SWR 925
20	322	13	17.38	32.00	13.4	8.78	924	-41	1.05
40	642	13	17.37	26.71	13.4	8.82	900	-124	1.15
80	1282	13	17.35	24.23	13.4	8.82	885	-174	1.22
Triple-Wire Design with 3 End Wires, TL to Source, and Parallel Resistors; Midline Spacing 0.025 WL									
Seg/WL	Tot Segs	El Ang	Gn dBi	FB dB	HBW deg	F/SL dB	Feed R	Feed X	SWR 600
20	966	13	18.88	30.51	13.2	8.43	600	-52	1.09
40	1926	13	18.87	25.29	13.2	8.47	574	-106	1.20
80	3846	13	18.85	22.92	13.2	8.48	558	-136	1.28
Notes:	Seg/WL = Segments per wavelength in model								
	Tot Segs = Total number of segments in model								
	El Ang = Elevation angle in degrees								
	Gn dBi = Maximum gain in dBi								
	FB dB = 180-degree front-to-back ratio in dB								
	HBW deg = Horizontal half-power beamwidth in degrees								
	F/SL dB = Front-to-sidelobe ratio in dB								
	Feed R = Feepoint resistance in Ohms								
	Feed X = Feedpoint reactance in Ohms								
	SWR nnn = SWR referenced to value of terminating resistor in Ohms								Table 5-11

The 1-wire and 3-wire rhombics show quite precise parallels in the progression of values in each data column, indicating that the models are appropriate comparators. The only small divergence occurs in the reactance data, as the 1-wire rhombic model has a 133-Ω total range, while the 3-wire model varies by only 84 Ω. In both cases, the capacitive reactance increases as the end-wires become shorter. (However, even at the shortest length with the highest segmentation density, the modeled end wires are long compared to typical physical structures until we reach the high end of the upper HF range.)

The claims for 3-wire rhombics with which we began this section of notes find only partial confirmation in the models used to evaluate them. Using 3 wires does raise forward gain by an average of 1.5 dB for a 4-λ leg rhombic. The exact gain advantage depends on the wire spacing at the midline. As well, the optimum value for the terminating resistor drops from a value between 800 and 900 Ω down to 600 Ω. In both cases, the models reflect both calculations and practical experience with rhombics. However, reports of quieter operation–presumably meaning freedom from what Bruce called "static" in 1931–do not find confirmation in any property of the models. For a given leg length and value of α, the 3-wire rhombics produce patterns that are congruent in almost every detail with those produced by 1-wire rhombics. If 3-wire rhombics are in fact quieter than their 1-wire counterparts, the reasons must lie outside the realm of properties that NEC models can reveal.

Among the claims associated with 3-wire rhombics is a flatter SWR curve over an extended frequency range. Over the intervening decades since the appearance of the original literature on rhombic design, accounts have undergone truncation, especially after the heyday of rhombics had passed into the history of radio communications. My suspicion is that the claim of a flatter extended-frequency SWR applies only to the use of 600-Ω transmission lines, likely occasioned by early difficulties in constructing mechanically stable wider lines with a higher characteristic impedance. If we match the line impedance to the terminating resistor, then extended-frequency SWR curves show no significant differences. For example, **Fig. 5-12** provides SWR curves for the 1-wire blunt-end model and for the narrow-spaced 3-wire rhombic, with each using the terminating resistor as the SWR reference impedance.

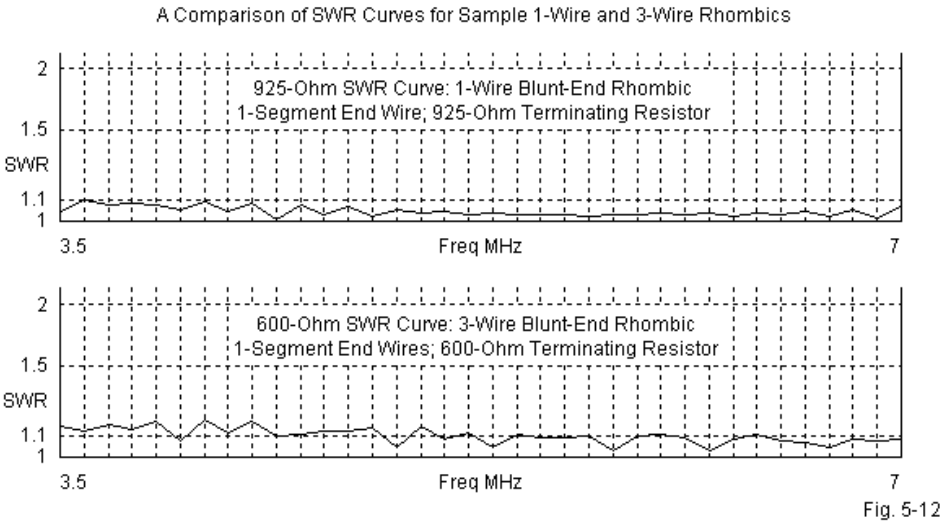

Fig. 5-12

The curves use a 0.1-MHz increment, which is sufficient to pick up at least some of the peak values that might occur. However, the peak SWR is 1.2:1 or less for both antennas, suggesting that there is no significant difference between them. The slightly higher values in the 3-wire curve result from the fact that the similar reactive components in both antennas represent a high percentage of the resistive component in the more complex array. In the end, reactance compensation during final design and construction, when combined with the selection of the correct feedline impedance, will do more for the flatness of the SWR curve than the presence of 3 wires.

(In fact, one account of single-wire rhombics suggested in one paragraph the use of 600-Ω transmission line to the feedpoint and in another suggested that the terminating load might be placed conveniently near ground level by the use of another transmission line. If the termination line had a characteristic impedance of 800 Ω, then line length would make no difference to performance, since it would match the presumed impedance of the terminating load and the antenna when viewed as a transmission line over ground. The account reflected common

practice at the time of writing, and common practice is often the source of unnoticed inconsistencies.)

In the end, a 3-wire rhombic appears to have no calculable properties other than those associated with the simulation of a very large diameter wire through the use of multiple conductors. Cage antenna elements and multiple-conductor dipole and quad loop elements are fairly common practices to increase the effective diameter of an element without resorting to excessively heavy single large elements. The rhombic 3-conductor side wires function in much the same way, although their tapered arrangement makes the determination of a single effective diameter a somewhat uncertain calculation. The use of multiple side wires is optional unless one requires either the small gain advantage or the use of 600-Ω lines and an equal value of terminating resistor.

Our small side-trip into 3-wire rhombics has had two goals. The first was to find an effective technique for modeling the antenna, a technique that would produce results that are fully consistent with both good NEC modeling practices and reports emerging from relevant 1-wire rhombic models. "Option B," the triple end-wire model accomplished this goal. The second goal was to understand within the limits of what models can tell us whether a 3-wire rhombic might have advantages over a 1-wire version of the same rhombic. Although we focused on a single mid-size rhombic (with 4-λ legs) designed to optimize gain, the results are suggestive for the entire range of possible rhombic sizes.

Multi-Element Rhombics

Since the first long-wire beam emerged as a means of improving HF communications, designers have troubled over the high sidelobe content of the radiation pattern. Indeed, a combination of the required rhombic acreage ad the high sidelobe strength eventually led to the demise of general use of long-wire technology, including rhombics. However, until the end of the rhombic era, engineers continued to seek out ways to reduce the number and size of rhombic sidelobes. Laport especially deserves note for one solution to the problem that he published in 1960: the use of closely space rhombics of different sizes using the same radiation centerline.

Fundamental Physical Dimensions
of Dual Rhombic Beams

Fig. 5-13

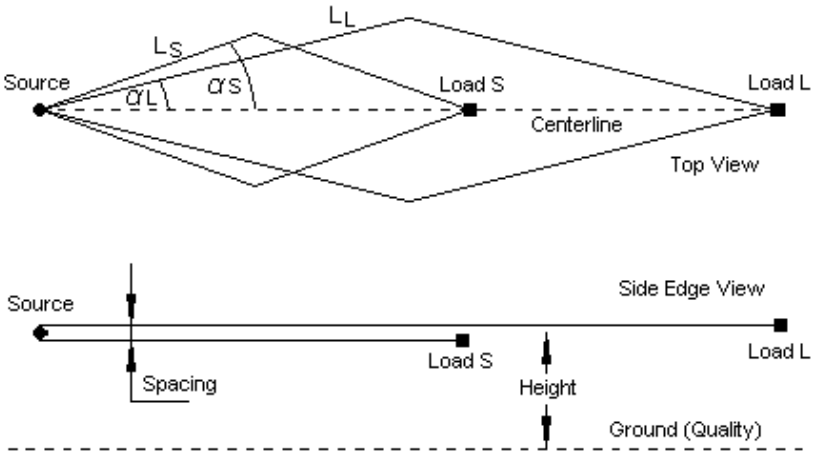

Fig. 5-13 shows the general outline of the rhombic design developed to reduce the sidelobe content of rhombic radiation patterns. If we carefully match single rhombics, and closely space them, then the side nulls in one pattern will counteract the sidelobes in the other pattern, especially for the strongest forward sidelobes. **Fig. 5-14** shows the evolution of the dual rhombic pattern, beginning with a pair of single rhombics that display the necessary properties. The upper portion of the figure shows the individual azimuth patterns for a rhombic with 3.5-λ legs and a rhombic with 6.0-λ legs. At the lower left, the large pattern has overlaid the two individual patterns to show how the side lobes and nulls interlace in compensatory ways. All models use the standard structures that permeate these notes: 0.16" diameter lossless wire. These models use 850-Ω terminating resistors and are vertically centered at 1 λ over average ground.

At the lower right of the figure, we have the composite pattern of the 2 rhombics when we feed tem in parallel. The sidelobe structures of the dual rhombic shows a very noticeable decrease not only in the forward direction, but

as well, throughout the side and rear quadrants.

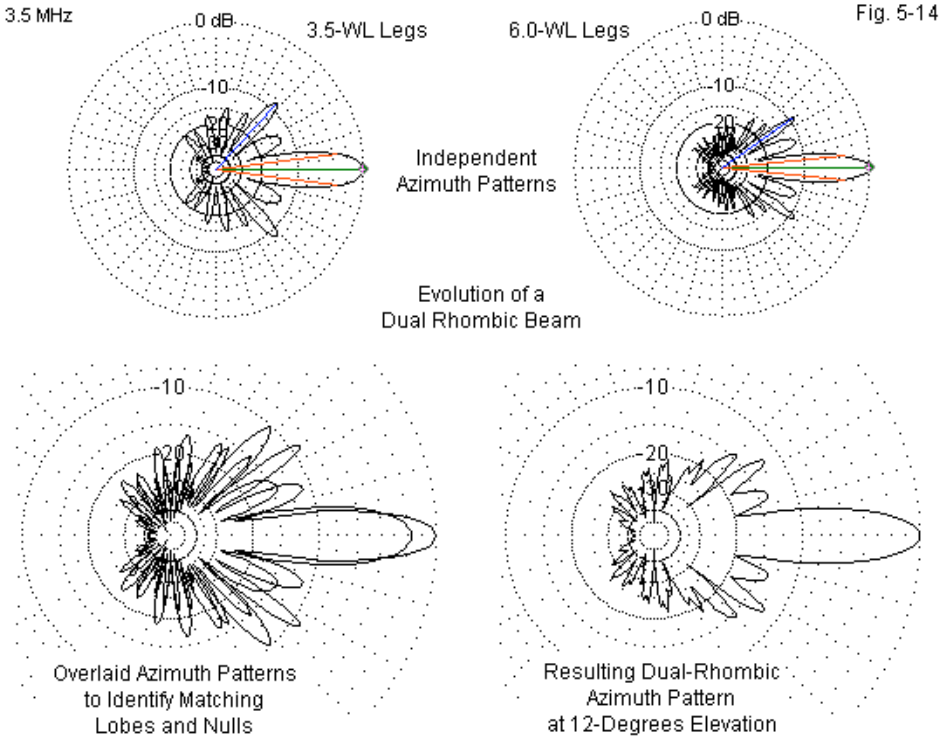

The initial modeling tests with the dual rhombic employed single rhombic designs that had been optimized in previous chapters for maximum forward gain. The performance data appears in **Table 5-12**, along with data on the original single rhombics that we combined. The first dual rhombic in the table records information for the models combined in **Fig. 5-14**. The dual rhombic achieves about 1.3-dB higher forward gain than the longer single rhombic. Its beamwidth is intermediate between the two single rhombics. The most noticeable improvement shows up in the front-to-sidelobe column: a full 3-dB improvement

in the ratio of the main lobe to the strongest sidelobe. For reference, the next column lists the azimuth angle (relative to the main lobe) of the strongest sidelobe. The 34° angle indicates that, as in the case of single rhombics, the second sidelobe is stronger than the first sidelobe.

Data on Dual Rhombics and Their Component Single Rhombics										Table 5-12
All antennas 1 wavelength above average ground; for dual antennas, 1 wavelength = average height										
Antenna	Sp WL	alpha	El Ang	Gn dBi	FB dB	BW Deg	F/SI dB	SL Ang	Feed R	Feed X
S-3.5		26.5	13	16.95	41.50	14.2	8.58	47	869	29
S-6.0		19.0	12	18.62	43.51	11.2	8.97	35	865	26
D-3.5/6.0	0.18	26.5-19.0	12	19.95	43.42	12.2	12.08	34	446	75
D-3.5/6.0	0.18	28.0-19.0	12	19.91	38.98	12.0	12.22	20	452	76
D-3.5/6.0	0.18	28.0-18.5	12	19.88	39.53	12.2	12.39	20	454	73
D-3.5/6.0	0.1	28.0-18.5	12	19.91	33.41	12.2	12.28	20	480	67
D-3.5/6.0	0.02	28.0-18.5	12	19.91	24.77	12.2	12.12	20	614	85
Notes:	Antenna = Single (S) or Dual (D) rhombic and leg length(s) in wavelengths									
	Sp WL = spacing of dual rhombics in wavelengths									
	alpha = Wire angle to centerline in degrees									
	El Ang = Elevation angle in degrees									
	Gain dBi = Maximum gain in dBi									
	FB dB = 180-degree front-to-back ratio in dB									
	BW deg = main lobe beamwidth in degrees									
	F/SL dB = Front-to-sidelobe ratio in dB									
	SL Ang = Strongest sidelobe azimuth angle relative to main lobe in degrees									
	Feed R = Feepoint resistance in Ohms									
	Feed X = Feedpoint reactance in Ohms									

The next two entries in the table record successive attempts to see if we might improve the sidelobe performance, and to what degree. As we saw in the case of multi-band rhombics, a design optimized for maximum gain might not yield a particular result that stresses a different performance parameter. To better align the sidelobe structure, I first widened the α angle of the shorter rhombic and then narrowed the α angle of the longer rhombic. The results are likely operationally insignificant, but they are numerically noticeable with a further 0.3-dB improvement in the front-to-sidelobe ratio. Equally important is the fact that the strongest sidelobe angle is now 20° away from the main lobe. An interesting aspect of rhombic behavior is that the first and second azimuth sidelobes tend to show reverse behaviors as we change the α angle of a rhombic. As one diminishes, the other enlarges.

Fig. 5-15 compares the details of the dual rhombic azimuth patterns for the original version and for the tweaked version. The patterns use a larger format

than normal for these notes, since the sidelobe detail is critical to the design considerations for dual rhombics. Both designs use the same vertical separation: 0.18λ or 0.09λ above and below the 1-λ nominal array height.

Tweaking alpha Angles for Improved Sidelobe Attenuation in a Dual Rhombic Beam (Legs = 3.5 WL and 6.0 WL) Fig. 5-15

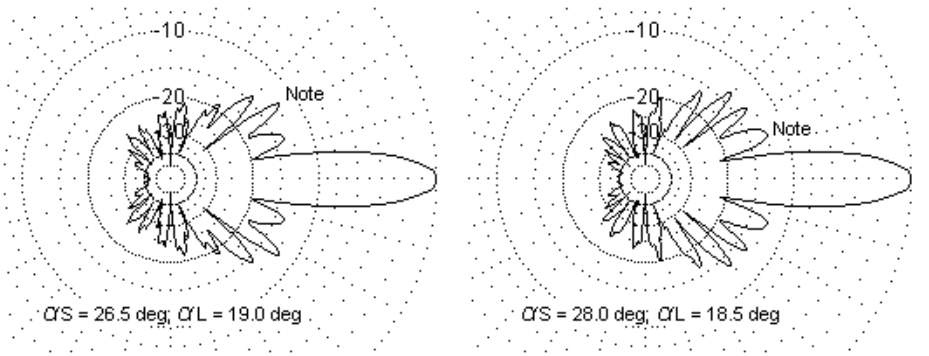

Consequences of Vertical Spacing Between Arrays in a Dual Rhombic Beam Fig. 5-16

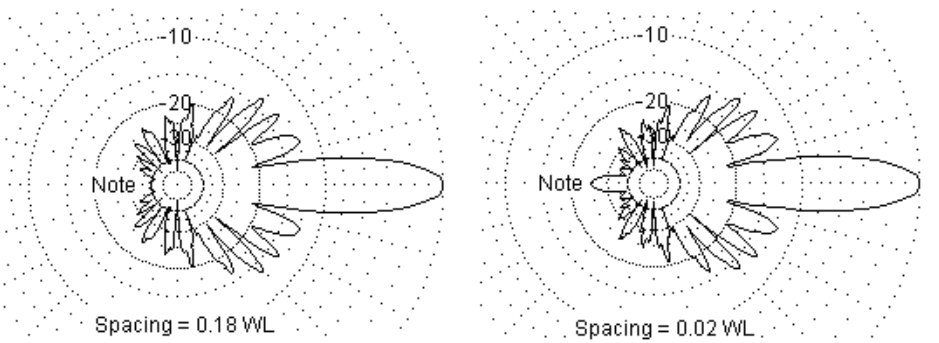

Laport's original 1960 article implies the use of very close spacing between

the individual rhombics. Therefore, the final 3 entries in **Table 5-12** show the optimized dual rhombic at 3 different spacing values. The 0.18-λ spacing value minimizes interactions between the individual antennas that are sufficient to alter the feedpoint impedance. The closest spacing (0.02 λ) shows an elevated feedpoint impedance that results from interaction. Equally prominent is the degradation in the front-to-back ratio. **Fig. 5-16** puts a graphic face on the tabular data. The data for the intermediate spacing (0.1 λ) simply indicates a progressive development of the numerical trends. The most important aspect of the data, relative to the reason for using a dual rhombic, is the decay of the front-to-sidelobe ratio, although the innermost sidelobe remains the strongest one.

One of the most ingenious aspects of Laport's design work was the development of dual offset rhombics to replace the straightforward dual rhombic structure that we have so far explored. His goal was to obtain the same performance, but to reduce the overall size of the rhombic structure. **Table 5-13** provides the relative dimensions of a standard dual rhombic and a Laport dual offset rhombic using the single rhombics with 3.5-λ and 6.0-λ legs as a foundation. The maximum dimensions of the dual rhombic are highlighted. In contrast to the 11.4-λ total length of the dual rhombic, the Laport offset version requires only 8.8 λ.

Dimensions of Dual and Dual Offset Rhombics									Table 5-13
Dual Rhombic: 3.5 WL @ 28.0 Degrees and 6.0 WL @ 18.5 Degrees									
Element	Leg WL	Midline	CenterLine		Element	Leg WL	Midline	CenterLine	
Short	3.5	3.286	6.181		Long	6	**3.808**	**11.445**	
Dual Offset Rhombic: See Fig, 5-17									
alpha S	L-S	alpha L	L-L	a	b	c	d	e	f
28	3.5	18.5	6	1.643	1.904	0.261	3.09	5.69	8.78

The dimensions of the dual offset rhombic require special explanation and key to **Fig. 5-17**. The upper portion of the figure shows a pair of rhomboids that mirror each other. The factor that produces the offset is the use in each rhombic of the α angle for the shorter single rhombic in one direction and the α angle for the longer rhombic in the other. The lower portion of the figure shows only one of the two rhombics, but provides an orientation to the angles and to the key dimensions for calculating the antenna.

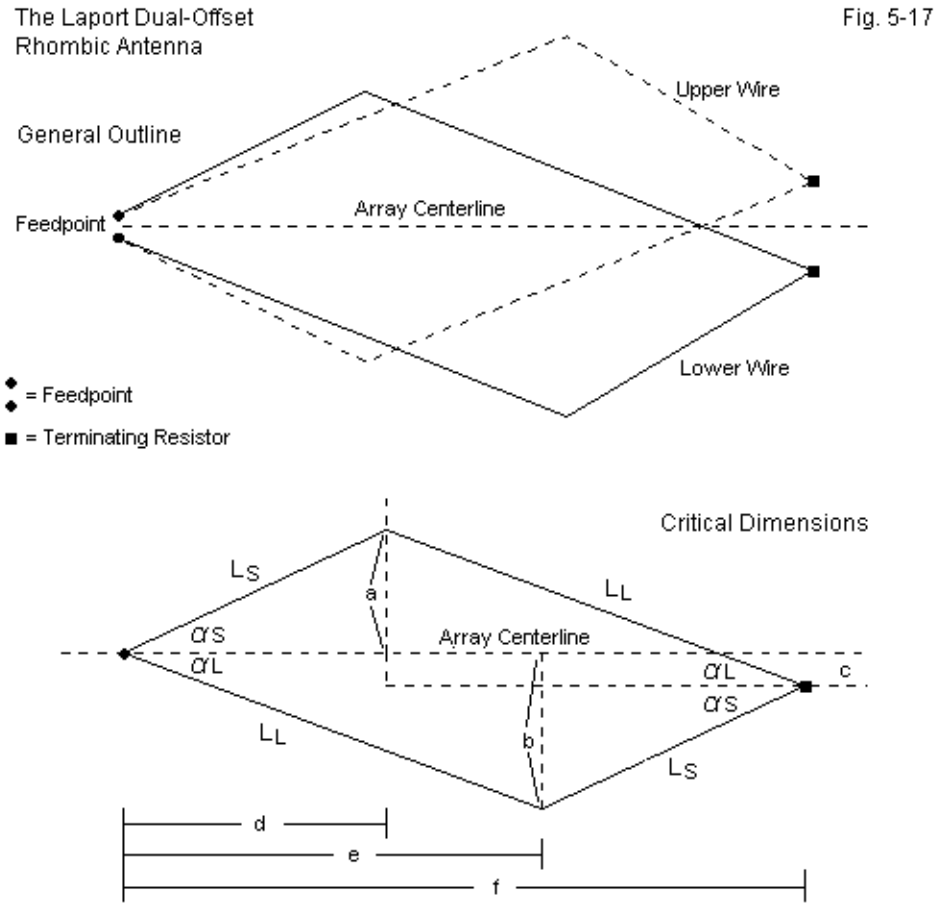

Certain key dimensions are givens, based on the selection of the short and long rhombic.

$\alpha_S = 28.0°$ $L_S = 3.5\ \lambda$ $\alpha_L = 18.5°$ $L_L = 6.0\ \lambda$

The remaining dimensions emerge from a few trig functions and a little arithmetic.

$a = \sin \alpha_S \, L_S = 1.643\ \lambda$ $\quad b = \sin \alpha_L \, L_L = 1.903\ \lambda$ $\quad c = b - a = 0.261\ \lambda$
$d = \cos \alpha_S \, L_S = 3.090\ \lambda$ $\quad b = \cos \alpha_L \, L_L = 5.690\ \lambda$ $\quad f = d + e = 8.780\ \lambda$

If we model the prescribed offset dual rhombic, we obtain the data in **Table 5-14**. The table records information for 3 versions of the antenna, using separation values that correspond to those used by the standard dual rhombic.

Data on Dual Offset Rhombics: 3.5 WL @ 28.0 Degrees and 6.0 WL @ 18.5 Degrees									Table 5-14
All antennas 1 wavelength average above average ground									
Sp WL	alpha	El Ang	Gn dBi	FB dB	BW Deg	F/Sl dB	SL Ang	Feed R	Feed X
0.18	28.0-18.5	12	19.81	38.33	12.1	11.53	20	427	3
0.1	28.0-18.5	12	19.82	32.44	12.0	11.52	20	423	-14
0.02	28.0-18.5	12	19.77	22.55	12.0	11.57	20	435	-49
Notes:	Sp WL = spacing of dual rhombics in wavelengths								
	alpha = Wire angle to centerline in degrees								
	El Ang = Elevation angle in degrees								
	Gain dBi = Maximum gain in dBi								
	FB dB = 180-degree front-to-back ratio in dB								
	BW deg = main lobe beamwidth in degrees								
	F/SL dB = Front-to-sidelobe ratio in dB								
	SL Ang = Strongest sidelobe azimuth angle relative to main lobe in degrees								
	Feed R = Feepoint resistance in Ohms								
	Feed X = Feedpoint reactance in Ohms								

The dual offset rhombic does not quite achieve the maximum forward gain of standard dual rhombic, although the difference is very small. The other difference between the two design configurations appears in the front-to-sidelobe column. The offset rhombic pair shows a sidelobe ratio that is nearly a dB lower than for the standard design. The value remains about 2.5-dB higher than for the single 6.0-λ rhombic. Like the standard dual rhombic, the offset design shows a gradually degradation in certain performance categories as we pull the two component rhombics closer together

In fact, the azimuth patterns of the two versions of the dual rhombic are not identical, even when we widely space the components for maximum performance. **Fig. 5-18** shows the azimuth patterns for the wide-spaced versions of each configuration. The offset version shows a somewhat different pattern of

sidelobe combinations in virtually every azimuth direction. The differences have no practical consequences, but they do suggest subtle differences at the theoretical level. The irregularities in the shapes of some sidelobes result from the slight offset in sidelobe angle for the two component rhombic sidelobes.

Fig. 5-18

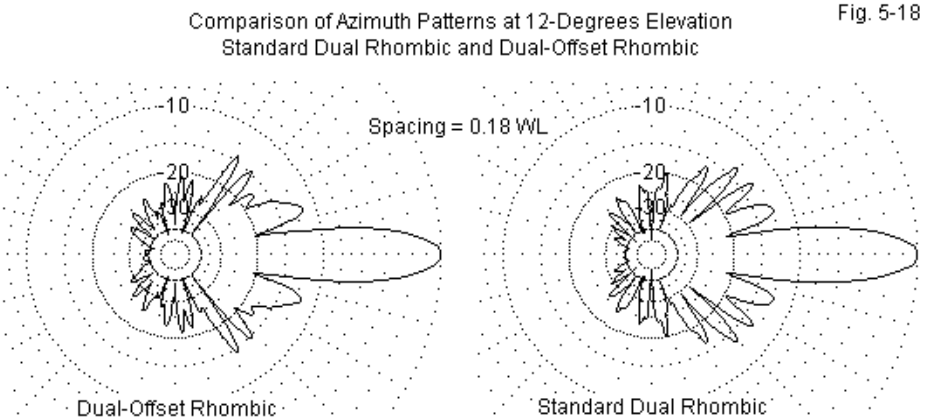

Laport equally emphasized the reduction of sidelobes in the vertical plane. **Fig. 5-19** presents elevation patterns for the original single rhombics and for the two versions of the dual rhombic. The single short rhombic shows its strongest vertical sidelobe (the 2nd) at 49° relative to the horizon, and it is about 10.5 dB weaker than the main lobe. The more relevant longer single rhombic has a first sidelobe at 38° and down by about 13.6 dB relative to the main lobe.

In contrast, both versions of the dual rhombic reduce the strength of the first elevation sidelobe at 37°, leaving the second sidelobe at a relatively harmless 51° as the stronger–down about 13.6 to 14.0 dB. The first elevation sidelobe is between 17 and 20 dB weaker than the main lobe. For HF communications, the very significant reduction in the strength of the first elevation sidelobe contributes to a very significant reduction in various forms of interference from shorter-range sources. With respect to the first elevation sidelobe, the dual offset design is about 3-dB superior to the standard dual rhombic design.

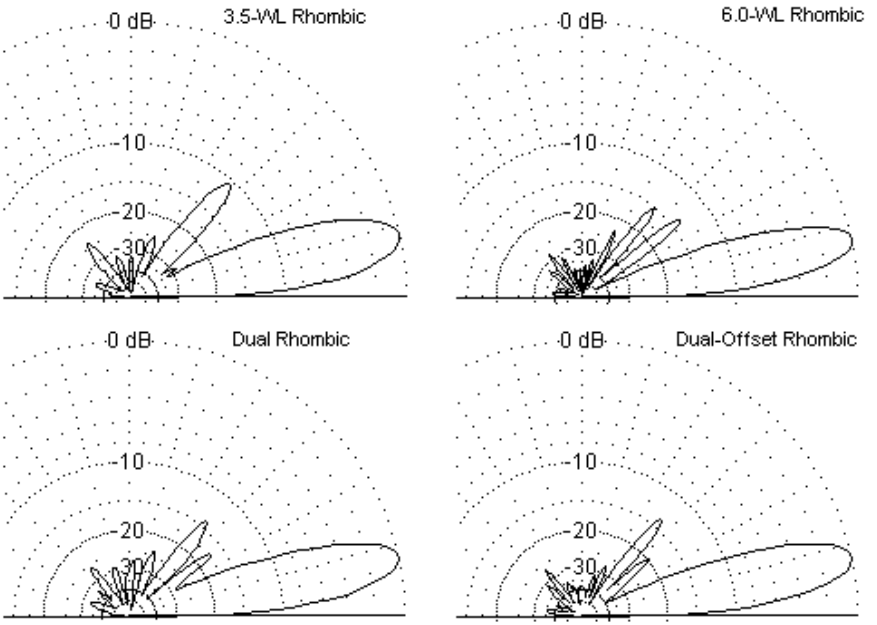

Comparative Elevation Patterns
Single and Dual Rhombic Beams

Fig. 5-19

The models used in these comparisons do not correspond perfectly to Laport's designs. He used a collection of stereographic design aids, derived from Foster's 1937 work. In many ways, the use of NEC models updates those aids by taking into account on a running basis all of the environmental factors that affect rhombic performance. Furthermore, using a uniform scale for all patterns removes much of the difficulty in reading the relatively more exact improvements achieved by the design over a single rhombic. In general, the dual rhombic adds about 1.5-dB forward gain to the longer component single rhombic and reduces sidelobes by about 3 dB in the E-plane and by even more in the H-plane (with special reference to the first elevation sidelobe). Results may vary slightly with the antenna height above ground and with the ground quality for antennas whose

height is below about 2 λ.

Laport's vision for rhombic applications did not end with either the dual rhombic or with the HF range. An offset dual rhombic–constructed from wire around a wood frame–managed to win an antenna competition at 1296 MHz in the 1990s. The design has also been used for fringe area television reception in the days before cable and satellite television. As well, Laport envisioned a 4-rhombic design as perhaps the ultimate step in rhombic sidelobe reduction.

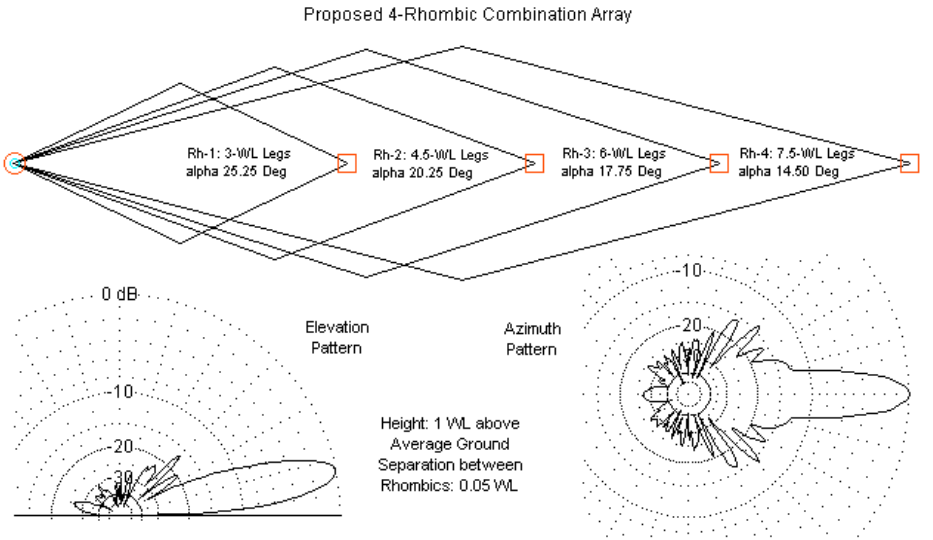

Fig. 5-20

Fig. 5-20 shows the design as modeled using standard techniques, rather than as two pairs of offset rhombic. However, the standard formulation will suffice to hint at the limits of sidelobe reduction in rhombics using the technique of offsetting lobes with corresponding nulls from other rhombics in the set. The upper portion of the figure supplies Laport's dimensions, translating his full apex angles into values of α.

The elevation pattern shows a further reduction in sidelobe strength past the first two elevation sidelobes. The critical first elevation sidelobe is down by over 20 dB, while the second is 3-dB weaker than for the dual rhombics explored earlier. The azimuth pattern shows similar improvements, except for forward gain. The maximum forward gain for this configuration is 19.92 dBi, suggesting that there may be a gain limit relative to adding rhombics to the collection. Because the model spaces the rhombics at 0.05-λ intervals, we find a reduction in the front-to-back ratio down to about 27 dB. We have seen a reduction in feedpoint impedance from well over 800 Ω for single rhombics to somewhat over 400 Ω for dual rhombics. The set of 4 rhombics in the present model reduces the impedance to about 200 Ω.

The azimuth pattern also shows that considerable design work might be required to perfect the 4-rhombic combination for any given height above ground. The main lobe has a standard 12.1° beamwidth, but the first sidelobes have folded into the main lobe and appear as "bulges" on each side. These bulges are only about 12-dB below the level of the main lobe. As well, the strongest lobe is 2 lobes over from the bulges at 44° from the main forward lobe. Relative to this strongest identifiable sidelobe, the front-to-sidelobe ratio is 13.85 dB, about 1.5-dB better than for the dual rhombics at their best. It may be possible to effect further improvements in performance both by further adjustments to the α angles of the component rhombics and also by make slight changes in their leg lengths. All of these designs have used leg lengths that are multiples of a half-wavelength. Of course, some of these values may change if we convert the design to an offset version. The technique–which we shall not pursue here–involves combining the shortest and the longest component rhombics and then combining the two intermediate-length components. The results would be 4 rhomboid structures with approximately the same overall length. Laport did install a dual offset rhombic for the HF range, and there have been VHF and UHF versions as well. However, I have not come across an implementation of the most complex of the multiple rhombics.

Conclusion

Although we might go further in the study of rhombics using NEC as our

examination tool, we likely should end at this point. We have seen enough to appreciate the general trends in rhombic performance. Hopefully, in the course of meandering through the maize of multiplicities, we have also come to appreciate that the design of rhombic antennas is not locked into a simple (or even a single complex) set of equations.

We began by demonstrating that there are virtually always multiple rhombic designs that may fulfill a given need. By juggling the leg length, the value of α, and the antenna height, we can arrive at a design that will fit a set of property limits with the best possible gain. That design may not be the same as the designs in the previous chapter that optimize values for maximum gain regardless of the required acreage. We also discovered that some older design methods rely heavily on calculations applicable to rhombics with legs that are multiples of half-wavelengths. NEC and similar antenna design software allow us to determine properties for any length whatsoever, and these properties do not form straight-line curves from one to the next half-wavelength multiple.

We next examined multi-band rhombics. We found that by modifying the value of α for any given basic design initially optimized for maximum gain, we could spread operation over a 2:1 frequency range. Indeed, the proper selection of the value of α allows one to tailor the rhombic design to a desired frequency range up to at least 2:1. The value of α also allows us to place peak gain closer to or farther from the base design frequency. Like any horizontally polarized antenna, as we raise the operating frequency, the antenna grows longer and the height goes up when measured as a function of a wavelength. These factors lower the elevation angle of maximum radiation as the frequency climbs.

As a check upon our modeling exercises, we explored multiple ways to model even simple rhombic structures. By comparing the pointed-end models used in all preceding chapters with blunt-end models, we determined that the use of a one-segment wire at each end of the rhombic allowed us to replace the series terminating resistors with a single resistance value. As well the split source became a single source. The only significant difference between the models occurred in the feedpoint reactance, which has its most likely source in the altered capacitance across the terminating resistor(s). With a single load resistor,

data showed a higher capacitive reactance at the source than with the series resistors, a phenomenon that roughly corresponds with rhombic construction practices that recommend the use of series resistance terminations.

The blunt-end models allowed us to examine the use of multiple side wires in the rhombic, and to compare performance with single-wire models. The results tallied well with rhombic experience, as the termination resistance dropped from over 800 Ω down to about 600 Ω. As well, the 3-wire models showed a small gain advantage over their 1-wire counterparts. However, a past claim about the flatness of SWR curves over an extended frequency range turned out to depend less on the use of multiple side wires than on the degree to which the builder matches the feedline and the terminating load resistance.

We concluded our foray into multiplicity with Laport's multi-element rhombic designs that aimed to attenuate both vertical and horizontal sidelobes well beyond the levels possible with single-element rhombics. By combining rhombic lengths whose patterns tend to overlap lobes with nulls, and vice versa, we obtained a dual rhombic with about 3-dB of sidelobe reduction, especially with respect to the strongest forward sidelobes. The elevation advantage proved to be even greater with respect to the first vertical sidelobe (or second elevation lobe). However, once more, the optimal values of α for the suppression of sidelobes did not generally correspond precisely with the angles needed for other single-element rhombic designs, and the necessary design angles also are quite likely to depend on antenna height and ground quality if the antenna is below about 2 λ. We also examined 2 of Laport's most creative designs. First was the offset dual rhombic, which shortens the overall antenna length without a significant change from dual rhombic dual rhombic performance. We closed with a glimpse at the 4-rhombic combination that revealed both the potential and the limitations of the design.

Like all of the long-wire arrays that we have surveyed, we have treated the rhombic on its own ground, avoiding comparisons with other antenna technologies. We have sought to understand long-wires, not to judge them. However, we must eventually face an important question for the amateur radio operator with more acreage than cash: should I ever build one?

Afterword: Should I or Shouldn't I

> The horizontal rhombic antenna provides an economical means for obtaining signal and directivity gains comparable with those secured by other more costly antennas of limited frequency range. The first and annual costs of single rhombic antennas compare favorably with those of known types of single channel arrays, and the rhombic type has the advantage that although optimum performance is obtained only in the neighborhood of a predetermined frequency, it will operate reasonably satisfactorily over a wide range of adjacent frequencies.
>
> A. E. Harper, *Rhombic Antenna Design*, p. 15

Except for a few comments along the way regarding the best use of the long-wire beams and bi-directional arrays, we have tried to examine the antennas within their own context. These notes have aimed to naturalize the performance of long-wire antennas by presenting a staged development from the simplest long center-fed doublet to the most refined multiple rhombic beam. Hopefully, you may now have rational expectations of any member of the long-wire technology family.

Long-wire technology provides a number of fundamental lessons and principles relating to antenna performance. These alone make our trek through them sufficiently worthwhile, despite the gradual disappearance of long-wire arrays from active use. In some cases, modern technology, such as satellite communication, has supplanted large HF arrays as the mainstay of long-haul point-to-point message handling. In other cases, better antennas have emerged for the changing communications needs. Nonetheless, many facets of long-wire technology remain in place at both government and amateur installations. Amateurs regularly use 135' and 270' doublets to cover the entire HF spectrum. Military and other government installations use such doublets as back-up antennas. Their simplicity lets them continue working when complex rotating mechanisms and the antennas they turn have broken down from use or weather fatigue. Some installations use terminated long-wire beams in addition to other antennas, again for their simplicity, reliability, and broad frequency response. Some form of V array remains a popular amateur field antenna. Most of the HF

rhombics in service are remnants of bygone days, although they provide broadcast and other communications coverage just as in earlier days.

For the radio amateur, the V and rhombic arrays have two major drawbacks: acreage and beamwidth. A limited number of amateurs have the necessary acreage. Unlike the situation in the 1930s, copper wire is now a relatively cheap commodity. Even copperweld is cheap enough to support a very large array that will endure until time wears away the bonded copper coating and rust dissolves the steel beneath it. As well, radio amateurs are very much attuned to the history of their avocation and regularly dream of antenna farms. Long-wire arrays have more than a rational appeal to many.

Hence, a certain question arises at least for a limited subset of the amateur radio operators world wide. Should I or shouldn't I build a large long-wire array?

Since the question can only arise for someone with the requisite acreage, we can focus on the beamwidth question. **Table 6-1** provides a summary of the beamwidths that we uncovered in free-space models for V and rhombic antennas. We shall bypass the more complex question of long-wire array beamwidths, since they usually are a function of a split lobe at equal angles relative to the wire axis. All V and rhombic arrays have a strong main lobe aligned with the array centerline. (Tabular values for the unterminated rhombic are for the closed version, but the open version does not vary by much from the values shown.)

Once we align main lobes from at least two wires, the main lobe that we create has a very narrow beamwidth. The values in the table are for arrays optimized for maximum gain. We can broaden the beam slightly by using an α angle that departs from the value for maximum gain, but the resulting antenna will lose gain faster than it significantly increase the beamwidth.

Moreover, note that we find very little difference in the beamwidth values for V and rhombic antennas, whether unterminated or terminated. The rhombic adds considerable strength to the main lobe as it doubles the length of a V array with the same leg length, but the main lobe maintains its essential needle-nose shape.

Beamwidths of V and Rhombic Arrays				Table 6-1
	Free-Space Beamwidth in Degrees			
Len WL	V Array	V Beam	Un Rhom	Ter Rhom
2	19.4	19.8	18.4	18.2
3	15.4	15.8	14.9	14.6
4	13.6	13.2	12.4	12.4
5	12.2	12.0	11.0	11.0
6	10.8	10.8	10.0	10.0
7	10.2	10.0	9.2	9.2
8	9.6	9.2	8.6	8.6
9	8.8	8.6	8.0	8.0
10	8.4	8.4	7.6	7.6
11	8.2	7.8	7.4	7.4

Most amateurs only recognize some of the implications of having an antenna with a very narrow beamwidth. For example, we can know from the start that we shall have to aim the antenna carefully–by way of an initial property survey rather than a well-calibrated rotator–in order to be assured that it points at a target area. At the same time, we may fail to realize just how restrictive the narrow beamwidth can be.

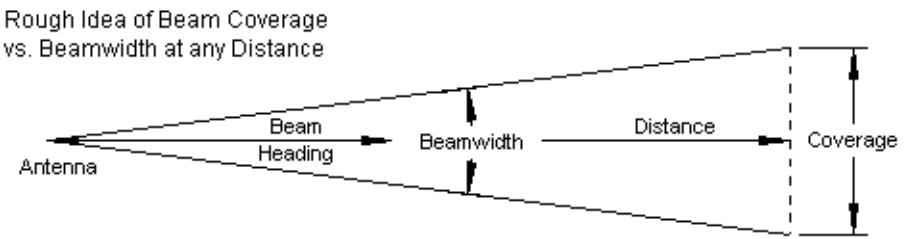

Fig. 6-1

Let's perform a little exercise using a flat earth as its foundation. The earth is round, which will make the results of the exercise slightly inaccurate. However, refraction of HF signals in the ionosphere is an inherently imprecise matter, much like the reflections from an out-of-focus mirror. Transmitted waves strike regions

of the ionosphere, not points. They also descend in broad fronts rather than straight rays. The ionosphere will create much larger variances from a truly spherical analysis than will our use of flatland trig. In any event, given a certain beamwidth angle, we can calculate a very rough azimuth coverage equation:

C = 2 D sin (BW/2)

C is the coverage distance across the beamwidth limits in the same units of measure as the distance, D. BW is the beamwidth angle. We take half the beamwidth angle to create our erstwhile right triangle, and then calculate the distance from the centerline to the outer limits for a given distance. Doubling that distance gives us the total span of coverage, at least as a first order estimate.

Long-Wire Coverage at Selected Distances and Beamwidths					
Distance	Half-Power Beamwidth in Degrees				
Miles	23 Deg	19 Deg	15 Deg	11 Deg	7 Deg
1000	399	330	261	192	122
2000	797	660	522	383	244
3000	1196	990	783	575	366
4000	1595	1320	1044	767	488
Table 6-2	Coverage at Right Angles to Beam Centerline in Miles				

Table 6-2 provides some sample numbers for representative beamwidths. Even at 4000 miles distance, a rhombic with 11-λ legs will cover about 500 miles, and the edges will be at half power. Fortunately, a strong ionospheric layer will enlarge that area, although not by too much. As well, a V beam or a rhombic is a fixed antenna, a fact that requires us to know in advance with whom we wish to communicate. Since either type of antenna losses nothing in performance if we remove the termination, we can obtain a bi-directional array if we have communications targets both fore and aft. Nevertheless, much of the horizon remains uncovered except by the weaker sidelobes of the array that we choose.

Perhaps we can understand the limitations of rhombics by a few comparisons. As a reference table, let's replicate in **Table 6-3** the free-space performance of rhombic beams with legs from 2 λ to 11 λ.

Performance of Terminated Rhombic Beams Optimized for Maximum Gain (R = 850 Ohms)									Table 6-3
Free Space									
Len WL	Ttl Len	alpha	Gn dBi	FB dB	BW deg	F/SL dB	Feed R	Feed X	SWR 850
2	3.13	38.5	9.43	29.22	18.2	7.52	851	8	1.01
3	5.14	31.0	11.30	45.38	14.6	8.94	865	22	1.03
4	7.13	27.0	12.59	44.22	12.4	9.32	868	18	1.03
5	9.14	24.0	13.57	38.68	11.0	9.10	872	22	1.04
6	11.13	22.0	14.36	37.26	10.0	8.94	872	20	1.04
7	13.11	20.5	15.03	36.44	9.2	8.86	871	22	1.04
8	15.13	19.0	15.60	36.16	8.6	8.87	871	22	1.04
9	17.12	18.0	16.11	36.14	8.0	8.96	869	22	1.03
10	19.13	17.0	16.56	36.17	7.6	9.00	867	22	1.03
11	21.15	16.0	16.96	36.46	7.4	8.95	866	23	1.03
Len WL = Leg length in Wavelengths					BW deg = Half-power beamwidth in degrees				
Ttl Len = Overall rhombic length in wavelengths					F/SL dB = Front-to-sidelobe ratio in dB				
alpha = Wire angle to V centerline					Feed R = Feepoint resistance in Ohms				
Gn dBi = Maximum gain in dBi					Feed X = Feedpoint reactance in Ohms				
FB dB = 180-degree front-to-back ratio in dB					SWR 850 = 850-Ohm SWR				

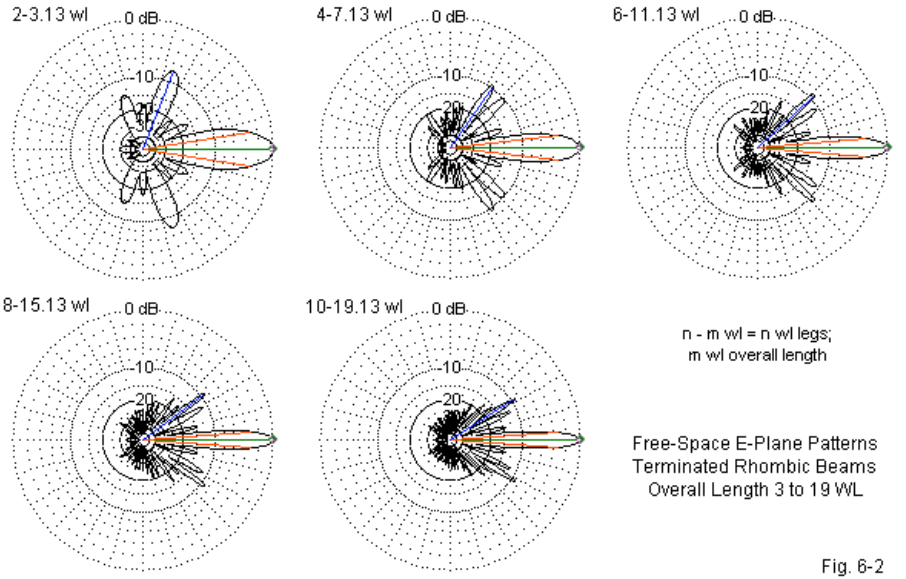

Fig. 6-2

The table provides us with not only the beamwidth values, but also with the leg length, total overall length, and free-space gain of the associated rhombic beam. The gallery of E-plane plots in **Fig. 6-2** supplies corresponding glimpses into the sidelobe structure of the patterns that go with the data. Since the rhombic data is for free space and uses wavelengths as the unit of physical and electrical measure, the data would apply at virtually any frequency.

DL6WU Yagis: 10-40 Elements			Single-Unit Free-Space Performance at 432 MHz					Elements: 4-mm aluminum		
Elements	Bm-Ln	Gain	180 F-B	H BW	H F/SL	V BW	V F/SL	FP Resis	FP React	SWR-50
10	2.15	13.88	31.92	37.6	19.08	41.6	13.40	49.65	13.75	1.32
11	2.49	14.26	16.96	35.8	18.19	39.0	13.32	46.34	-2.13	1.09
12	2.85	14.76	15.49	34.0	17.81	36.6	13.63	60.77	-7.83	1.27
13	3.22	15.28	19.31	32.4	17.82	34.8	14.14	67.77	7.43	1.39
14	3.62	15.69	28.63	31.2	17.78	33.2	14.50	55.32	14.59	1.34
15	4.02	15.99	21.14	30.0	17.58	31.8	14.62	46.94	8.07	1.20
16	4.42	16.27	17.54	29.0	17.40	30.6	14.69	47.93	-0.75	1.05
17	4.81	16.59	17.68	28.0	17.32	29.5	14.88	56.06	-4.27	1.15
18	5.21	16.92	21.43	27.2	17.37	28.6	15.08	62.63	2.50	1.26
19	5.61	17.21	33.20	26.6	17.33	27.6	15.19	57.93	10.14	1.27
20	6.02	17.43	24.37	25.8	17.16	26.8	15.17	50.63	8.35	1.18
21	6.42	17.61	19.80	25.2	16.96	26.2	15.11	49.36	2.04	1.04
22	6.82	17.82	19.51	24.6	16.85	25.6	15.11	54.25	-1.79	1.09
23	7.22	18.06	22.92	24.0	16.77	24.8	15.15	59.80	1.50	1.20
24	7.61	18.28	35.99	23.6	16.68	24.4	15.17	58.13	7.62	1.23
25	8.01	18.45	26.69	23.0	16.57	23.8	15.08	52.51	7.76	1.17
26	8.41	18.59	21.48	22.6	16.38	23.4	14.99	50.53	3.24	1.07
27	8.82	18.74	20.94	22.2	16.32	22.8	15.02	53.68	-0.27	1.07
28	9.22	18.92	24.14	21.8	16.24	22.4	14.96	58.18	1.45	1.17
29	9.62	19.09	37.43	21.4	16.16	22.0	14.96	57.81	6.21	1.20
30	10.02	19.23	28.42	21.2	16.04	21.6	14.86	53.52	7.11	1.17
31	10.41	19.35	22.83	20.8	15.98	21.2	14.88	51.42	3.80	1.08
32	10.81	19.47	22.14	20.4	15.88	21.0	14.79	53.55	0.72	1.07
33	11.21	19.61	25.20	20.2	15.91	20.6	14.84	57.21	1.64	1.15
34	11.62	19.75	38.02	20.0	15.76	20.4	14.75	57.40	5.39	1.19
35	12.02	19.87	29.70	19.6	15.72	20.0	14.72	54.09	6.55	1.16
36	12.42	19.97	23.93	19.4	15.67	19.8	14.75	52.08	4.06	1.09
37	12.82	20.07	23.15	19.0	15.58	19.6	14.66	53.56	1.40	1.08
38	13.21	20.18	26.12	18.8	15.57	19.2	14.66	56.58	1.88	1.14
39	13.61	20.30	38.19	18.6	15.55	19.0	14.71	57.02	4.89	1.17
40	14.01	20.40	30.61	18.4	15.43	18.8	14.60	54.40	6.10	1.16
Elements = Total number of Yagi elements					V BW = Vertical beamwidth in degrees					
Bm-Ln = Boom length in wavelengths					V F/SL = vertical front-to-sidelobe ratio in dB					
Gain = forward gain in dBi					FP Resis = Feedpoint resistance in Ohms					
180 F-B = 180-degree front-to-back ratio in dB					FP React = Feedpoint reactance in Ohms					
H BW = Horizontal beamwidth in degrees					SWR-50 = 50-Ohm SWR					
H F/SL = horizontal front-to-sidelobe ratio in dB										Table 6-4

One type of antenna that has supplanted the rhombic beam is the ubiquitous Yagi. The typical HF Yagi does not reach rhombic gain levels until it has 5 to 6 elements for a gain of 9 to 10 dBi in free space. We may perhaps draw a more relevant comparison by using VHF and UHF Yagis. The DL6WU trimming series of Yagis has performance levels and physical measurements as shown in **Table 6-4**. There are Yagis with better sidelobe performance and individual length designs that achieve more gain. But the classic antennas designed by Guenter Hoch have become a standard against which we tend to measure all VHF and UHF beams. **Fig. 6-3** provides a gallery of sample E-plane patterns.

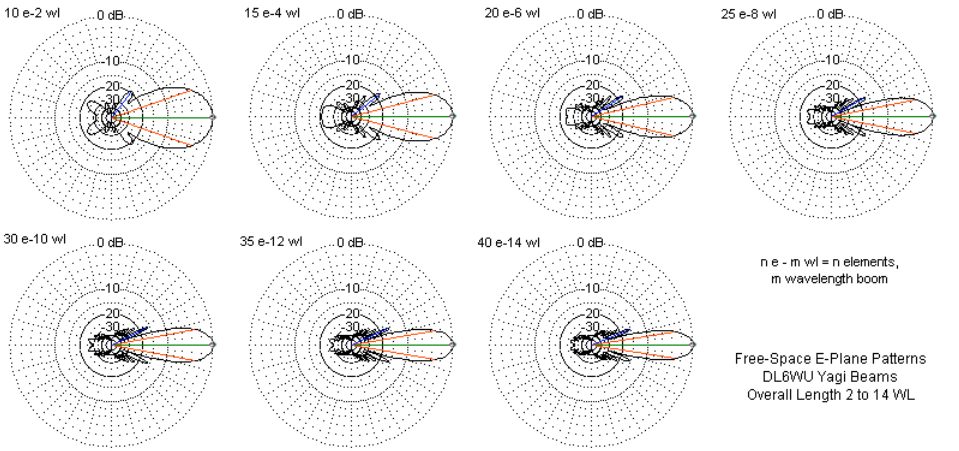

Fig. 6-3

Perhaps the most vivid comparison that we can make appears in **Fig. 6-4**. I selected a rhombic and a Yagi with almost identical gain values: about 16 dBi. The upper portion of the graphic shows the relative sizes of the two antennas, one a rhombic with 9-λ legs, the other a 15-element Yagi on a 4-λ boom. Even though both antennas have the same maximum gain, the Yagi provides the gain over a 30° beamwidth to the half-power points, while the rhombic manages an 8° beamwidth. The Yagi has a front-to-sidelobe ratio that is double the value of the rhombic. Moreover, it confines the major sidelobes to a much smaller region of the horizon. When we add to the equation that the Yagi is–in the VHF and UHF

ranges–small enough to rotate to a desired direction, we begin to understand why early use of V beams and rhombics at very high frequencies gave way to modern Yagi designs.

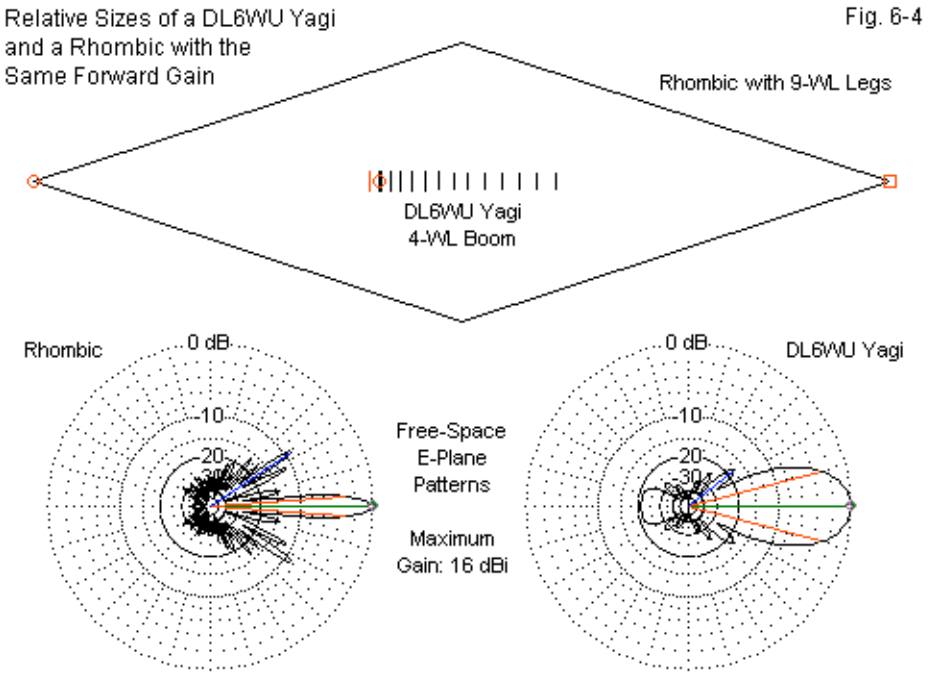

Although the Yagi enjoys a very large performance-vs.-size advantage over the rhombic, it has a notable disadvantage. The operating bandwidth is generally quite narrow. A Yagi capable of good performance over a 7% bandwidth falls into the "wide-band Yagi" category. (A bandwidth as a percentage calls for a simple calculation. Divide the covered frequency range by the center frequency, and multiply by 100. To cover the 70-cm band, we subtract 420 from 450 to get a 30-MHz range, and divide by 432 MHz, the center frequency. The result is, when multiplied by 100, 6.9%.) For a 2:1 or larger operating bandwidth, we must turn to

a different type of antenna. One currently useful type of antenna is the log periodic dipole array (LPDA).

Performance of a 40-Element LPDA in Free Space						Table 6-5
Tau = 0.97; Sigma = 0.18; Boomlength = 4.26 WL at Lowest Frequency						
Freq	Gn dBi	FB dB	BW deg	Feed R	Feed X	SWR 75
1 F	13.50	43.51	41.8	82	-5	1.11
1.25 F	13.50	42.93	42.0	80	-10	1.15
1.5 F	13.30	35.95	42.6	76	-13	1.19
1.75 F	13.16	48.10	42.4	83	-11	1.18
2 F	12.60	30.62	44.2	90	-24	1.40
Freq = Frequency relative to lowest frequency						
Gn dBi = Maximum gain in dBi						
FB dB = 180-degree front-to-back ratio in dB						
BW deg = Half-power beamwidth in degrees						
Feed R = Feepoint resistance in Ohms						
Feed X = Feedpoint reactance in Ohms						
SWR 75 = 75-Ohm SWR						

Table 6-5 present data for a 40-element LPDA design using nearly optimal values of τ and σ, the standard calculating increments for such antennas. The sample antenna is larger than we would ever find in the HF region, but well within the capabilities of support mechanisms at VHF and UHF frequencies. The boom length is 4.26 λ. The table presents performance values at selected points on the 2:1 design frequency range. It is possible–with some added elements–even to improve the performance at twice the lowest frequency to match the performance elsewhere in the operating range.

The performance of the sample LPDA comes close to the absolute limits of what we may squeeze out of these broadband antennas. In fact, we rarely use an LPDA for its raw gain. Rather, our concern is the evenness of the gain and the beamwidth across the operating spectrum. We are also interested in obtaining an acceptable SWR performance at every frequency. Next, LPDA users wish to obtain the highest front-to-back ratio possible. In general, the front-to-back ratio and the rearward pattern improve automatically as the gain

increases in a well-designed antenna. Finally, the LPDA yields a very clean forward lobe with no significant sidelobes at all. **Fig. 6-5** provides samples for the lines in the data table. The only detectable forward sidelobes occur in the E-plane pattern for 1.5F, and they are 35-dB weaker than the main lobe.

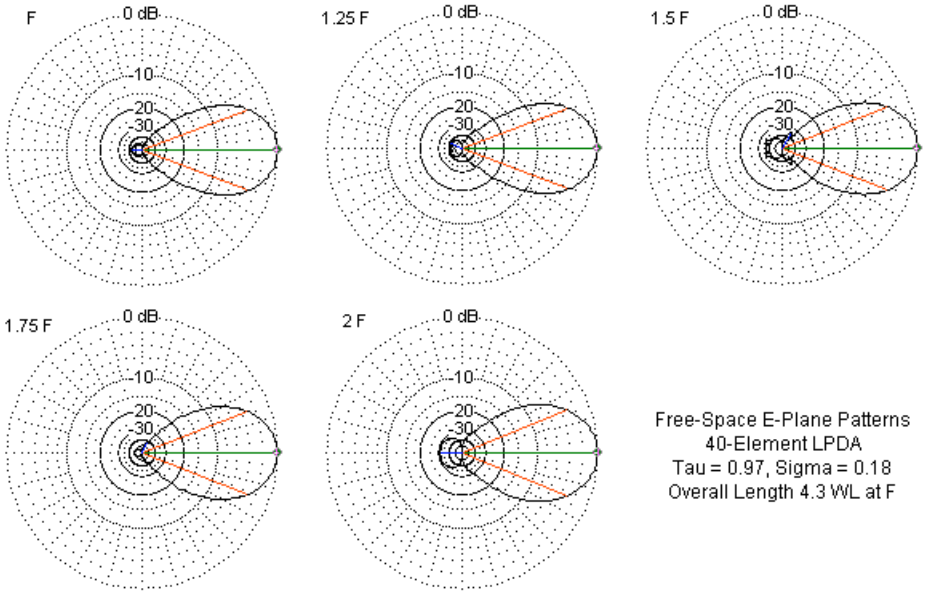

Fig. 6-5

Although the sample LPDA shown in the table and figure are for the UHF range, it is possible to design similar antennas for HF use. Although they are too long to rotate, we may build them with wire elements and use them in a fixed installation. The broad beamwidth and bandwidth make them good candidates for short-wave broadcast antennas directed at large regions of the globe.

We can contrast the 40-element LPDA with a rhombic having roughly equivalent gain performance. A rhombic with 5-λ legs has about the same gain, although its total length is well over twice that of the LPDA on its 4.3-λ boom. The

top portion of **Fig. 6-6** provides the in-scale comparison.

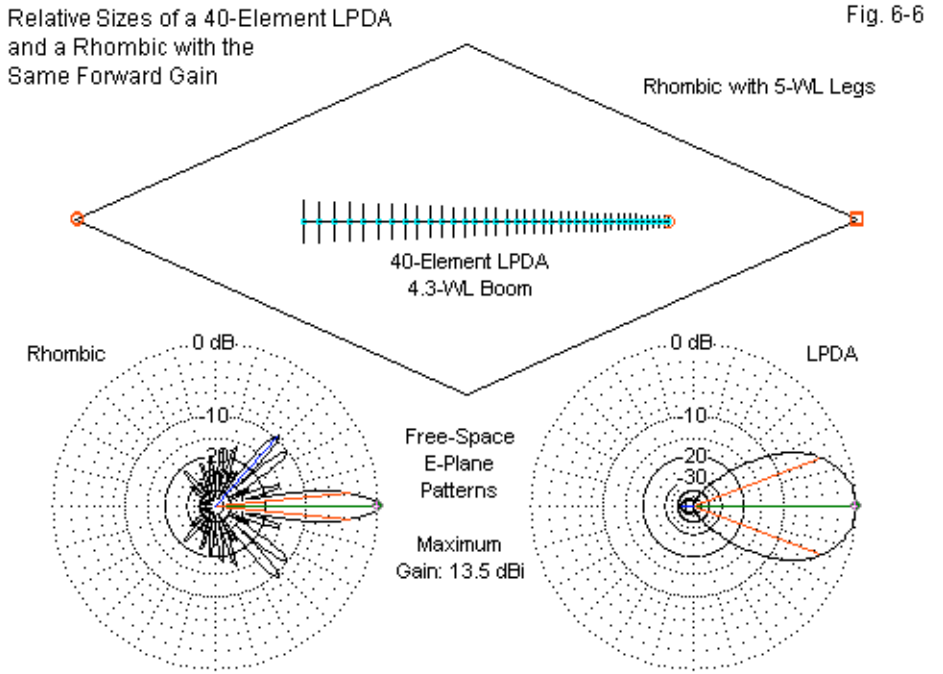

More vivid than the size difference is the shape of the E-plane patterns for the two antennas, shown in the lower half of the graphic. The shear cleanliness of the LPDA pattern contrasts sharply with the many side and rear lobes of the rhombic. However, the 40° beamwidth of the LPDA is not appropriate for every communications application. Point-to-point HF communications call for a narrow beamwidth, while the LPDA is better for covering a broad portion of the horizon. Nine LPDAs of the sample design would cover the entire horizon, assuming an unlimited supply of wire, support ropes, and vertical poles to elevate the antenna.

We might extend these comparisons to include many other high gain antenna

types. For example, dipole arrays have become popular because we may electronically steer their patterns. They tend to require less acreage than rhombics, but may result in much taller and more complex structures. Still, the samples that we have explored suffice to show in a general way why long-wire arrays have ceased to be the mainstays of communications. If we add to the list of conditions that most radio amateur no longer have the space for even a small rhombic, then the tri-band Yagi on the suburban backyard tower becomes the de facto standard of contemporary operation.

The bottom line is simple. Although I would not recommend, except for well-defined special applications, the use of a long-wire beam or array beyond the multi-band doublet or end-fed wire, I do recommend that we learn as much as possible about this class of antennas. They have much to teach us about the electronic aspects of antenna performance. As a bonus, they also have much to teach us about the history of antenna development as we moved from mystery to mastery of the HF spectrum. Finally, long-wire arrays still have special applications based upon their simplicity, their reliability, and their geometry.

The Models Accompanying This Volume

Attached to this volume is a special directory called "models." The collection of models includes almost all of the models used in developing the data in the notes that fill the chapters. All models are in EZNEC format (filename.EZ).

The models subdivide according to what kind of long-wire antenna is involved. The subdirectories (or folders) are as follows:

Doublet
Long-Wire-Unterminated
Long-Wire-Terminated-Laport
Long-Wire-Terminated-Common
V-Unterminated
V-Terminated-Laport
V-Terminated-Common
Rhombic-Unterminated
Rhombic-Terminated
Rhombic-Multi-Band
Rhombic-Multi-Wire
Rhombic-Dual

Within each subdirectory, you will find models whose file names contain a number that indicates the leg length of the wire antenna. Some directories contain separate models for free-space and for over-ground; others require that you introduce the changes necessary to covert free-space models for analysis over ground. Most models are for the standard test frequency used in the volume: 3.5 MHz. All of these models use a standard lossless wire diameter of 0.16". Hence, you may scale them to other frequencies and still have a reasonable–although not always practical–wire size. A few models, such as the ARRL multi-band rhombic appear in versions for the standard test frequency and for the bands of use. Before using these models, you should copy them to a directory within your hard drive. Once on the hard drive, you may revise and save the revised file.

These files are presented as a convenience. Therefore, I do not certify that every one of them is in perfect shape relative to the data in the text. In the course of developing the data sets, many of the models have undergone significant revision. In some cases, the model file might not have returned to its initial form. However, using the techniques described in the various chapters of this volume, you can determine the applicable value of α and restore the original dimensions.

Some of the models, for example, the common-configuration terminated end-fed long-wire antennas and some of the terminated V-beams, may involve wires that are below the surface of the ground. If you use NEC-2, you may have to revise these models before they will run. Models with all wires above ground will run on either NEC-2 or NEC-4. Depending on the exact version of EZNEC that you use, some transmission lines used to created paralleled feedpoints may require lengthening to some fraction of an inch before the program will accept the value.

Other Publications

We hope you've enjoyed this Volume of the **Long Wire Notes.** You'll find many other very fine books and publications by the author L.B. Cebik, W4RNL in the ***antenneX Online Magazine BookShelf*** at the web site shown below.

Published by
antenneX Online Magazine
http://www.antennex.com/
POB 271229
Corpus Christi, Texas 78427-1229
USA

ISBN: 1-877992-77-1
